Zentime

Volume 3 Number 4; Dec. 31, 2025

PERIOPERATIVE PRECISION MEDICINE

ISSN:
2957-5443

Published by ZENTIME PUBLISHING CORPORATION

Perioperative Precision Medicine
ISSN: 2957-5443

Zentime

Perspective https://doi.org/10.61189/159279rpqbrp

A unified framework of cell death: Energy interdependence and multimodal interactions in disease pathogenesis

Qilu Yan[1,*], Haoling Zhang[2,*], Ting Hu[3,4,#], Wangzheqi Zhang[4,#]

[1]Cancer Center, Renmin Hospital of Wuhan University, 238 Jiefang Road, Wuhan 430060, Hubei, China. [2]Department of Biomedical Sciences, Advanced Medical and Dental Institute, Universiti Sains Malaysia, Penang 13200, Malaysia. [3]940th Hospital of PLA Joint Logistic Support Force, 333 Nanbinhe Road, Lanzhou 730050, Gansu, China. [4]Naval Medical University, 800 Xiangyin Road, Shanghai 200433, China.
[*]The authors contribute equally.
[#]Co-corresponding authors.

Corresponding authors: Ting Hu and Wangzheqi Zhang.

Declaration of conflict of interest: None.

Received November 19, 2025; Accepted November 24, 2025; Published December 3, 2025

Abstract

There are various cell death programs that require energy metabolism, redox balance, and the mitochondria–endoplasmic reticulum stress axis. These programs do not operate in isolation; they respond to microenvironmental changes. This review summarizes their networked organization and discusses how Adenosine Triphosphate balance, mitochondrial dynamics, and redox control shape death decisions. The paper also discusses how inflammatory signals integrate diverse modes of death, the diagnostic information contained in cross-death biomarkers, and why multi-target approaches are better suited to complex diseases.

Keywords: Cell death, energy metabolism, redox regulation, mitochondria–endoplasmic reticulum stress, multi-target interventions

Introduction

The latest discoveries in cell-death mechanisms like pyroptosis, apoptosis, ferroptosis, cuproptosis, and PANoptosis reveal a coherent network rather than isolated pathways [1]. Multi-omics and single-cell techniques indicate that these cell death programs affect important metabolic and stress nodes (energy balance, redox state, and the mitochondria–endoplasmic reticulum [ER] axis), and that they are shaped by metabolic pressure, inflammatory signals, and shifts in the microenvironment [2]. Under disease conditions, death pathways operate in parallel, compete with, or follow one another, thereby influencing intercellular communication and the overall immune and tissue responses. Viewing cell death as energy-dependent and multimodal enhances pathologic understanding and supports targeted interventions.

The network logic of cell death: Crosstalk, coupling, and feedback

Molecular nodes governing signaling interactions

Cell death signaling hinges on hub molecules that integrate metabolic stress, inflammation, and growth-factor signals. Klotho regulates ER–autophagy for tissue homeostasis. Interleukin-11 opposes the action of Signal Transducer and Activator of Transcription 1 and decreases reactive oxygen species (ROS) levels, blocking hepatocyte death induced by Interferon-gamma.

Address correspondence to: Ting Hu, 940th Hospital of PLA Joint Logistic Support Force, 333 Nanbinhe Road, Lanzhou 730050, Gansu, China. E-mail: huting@smmu.edu.cn. **Wangzheqi Zhang**, Naval Medical University, 800 Xiangyin Road, Shanghai 200433, China. E-mail: zwzq001031@smmu.edu.cn.

Urolithin A induces ER stress and decreases signaling of the AKT mTOR–4EBP1 pathway—a cascade involving the kinase AKT, the mechanistic target of rapamycin (mTOR), and eukaryotic translation initiation factor 4E-binding protein 1 (4EBP1)—to promote cell death through a different mechanism [3]. As these examples show, cell death relies on signal-integrating molecular nodes rather than linear pathways.

Pathway-level interaction models

Cell death pathways form interconnected networks centered on common axes. Visfatin affects both systemic glucose metabolism and the function of adipocytes. It also activates AMP-activated protein kinase and extracellular signal-regulated kinases 1 and 2 in pancreatic β cells, which prevents apoptosis. Ursolic acid blocks pyroptosis to reduce inflammation through the NF-κB–NLRP3–GSDMD axis (comprising Nuclear Factor Kappa B, NLR Family Pyrin Domain Containing 3, and Gasdermin D) [4]. Overall, the observations show that death pathways operate as modifiable interactive signaling systems rather than as linear causes.

System-level spatiotemporal coordination

Cell-death pathways are shaped by intracellular communication and the action of non-epithelial cells. Studies on mixed-target nanoplatforms have demonstrated the importance of targeting signaling in both tumor cells and tumor-associated macrophages. This approach can align innate and adaptive immunity and alter the dominant death programs in the tumor microenvironment [5]. This suggests that control over cell death is multilayered and constantly modulated by intercellular communication and microenvironmental cues. The major pathways and key nodes mapped in the molecular atlas are shown in **Figure 1**.

The foundational logic of cell death: Energy homeostasis and metabolic disassembly

Adenosine triphosphate (ATP) homeostasis and the turning points of death decisions

ATP plays a distinctly dual role in determining cell fate. Under normal physiological conditions, it ensures the requisite supply of energy. However, once ATP starts to accumulate abnormally outside the cell, its signaling shifts towards a pro-death mode almost immediately. Research has shown that increasing ATP causes breast cancer cells to die. Furthermore, under hypoxia stress, it induces even faster cell death while suppressing autophagy. The variations in ATP levels can also cause cell death. When ATP homeostasis is disrupted repeatedly, it marks a point of no return, leading to cell death.

Mitochondria: The energetic hub and resonance center of cell death

Mitochondria are not only the primary energy source of cells but also a key initiator of death pathways. When their balance is disturbed, there is often an escalation in metabolic dysfunction and death signaling. Palmitic acid damages mitochondrial DNA and the respiratory chain directly and renders myoblasts more death-prone. Since the electron transfer chain generates ATP and ROS, too much oxidative pressure can drive the crosstalk between apoptosis, ferroptosis, and other death phenotypes toward a convergent and amplifying response. The mitochondria-targeted compound CQ-Mito induces ferroptosis and apoptosis according to therapeutic studies, illustrating the organelle's important role in orchestrating multiple death programs [6]. Hence, mitochondria are not purely energy producers but key points where life or death diverge. **Figure 2** highlights the core nodes and regulatory signals through which mitochondrial dysfunction links energy imbalance to redox-driven cell death (apoptosis, autophagy, necroptosis, ferroptosis).

Integrated regulation within the redox network

The metabolic framework for cell death positions redox state at the tipping point between different death programs. ROS are not just amplifiers. They are also shared mediators that are used by many pathways. In pancreatic cancer, SRN-19 produces an accumulation of ROS and activates the p38 Mitogen-Activated Protein Kinase signaling pathway, which causes a concurrent enhancement of apoptotic and cytostatic responses [7]. As such, the redox network can be seen as a common regulatory axis for all forms of cell death. Redox dynamics connect metabolic imbalance with death-decision execution, thus providing a common molecular linkage among different death programs.

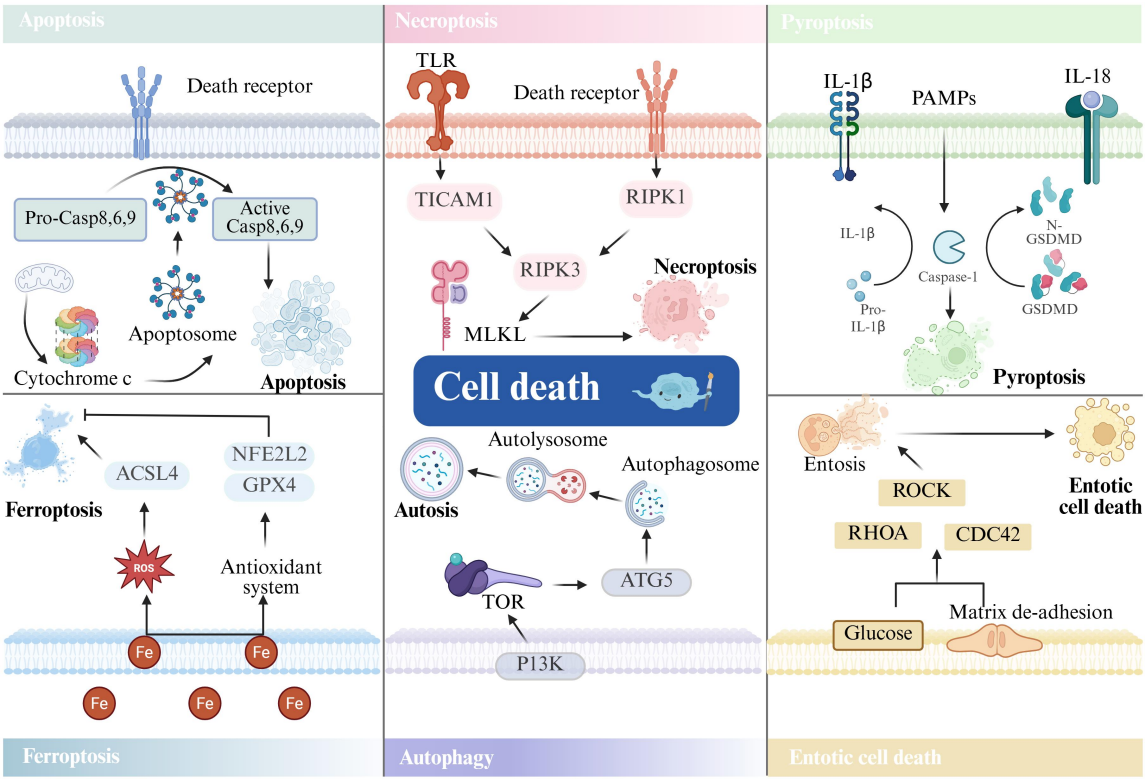

Figure 1. Molecular Atlas of Signaling Pathways and Key Molecules in Cell Death. This figure illustrates the molecular mechanisms of six cell death pathways: Apoptosis is initiated either via death receptors, activating Caspase-8, -6, and -9, or through cytochrome c release from mitochondria, forming apoptosomes; both pathways ultimately lead to programmed cell death; Necroptosis is triggered by TLR or death receptors, inducing necrosis-like cell death via the RIPK1-RIPK3-MLKL signaling pathway; Pyroptosis involves PAMPs activating Caspase-1, which then cleaves both GSDMD to form membrane pores and pro-IL-1β/IL-18 into their mature forms, resulting in inflammatory cell death; Ferroptosis is driven by iron ions inducing ROS accumulation, promoting lipid peroxidation via ACSL4, while the NFE2L2/GPX4 antioxidant system counteracts this process, leading to iron-dependent cell death; Autophagy is regulated by PI3K and TOR signaling, a process that controls autophagosome formation through proteins like ATG5 and culminates in the fusion of these autolysosomes with lysosomes, enabling the degradation of contents within autolysosomes; Entotic cell death occurs when glucose deprivation and matrix de-adhesion activate the ROCK-RHOA-CDC42 pathway, promoting cell entosis and subsequent death. Note: Casp, Caspase; TLR, Toll-like receptor; RIPK1, Receptor-interacting serine/threonine-protein kinase 1; RIPK3, Receptor-interacting serine/threonine-protein kinase 3; MLKL, Mixed lineage kinase domain-like pseudokinase; TICAM1, TIR-domain-containing adapter molecule 1; PAMP, Pathogen-associated molecular pattern; GSDMD, Gasdermin D; N-GSDMD, N-terminal fragment of Gasdermin D; IL-1β, Interleukin-1 beta; L-18, Interleukin-18; Fe, Iron ions; ROS, Reactive oxygen species; ACSL4, Acyl-CoA synthetase long-chain family member 4; NFE2L2, Nuclear factor erythroid 2-related factor 2; GPX4, Glutathione peroxidase 4; PI3K, Phosphatidylinositol 3-kinase; TOR, Target of rapamycin; ATG5, Autophagy-related protein 5; ROCK, Rho-associated coiled-coil-containing protein kinase; RHOA, Ras homolog family member A; CDC42, Cell division control protein 42.

Shared mechanisms and biomarkers across multiple cell death modalities

Convergence of inflammation and immune responses

Inflammation and immune activation share regulatory circuits. During β-coronavirus infection, the entry of the viral particle activates innate immunity and induces PANoptosis, a process in which the two pathways engage in a vicious cycle that drives the development of a cytokine storm. In cancers, though, persistent inflammation causes an exhaustion of $CD8^+$ T cells and weakens responses to immunotherapy, whereas Janus Kinase 1 inhibition externally reroutes T-cell differentiation and reinstates anti–Programmed Cell Death Protein 1 (PD-1) sensitivity [8]. These examples suggest that inflammatory signaling amplifies cell-death

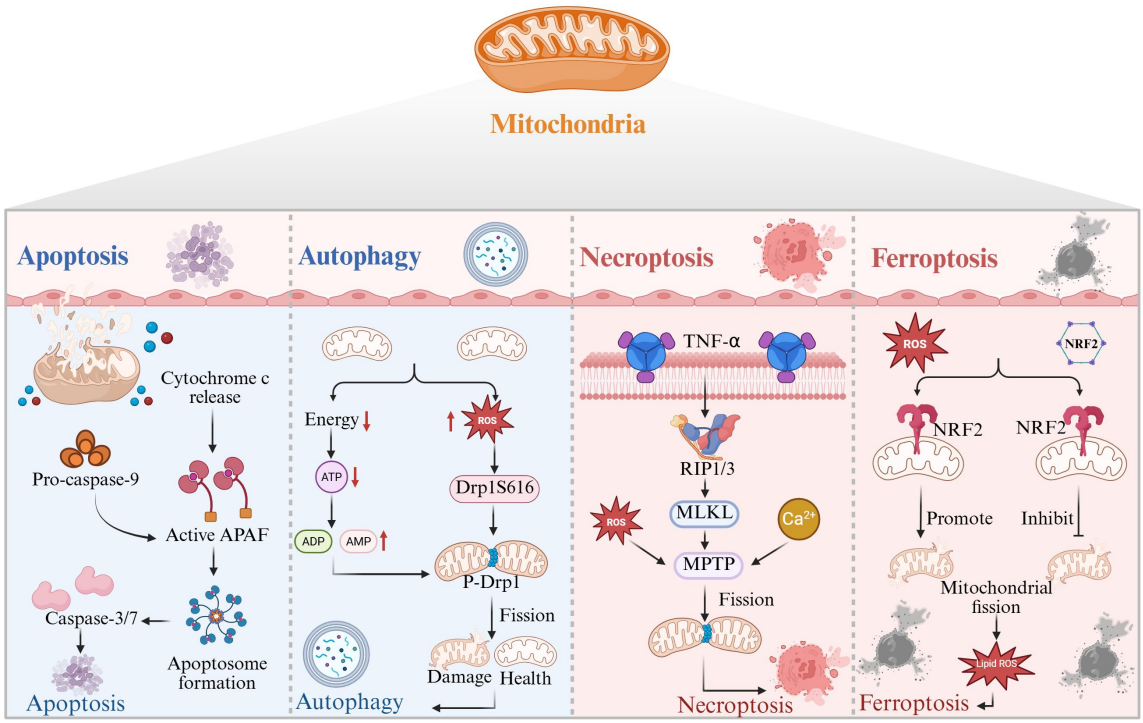

Figure 2. Mitochondria as a Central Node in Multiple Cell Death Pathways. This figure illustrates the central regulatory role of mitochondria in four cell death pathways: apoptosis, autophagy, necroptosis, and ferroptosis. In apoptosis, mitochondria release cytochrome c, which forms an apoptosome with pro-caspase-9 and others, activating Caspase-3/7 to induce cell death. In autophagy, changes in energy levels (decreased ATP, increased AMP), ROS, and others promote mitochondrial fission, and damaged mitochondria are degraded through autophagy to maintain intracellular homeostasis. In necroptosis, TNF-α signaling activates RIP1/3, which in turn regulates MLKL and MPTP; this process, along with changes in Ca^{2+} and production of ROS, promotes mitochondrial fission and ultimately triggers necroptosis. In ferroptosis, ROS activate NRF2, which can promote or inhibit mitochondrial fission, ultimately leading to ferroptosis through processes such as lipid peroxidation. Note: APAF, Apoptotic protease-activating factor; ATP, Adenosine triphosphate; ADP, Adenosine diphosphate; AMP, Adenosine monophosphate; TNF-α, Tumor necrosis factor-alpha; RIP1/3, Receptor-interacting serine/threonine-protein kinase 1/3; MLKL, Mixed lineage kinase domain-like pseudokinase; MPTP, Mitochondrial permeability transition pore; Drp1, Dynamin-related protein 1; p-Drp1, Phosphorylated Drp1; Drp1S616, Drp1 Serine 616; ROS, Reactive oxygen species; Ca^{2+}, Calcium ion; NRF2, Nuclear factor erythroid 2-related factor 2.

pathways and rewires immune behavior to create a common axis linking diverse death modes to immune dysfunction.

Coupling between mitochondrial and ER stress

ER and mitochondria act coordinately under stress. Macrophages undergo different mitochondrial changes in response to various nanoparticles. Some hyperpolarize with ER stress; others depolarize with high levels of ROS. Cell death relies on communication between the ER and mitochondria.

Likewise, in mechanical asphyxia, hypoxia induces C/EBP Homologous Protein, which subsequently translocates to the mitochondria and initiates apoptotic signaling. When these conditions are viewed together, they suggest something simple that often recurs. The coordinated stress of the ER and mitochondria is a common mechanism driving various cell death processes.

Reassessment of cross-death biomarkers

In a disease context, one cell-death program will often present an incomplete picture, because multiple cell-death programs coexist. Multi-omics and machine-learning techniques will bring cross-death features to the field. In glioma, a composite cell death signature can reflect tumor heterogeneity, immune status, and risk of drug resistance at the same time, outperforming individual markers associated with any

one mode of death. A similar trend appears in ischemic stroke. The analysis of the ferroptosis, heat-shock–related death, parthanatos, and cuproptosis pathways revealed sex-specific diagnostic markers: Solute Larrier Camily 2 Member 3 and Matrix Metallopeptidase 9 for men; Pyruvate Dehydrogenase Kinase 4 and Cluster of Differentiation 163 for women.

Determining diagnosis from single-pathway readouts may be limited. Findings suggest that cross-death biomarkers may provide a more accurate multi-modal framework for diagnosis.

Integrated intervention strategies: From single targets to system-level control

Limitations of traditional single-target approaches

Single pathway interventions face limitations. Blocking PD-1/Programmed Cell Death Ligand 1 has little utility for prostate cancer. However, coupling a therapeutic vaccine with checkpoint blockade broadens T-cell activation, bolsters T-cell infiltration, and overcomes resistance driven by the microenvironment. PARP inhibitors similarly impair tumor DNA damage repair, but can be detrimental to T cells, thereby compromising antitumor immunity. As standard cytotoxic therapies are largely unsuccessful due to the existence of long-lasting dormant tumor cells, it is essential to target autophagy and mTOR to eliminate the dormant survival state [9]. Based on these findings, one single switch to achieve tumor elimination while preserving immunity and reshaping the microenvironment will not be adequate. Thus, meaningful benefits will require more integrated multi-pathway strategies.

Potential of multi-target and multi-modal therapeutics

As different types of cancer cells behave differently and resistance against drugs becomes common in cancer treatment, the drugs that hit cancer cells from different targets are better than those just hitting a single target. One example is LCC-09. By blocking Dopamine Receptor D2/D4 and simultaneously suppressing AKT, mTOR and β-catenin signaling, it reverses temozolomide resistance and disrupts glioma stem-cell maintenance [10]. Sodium selenite in high doses puts pressure on cells in different ways. It causes a surge of ROS, lowers levels of glutathione and inhibits Glutathione Peroxidase 4, which together cause ferroptosis through oxidative stress and lipid peroxidation.

The findings suggest that broader regulatory leverage across metabolic and cell-death signaling networks could be expected from multi-target or multi-modal agents that fill an important gap left by single-target agents.

Contributions of artificial intelligence (AI) and network pharmacology

AI and network pharmacology offer a powerful approach for dissecting pathway interactions in the system-level intervention of complex diseases. Multi-omics techniques and molecular-docking analyses showed that DCH inhibits the Phosphatidylinositol 3-kinase/AKT/NF-κB axis and PANoptosis-related nodes, thereby improving sepsis-induced lung injury. Separately, puralne extra blocks AXL Receptor Tyrosine Kinase, mitigates ER stress, and induces immunogenic cell death. Overall, these examples signify a change. AI and networks are shifting drug discovery from single-target trial-and-error to system-wide, mechanism-based precision.

Discussion

According to recent studies, multiple cell-death programs seldom operate independently in disease. As a result, they point to a small set of metabolic and stress-response nodes—energy state, redox balance, and the mitochondria–ER interface. A change in these nodes due to metabolic or inflammatory pressures can drive death pathways to run in parallel, compete or trigger each other. Differences in ATP levels, mitochondrial stability, and inflammatory tone can help explain why diseases—and even patients—appear differentially susceptible to, and have different responses to, treatments. Therapeutically, this layered interplay limits the effects of single-target therapies. For example, in non-small cell lung cancer, the combination of Janus Kinase inhibition and PD-1 immunotherapy targets the redox-immune crosstalk and mitochondria-related death pathways, significantly improving patient response rates; in sepsis-induced lung injury, multi-target agents inhibiting the Phosphatidylinositol 3-kinase/AKT/NF-κB axis and PANoptosis-related nodes have shown promising therapeutic effects.

The use of multi-target agents, cross-death biomarkers, and AI-based network analyses offers more realistic ways to modulate the system as a whole. As the technologies behind single-cell, spatial-omics and live-imaging mature, they may help chart these death networks at improved resolution, enabling true system-level precision interventions.

Author contributions: Qilu Yan, Haoling Zhang contributed to the manuscript writing and figure preparation. Ting Hu and Wangzheqi Zhang designed and supervised the work. All authors read and approved the final manuscript.

References

[1] Zhang W, Liu Y, Liao Y, et al. GPX4, ferroptosis, and diseases. Biomed Pharmacother 2024; 174:116512.

[2] Chen L, Hu Y, Li Y, et al. Integrated multiomics analysis identified comprehensive crosstalk between diverse programmed cell death patterns and novel molecular subtypes in Hepatocellular Carcinoma. Sci Rep 2024;14(1):27529.

[3] Remadevi V, Jamadar A, Varghese MM, et al. Urolithin A, induces apoptosis and autophagy crosstalk in Oral Squamous Cell Carcinoma via mTOR/AKT/ERK1/2 pathway. Phytomedicine 2024;130:155721.

[4] Lei P, Li Z, Hua Q, et al. Ursolic acid alleviates neuroinflammation after intracerebral hemorrhage by mediating microglial pyroptosis via the NF-κB/NLRP3/GSDMD pathway. Int J Mol Sci 2023;24(19):14771.

[5] Guo Y, Li Y, Zhang M, et al. Polymeric nanocarrier via metabolism regulation mediates immunogenic cell death with spatiotemporal orchestration for cancer immunotherapy. Nat Commun 2024;15(1):8586.

[6] Zhao X, Wang T, Shang F, et al. Coumarin-Quinazolinone based photosensitizers: Mitochondria and endoplasmic reticulum targeting for enhanced phototherapy via different cell death pathways. Eur J Med Chem 2024;280:116990.

[7] Yoon B, Suresh RN, Shivakumara CS, et al. Triazolyl-indolo-quinoxaline triggers differential cell death pathways in pancreatic cancer via ROS/p38 axis. Chem Biol Interact 2025; 420:111668.

[8] Mathew D, Marmarelis ME, Foley C, et al. Combined JAK inhibition and PD-1 immunotherapy for non-small cell lung cancer patients. Science 2024;384(6702):eadf1329.

[9] DeMichele A, Clark AS, Shea E, et al. Targeting dormant tumor cells to prevent recurrent breast cancer: a randomized phase 2 trial. Nat Med 2025;31(10):3464-3474.

[10] Wen YT, Wu AT, Bamodu OA, et al. A novel multitarget small molecule, LCC-09, inhibits stemness and therapy-resistant phenotypes of glioblastoma cells by increasing miR-34a and deregulating the DRD4/Akt/mTOR signaling axis. Cancers (Basel) 2019;11(10):1442.

Perioperative Precision Medicine
ISSN: 2957-5443

Zentime

Review Article https://doi.org/10.61189/579841iexakc

Research progress on the mechanisms of traditional Chinese medicine extracts in improving acute lung injury in sepsis

Sixu Chen[1,2,5,*], Jiayin Wang[3,5,*], Weiqi Lin[4,5,*], Xinyi Xie[3,5], Yutong Sun[4,5], Haiyi Qian[3,5], Yichen He[1,2,5], Cuifeng Zhang[1,2,5]

[1]School of Anesthesiology, Wannan Medical College, Wuhu, Anhui Province, China. [2]Anesthesia Laboratory and Training Center, Wannan Medical College, Wuhu, Anhui Province, China. [3]School of Pharmacology, Wannan Medical College, Wuhu, Anhui Province, China. [4]School of Clinical Medicine, Wannan Medical College, Wuhu, Anhui Province, China. [5]Wuhu Perioperative Monitoring and Prognostic Technology Research and Development Center, Wannan Medical College, Wuhu, Anhui Province, China.
[*]The authors contribute equally and co-first authors.

Corresponding author: Cuifeng Zhang.

Acknowledgement: This work was supported by The Foundation of Wannan Medical College (WK2023ZQNZ08), National university innovation and entrepreneurship training program (202310368014, 202310368049, 202410368014), Anhui Province university innovation and entrepreneurship training program (S202310368095, S202310368087, S202410368004, S202410368009).

Declaration of conflict of interest: None.

Received March 5, 2025; Accepted May 12, 2025; Published December 31, 2025

Highlights

- The pathogenesis of sepsis-induced acute lung injury is outlined.
- A comprehensive overview of the role of TCM extracts in sepsis-induced acute lung injury is provided.
- The clinical application of classical TCM extracts is summarized in detail.

Abstract

Acute lung injury (ALI) is a severe and life-threatening condition. Traditional Chinese medicine (TCM) extracts, which are rich in bioactive compounds with demonstrated efficacy against ALI, have exhibited considerable therapeutic potential. This review provides a comprehensive analysis of the therapeutic effects of TCM extracts in mitigating sepsis-induced ALI, synthesizing current evidence on their clinical advantages and the underlying molecular and cellular mechanisms. Furthermore, it outlines the major challenges and unresolved issues in the field, offering insights that may guide future research and enhance the application of TCM in managing sepsis-associated respiratory complications.

Keywords: Traditional Chinese medicine extracts, sepsis, acute lung injury, mechanisms, research progress

Introduction

Acute lung injury (ALI) due to pulmonary sepsis is a systemic inflammatory response caused by infection and is often life-threatening [1]. It can lead to severe lung inflammation, gas exchange dysfunction and multiple organ failure, so it has a high incidence and fatality rate. Although modern medicine have made progress, but the treatment of ALI option

Address correspondence to: Cuifeng Zhang, School of Anesthesiology, Wannan Medical College, Wuhu, Anhui Province, China, No. 22 Wenchang West Road, Yijiang District, Wuhu 241002, Anhui Province, China. Tel: +86-15551257181. E-mail: zhangcuifeng@wnmc.edu.cn.

is still limited, existing therapies are often ineffective.

TCM for its long history and unique pharmacological properties, complementary or alternative therapy in acute lung injury in shows a good application prospect. This article focuses on the effect and progress of Chinese herbal extracts in alleviating acute lung injury in sepsis, providing more ideas for future research and clinical application.

TCM extracts have anti-inflammatory, antioxidant, immunoregulatory, and other therapeutic effects, which can reduce the adverse effects of sepsis-induced ALI. ALI is caused by the multifaceted interaction among inflammatory mediators, oxidative stress, and apoptosis. The initial inflammatory cascade triggered by sepsis promotes the release of key pro-inflammatory cytokines, such as tumor necrosis factor -α (TNF-α) and interleukin-6 (IL-6), resulting in pulmonary edema and impaired lung function [2]. This pathological progression is further exacerbated by the excessive production of ROS, which exacerbate tissue damage and perpetuate a destructive cycle of inflammation and organ dysfunction [3]. Under this background, TCM extracts represent a promising treatment approach, owing to their well-known anti-inflammatory, antioxidant. and immunoregulatory characteristics that counteract sepsis-induced ALI.

The protective effect of TCM extracts on sepsis-induced ALI is mainly reflected in two aspects: inflammatory regulation and oxidative stress intervention. In terms of inflammatory regulation, *Scutellaria baicalensis* extract alleviates lung inflammation and damage by inhibiting the NF-κB signaling pathway (a key regulatory factor for pro-inflammatory cytokine production), while promoting the transformation of macrophages from the pro-inflammatory M1 phenotype to the anti-inflammatory M2 phenotype, thereby accelerating inflammation resolution and supporting the repair of damaged lung tissue [4, 5]. In terms of antioxidation, active ingredients such as hyperoside and salvianolic acid A promote the generation of antioxidant enzymes and reduce the level of reactive oxygen species (ROS) by activating the Nrf2 pathway [6]. This dual mechanism not only enhances the body's antioxidant capacity but also effectively protects the lung tissue structure. Compared with traditional single-target therapy, Chinese herbal extracts can simultaneously intervene in two key pathological links, inflammation and oxidative stress, and have a more comprehensive therapeutic effect. In addition to their anti - inflammatory and antioxidant properties, TCM extracts also play a role in regulating immune responses during sepsis. For instance, certain herbal formulations have been shown to enhance the phagocytic activity of macrophages and improve their ability to clear pathogens, thereby reducing the burden of infection and inflammation [7]. Existing studies have confirmed that these natural compounds have the potential to become important treatment options for ALI. Their multi-target intervention characteristics provide new ideas for developing more comprehensive treatment strategies for acute lung injury, which is worthy of further in-depth research and clinical exploration.

Overview of TCM extracts

Common TCM extracts

Various herbal extracts from different parts of medicinal plants are widely used in TCM, which have unique therapeutic effects. Take *Scutellaria baicalensis* extract as an example. It because of its remarkable anti-inflammatory and antibacterial properties and was highly valued. Ginseng extract is renowned for its ability to enhance stress resistance and relieve fatigue. Angelica is often used in the field of female health care, for blood beautification. Licorice root in the herbal formula as major additives play an important role. *Rehmannia* is famous for its restore body function in the field of TCM. These extracts mainly adopts decoction, dipping the traditional methods of solvent extraction and preparation. The preparation process optimized over a long period of time can effectively retain the therapeutic effect and efficacy of the active compounds [8, 9]. The TCM treatment concept as a whole, the synergistic use of these herbal extracts makes the various ingredients work together to restore the body's balance and promote recovery. The extraction process after hundreds of years of practice continuous improvement and optimization, to ensure the effective components in medicinal plants of therapeutic value into full play in the clinical application. Continuous research and application of these herbs extract

fully proves that they are in the important value of traditional and modern medical practice.

Major active ingredients in TCM extracts

The therapeutic effects of TCM extracts stem from their various bioactive compounds, including flavonoids, alkaloids, terpenoids and polysaccharides, each of which has unique pharmacological effects. For instance, baicalin, a flavonoid extracted from *Scutellaria baicalensis*, has remarkable antioxidant and anti-inflammatory properties and can effectively treat inflammatory diseases such as sepsis [1, 2]. The alkaloids in *Sophora flavescens* exhibit obvious anti-cancer activity and are of great significance in tumor research [10]. Terpenoids, especially the extract of *Salvia miltiorrhiza*, can improve microcirculation and protect heart function, while the polysaccharide components in herbs such as *Astragalus* play a key role in immune regulation and can enhance the body's anti-infection ability [4, 5]. The synergistic effects of these active ingredients illustrate the holistic treatment philosophy of TCM. For instance, the combination of ginsenosides and glycyrrhizin enhances anti-inflammatory effects by inhibiting the NF-κB and MAPK signaling pathways. This multi-component synergistic strategy exemplifies the comprehensive treatment characteristics of TCM [8, 9].

Pharmacological properties of TCM extracts

Herbal extracts have a wide range of pharmacological properties, including anti-inflammatory and anti-oxidant effects, which support the widespread use of TCM in the treatment of various diseases. For example, turmeric extract attenuates inflammation by blocking key signaling pathways such as NF-κB [2, 8]. In the treatment of chronic diseases, TCM extracts have shown unique advantages, including improving diabetes and cardiovascular disorders by optimizing metabolic pathways and enhancing insulin sensitivity [9]. In particular, their significant immunomodulatory effects are of particular importance [5]. *Astragalus* extract, for instance, enhances the activity of macrophages and promote the secretion of cytokines, thus strengthening the body's immune defense. Meanwhile, the hepatoprotective properties of *Schisandrae chinensis* extract provide new insights into the treatment of liver diseases and the prevention of liver injury. Collectively, these findings not only verify the application value of TCM but also provides a scientific basis for transforming ancient medical wisdom into modern medical practice.

Pathological mechanisms of sepsis-induced ALI

Sepsis is a life-threatening condition in which the host response to infection becomes dysregulated, leading to widespread inflammation and potential multi-organ failure. The syndrome develops through a cascade of immune responses that can culminate in ALI, characterized by pulmonary vascular leakage, lung effusion, and dyspnea [1]. In the early stage of sepsis, immune cells such as neutrophils and macrophages are excessively activated and release pro-inflammatory cytokines, including TNF-α and IL-6, which cause endothelial injury, increased vascular permeability, and alveolar fluid accumulation [2]. Interestingly, the immune system may later shift toward immunosuppression, making the patient more susceptible to secondary infections, a challenging complication for physicians treating sepsis [11]. Current research is focused on understanding the delicate balance between inflammatory and anti-inflammatory processes, which may lead to better treatment of sepsis and its dangerous consequences, such as ALI.

Cellular pathomechanisms

Dysregulated neutrophil activation

In sepsis, the excessive activation of neutrophils is closely related to tissue damage. After stimulation, white blood cells are activated by NOX2 enzyme to release reactive oxygen species, and then release matrix metalloproteinase-9 and other harmful substances through particles. These substances destroy VE-cadherin, an important structural protein, and degrade collagen IV and laminin in the lung tissue barrier, leading to fluid leakage and hemorrhage in the air sacs. The problem is exacerbated when neutrophils shed their DNA and form sticky webs called neutrophil extracellular traps, which promote clotting and inflammation.

Macrophage phenotypic polarization

The progression of sepsis also involves a dynamic shift in macrophage behavior. Early stages (0-48 hours) are marked by pro-inflam-

matory M1 macrophage dominance, driven by IFN-γ and LPS-TLR4 signaling, which leads to elevated expression of CD86 and excessive secretion of IL-1β, IL-6, and TNF-α, fueling the cytokine storm. Beyond 72 hours, a transition to reparative M2 macrophages occurs, stimulated by IL-4/IL-13-induced STAT6 activation, resulting in increased CD206 and arginase-1 expression. While this shift promotes TGF-β1-mediated collagen deposition, excessive M2 activity is linked to a 58% incidence of fibroproliferative ARDS in survivors [11].

Molecular signaling networks

Hyperinflammatory signaling cascades

The molecular signaling networks involved in hyperinflammatory cascades demonstrate convergent activation of canonical pathways. The NF-κB pathway is triggered through IKKβ-mediated phosphorylation of IκBα at Ser32/36, enabling nuclear translocation of NF-κB p65 and subsequent upregulation of over 200 proinflammatory genes, including IL6, TNF, and CXCL8 [12].

Simultaneously, NLRP3 inflammasome assembly occurs via dual signals—LPS priming combined with ATP/K+ efflux—leading to the formation of the NLRP3-ASC-pro-caspase-1 complex, which generates active IL-1β (17 kDa) and induces gasdermin D-mediated pyroptosis [12].

Redox imbalance and oxidative injury

In septic lungs, NOX4-derived superoxide (O_2•-) production increases 2.7-fold, overwhelming endogenous antioxidants (43% reduction in SOD1 and 39% reduction in catalase). This redox imbalance result in:

• Oxidation of endothelial caveolin-1, disrupting tight junctions (72% reduction in occludin).

• Activation of MMP-2 via ERK1/2 signaling, leading to degradation of elastin fibers.

• Generation of lipid peroxidation products (3.9-fold increase in MDA and 4.5-fold increase in 4-HNE) that impair surfactant protein-B (SP-B) function.

Ferroptosis-driven fibrogenesis

In sepsis-induced ALI, GPX4 activity decreases by 61% due to glutathione depletion (GSH/GSSG ratio 1.2 vs. 8.7 in controls), permitting iron-catalyzed phospholipid peroxidation (6.8-fold increase in AA/DHA-PE-OOH). Concurrent hepcidin suppression elevates labile iron pool (LIP) concentrations (4.3 μM vs. 1.1 μM), which contributes to the following:

• Fenton reactions: $Fe^{2+} + H_2O_2 \rightarrow Fe^{3+} + \bullet OH + OH^-$, accelerating oxidative damage.

• Upregulation of TGF-β1/Smad3 signaling (3.1-fold increase in p-Smad3), promoting α-SMA+ myofibroblast differentiation and collagen I deposition (↑82%).

Immune response in lung injury

The immune response is central to the development of ALI, with the lungs being especially susceptible due to their direct exposure to pathogens and inflammatory mediators. Key events in this process include the activation of alveolar macrophages and the influx of neutrophils into lung tissue, both of which drive inflammation by releasing a flood of cytokines and chemokines that worsen lung injury through mechanisms like edema formation, disruption of the epithelial barrier, and triggering lung cell death [12]. Additionally, neutrophil extracellular traps (NETs) contribute to tissue damage, further aggravating ALI [13]. Striking the right balance between inflammatory and anti-inflammatory signals is critical—while a controlled immune response helps fight infection, excessive inflammation can cause significant tissue harm and impair lung function [14]. Emerging therapeutic approaches that fine-tune the immune response, such as targeting specific cytokines or immune pathways, show potential in reducing sepsis-related ALI severity.

Role of inflammatory factors in ALI

Inflammatory factors, especially cytokines and chemokines, play a crucial role in the development of sepsis-induced acute lung injury (ALI). During sepsis, excessive production of pro-inflammatory cytokines like TNF-α, IL-1β, and IL-6 creates a harmful inflammatory environment that damages lung tissue [15]. These cytokines not only worsen inflammation but also attract and activate immune cells in the lungs, creating a vicious cycle of injury [16]. Another important player is the NLRP3 inflammasome, part of the body's innate immune defense, which when activated releases IL-1β

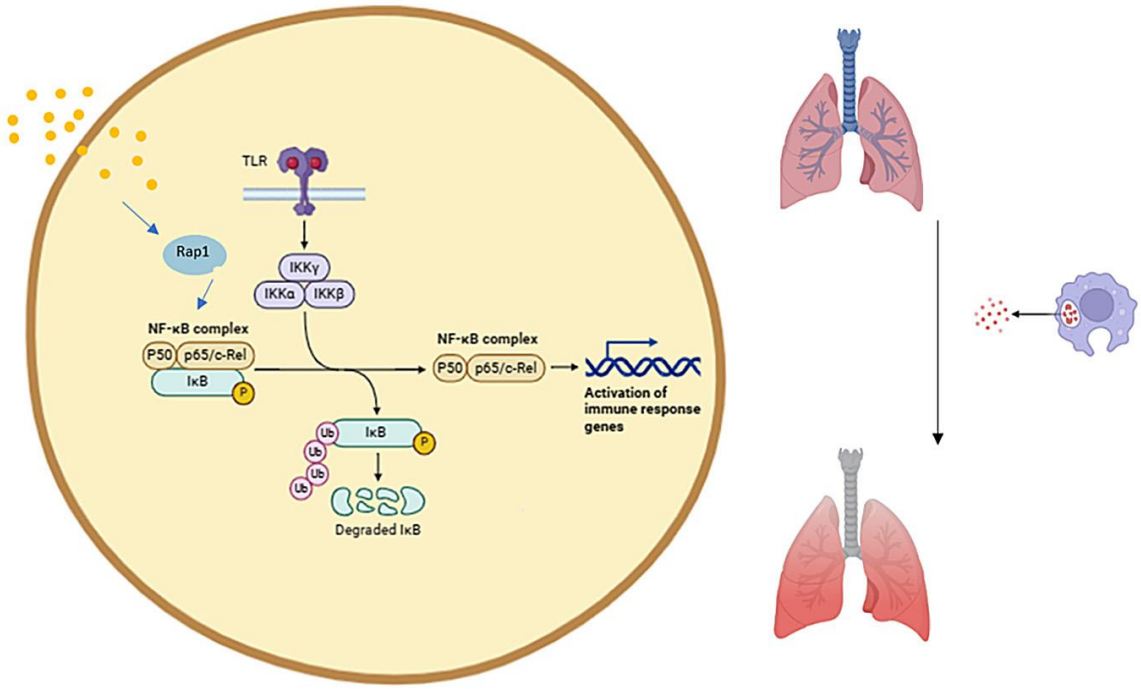

Figure 1. Sepsis-induced acute lung injury. Upon TLR stimulation, downstream effectors such as Rap1 and NK-associated molecules initiate signaling cascades that trigger NF-κB degradation, releasing the NF-κB complex.

and IL-18, further intensifying the inflammatory response [17]. Additionally, the overproduction of reactive oxygen species (ROS) leads to oxidative stress, causing damage to blood vessels and air sacs in the lungs [18]. Potential treatment approaches could involve targeting these inflammatory pathways, such as blocking the NLRP3 inflammasome or specific cytokine receptors, which might help prevent or treat sepsis-related lung injury [19]. The complex interactions between these inflammatory components demonstrate how challenging sepsis can be and emphasize the importance of developing precise treatments that can effectively control the immune response to minimize lung damage (**Figure 1**).

Effects of TCM extracts on sepsis-induced ALI

Improvement in lung function

TCM extracts have demonstrated considerable therapeutic potential in the treatment of sepsis-induced ALI, which remains a major clinical challenge due to the high mortality of sepsis and its complications. TCM preparations, such as *Xuebijing* Injection, have shown significant improvement in lung function in sepsis models by reducing oxidative stress and regulating inflammatory responses. Animal experiments have confirmed that Xuebijing can effectively inhibit the excessive production of key pro-inflammatory factors such as IL-1β and TNF-α, which are hallmarks of sepsis progression [5]. In addition, *Salvia miltiorrhiza* extract also shows promising therapeutic prospects, promoting lung function recovery through a dual mechanism of action: inhibiting inflammatory responses and improving microcirculation [1]. Collectively, these findings indicate that TCM extracts not only alleviate clinical symptoms but also target the core pathological processes of sepsis-induced ALI, providing a multi-target, multi-pathway treatment strategy for clinical treatment.

Studies have shown that certain phytochemicals in TCM, such as *Hyperoside* and *Salirin*, exhibit potent anti-inflammatory and antioxidant effects that effectively protect the lung function in sepsis [6]. *Hyperoside* improves lung function in sepsis models by reducing lung tissue inflammation and oxidative stress, while *Salirin* exerts its effect by blocking the activation of key pro-inflammatory signaling pathways, such as NF-κB and MAPK, which play significant roles in the septic inflammatory response [12]. These findings suggest that TCM extracts hold great promise in treating sepsis-induced ALI, as they can enhance lung function

Table 1. Key TCM extracts and their mechanisms in sepsis-induced ALI

TCM Extract	Active Compound	Mechanism	Synergistic Partners
Scutellaria baicalensis	Baicalin	Inhibition of NF-κB, antioxidant	Glycyrrhizin
Salvia miltiorrhiza	Tanshinones	Anti-apoptotic, improves microcirculation	Astragalus polysaccharides
Astragalus membranaceus	Astragalosides	Immunomodulation, M2 macrophage polarization	Ginsenosides

through multiple mechanisms in a synergistic manner (**Table 1**).

Anti-inflammation mechanisms

TCM extracts play a key role in mitigating inflammation during sepsis-induced ALI by regulating macrophage polarization. Studies have shown that these extracts promote macrophage polarization from the pro-inflammatory M1 to the anti-inflammatory M2 phenotype, which is important for suppressing excessive inflammation and facilitating tissue repair. For example, *Dichondra repens* extract inhibits its NLRP3 inflammasome activation, thereby reducing the release of proinflammatory cytokines while enhancing M2 macrophage responses [3].

Xuebijing injection and other TCM extracts not only regulate macrophage function but also suppress the expression of key inflammatory mediators such as IL-6 and TNF-α by inhibiting the NF-κB signaling pathway, a main regulator of inflammation [5]. In addition, active components of TCM, including curcumin and echinoside, effectively reduce oxidative stress and pulmonary inflammation by scavenging ROS and enhancing antioxidant enzyme activity, thereby exerting robust anti-inflammatory effects. These multifaceted synergistic effects fully demonstrate the efficacy of TCM extracts in combating the inflammatory process of ALI [20].

TCM also contributes to immune homeostasis. Studies have shown that TCM extracts improve host immune status by enhancing immune cell function, promoting balanced immune response, preventing excessive inflammation, and assisting pathogen clearance. Specifically, their ability to modulate T cell responses is particularly critical for ameliorating the immune impairment commonly seen in sepsis patients [21]. Collectively, these findings not only validate the clinical value of TCM in alleviating symptoms of ALI but also reveal its therapeutic potential in regulating the underlying inflammatory and immune mechanisms driving lung injury.

Inhibition of apoptosis

TCM extracts not only have significant anti-inflammatory effects but also effectively inhibit the apoptotic process in sepsis-induced ALI. Apoptosis of lung epithelial cells is a critical event in the pathogenesis of ALI. By regulating apoptotic signaling pathways, TCM extracts can significantly alleviate this pathological process, thereby preserving lung function during sepsis. Various active ingredients of TCM exert protective effects through different mechanisms, providing new therapeutic possibilities.

For example, turmeric extract inhibits lung cell apoptosis by regulating key apoptotic proteins such as Bax and Bcl-2, which are essential for maintaining cell viability and function in sepsis-related inflammation [22]. In addition, TCM extracts enhance the expression of anti-apoptotic proteins while reducing pro-apoptotic factors, thereby promoting cell survival. These findings suggest that TCM may alleviate sepsis-induced lung injury by regulating apoptosis [23].

Beyond apoptosis, TCM extracts also influence other survival pathways such as autophagy. Autophagy can remove damaged organelles and proteins, thereby enhancing cellular resilience under stress. Studies have shown that active components of TCM extracts such as emodin can effectively induce autophagy in lung cells, thereby inhibiting apoptosis and improving lung function during sepsis [24]. In addition, the extract could also regulate immune response by promoting macrophage polarization from the pro-inflammatory M1 to the anti-inflammatory M2 phenotype and by inhibiting NLRP3 inflammasome activation [3, 5]. *Astragalus membranaceus* extract, for example, shows a unique dual regulatory function: it can moderately enhance the inflammatory response to fight infection in the early stage of sepsis, and inhibit excessive inflamma-

tory response to prevent tissue damage in the later stage. This dynamic regulatory mechanism explains the contradictory reports on the pro- versus anti-inflammatory effects of TCM in previous studies. This multi-targeted protective effect of TCM is particularly important because uncontrolled cellular stress and inflammatory responses in sepsis lead to widespread cell death.

TCM extracts can inhibit ALI by targeting the apoptotic pathway and promoting cell survival, which has broad therapeutic prospects. They not only preserve lung function in sepsis patients but also improve clinical prognosis. Owing to their multi-targeted mechanism of action, TCM extracts represent a promising complementary therapy in the management of sepsis and its complications.

Research progress on clinical application of classic TCM extracts

Hesperidin

Hesperidin, a flavonoid widely present in citrus fruits, has attracted much attention due to its significant anti-inflammatory, antioxidant, and cardiovascular protective effects. Recent studies have demonstrated its beneficial effects in ameliorating metabolic disorders and cardiovascular diseases. These therapeutic effects are mainly achieved by regulating inflammatory and oxidative stress-related signaling pathways, such as activation of the Nrf2 pathway, which induces antioxidant enzymes, thereby reducing cell oxidative damage [25]. In terms of cardiovascular protection, hesperidin improves endothelial function and lowers blood pressure [21]. Clinical studies have also found that hesperidin can reduce peak postprandial blood glucose by inhibiting α-glucosidase activity, a finding of particular relevance for diabetes management. In addition, hesperidin exerts significant anti-inflammatory effects by inhibiting pro-inflammatory cytokine production, shows promise in the treatment of chronic inflammatory diseases such as arthritis and metabolic syndrome [26]. However, current evidence remains limited by small sample size and short observation period, highlighting the need for more in-depth exploration [1]. It is important to note that studies on the pharmacokinetics of hesperidin, especially bioavailability and metabolic pathways, are essential to optimize its clinical application [21]. These findings not only confirm the value of hesperidin in TCM but also highlight its potential as a modern therapeutic drug.

Astragalus extracts

Astragalus membranaceus, a core herb in TCM, has attracted much attention due to its significant immune-enhancing and anti-inflammatory effects, which are mainly derived from the active ingredients such as astragaloside IV. A large number of clinical studies have shown that Astragalus not only enhances host immune function but also improves treatment outcomes in a variety of chronic diseases and infections. Specifically, *Astragalus* activates macrophages, enhances their ability to phagocytize pathogens, and promote the release of key cytokines, which are essential for maintaining immune system homeostasis [2]. In the treatment of sepsis, *Astragalus* extract significantly reduces patient mortality and organ damage by inhibiting excessive inflammatory response and improving microcirculatory blood flow [1]. When used in combination with conventional treatment, *Astragalus* has also shown adjunctive benefits in chronic obstructive pulmonary disease (COPD) and heart failure. A meta-analysis of 15 clinical trials involving 1200 participants reported a 28% reduction in sepsis-related mortality with *Astragalus* treatment [1]. Current evidence suggests that the therapeutic effects of *Astragalus membranaceus* are mainly attributed to its regulation of key inflammatory and immune signaling pathways, such as NF-κB and MAPK. With the deepening of research, as a safe and effective immunomodulator, *Astragalus* has shown increasingly broad application prospects in the adjuvant treatment of immune-related diseases.

Salvia miltiorrhiza

Salvia miltiorrhiza has been traditionally used for centuries, especially in the treatment of cardiovascular diseases and improvement of blood circulation. Its core active ingredients, tanshinone and salvianolic acid, exhibit multiple pharmacological effects, including anti-inflammatory, antioxidant, and cardioprotective functions. Recent studies have confirmed that *Salvia miltiorrhiza* effectively regulates oxidative stress and inflammatory response, significantly attenuates myocardial ischemia-reperfusion injury and improves cardiac function [27]. Clinical

practice has shown that its combination with conventional therapy yields significant benefits in patients with coronary heart disease, providing strong evidence on its role as an adjuvant treatment [28]. Mechanistically, *Salvia miltiorrhiza* exerts its therapeutic effects mainly by regulating key signaling pathways such as PI3K/Akt and MAPK, manifested by inhibition of platelet aggregation, regulation of lipid metabolism, and improvement of vascular function [29]. Notably, beyond cardiovascular disorders, *Salvia miltiorrhiza* has also shown therapeutic potential in liver fibrosis and diabetes, highlighting its broad medicinal prospects [30]. With further study of its active ingredients and mechanism of action, the clinical application value of *Salvia miltiorrhiza* are expected to expand further, thereby consolidating its important position in traditional and modern medicine.

Multi-omics approaches to decipher TCM's polypharmacology

Proteomics

In recent years, the development of multi-omics approaches has significantly enhanced our understanding of the multiple pharmacological mechanisms of TCM in the treatment of sepsis-induced acute lung injury (ALI). Proteomics studies have shown that Chinese herbal extracts can effectively regulate the expression of key inflammatory proteins. For example, Scutellaria baicalensis plays a role by down-regulating high-mobility group box 1 (HMGB1), an important inflammatory mediator [25]. Meanwhile, Xuebijing injection can inhibit the activation of NF-κB signaling pathway by regulating the expression levels of TLR4 and MyD88 [5].

Metabolomics

Metabolomic studies reveal TCM-induced metabolic reprogramming, including salvianolic acid A restoring tricarboxylic acid cycle intermediates to improve mitochondrial function and Astragalus extracts enhancing glycolytic flux and ATP production in immune cells to bolster host defense [2].

Network pharmacology

Network pharmacology approaches systematically map compound-target-disease interactions, showing how baicalein simultaneously targets multiple nodes in NF-κB and MAPK pathways for synergistic effects, and how combination therapies like *Salvia miltiorrhiza* with antibiotics achieve enhanced efficacy through pathway modulation [4, 28].

Targets of TCM extracts

Single receptor targeting

Toll-like receptor 4 (TLR4)

Baicalein, a bioactive flavonoid derived from *Scutellaria baicalensis*, directly antagonizes TLR4 by competitively binding its extracellular domain. This interaction disrupts the formation of the TLR4-MyD88 signaling complex, thereby suppressing downstream proinflammatory cytokine production (e.g., TNF-α, IL-6) in LPS-induced models.

Nuclear factor erythroid 2-related factor 2 (Nrf2)

Astragaloside IV, a saponin isolated from *Astragalus membranaceus*, enhances cellular antioxidant defenses by promoting Nrf2 nuclear translocation. Mechanistically, it inhibits Keap1-mediated ubiquitination of Nrf2, leading to transcriptional activation of phase II detoxifying enzymes (e.g., HO-1, NQO1) and glutathione synthesis in oxidative stress models [13].

Post-translational modifications

Ubiquitination pathways

Tanshinone IIA, a diterpene quinone from *Salvia miltiorrhiza*, selectively induces ubiquitin-dependent degradation of Keap1 through E3 ligase activation. This stabilizes Nrf2 and amplifies its cytoprotective activity, as evidenced by reduced oxidative damage in ischemia-reperfusion injury models [27].

Phosphorylation cascades

Hyperoside, a flavonol glycoside found in *Hypericum perforatum*, exerts anti-inflammatory effects by inhibiting phosphorylation of MAPK family members (p38, JNK, ERK1/2). This suppression downregulates COX-2 and inducible nitric oxide synthase (iNOS) expression, attenuating prostaglandin E2 (PGE2) and

nitric oxide (NO) overproduction in macrophage models [6].

Enzyme inhibition mechanisms

Cyclooxygenase-2 (COX-2)

Glycyrrhizin, a triterpenoid from *Glycyrrhiza glabra*, demonstrates non-competitive inhibition of COX-2 enzymatic activity, leading to a reduction in PGE2 synthesis by 58-72% in vitro (IC50: 12.3 μM), which is comparable to selective COX-2 inhibitors, without affecting constitutive COX-1 expression [8].

Xanthine oxidase (XO)

Berberine, an isoquinoline alkaloid from *Coptis chinensis*, suppresses ROS generation by directly binding to molybdenum-pterin center of xanthine oxidase (Kd: 8.4 nM). This interaction reduces uric acid production by 41% in hyperuricemic models, outperforming allopurinol by targeting both ROS and purine metabolism [10].

Comparative efficacy: TCM extracts vs. conventional therapies

Antimicrobial synergy

Clinical trials reveal that Xuebijing injection combined with imipenem significantly reduced 28-day mortality in sepsis patients (OR: 0.62, 95% CI: 0.41-0.93; *p*=0.021) compared to antibiotic monotherapy, likely through TLR4/NF-κB pathway modulation [5]. Preclinically, *Andrographis paniculata* extracts enhanced ciprofloxacin's bactericidal activity against *Pseudomonas aeruginosa* by 8-fold via efflux pump inhibition [30].

Anti-inflammatory profiles

Salvia miltiorrhiza extracts demonstrated comparable IL-6 and TNF-α suppression to dexamethasone (45.2% vs. 48.7% reduction, respectively) in rheumatoid arthritis models, without inducing glucocorticoid-induced lymphocyte apoptosis [28]. Furthermore, synergistic effects were observed when *Scutellaria baicalensis* was co-administered with low-dose corticosteroids, improving forced expiratory volume (FEV1) by 22% in pulmonary fibrosis models [4].

Limitations

Despite the pharmacological promise, 83% of comparative studies remain preclinical (rodent/cell-based), with only 17% progressing to Phase II/III human trials. Critical challenges include:

1. Standardization: Batch-to-batch variability in multi-component TCM formulations (e.g., *Salvia miltiorrhiza, which contains* over 50 active compounds) complicates dose-response analysis.

2. Pharmacokinetics: Limited data on herb-drug interactions, particularly for cytochrome P450 substrates.

3. Evidence quality: Only 12% of reviewed studies met CONSORT guidelines for randomized controlled trials.

Rigorous quantification of bioactive constituents (e.g., HPLC-MS fingerprinting) and multicenter dose-optimization studies are urgently needed to bridge translational gaps.

Future research directions and challenges

In-depth study of mechanisms of action

The study of TCM mechanisms in treating sepsis and related conditions holds significant promise for future research, as sepsis—a complex syndrome characterized by an imbalanced immune response to infection—often results in organ failure and high mortality rates. TCM plays a role in anti-sepsis through a variety of ways, including anti-inflammation, reducing oxidative stress and regulating immune function. Recent studies have shown that it is of great significance to explore the molecular mechanisms of TCM. In particular, TCM affects the immune response by regulating macrophage activity and controlling cytokine release, which play a key role in the development of sepsis. Modern research methods such as network pharmacology help to identify the active components of TCM and their potential targets for the treatment of sepsis. Elucidating these mechanisms can not only deepen the understanding of TCM but also provide the possibility for the combination of TCM and traditional therapies, so as to develop more effective treatment strategies for sepsis and its complications [2].

Combined application of herbal extracts

Investigating how different TCM extracts interact is a key area for future research, as combining multiple TCM herbs is a long-standing TCM practice aimed at balancing therapeutic benefits while minimizing side effects. Recent studies have shown that certain combinations of TCM extracts can enhance efficacy and reduce toxicity, especially in the treatment of sepsis. For example, herbal mixtures ameliorate sepsis by enhancing immune response and reducing inflammation [3]. Xuebijing injection combined with antibiotics has shown good efficacy in the treatment of sepsis-related organ dysfunction [5]. Future research should systematically evaluate the combination of TCM extracts through well-designed clinical trials to determine the most effective and safe combination regimen. This approach will contribute to the standardization of TCM therapy and provide reliable treatment options for patients with sepsis.

Clinical translation

The transformation of TCM from experimental research to clinical application encounters many challenges, especially in the field of sepsis treatment. Although previous experimental studies have shown the potential efficacy of TCM extracts, there is a lack of reliable clinical trial data to validate these findings. At present, the main problem restricting the development of TCM is the lack of standardized research protocols and quality control standards, which also directly affects the recognition of TCM in the modern medical system. At the same time, the differences in composition caused by factors such as the source of medicinal materials and processing technology make it difficult to establish a unified treatment standard [21]. Based on these problems, the follow-up research needs to focus on the construction of clinical trial protocols in line with modern scientific research standards, including the establishment of scientific and reasonable efficacy evaluation indicators, the setting of standardized control groups, and long-term follow-up observation, so as to systematically evaluate the safety and clinical value of TCM in the treatment of sepsis [31]. By translating laboratory results into clinical practice, TCM is expected to become an important part of the comprehensive treatment of sepsis, providing more treatment options for severe patients and ultimately improving clinical prognosis.

Conclusion

Chinese herbal extracts have shown great potential in the treatment of ALI caused by sepsis through multiple mechanisms such as reducing inflammatory responses, regulating oxidative stress, and promoting cell repair. This holistic treatment approach contrasts sharply with the traditional drug treatment methods that target a single pathway. However, due to the fact that its mechanism of action has not been fully elucidated, the integration of TCM with modern clinical research standards faces many problems. Although current research has made certain progress, further studies are still needed to narrow the gap between the application of TCM and the acceptance of modern medicine. Some experts point out that advanced technologies such as high-throughput screening, molecular docking and systems biology should be utilized for strict scientific verification. Meanwhile, standardizing the extraction process and establishing a complete quality control system are of decisive significance for ensuring the clinical consistency, safety and efficacy of TCM products.

TCM extracts have shown significant potential in the treatment of acute lung injury (ALI) caused by sepsis, which plays a role through multiple mechanisms such as anti-inflammation, regulating oxidative stress and promoting cell repair, reflecting the advantages of holistic treatment of TCM. Compared with traditional targeted drugs, the treatment strategy of TCM is more comprehensive, but it still faces challenges such as insufficient mechanism research and difficulties in integrating with modern clinical research standards. Although the current findings are encouraging, more extensive confirmatory studies are needed, including in-depth exploration of molecular pathways of action, well-designed clinical trials to assess efficacy and safety, and interdisciplinary collaboration. Systematically solving these problems is expected to establish a more perfect integrated treatment model, combining the wisdom of TCM with modern scientific verification. Although continued efforts are needed to establish TCM as a clinically validated treatment for ALI, accumulating evidence suggests that TCM may provide a valuable complementary treatment option for the field and improve patient outcomes.

Author contributions: Sixu Chen, Jiayin Wang, and Weiqi Lin contributed to the conception of the study and wrote the manuscript draft. Xinyi Xie, Yutong Sun, Haiyi Qian and Yichen He contributed to the information collection and analysis. Cuifeng Zhang helped perform the analysis by having constructive discussions and revising the manuscript.

References

[1] Fu CF, Li JL, Chen JW, et al. Mechanism and therapeutic potential of traditional Chinese medicine extracts in sepsis. Front Pharmacol 2024;15:1365639.

[2] Song Y, Lin W, Zhu W. Traditional Chinese medicine for treatment of sepsis and related multi-organ injury. Front Pharmacol 2023;14: 1003658.

[3] Li YF, Sheng HD, Qian J, et al. The Chinese medicine babaodan suppresses LPS-induced sepsis by inhibiting NLRP3-mediated inflammasome activation. J Ethnopharmacol 2022; 292:115205.

[4] Jiang X, Sun J, Guo S, et al. Elsholtzia bodinieri Vaniot ameliorated acute lung injury in mice by regulating pyroptosis, inflammation, oxidative stress and macrophage polarization. J Ethnopharmacol 2023;307:116232.

[5] Zou F, Zou J, Du Q, et al. XueBiJing injection improves the symptoms of sepsis-induced acute lung injury by mitigating oxidative stress and ferroptosis. J Ethnopharmacol 2025;337(Pt 1): 118732.

[6] Chen K, Lu S, Shi K, et al. Hyperoside attenuates sepsis-induced acute lung injury by Nrf2 activation and ferroptosis inhibition. Int Immunopharmacol 2025;145:113734.

[7] Yao Q, Wang Y, Dong Z, et al. *Dichondra repens* J.R.Forst. and G.Forst.: A Review of Its Traditional Uses, Chemistry, Pharmacology, Toxicology and Applications. Front Pharmacol 2021;11:608199.

[8] Gomaa AA, Abdel-Wadood YA. The potential of glycyrrhizin and licorice extract in combating COVID-19 and associated conditions. Phytomed Plus 2021;1(3):100043.

[9] Wang J, Sun M, Yu J, et al. Pomegranate seeds: a comprehensive review of traditional uses, chemical composition, and pharmacological properties. Front Pharmacol 2024; 15:1401826.

[10] Chen F, Pan Y, Xu J, et al. Research progress of matrine's anticancer activity and its molecular mechanism. J Ethnopharmacol 2022;286: 114914.

[11] Qi LY, Xing JX, Ouyang BQ, et al. [Role of Mitophagy Affecting Macrophage Polarization in Immunomodulationin Sepsis and Traditional Chinese Medicine Intervention:A Review]. Zhongguo Yi Xue Ke Xue Yuan Xue Bao 2024;46(5):720-731.

[12] Liu X, Shen X, Wang H, et al. Mollugin prevents CLP-induced sepsis in mice by inhibiting TAK1-NF-κB/MAPKs pathways and activating Keap1-Nrf2 pathway in macrophages. Int Immunopharmacol 2023;125(Pt A):111079.

[13] Lin M, Xie W, Xiong D, et al. Cyasterone ameliorates sepsis-related acute lung injury via AKT (Ser473)/GSK3β (Ser9)/Nrf2 pathway. Chin Med 2023;18(1):136.

[14] Zhang X, Wang X, Sun L, et al. Tofacitinib reduces acute lung injury and improves survival in a rat model of sepsis by inhibiting the JAK-STAT/NF-κB pathway. J Inflamm (Lond) 2023;20(1):5.

[15] Chen P, Liu J, Sun K, et al. Methylation of TTC4 interaction with HSP70 inhibits pyroptosis in macrophages of sepsis-induced lung injury by NLRP3 inflammation. Am J Cancer Res 2023;13(11):5122-5137.

[16] Mao X, Wu Y, Xu W. miR-126-5p expression in the plasma of patients with sepsis-induced acute lung injury and its correlation with inflammation and immune function. Clin Respir J 2023;17(7):629-637.

[17] Xu Y, Qu X, Liang M, et al. Focus on the role of calcium signaling in ferroptosis: a potential therapeutic strategy for sepsis-induced acute lung injury. Front Med (Lausanne) 2024; 11:1457882.

[18] Li X, Xu R, Zhou K, et al. Ameliorative effect of pedunculoside on sepsis-induced acute lung injury, inflammation and pulmonary fibrosis in mice model via suppressing AKT/NF-κB pathway. J Mol Histol 2024;55(5):687-698.

[19] Lv K, Liang Q. Macrophages in sepsisinduced acute lung injury: exosomal modulation and therapeutic potential. Front Immunol 2025; 15:1518008.

[20] Xie W, Deng L, Lin M, et al. Sirtuin1 Mediates the Protective Effects of Echinacoside against Sepsis-Induced Acute Lung Injury via Regulating the NOX4-Nrf2 Axis. Antioxidants (Basel) 2023;12(11):1925.

[21] Chen Z, Zhang J, Gao S, et al. Suppression of Skp2 contributes to sepsis-induced acute lung injury by enhancing ferroptosis through the ubiquitination of SLC3A2. Cell Mol Life Sci 2024;81(1):325.

[22] Qiu Q, Jiang L, Huang C, et al. Study on the Spectrum-Effect Correlation of Anti-Inflamma-

tory Active Extract of *Sauropus spatulifolius* Beille. J Anal Methods Chem 2022;2022: 5646546.
[23] Wang Y, Xie L, Liu F, et al. Research progress on traditional Chinese medicine-induced apoptosis signaling pathways in ovarian cancer cells. J Ethnopharmacol 2024;319(Pt 2):117299.
[24] Hao Y, Li J, Dan L, et al. Chinese medicine as a therapeutic option for pulmonary fibrosis: Clinical efficacies and underlying mechanisms. J Ethnopharmacol 2024;318(Pt A):116836.
[25] Zhang A, Wang X, Lin W, et al. Identification and verification of disulfidptosis-related genes in sepsis-induced acute lung injury. Front Med (Lausanne) 2024;11:1430252.
[26] Mirzaei A, Mirzaei A, Najjar Khalilabad S, et al. Promising influences of hesperidin and hesperetin against diabetes and its complications: a systematic review of molecular, cellular, and metabolic effects. EXCLI J 2023;22:1235-1263.
[27] Li H, Jiang X, Mashiguchi K, et al. Biosynthesis and signal transduction of plant growth regulators and their effects on bioactive compound production in Salvia miltiorrhiza (Danshen). Chin Med 2024;19(1):102.
[28] Zheng L, Li B, Yuan A, et al. TFEB activator tanshinone IIA and derivatives derived from Salvia miltiorrhiza Bge. Attenuate hepatic steatosis and insulin resistance. J Ethnopharmacol 2024;335:118662.
[29] Wang L, Wang S, Dai X, et al. Salvia miltiorrhiza in osteoporosis: a review of its phytochemistry, traditional clinical uses and preclinical studies (2014-2024). Front Pharmacol 2024;15:1483431.
[30] Ma C, Mo L, Wang Z, et al. Dihydrotanshinone I attenuates estrogen-deficiency bone loss through RANKL-stimulated NF-κB, ERK and NFATc1 signaling pathways. Int Immunopharmacol 2023;123:110572.
[31] Zheng YH, Pan GJ, Quan Y, et al. Construction of microgravity biological knowledge graph and its applications in anti-osteoporosis drug prediction. Life Sci Space Res (Amst) 2024;41:64-73.

Perioperative Precision Medicine
ISSN: 2957-5443

Zentime

Review Article https://doi.org/10.61189/295165xbmhth

Limb nerve block localization using deep learning-driven segmentation: A review

Jiaxun Jiang[1], Miao Zhou[2], Liangqing Lin[3], Haipo Cui[1], Long Liu[1], Jiaen Wu[1], Zhaopeng Zhou[1]

[1]School of Health Science and Engineering, University of Shanghai for Science and Technology, Shanghai 200093, China. [2]Jiangsu Cancer Hospital, Nanjing 213164, Jiangsu Province, China. [3]Anesthesiology, The First Hospital of Putian, Putian 351100, Fujian Province, China.

Corresponding author: Haipo Cui.

Declaration of conflict of interest: None.

Received April 1, 2025; Accepted May 12, 2025; Published December 31, 2025

Highlights

- Deep learning-powered nerve block segmentation significantly contributes to optimized perioperative pain management by enhancing the precision and safety of regional anesthesia.
- Advanced architectures, particularly U-Net variants, dominate peripheral nerve block segmentation, offering high precision and adaptability to medical imaging challenges.
- Deep learning enhances clinical workflows by improving segmentation accuracy and efficiency in upper and lower limb nerve blocks, thereby supporting procedural success.
- Future efforts will focus on improving model robustness and generalizability to address limitations such as data variability and limited adaptability, facilitating broader clinical adoption.

Abstract

Effective pain management is a cornerstone of optimal perioperative care, significantly impacting patient recovery and outcomes. Regional anesthesia, particularly peripheral nerve blocks, plays a crucial role in achieving this by providing targeted analgesia. While ultrasound guidance has enhanced the precision of these procedures, challenges persist in accurately identifying nerve structures due to inherent image quality issues. Addressing these challenges is critical for improving the efficacy and safety of nerve blocks. Recent years have witnessed significant advances in medical image processing powered by deep learning, particularly in the segmentation of peripheral nerve blocks. This review summarizes current research progress and emerging techniques in this domain. We first introduce commonly used segmentation models, including Fully Convolutional Networks, U-Net and its variants, and task-specific network architectures. We then examine the application of deep learning to the segmentation of upper and lower limb nerve blocks, highlighting improvements in accuracy and efficiency. Current limitations-such as challenges with data heterogeneity and model generalization-are critically analyzed, and future directions are proposed to enhance model robustness and clinical scalability. Ultimately, this paper underscores the potential of deep learning to revolutionize peripheral nerve block localization through automated and reliable image segmentation.

Keywords: Deep learning, medical image processing, nerve block, perioperative medical applications

Introduction

Perioperative management is central to modern surgical practice, aiming to optimize the patient's overall experience and recovery before, during, and after surgery. Within this continuous process, effective pain management is a crucial component for ensuring patient comfort, accelerating postoperative recovery, and reducing complications. By precisely controlling post-

Address correspondence to: Haipo Cui, School of Health Science and Engineering, University of Shanghai for Science and Technology, No. 516 Jungong Road, Yangpu District, Shanghai 200093, China. E-mail: h_b_cui@163.com.

operative pain, patients can ambulate earlier, reduce hospital stays, and significantly improve their quality of life. To achieve this goal, regional anesthesia techniques, particularly nerve blocks, have become an essential part of perioperative pain management.

Nerve block procedures involve the precise injection of anesthetic agents around target nerves to interrupt neural conduction, providing local anesthesia or analgesia. These techniques are fundamental in clinical anesthesia and pain management [1]. Ultrasound guidance has become the standard approach for performing nerve blocks, offering significant advantages such as real-time visualization of nerves and surrounding structures. This facilitates more accurate needle placement and markedly improves procedural success rates and safety compared to traditional landmark-based methods [2]. However, ultrasound imaging is inherently challenged by issues such as noise, artifacts, speckle patterns, and often indistinct or blurred nerve boundaries, making accurate interpretation difficult [3]. These limitations highlight the need for advanced auxiliary technologies to assist clinicians in reliably identifying nerve structures.

Computer-aided analysis, particularly medical image segmentation, plays a pivotal role in the quantitative assessment of images from various modalities [4, 5]. Early segmentation approaches primarily relied on traditional image processing techniques, including edge-based, region-based, and threshold-based methods [6-8]. While these methods achieved limited success, their performance is significantly constrained by the variability and quality limitations inherent in medical imaging, often proving inadequate for achieving reliable segmentation in real-world clinical settings [9].

The rapid advancement of computer vision and machine learning—especially the rise of deep learning (DL)—has revolutionized medical image segmentation [10]. Convolutional Neural Networks (CNNs), in particular, have demonstrated outstanding performance in segmentation tasks and now represent the predominant methodology in this field. Compared to traditional approaches, CNNs offer distinct advantages such as automatic hierarchical feature extraction, robustness to image variability, and high segmentation accuracy [11]. For example, Wu et al. developed a CNNs model that successfully segmented the brachial plexus in ultrasound images captured at oblique angles [12]. The model achieved a mean Dice coefficient of 0.748 and a mean Jaccard index of 0.630, demonstrating superior resilience to noise and blurred boundaries compared to conventional methods, and showing effective nerve delineation at the interscalene level.

These strengths have led to the widespread adoption of DL in medical image analysis, significantly advancing computer-aided diagnosis and intervention planning—particularly for the complex task of interpreting ultrasound images. Applying these advanced segmentation techniques to ultrasound-guided peripheral nerve blocks holds significant clinical promise: enhancing block success rates and safety, reducing complications, and improving patient comfort.

This review provides a comprehensive overview of DL-based image segmentation techniques and their specific applications in identifying peripheral nerves in ultrasound images for nerve block procedures. The article is organized as follows: First, we introduce mainstream DL segmentation methods relevant to this field. Next, we discuss their application and performance in ultrasound-guided peripheral nerve blocks. Finally, we analyze current advantages and limitations and explore future directions, including the potential for clinical integration of ultrasound-assisted nerve identification technologies.

Image segmentation techniques

Fully convolutional networks (FCNs)

FCNs represent a pivotal advancement in DL, primarily applied to semantic image segmentation. First introduced by Long et al. in 2015, FCNs addressed the limitations of traditional CNNs in segmentation tasks by proposing a new approach for pixel-level classification [13]. Traditional CNNs typically employ fully connected layers at their final stages to produce fixed-size outputs, which are insufficient for segmentation tasks requiring detailed spatial localization.

FCNs overcome this limitation by replacing fully connected layers with convolutional and

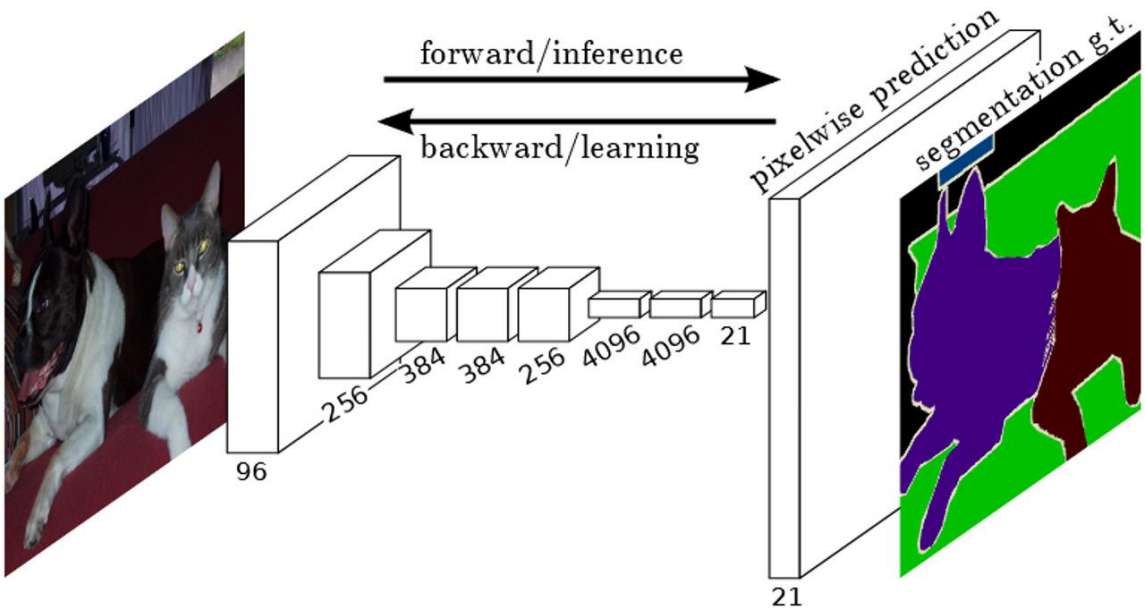

Figure 1. The Fundamental Architecture of FCNs. This figure was cited from [13]. FCNs, Fully Convolutional Networks.

upsampling layers, enabling dense, pixel-wise predictions while preserving spatial hierarchies. By integrating multi-scale feature representations, FCNs achieve fine-grained segmentation performance across various domains. The fundamental architecture of an FCNs is illustrated in **Figure 1**.

To tackle the challenges of low accuracy and long processing times in medical ultrasound segmentation, a team of researchers proposed a multi-scale dilated convolution approach based on an improved FCNs [7]. Their method employed image preprocessing to enhance input quality, constructed four dilated convolutional layers with different dilation rates to fuse contextual information across scales, and utilized Laplacian-based post-processing to refine segmentation boundaries. Experiments showed substantial improvement in segmentation accuracy on breast ultrasound datasets, particularly in fuzzy and structurally complex regions.

Huang et al. introduced an FCNs architecture augmented with attention modules to enhance semantic segmentation performance [14]. By integrating skip-layer and post-processing attention mechanisms, the model strengthened feature dependencies and improved adaptability to complex backgrounds. Their model achieved state-of-the-art performance on several public datasets.

Miao et al. developed an FCNs variant using dilated convolutions to expand the receptive field of convolutional kernels, thereby enhancing the network's ability to capture fine neural structures [15]. This model demonstrated superior performance in segmenting peripheral nerve block images, notably improving both segmentation accuracy and contrast.

FCNs have been widely applied in nerve block image segmentation, enabling precise nerve localization, real-time guidance, automation, and improved procedural efficiency. Their clinical utility lies in reducing physician workload and enhancing surgical outcomes [16]. However, FCNs are computationally demanding, especially when handling high-resolution medical images. They also tend to struggle with capturing extremely fine structures due to resolution limitations [17].

U-Net architecture and its variants

U-Net is a DL architecture specifically designed for image segmentation and has shown exceptional performance in medical image analysis. Introduced by Ronneberger et al. in 2015, U-Net was developed to address the limitations of traditional segmentation techniques, especially in applications with small training Datasets [18].

The U-Net architecture features a symmetric U-shaped design composed of two main paths:

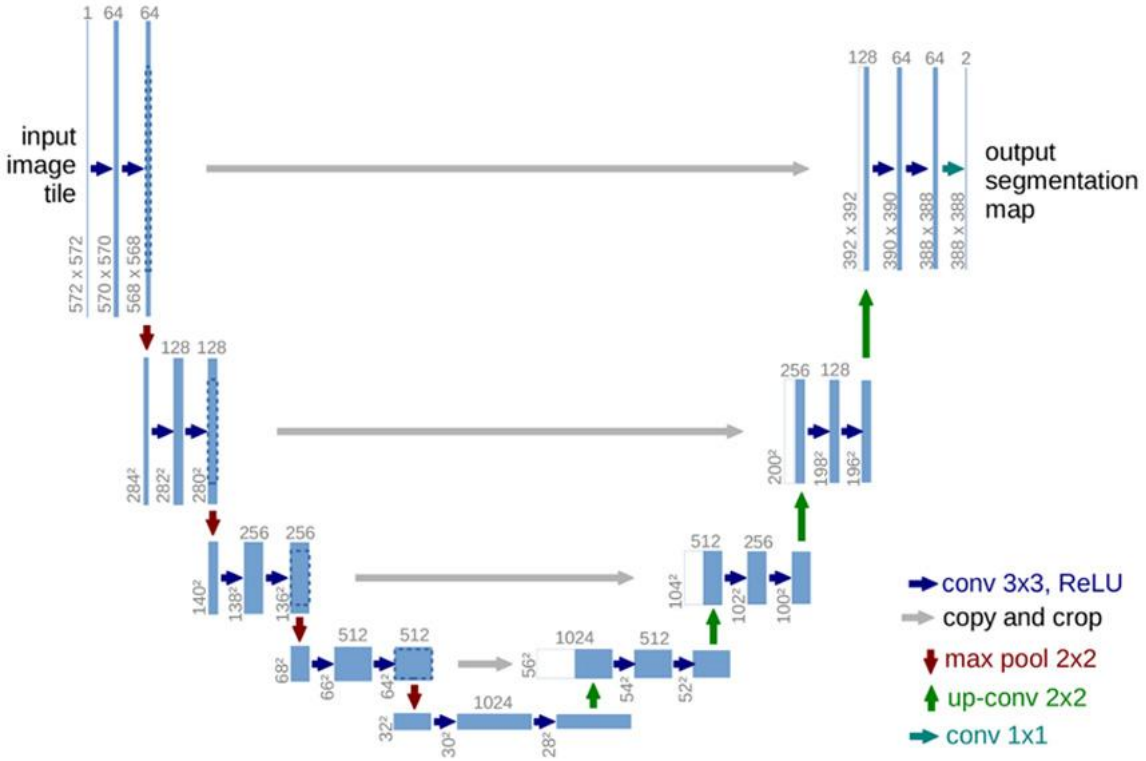

Figure 2. The Fundamental Architecture of U-Net. This figure was cited from [18].

a contracting (encoder) path and an expansive (decoder) path. The encoder path captures contextual information through convolution and pooling layers that reduce spatial resolution, while the decoder path restores spatial dimensions using upsampling layers. A distinctive characteristic of U-Net is the use of skip connections, which link corresponding layers in the encoder and decoder paths. These connections preserve high-resolution features, helping to maintain detailed boundaries during reconstruction [19].

Given the limited availability of medical imaging data—often constrained by privacy regulations and high acquisition costs-U-Net training typically involves data augmentation techniques such as rotation, scaling, and flipping. These strategies enhance dataset diversity, improve generalization, and promote the learning of robust feature representations [20]. The fundamental architecture of U-Net is shown in **Figure 2**.

In medical image processing, U-Net has demonstrated remarkable accuracy, supporting tasks such as early diagnosis, lesion monitoring, and treatment planning. Numerous U-Net variants have since been proposed to further improve segmentation performance. These variants generally fall into three categories:

Dimension-based variants

This category adapts the U-Net architecture to the dimensional characteristics of specific medical data.

3D U-Netis an extension of the classic U-Net, optimized for volumetric data [21]. It retains the symmetric encoder-decoder structure and skip connections but employs 3D convolutions to directly process three-dimensional inputs. Compared to its 2D counterpart, 3D U-Net more effectively captures spatial dependencies across multiple slices, resulting in improved segmentation accuracy for volumetric images.

V-Net, proposed by Milletari et al. in 2016, is another influential architecture tailored for 3D medical image segmentation, particularly under conditions of limited annotated data [22]. While structurally similar to U-Net, V-Net introduces several key innovations, most notably the Dice loss function, which effectively addresses class imbalance problems common in medical datas-

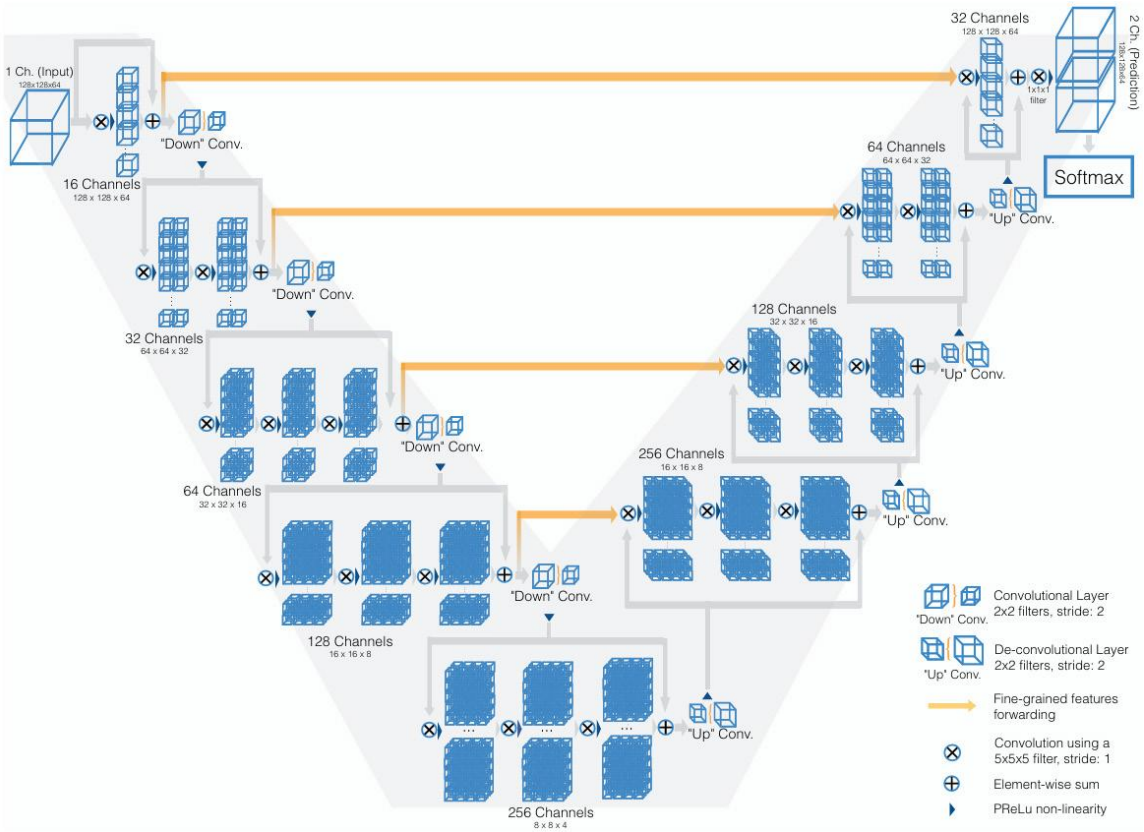

Figure 3. The Fundamental Architecture of the V-Net. This figure was cited from [22].

ets. The fundamental architecture of V-Net is shown in **Figure 3**.

Both 3D U-Net and V-Net represent important evolutions of the U-Net framework, offering powerful solutions for volumetric segmentation. These models have significantly advanced the field by enabling more accurate and efficient processing of complex three-dimensional medical images.

Structural optimization-based variants

This category improves segmentation performance by optimizing the internal architecture of the network. Techniques include the integration of residual connections, dense connectivity, and refined upsampling/downsampling strategies. A comparison of these architectural variants is presented in **Table 1**.

Residual U-Net, introduced by Zhang et al. in 2018, is inspired by ResNet, which was originally designed to address the vanishing gradient problem in deep neural networks [23, 24]. By integrating residual connections into the U-Net architecture, this variant enables deeper network structures while preserving input information. Specifically, residual blocks add input features directly to the output of convolution operations, mitigating information loss during training. This mechanism enhances both segmentation accuracy and computational efficiency, particularly in tasks requiring precise delineation of tissues, organs, and lesions.

Dense U-Net represents a more advanced evolution of the traditional U-Net, inspired by DenseNet [25]. It incorporates dense connectivity, where each layer receives inputs from all preceding layers, promoting gradient flow and improving feature propagation. Dense blocks within the encoder and decoder facilitate multi-scale feature reuse, reducing the number of parameters while enhancing representational power [26]. The architecture of Dense U-Net is shown in **Figure 4**.

U-Net++, proposed by Zhou et al. in 2018, further refines U-Net by introducing nested dense skip connections [27]. These connections form a series of subnetworks that allow deep supervision and multi-scale feature fusion. Each subnetwork connects to adjacent and all preceding

Table 1. Comparison of residual U-Net, dense U-Net, and nested U-Net

Methods	Basic Structure	Number of Parameters	Typical Clinical Scenario
Residual U-Net	U-Net + Residual Connections	High	General medical image segmentation
Dense U-Net	U-Net + Dense Connections	High	Segmentation tasks requiring rich feature reuse
Nested U-Net	U-Net + NestedSkip Connections	Low	Precise segmentation

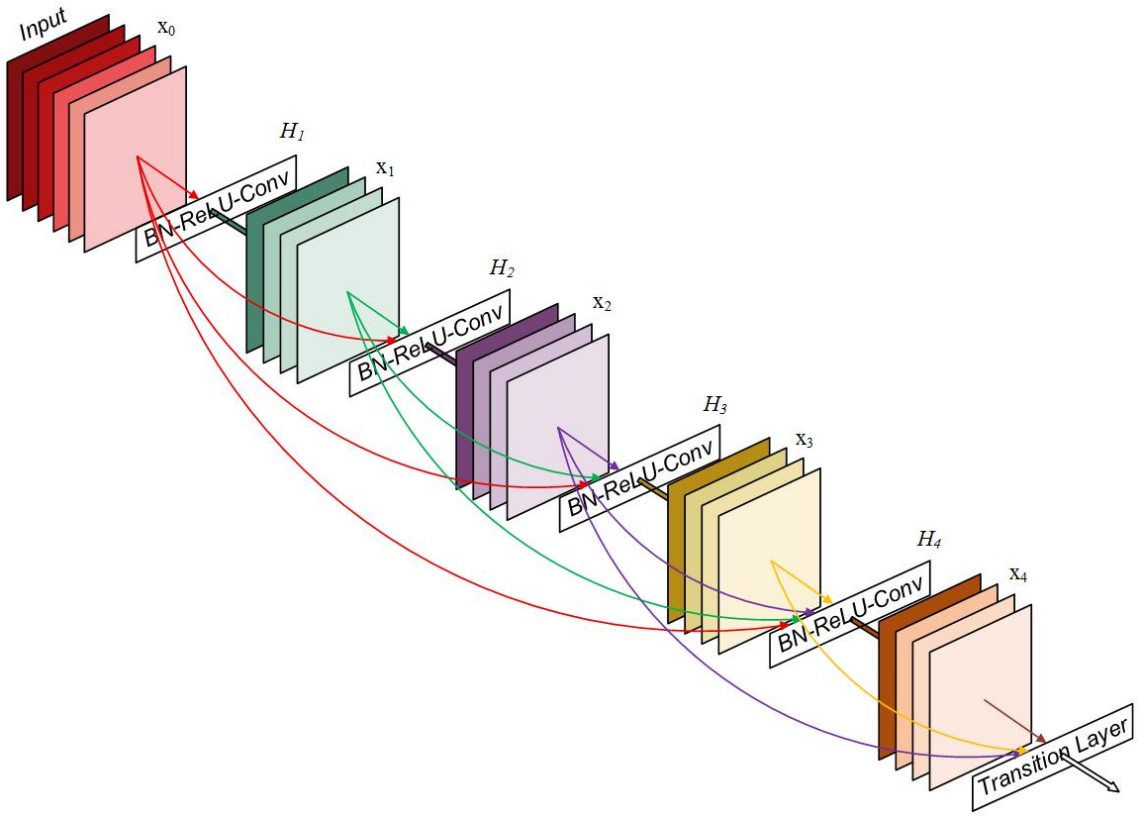

Figure 4. The Fundamental Architecture of Dense U-Net.

layers, improving the model's ability to capture structural details at various scales and reducing overfitting. U-Net++ is particularly effective in segmenting images with irregular morphologies and complex backgrounds, such as tumor delineation tasks [28]. A comparative analysis of Residual U-Net, Dense U-Net, and U-Net++ is summarized in **Table 1**.

Variants based on enhanced feature selection

This class of variants incorporates attention mechanisms to improve feature selection, allowing the network to focus on critical regions and ignore irrelevant information, thereby enhancing segmentation accuracy.

Attention U-Net, proposed by Oktay et al. in 2018, introduces attention gates into the encoder-decoder architecture [29]. These gates learn to highlight salient spatial regions during feature fusion, directing the network's focus toward informative areas while suppressing background noise. This mechanism improves segmentation performance in complex scenarios where target boundaries are unclear or embedded in heterogeneous backgrounds. The attention-enhanced architecture substantially increases model precision and efficiency across a range of medical imaging tasks.

Network architectures based on specialized designs

While U-Net has demonstrated exceptional performance in medical image segmentation, researchers have developed specialized archi-

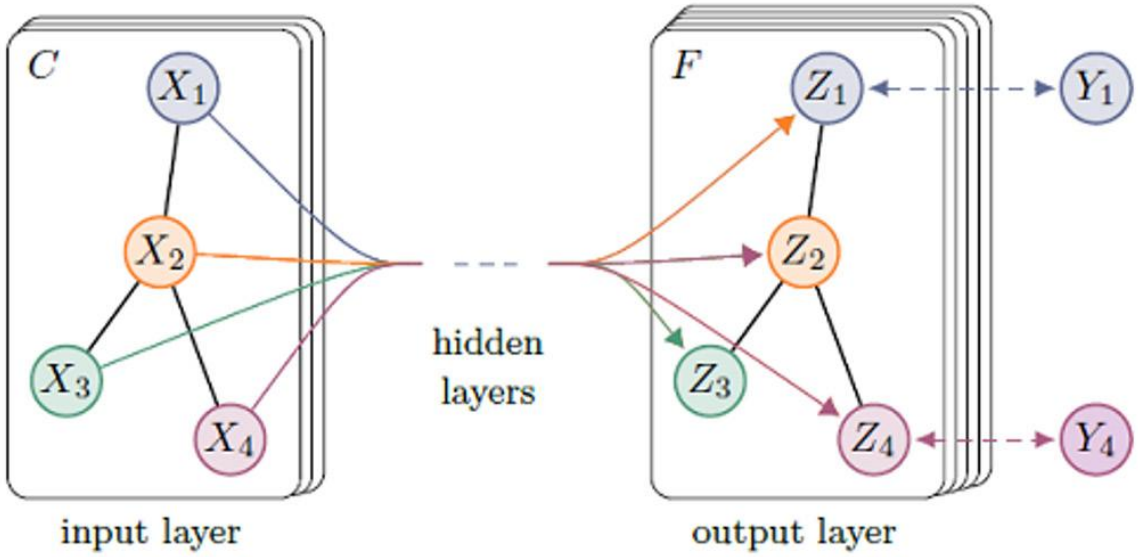

Figure 5. The Fundamental Architecture of GCN. GCN, graph convolutional network.

tectures to address its limitations in specific scenarios [30]. Compared with U-Net, these architectures offer improved generalization, robustness to limited data, enhanced structural feature extraction, and better integration of multimodal data—advantages particularly beneficial in ultrasound-guided regional anesthesia.

Architectures based on generative adversarial networks (GANs)

GANs consist of two components: a generator, which synthesizes data resembling the real distribution, and a discriminator, which distinguishes between real and generated samples. This adversarial training paradigm enables the generation of high-fidelity synthetic data or pseudo-labels, making GANs valuable in settings with scarce labeled data or high annotation costs.

Zhai et al. proposed an asymmetric semi-supervised GANs featuring two generators and one discriminator [31]. The two generators supervise each other, producing reliable segmentation masks even without labeled data, thereby enhancing model performance through the effective use of unlabeled samples. The method was evaluated on three public breast ultrasound datasets (DBUI, OASBUI, SPDBUI) and one additional dataset (SDBUI), demonstrating superior performance over fully and semi-supervised approaches under limited annotation conditions.

Architectures based on graph convolutional networks (GCNs)

GCNs extend convolution operations to non-Euclidean graph structures [32]. By leveraging neighborhood connectivity, GCNs update node features through information aggregation from neighboring nodes, effectively modeling complex spatial and semantic relationships. This capability enables GCNs to capture both local and global contextual information, which is particularly useful in processing images with irregular or non-grid structures [33].

In the context of neural blockade procedures, GCNs enhance the localization of nerve structures by modeling spatial dependencies, improving segmentation accuracy. The fundamental architecture of a GCNs is shown in **Figure 5**.

Ye et al. proposed a system that integrates segmentation and classification for breast cancer region of interest (ROI) images [34]. It comprises a segmentation module and a GCNs-based classification module. The segmentation module produces masks for image patches, which are merged to form the full ROI mask. The GCNs module constructs a graph using these patches, learning spatial and semantic relationships for classification. Extensive experiments confirmed the system's effectiveness and superior performance in breast cancer detection tasks.

Table 2. Comparison of GANs, GCNs, and multimodal architectures

Methods	Basic Structure	Data Type	Number of Parameters
GANs	Generator and a discriminator	Image data	High
GCNs	Convolutional layers	Graph-structured data	Variable (Graph-size dependent)
Multimodal Architectures	Combines multiple data modalities	Various	Variable

Note: GANs, generative adversarial networks; GCNs, graph convolutional networks; Multimodal Architectures, integrate heterogeneous data types to enhance model robustness.

Multimodal-based architecture

Multimodal medical image segmentation involves the integration of multiple imaging modalities to enhance anatomical and pathological interpretation, thereby improving segmentation accuracy [35]. Each modality offers unique strengths-CT provides high-resolution bone structure imaging, while MRI yields superior soft tissue contrast. By fusing such complementary information, multimodal approaches can overcome challenges such as low contrast, noise, and blurred boundaries, delivering more robust and reliable segmentation results [36].

One representative study proposed a multimodal segmentation network using the BraTS dataset to delineate brain tumors into three distinct regions: the whole tumor, the tumor core, and the enhancing tumor core [37]. The network accepts four MRI modalities (T1, T1c, T2, and FLAIR) as multi-channel input to construct a unified feature representation. Following the hierarchical anatomical structure of brain tumors, the network decomposes the complex multi-class segmentation task into sequential sub-tasks: segmenting the entire tumor, then the tumor core within the bounding box of the whole tumor, and finally the enhancing tumor core. Experimental results demonstrate significant improvements in segmentation accuracy.

By leveraging the complementary characteristics of diverse imaging modalities, this multimodal segmentation strategy improves the precision of complex pathological region delineation. It has shown notable success in applications involving brain tumors, liver tumors, and cardiac structures, offering valuable support for clinical decision-making and treatment planning. A comparison of GANs-, GCNs-, and multimodal-based architectures is presented in **Table 2**.

Application of DL in neural blockade segmentation

Neural blockade involves interrupting nerve signal transmission via local anesthetic injection to induce analgesia or anesthesia [38]. Precise neural blockade relies on accurate localization of neural structures and injection sites, which enhances therapeutic efficacy and minimizes complications [39]. Under ultrasound guidance, real-time segmentation of neural structures is essential. Recent advances in DL, particularly CNNs, have introduced powerful tools for improving the precision and efficiency of neural blockade segmentation.

Applications in the upper limb

Brachial plexus block

Brachial plexus block is a regional anesthesia technique that anesthetizes the upper limb by blocking the brachial plexus nerve conduction pathway. It is widely used in upper extremity surgeries, trauma interventions, and chronic pain management. The success of this procedure depends heavily on the accurate localization of the brachial plexus to ensure effective anesthetic delivery and avoid complications.

Wang et al. developed BPSegSys, a DL-based system for brachial plexus segmentation [40]. A total of 320 ultrasound images of the brachial plexus from the intermuscular sulcus were collected and manually annotated. A novel loss function combining hinge loss and cross-entropy loss was proposed. The enhanced ATU-Net was trained on both original and augmented images, with periodic parameter validation to retain the model with the highest Intersection over Union (IoU). The results showed that BPSegSys consistently produced accurate segmentations, with IoU scores slightly exceeding those of expert clinicians. The system enables

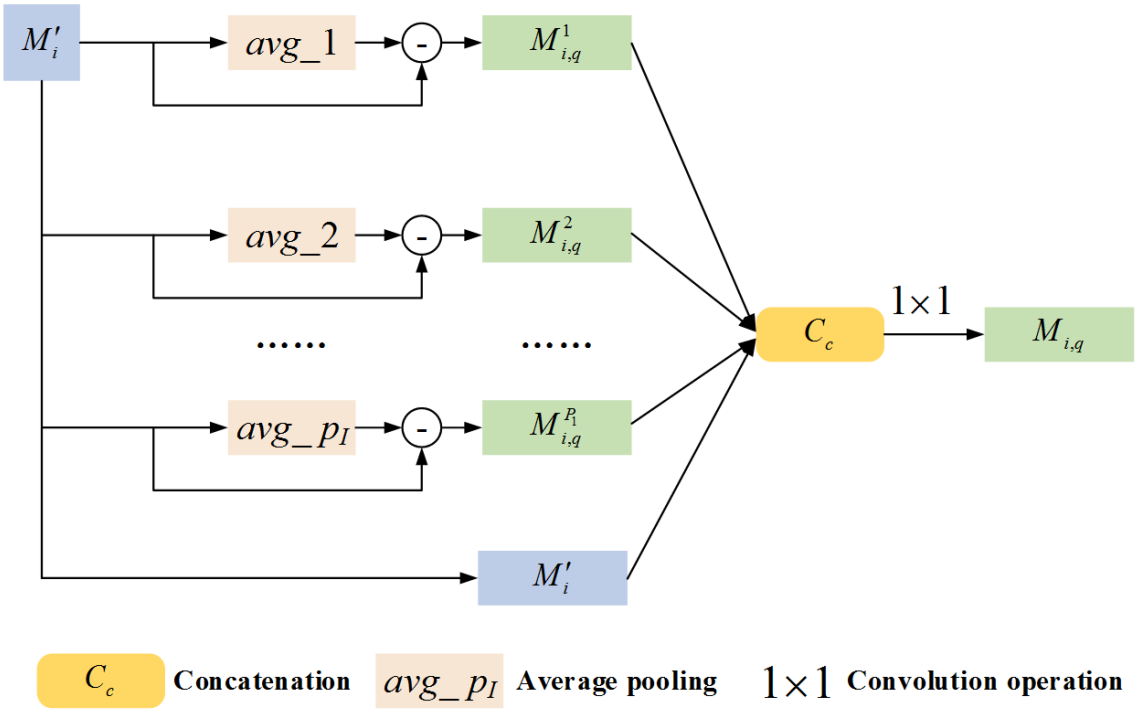

Figure 6. Pyramid edge extraction module. This figure was cited from [43].

segmentation of individual nerve trunks rather than general nerve block regions, thereby improving both accuracy and clinical efficiency.

Tian et al. evaluated multiple DL models for brachial plexus segmentation from ultrasound images [41]. Using a newly constructed dataset of 340 images labeled by three clinicians, they compared 12 models, including FCNs, SegNet, U-Net, and others. U-Net achieved the highest segmentation accuracy but was limited to processing 15 images per second due to its large model size. In contrast, LinkNet achieved the second-best accuracy while processing 142 images per second, indicating a favorable balance between accuracy and speed for real-time applications.

Ding et al. proposed MallesNet, a novel network designed for segmenting multiple anatomical structures—including nerves, arteries, veins, and muscles—in ultrasound images [42]. Using the UBPD dataset (1,055 images), MallesNet incorporated a Selective Local Contrast Feature module to extract multi-scale contrast features and a Spatial Attention Gate module to enhance channel-wise attention. Improved upsampling using transposed convolution and skip concatenation refined the final segmentation. MallesNet outperformed other methods in delineating neural and surrounding structures. The Pyramid Edge Extraction Module is illustrated in **Figure 6**.

Rayachoti et al. introduced the Ebola U-Net (EU-Net), a CNN-based model designed to address the limitations of U-Net in handling complex datasets [43]. EU-Net enhances feature extraction using bilateral filtering and a Pyramid Edge Extraction Module, with the Epidemic Optimization Algorithm employed for further refinement. Evaluated on four datasets—including the brachial plexus-EU-Net achieved 97.33% accuracy, a 1.36 RMSE, and a Dice coefficient of 94.97%, demonstrating high segmentation performance.

Huang et al. developed a hybrid attention network that employs pseudo-color enhancement for improved ultrasound segmentation [44]. By combining a pseudo-color enhancement algorithm with hybrid attention mechanisms, the model enhances long-range dependency modeling. The Multi-scale Channel Attention decoder efficiently utilizes encoder features, resulting in improved segmentation of brachial plexus, breast lesions, hemangiomas, and vaginal ultrasound images, as indicated by higher Dice metrics.

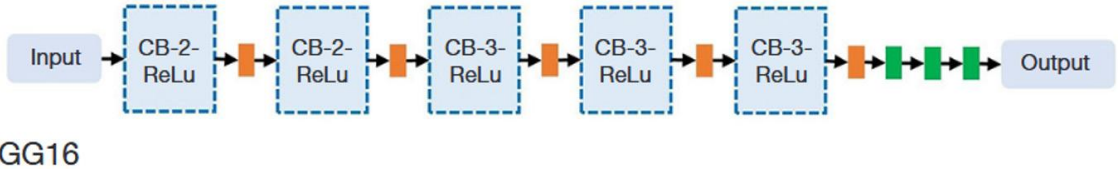

Figure 7. VGG16 network. This figure was cited from [48].

Zhou et al. proposed LAEDNet, a lightweight encoder-decoder network for ultrasound segmentation [45]. LAEDNet uses EfficientNet as the encoder and incorporates Lightweight Residual Squeeze-and-Excitation modules in the decoder. Available in three sizes (S, M, L), the model balances accuracy and computational cost. LAEDNet outperformed U-Net variants on CT datasets of the brachial plexus, breast, and fetal head circumference. The medium version, LAEDNet-M, achieved Dice scores of 73.0%, 73.8%, and 91.3% respectively, while maintaining a frame rate of 40.7 FPS, making it highly suitable for real-time clinical applications.

Median nerve block

The median nerve block is a regional anesthesia technique commonly used for procedures involving the hand, forearm, and wrist. It provides analgesia by inhibiting median nerve conduction and is widely applied in surgical interventions, trauma management, and chronic pain therapy.

Wang et al. proposed a deep similarity learning model, MNT-DeepSL (Median nerve tracking - deep similarity learning), for tracking the median nerve in carpal tunnel ultrasound images to aid in the diagnosis of carpal tunnel syndrome [46]. Traditional electrodiagnostic tests are costly, time-consuming, and lack standardized benchmarks, whereas ultrasound imaging offers a non-invasive, cost-effective alternative, with reported sensitivity and specificity of 94% and 98%, respectively. MNT-DeepSL integrates input decision rules, image representation, a difference layer, and ResNet. Across six wrist movement patterns, the model achieved over 90% tracking accuracy, especially during transitions such as from hook fist to full fist. This model provides precise localization of the median nerve in dynamic ultrasound sequences, enabling efficient and reliable tracking across various wrist positions, and offering a promising approach for rapid carpal tunnel syndrome screening.

Shao et al. assessed an improved U2-Net model for segmenting ultrasound images of the median nerve [47]. A total of 402 images were used, including 249 from carpal tunnel syndrome patients and 153 from healthy volunteers. Evaluation metrics included the Dice coefficient, pixel accuracy, and average Hausdorff distance. The improved U2-Net achieved a Dice score of 72.85%, mean IoU of 79.66%, and pixel accuracy of 95.92%, significantly outperforming conventional U-Net and Res-U-Net models. These findings demonstrate the enhanced segmentation performance of the improved U2-Net and its potential utility for early carpal tunnel syndrome diagnosis. The architecture based on the VGG (Visual Geometry Group) 16 network is illustrated in **Figure 7**.

Huang et al. developed an enhanced VGG16-UNet architecture incorporating a contracting path and an expanding path [48]. The contracting path employs a VGG16 backbone with the fully connected layers removed, while the expanding path mirrors the upsampling structure of U-Net. By integrating attention mechanisms and residual modules, several variants—A-UNet, S-UNet, and AS-UNet—were proposed and tested on 910 median nerve images. Results showed that AS-UNet achieved the best performance among U-Net-based models, while VGG16-UNet variants outperformed standard U-Net. Among these, attention-based architectures consistently outperformed residual-based ones, with A-VGG16-UNet delivering the highest accuracy, improving visualization of the median nerve and reducing the risk of iatrogenic injury to adjacent vessels and nerves.

Wu et al. evaluated multiple DL models pretrained on ImageNet, including DeepLabV3+, U-Net, FPN (Feature Pyramid Network), and Mask R-CNNs (Mask Region-based Convolutional Neural Networks), for automatic segmentation of the median nerve in dynamic ultrasound images [49]. U-Net, DeepLabV3+, and FPN were employed for semantic segmentation, while Mask R-CNNs was used for instance seg-

mentation. Results indicated that DeepLabV3+ and Mask R-CNNs provided the best performance, with average IoU scores approaching 0.83, significantly improving the accuracy of nerve localization.

Horng et al. proposed a novel convolutional neural network, DeepNerve, for localizing and segmenting the median nerve in ultrasound video sequences [50]. The DeepNerve model comprises a convolutional layer, pooling layer, two fully connected layers, and a softmax layer. By incorporating spatial-temporal consistency techniques with CNNs, the model effectively reduces false positives caused by ultrasound image noise. It was evaluated on ultrasound sequences from 20 patients, each containing 400-600 frames, using cross-validation. Segmentation performance was primarily assessed by Dice coefficient and Hausdorff distance. Results demonstrated that DeepNerve outperformed both traditional CNNs and support vector machine (SVM) methods in nerve localization and segmentation, achieving superior accuracy.

Ulnar nerve block

Ulnar nerve block is an effective regional anesthesia technique for controlling pain in the hand and medial forearm. It is particularly suitable for surgical procedures and pain management in areas such as the wrist, elbow, and hand, including trauma repair.

Smistad et al. investigated the real-time segmentation of blood vessels, nerves, and bones during regional anesthesia using DL applied to ultrasound guidance [51]. The primary objective was to develop a system that assists non-expert users in interpreting ultrasound images, particularly for performing nerve blocks, by enabling real-time anatomical segmentation. The study collected 108 axillary ultrasound videos from healthy volunteers and patients, with annotations for the musculocutaneous, median, and ulnar nerves, and an additional 20 groin ultrasound videos for femoral nerve labeling. A U-Net architecture was applied with 10-fold cross-validation. For axillary nerve blocks, F1 scores for the musculocutaneous, median, and ulnar nerves were 0.72, 0.84, and 0.54, respectively. For femoral nerve blocks, the F1 scores for the femoral nerve, vascular structures, and bones were 0.79, 0.90, and 0.78, respectively. These findings demonstrate the potential of DL-based segmentation in enhancing the accuracy and efficiency of ultrasound-guided regional anesthesia, particularly for less experienced users.

Jimenez et al. proposed a method for automatic neural structure segmentation in ultrasound images using Random Under-Sampling (RUS) and SVM classifiers [52]. First, the ROI was defined using graph-cut-based techniques. The Simple Linear Iterative Clusteringalgorithm was then applied to divide the ROI into superpixels. Relevant features were extracted using a nonlinear wavelet transform. Finally, classification was performed using RUS and SVM-based schemes to label each parameterized "hyperpixel", addressing the class imbalance between neural and non-neural regions. The dataset included 38 ultrasound images, with 22 depicting the median nerve and 16 depicting the ulnar nerve. Four classification approaches were compared: Gaussian Process Classifier, standard SVM, RUS-free SVM, and Weighted Lagrange Twin Support Vector Machine. Segmentation performance was assessed using the Dice coefficient and Geometric Mean. Results showed that the RUS-SVM method outperformed the other baselines, effectively identifying neural structures and providing technical support for peripheral nerve block applications. A comparison of medical image segmentation algorithms for upper limb nerve blocks is presented in **Table 3**.

Application in lower limbs

Lumbar plexus block

The lumbar plexus block is a commonly used anesthesia technique for lower limb surgeries and pain management. It involves injecting local anesthetics to block the lumbar plexus, resulting in partial or complete sensory and motor loss in the lower limb. Ultrasound guidance enhances the accuracy of this technique by providing real-time visualization of nerves and surrounding anatomy, thereby reducing the risk of complications.

Berggreen et al. employed a U-Net architecture to identify the femoral nerve in high-resolution ultrasound images, significantly improving visualization accuracy essential for precise nerve blocks [53]. Built using the TensorFlow frame-

Table 3. Comparison of medical image segmentation algorithms for upper limb nerve blockade

Nerve Type	Author	Model/Method	Core Innovation
Brachial Plexus	Wang et al. [40]	BPSegSys	Hybrid loss (hinge + cross-entropy) driven attention U-Net
	Tian et al. [41]	Multi-model comp.	LinkNet balances accuracy (Dice: 0.85) and speed (142 FPS)
	Ding et al. [42]	MallesNet	Multi-target segmentation + SLCF module for small objects
	Rayachoti et al. [43]	EU-Net	Pyramid Edge Extraction Module edge extraction + EOA optimization (Dice: 94.97%)
	Huang et al. [44]	HybridAttNet	Pseudo-color enhancement + MSCA decoder
	Zhou et al. [45]	LAEDNet	EfficientNet encoder + Lightweight Residual Squeeze-and-Excitation module (40.7 FPS)
Median Nerve	Wang et al. [46]	MNT-DeepSL	ResNet-based tracking (accuracy >90%)
	Shao et al. [47]	U2-Net+	Architecture optimization (Dice: 72.85%)
	Huang et al. [48]	AS-UNet	VGG16-UNet + attention fusion
	Wu et al. [49]	Mask R-CNNs	Pretrained instance segmentation (IoU: 0.83)
	Horng et al. [50]	DeepNerve	Spatiotemporal CNNs (Dice: 0.81, HD: 1.2 mm)
	Smistad et al. [51]	Real-time U-Net	Multi-structure segmentation (F1: 0.54-0.84)
	Jimenez et al. [52]	RUS-SVM	Graph-cut + imbalanced classification (Dice coefficient: 0.78)

Note: SLCF, Small Lesion Context Fusion; EOA, Edge Optimization Algorithm; EU-Net, Ebola U-Ne; MSCA, Multi-Scale Context Attention; CNNs, Convolutional Neural Networks; RUS-SVM, Random Under-Sampling-Support Vector Machine; HD, Hausdorff Distance.

work, the model utilized the Adam optimizer and categorical cross-entropy loss. A dataset of 1,410 ultrasound images from 48 patients was manually annotated by clinical experts. After 350 training epochs and 10-fold cross-validation, the model achieved an IoU score of 74%, indicating strong performance. The study also examined the influence of demographic variables such as height, weight, age, and BMI through t-tests and chi-square analysis. Results confirmed that DL-based semantic segmentation using U-Net can accurately segment the femoral nerve even with limited training data.

Similarly, Huang et al. applied a U-Net model to a dataset of 562 ultrasound images [54]. The training, validation, and test sets achieved IoU scores of 0.713, 0.633, and 0.638, respectively. The model attained an overall accuracy of 88.4%, demonstrating satisfactory performance and potential for clinical adoption.

Hong et al. explored image reconstruction, processing, and analysis using data-driven and AI techniques [55]. Focusing on knee ligament reconstruction and femoral arteriography, they proposed a constrained data exploration method combined with an iterative algorithm to reconstruct high-resolution images from low-frequency K-space data. Simulated experiments using enhanced images of knee ligaments and femoral nerve arteriography supported the approach. A multi-input segmentation network was designed to leverage the spatial continuity of knee ligaments and femoral nerves. The multi-supervision output yielded excellent segmentation results, providing clinically valuable information for pain management.

Smistad et al. developed a novel algorithm in 2016 for real-time automatic detection of the femoral artery [56]. **Figure 8** shows a segmented and visualized ultrasound image of the femoral artery using the FAST (Framework for Heterogeneous Medical Image Computing and Visualization) framework. The algorithm models the artery as an ellipse and assigns an ellipse score to each pixel. The best-scoring ellipse is selected as the arterial candidate, and a Kalman filter is applied for robust tracking under noisy and dynamic conditions. The algorithm also includes anatomical registration to align real-time ultrasound images with known anatomical structures, improving visualization accuracy.

Building on this, a subsequent study introduced a real-time automatic segmentation and

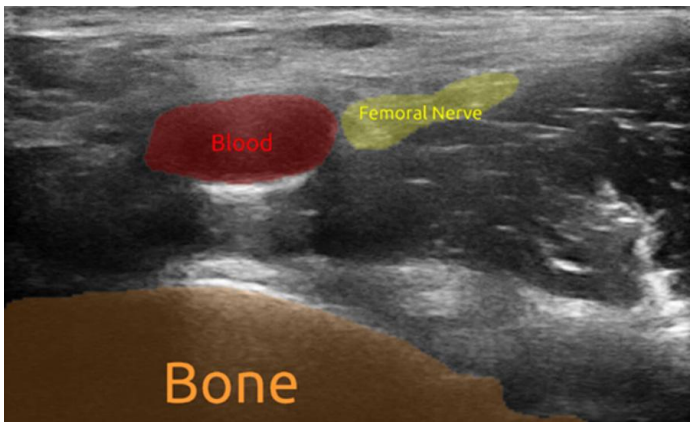

Figure 8. Example of an ultrasound femoral image segmented and visualized in real-time with FAST. This figure was cited from [57].

probe guidance system for ultrasound-guided femoral nerve blocks [57]. Utilizing modern GPUs (Graphics Processing Units) and the FAST framework, the system segments the femoral artery, femoral nerve, and fascial layers (fascia lata and fascia iliaca) in real time. Segmentation accuracy improved significantly, with positional errors between 1 and 3 mm and an average deviation of 8.5 mm from expert annotations. The system also featured transparent probe visualization and dynamic indicator updates, helping clinicians intuitively interpret ultrasound images. The study concluded that such computer-assisted tools are clinically feasible and may enhance success rates in femoral nerve blocks.

Accurate segmentation of the lumbosacral plexus is crucial for diagnosing and analyzing nerve injuries. While many DL models for spinal segmentation exist, they mainly focus on vertebrae and intervertebral discs rather than neural structures. Zhao et al. addressed this by proposing RA2-Net, a Residual Attention Network designed specifically for lumbosacral plexus segmentation [58]. RA2-Net consists of three key components: (1) an atrous encoder module that extracts multi-scale contextual features from MRI; (2) residual skip connections that merge high-resolution encoder features with high-level decoder outputs; and (3) a scale attention block that fuses multi-scale features in the decoder. Evaluated on spinal MR images from 10 patients, RA2-Net outperformed several state-of-the-art methods in segmenting the lumbosacral plexus.

Sciatic nerve block

The sciatic nerve block is commonly used in foot, ankle, and knee surgeries. To achieve complete anesthesia of the lower extremity, it is often combined with a femoral nerve block. This combined approach provides comprehensive coverage of the lower limb's sensory regions, making it suitable for extensive procedures involving the thigh, knee, and areas below.

Jimenez-Castaño et al. proposed a method using Random Fourier Features (RFF) to enhance ultrasound image segmentation of peripheral nerves via DL [59]. This method improved three semantic segmentation architectures—FCNs, U-Net, and ResUnet—by integrating RFF, resulting in RFF-FCNs, RFF-U-Net, and RFF-ResUnet. Two ultrasound datasets, Nerve UTP and NSD, were used, including images of the sciatic, ulnar, median, and femoral nerves. Results showed that RFF integration improved generalization in nerve segmentation. On the Nerve UTP dataset, RFF-FCNs and RFF-U-Net improved segmentation accuracy in most cases, although ResUnet and RFF-ResUnet experienced overfitting. On the NSD dataset, RFF-U-Net yielded the best segmentation results. This approach demonstrates strong potential for enhancing peripheral nerve segmentation while maintaining interpretability.

Díaz-Vargas et al. developed a variant of the U-Net, termed Conditional U-Net (C-U-Net), for improved automatic segmentation of peripheral nerves in ultrasound images [60]. By introducing a conditional input at the network's bottleneck to specify the target nerve type, the model learns structure-specific features, enhancing segmentation accuracy. Trained on a dataset comprising images of the sciatic, ulnar, median, and femoral nerves, C-U-Net outperformed the conventional U-Net. On 372 validation images, it achieved an average Dice coefficient of 0.70, accuracy of 0.73, sensitivity of 0.71, and an AUC of 0.85. These findings suggest that incorporating target-specific information significantly enhances model performance in multi-nerve ultrasound segmentation.

Sugino et al. investigated optimal scaling of network architectures and input image sizes for ultrasound-guided nerve block detection using CNNs [61]. The study focused on pixel-level labeling via deep CNNs, comparing an encoder-decoder model based on U-Net with a two-

stage model based on Mask R-CNNs. Both models performed well in nerve segmentation tasks. Two datasets were employed to examine the impact of model size and input resolution on performance. The public dataset contained 600 ultrasound images of the sciatic, ulnar, femoral, and median nerves. Results showed that smaller input sizes combined with larger network models significantly enhanced detection accuracy. A key finding was that optimized configurations not only improved precision but also enabled real-time processing, highlighting potential for clinical implementation in nerve localization during regional anesthesia.

Popliteal nerve block

The popliteal nerve block targets the sciatic nerve in the lower limb to provide anesthesia and analgesia below the knee. It is commonly applied in procedures involving the foot, ankle, and Achilles tendon.

Kawanishi et al. aimed to develop a DL algorithm to assess tibial nerve tension across different ankle positions [62]. The study used 204 ultrasound images from 68 healthy volunteers, covering maximum dorsiflexion and plantarflexion angles at -10° and -20°. The tibial nerve was manually segmented and subsequently classified using U-Net and a CNNs. Manual segmentation achieved an average maximum accuracy of 0.92, while the fully automated classification reached an accuracy of over 0.77, demonstrating feasibility in assessing nerve tension at varying ankle angles. The study noted the clinical potential of ultrasound imaging for screening but acknowledged limitations such as small sample size and variability in ultrasound device performance.

Kolluru et al. developed NerveTracker, a Python-based tool for visualizing and tracking peripheral nerve fibers using tandem block-face microscopy [63]. This approach integrates 3D microscopic imaging with UV surface excitation for high-resolution nerve imaging. A 2D U-Net-based segmentation model was designed for multi-class segmentation of 3D-MUSE image stacks, specifically targeting fascicles and epineurium. Pretrained weights from the ImageNet database were used to initialize the network, improving segmentation accuracy. Selective annotation (one out of every 100 slices) was applied during training, after which the model could automatically segment entire image stacks. The method demonstrated high accuracy in trajectory mapping for vagus and tibial nerves, with Dice similarity coefficients exceeding 0.75, and robustness across varying image characteristics.

A comparison of medical image segmentation algorithms for lower limb nerve blockade is presented in **Table 4**.

Discussion

The integration of DL with ultrasound imaging marks a significant advancement in the field of regional anesthesia, offering considerable potential to improve the accuracy and efficiency of peripheral nerve blockade. As demonstrated in numerous studies reviewed herein, DL algorithms—particularly those based on convolutional neural networks such as U-Net and its variants—have shown impressive capabilities in automatically segmenting peripheral nerves in complex ultrasound images. Clinically, this promises to reduce operator dependency, improve procedural consistency, enhance patient safety by minimizing the risk of inadvertent punctures, and streamline workflows by automating a previously time-intensive interpretation step.

However, realizing the full clinical potential of this technology involves challenges beyond achieving high segmentation accuracy in controlled environments. A major limitation is the robustness and generalizability of current DL models. Ultrasound image quality and characteristics can vary significantly due to factors such as machine vendors, imaging settings, operator skill, and patient-specific anatomy. As a result, models trained on curated datasets often struggle to maintain performance in diverse real-world scenarios. This variability currently limits the feasibility of a universal model applicable across all nerve types and clinical contexts. In the near term, developing specialized or adaptive models may offer a more practical solution.

Beyond technical and data-related constraints, significant challenges exist at the clinical translation interface. The implementation of AI-assisted guidance systems requires rigorous validation to meet regulatory standards. This includes demonstrating not only accuracy, but also safety, reliability, and clinical utility across

Table 4. Comparison of medical image segmentation algorithms for lower limb nerve blockade

Nerve Type	Author	Model/Method	Core Innovation
Lumbar Plexus	Berggreen et al. [53]	U-Net	High-precision femoral nerve segmentation (IoU: 74%) with demographic analysis
	Huang et al. [54]	U-Net	Multi-stage dataset validation (train/test IoU: 0.713/0.638)
	Hong et al. [55]	Data-driven + AI	Iterative reconstruction + multi-layer input segmentation network
	Smistad et al. [56]	Elliptical scoring	Femoral artery modeling + Kalman filter-based dynamic tracking
	Smistad* et al. [57]	GPU real-time system	Multi-structure segmentation (error: 1-3 mm) with probe guidance
	Zhao et al. [58]	RA2-Net	Residual-attention network + multi-scale fusion (lumbosacral MRI)
Sciatic Nerve	Jimenez-Castaño et al. [59]	RFF-enhanced models	RFF for FCNs/U-Net/ResUnet generalization
	Díaz-Vargas et al. [60]	C-UNet	Conditional U-Net with nerve-type input (Dice: 0.70)
	Sugino et al. [61]	Multi-scale CNNs	Image/model scaling optimization + real-time validation
Popliteal Nerve	Kawanishi et al. [62]	U-Net + CNNs	Tibial nerve tension analysis (accuracy: 0.77+) across ankle positions
	Kolluru et al. [63]	NerveTracker	3D microscopy + 2D U-Net (Dice >0.75) for nerve fascicle/epineurium segmentation

Note: RA2-Net, Residual Attention Adaptive Network; RFF, Random Fourier Features; C-Unet, Conditional U-Net; FCNs, Fully Convolutional Networks; MRI, Magnetic Resonance Imaging; CNNs, Convolutional Neural Networks; 3D, Three-Dimensional.

varied populations and healthcare settings—often necessitating large-scale, prospective clinical trials. Equally important is clinician trust and seamless integration into existing workflows. For AI to be adopted widely, it must offer user-friendly interfaces, transparent decision-making processes, and tangible benefits without disrupting established clinical practices or contributing to skill degradation. Integration with existing ultrasound systems and hospital information infrastructures is also essential but often underestimated.

Moreover, ethical considerations must guide the development and deployment of these technologies. Ensuring patient data privacy and security throughout the AI lifecycle is non-negotiable. Responsible innovation in this field demands early and ongoing engagement with ethical principles, particularly when handling sensitive health information or making clinical recommendations.

Looking forward, several research priorities must be addressed to overcome these barriers. There is a need for models that are more robust to image variability and require less annotated data, potentially through techniques such as domain generalization, federated learning, or self-supervised learning. Developing lightweight, computationally efficient models that support real-time inference on portable ultrasound devices or edge hardware will be critical to enhancing accessibility. Additionally, the exploration of multimodal approaches could provide richer anatomical context, particularly in complex anatomical scenarios [64]. Ultimately, the field may evolve toward personalized guidance systems that adapt to individual patient anatomy and predicted clinical outcomes, advancing the vision of precision medicine in regional anesthesia.

Conclusion

The application of DL in ultrasound-guided peripheral nerve block identification is transforming the field of anesthesiology. This review comprehensively summarizes recent progress in the use of ultrasound and medical image segmentation techniques for nerve block applications in the extremities. It begins by categorizing and introducing mainstream segmentation algorithms, followed by detailed examples of their application in clinical scenarios. Finally, the review analyzes the advantages and limita-

tions of these technologies and discusses future directions for the development of AI-assisted ultrasound-guided nerve block systems.

Author contributions: Jiaxun Jiang: Responsible for the general framework design of the article, the planning and organization of the research direction, led the writing and editing of the literature review section, and participated in the discussion and writing of the research methodology section. Miao Zhou: Provided medically relevant theoretical support and was responsible for the collection and organization of literature. Liangqing Lin: Provides theoretical support for relevant parts of the development of ultrasound medicine. Haipo Cui: Corresponding Author: Led the revision of the article, participated in the final review and revision of the article, ensured that all authors' comments were integrated, and ultimately approved the article for submission. Long Liu: Provides theoretical support for relevant parts of the development of ultrasound medicine. Jiaen Wu: Participated in literature searches, provided experimental data support, and was responsible for producing some of the graphs. Zhaopen Zhou: Partial data collection and organization and production of partial tables.

References

[1] Helen L, O'Donnell BD, Moore E. Nerve localization techniques for peripheral nerve block and possible future directions. Acta Anaesthesiol Scand 2015;59(8):962-974.

[2] Verrill PJ. Principles and practice of regional anaesthesia. PAIN 1988;33(3):391.

[3] Wu L, Xin Y, Li S, et al. Cascaded Fully Convolutional Networks for automatic prenatal ultrasound image segmentation. 2017 IEEE 14th International Symposium on Biomedical Imaging (ISBI 2017) 2017;663-666.

[4] Norouzi A, Rahim MSM, Altameem A, et al. Medical Image Segmentation Methods, Algorithms, and Applications. IETE Tech Rev 2014;31(3):199-213.

[5] Rana M, Bhushan M. Machine learning and deep learning approach for medical image analysis: diagnosis to detection. Multimed Tools Appl 2022;1-39.

[6] Muthukrishnan R. Edge Detection Techniques For Image Segmentation. Int J Comput Sci Inf Technol 2011;3:259-267.

[7] Kaganami HG, Beiji Z. Region-Based Segmentation versus Edge Detection. Proceedings of the 2009 Fifth International Conference on Intelligent Information Hiding and Multimedia Signal Processing 2009;1217-1221.

[8] Otsu N. A Threshold Selection Method from Gray-Level Histograms. IEEE Trans Syst Man Cybern: Syst 1979;9(1):62-66.

[9] Cui H, Hu L, Chi L. Advances in Computer-Aided Medical Image Processing. Appl Sci 2023; 13(12):7079.

[10] Litjens G, Kooi T, Ehteshami Bejnordi B, et al. A Survey on Deep Learning in Medical Image Analysis. Med Image Anal 2017;42:60-88.

[11] Zhang S, Metaxas D. On the challenges and perspectives of foundation models for medical image analysis. Med Image Anal 2024;91: 102996.

[12] Wu R, Liu Y, Liang P, et al. H-vmunet: High-order Vision Mamba UNet for medical image segmentation. Neurocomputing 2025; 624:129447.

[13] Long J, Shelhamer E, Darrell T. Fully convolutional networks for semantic segmentation. 2015 IEEE Conference on Computer Vision and Pattern Recognition (CVPR) 2015;3431-3440.

[14] Huang Y, Xu H. Fully convolutional network with attention modules for semantic segmentation. Signal Image Video P 2021;15(5):1031-1039.

[15] Miao S, Piat S, Fischer P, et al. Dilated FCN for multi-agent 2D/3D medical image registration. Proceedings of the Thirty-Second AAAI Conference on Artificial Intelligence and Thirtieth Innovative Applications of Artificial Intelligence Conference and Eighth AAAI Symposium on Educational Advances in Artificial Intelligence 2018;32:575.

[16] Wang Z, Gao X, Wu R, et al. Fully automatic image segmentation based on FCN and graph cuts. Multimedia Syst 2022;28(5):1753-1765.

[17] Qian L, Huang H, Xia X, et al. Automatic segmentation method using FCN with multi-scale dilated convolution for medical ultrasound image. Visual Comput 2023;39(11):5953-5969.

[18] Ronneberger O, Fischer P, Brox T. U-Net: Convolutional Networks for Biomedical Image Segmentation. Medical Image Computing and Computer-Assisted Intervention – MICCAI 2015 2015;234-241.

[19] Singadkar G, Mahajan A, Thakur M, et al. Deep Deconvolutional Residual Network Based Automatic Lung Nodule Segmentation. J Digit Imaging 2020;33(3):678-684.

[20] Oyedotun OK, El Rahman Shabayek A, Aouada D, et al. Training Very Deep Networks via Residual Learning with Stochastic Input Shortcut Connections. Neural Inf Process 2017;23-33.

[21] Çiçek Ö, Abdulkadir A, Lienkamp SS, et al. 3D U-Net: Learning Dense Volumetric Segmentation from Sparse Annotation. Medical Image Computing and Computer-Assisted Intervention – MICCAI 2016 2016;424-432.
[22] Milletari F, Navab N, Ahmadi SA. V-Net: Fully Convolutional Neural Networks for Volumetric Medical Image Segmentation. 2016 Fourth International Conference on 3D Vision (3DV) 2016;565-571.
[23] Zhang Z, Liu Q, Wang Y. Road Extraction by Deep Residual U-Net. IEEE Geosci Remote Sens Lett 2018;15(5):749-753.
[24] He K, Zhang X, Ren S, et al. Deep Residual Learning for Image Recognition. 2016 IEEE Conference on Computer Vision and Pattern Recognition (CVPR) 2016;770-778.
[25] Iandola F, Moskewicz M, Karayev S, et al. DenseNet: Implementing Efficient ConvNet Descriptor Pyramids. arXiv - CS - Computer Vision and Pattern Recognition 2014.
[26] Zhang J, Zhang Y, Jin Y, et al. MDU-Net: multi-scale densely connected U-Net for biomedical image segmentation. Health Inf Sci Syst 2023;11(1):13.
[27] Zhou Z, Rahman Siddiquee MM, Tajbakhsh N, et al. UNet++: A Nested U-Net Architecture for Medical Image Segmentation. arXiv - CS - Computer Vision and Pattern Recognition 2018.
[28] Gab Allah AM, Sarhan AM, Elshennawy NM. Edge U-Net: Brain tumor segmentation using MRI based on deep U-Net model with boundary information. Expert Syst Appl 2023;213: 118833.
[29] Oktay O, Schlemper J, Folgoc L, et al. Attention U-Net: Learning Where to Look for the Pancreas. arXiv - CS - Computer Vision and Pattern Recognition 2018.
[30] Egger J, Gsaxner C, Pepe A, et al. Medical deep learning—A systematic meta-review. Comput Meth Prog Bio 2022;221:106874.
[31] Zhai D, Hu B, Gong X, et al. ASS-GAN: Asymmetric semi-supervised GAN for breast ultrasound image segmentation. Neurocomputing 2022;493:204-216.
[32] Hou J, Wei H, Liu B. iPiDA-GCN: Identification of piRNA-disease associations based on Graph Convolutional Network. PLoS Comput Biol 2022;18(10):e1010671.
[33] Tian F, Tian Z, Chen Z, et al. Surface-GCN: Learning interaction experience for organ segmentation in 3D medical images. Med Phys 2023;50(8):5030-5044.
[34] Ye H, Wang DH, Li J, et al. Improving Histopathological Image Segmentation and Classification using Graph Convolution Network. Proceedings of the 2019 8th International Conference on Computing and Pattern Recognition 2020;192-198.
[35] Azam MA, Khan KB, Salahuddin S, et al. A review on multimodal medical image fusion: Compendious analysis of medical modalities, multimodal databases, fusion techniques and quality metrics. Comput Biol Med 2022;144: 105253.
[36] Wang X, Li Z, Huang Y, et al. Multimodal medical image segmentation using multi-scale context-aware network. Neurocomputing 2022; 486:135-146.
[37] Wang G, Li W, Ourselin S, et al. Automatic Brain Tumor Segmentation Using Cascaded Anisotropic Convolutional Neural Networks. Brainlesion: Glioma, Multiple Sclerosis, Stroke and Traumatic Brain Injuries 2018;178-190.
[38] Asher Y. Hadzic's Peripheral Nerve Blocks and Anatomy for Ultrasound-guided Regional Anesthesia, Second Edition. Anesthesiology 2013; 119:493-493.
[39] Sinha A, Chan VW. Ultrasound imaging for popliteal sciatic nerve block. Reg Anesth Pain Med 2004;29(2):130-134.
[40] Wang Y, Zhu B, Kong L, et al. BPSegSys: A Brachial Plexus Nerve Trunk Segmentation System Using Deep Learning. Ultrasound Med Biol 2024;50(3):374-383.
[41] Tian D, Zhu B, Wang J, et al. Brachial Plexus Nerve Trunk Recognition From Ultrasound Images: A Comparative Study of Deep Learning Models. IEEE Access 2022;10:82003-82014.
[42] Ding Y, Yang Q, Wang Y, et al. MallesNet: A multi-object assistance based network for brachial plexus segmentation in ultrasound images. Med Image Anal 2022;80:102511.
[43] Rayachoti E, Vedantham R, Gundabatini SG. EU-net: An automated CNN based ebola U-net model for efficient medical image segmentation. Multimed Tools Appl 2024;83(30):74323-74347.
[44] Huang X, Wang Q, Chen J, et al. Effective hybrid attention network based on pseudo-color enhancement in ultrasound image segmentation. Image Vision Comput 2023;137:104742.
[45] Zhou Q, Wang Q, Bao Y, et al. LAEDNet: A Lightweight Attention Encoder–Decoder Network for ultrasound medical image segmentation. Comput Electr Eng 2022;99:107777.
[46] Wang YW, Chang RF, Horng YS, et al. MNT-DeepSL: Median nerve tracking from carpal tunnel ultrasound images with deep similarity learning and analysis on continuous wrist mo-

tions. Comput Med Imaging Graph 2020; 80:101687.
[47] Shao J, Zhou K, Cai YH, et al. Application of an Improved U2-Net Model in Ultrasound Median Neural Image Segmentation. Ultrasound Med Biol 2022;48(12):2512-2520.
[48] Huang A, Jiang L, Zhang J, et al. Attention-VGG16-UNet: a novel deep learning approach for automatic segmentation of the median nerve in ultrasound images. Quant Imaging Med Surg 2022;12(6):3138-3150.
[49] Wu CH, Syu WT, Lin MT, et al. Automated Segmentation of Median Nerve in Dynamic Sonography Using Deep Learning: Evaluation of Model Performance. Diagnostics (Basel) 2021; 11(10):1893.
[50] Horng MH, Yang CW, Sun YN, et al. DeepNerve: A New Convolutional Neural Network for the Localization and Segmentation of the Median Nerve in Ultrasound Image Sequences. Ultrasound Med Biol 2020;46(9):2439-2452.
[51] Smistad E, Lie T, Johansen KF. Real-time segmentation of blood vessels, nerves and bone in ultrasound-guided regional anesthesia using deep learning. 2021 IEEE International Ultrasonics Symposium (IUS) 2021;1-4.
[52] Jimenez C, Diaz D, Salazar D, et al. Nerve Structure Segmentation from Ultrasound Images Using Random Under-Sampling and an SVM Classifier. Image Anal Recognit 2018;571-578.
[53] Berggreen J, Johansson A, Jahr J, et al. Deep Learning on Ultrasound Images Visualizes the Femoral Nerve with Good Precision. Healthcare (Basel) 2023;11(2):184.
[54] Huang C, Zhou Y, Tan W, et al. Applying deep learning in recognizing the femoral nerve block region on ultrasound images. Ann Transl Med 2019;7(18):453.
[55] Hong G, Zhang L, Kong X, et al. Artificial Intelligence Image-Assisted Knee Ligament Trauma Repair Efficacy Analysis and Postoperative Femoral Nerve Block Analgesia Effect Research. World Neurosurg 2021;149:492-501.
[56] Smistad E, Lindseth F. Real-Time Automatic Artery Segmentation, Reconstruction and Registration for Ultrasound-Guided Regional Anaesthesia of the Femoral Nerve. IEEE Trans Med Imaging 2016;35(3):752-761.
[57] Smistad E, Iversen DH, Leidig L, et al. Automatic Segmentation and Probe Guidance for Real-Time Assistance of Ultrasound-Guided Femoral Nerve Blocks. Ultrasound Med Biol 2017;43(1): 218-226.
[58] Zhao J, Sun L, Zhou X, et al. Residual-atrous attention network for lumbosacral plexus segmentation with MR image. Comput Med Imaging Graph 2022;100:102109.
[59] Jimenez-Castaño CA, Álvarez-Meza AM, Aguirre-Ospina OD, et al. Random Fourier Features-Based Deep Learning Improvement with Class Activation Interpretability for Nerve Structure Segmentation. Sensors (Basel) 2021;21(22): 7741.
[60] Díaz-Vargas HM, Jimenez-Castaño CA, Cárdenas-Peña DA, et al. Peripheral Nerve Segmentation in Ultrasound Images Using Conditioned U-Net. Prog Artif Intell Pattern Recognit 2021;124-133.
[61] Sugino T, Onogi S, Oishi R, et al. Investigation of Appropriate Scaling of Networks and Images for Convolutional Neural Network-Based Nerve Detection in Ultrasound-Guided Nerve Blocks. Sensors (Basel) 2024;24(11):3696.
[62] Kawanishi K, Kakimoto A, Anegawa K, et al. Automatic Identification of Ultrasound Images of the Tibial Nerve in Different Ankle Positions Using Deep Learning. Sensors (Basel) 2023; 23(10):4855.
[63] Kolluru C, Joseph N, Seckler J, et al. NerveTracker: a Python-based software toolkit for visualizing and tracking groups of nerve fibers in serial block-face microscopy with ultraviolet surface excitation images. J Biomed Opt 2024;29(7):076501.
[64] Li X, Ma S, Xu J, et al. TranSiam: Aggregating multi-modal visual features with locality for medical image segmentation. Expert Syst Appl 2024;237:121574.

Perioperative Precision Medicine
ISSN: 2957-5443

Zentime

Review Article https://doi.org/10.61189/617079irudnn

A review of multimodal medical image fusion: Developments in traditional, model-based and learning-based approaches

Zhaopeng Zhou[1], Jiaen Wu[1], Jiaxun Jiang[1], Miao Zhou[2], Wenhui Guo[3], Yongchu Hu[4]

[1]School of Health Science and Engineering, University of Shanghai for Science and Technology, Shanghai 200093, China. [2]Jiangsu Cancer Hospital, Nanjing 213164, Jiangsu Province, China. [3]The Department of Anesthesiology, Naval Medical University, Shanghai 200433, China. [4]The Department of Anesthesiology, Second Affiliated Hospital of Navy Medical University, Shanghai 200003, China.

Corresponding author: Yongchu Hu.

Declaration of conflict of interest: None.

Received April 10, 2025; Accepted July 11, 2025; Published December 31, 2025

Highlights

- Significant Advantages of Multimodal Fusion: Multimodal medical image fusion enhances diagnostic accuracy and medical value by integrating multi-source data such as CT, MRI, and PET images, outperforming single-modality technologies.
- Benefits of Deep Learning: Deep learning technologies significantly advance multimodal medical image fusion, enabling more efficient and accurate fusion results.
- Perioperative clinical significance: Multimodal image fusion can provide important support for perioperative preoperative planning, intraoperative guidance, and postoperative evaluation, thereby improving surgical accuracy and patient safety.
- Future Research Directions: Future research should focus on improving model interpretability, enhancing modality alignment, and achieving breakthroughs in practicality, applicability, and efficiency.

Abstract

Multimodal medical image fusion technology optimizes image content by integrating images from diverse modalities, such as Computed Tomography (CT), Positron Emission Tomography (PET), Magnetic Resonance Imaging (MRI), and Single Photon Emission Computed Tomography (SPECT), while retaining critical information. With the rapid advancements in medical imaging technology, single-modal approaches have limitations in capturing comprehensive anatomical or functional characteristics. As a result, researchers are increasingly turning to multimodal fusion methods to enhance diagnostic accuracy and provide richer data for classification, detection, and segmentation tasks. In particular, during the perioperative period, multimodal image fusion plays a crucial role in surgical planning, intraoperative navigation, and postoperative evaluation, enabling precise localization of lesions and improving clinical decision-making. This paper presents a survey of the latest literature on medical image fusion, covering three major approaches: traditional methods, model-based methods, and learning-based methods. It discusses the advantages and limitations of each approach, with a particular emphasis on traditional image processing techniques, model-based fusion methods, and the integration of emerging deep learning (DL) technologies. Comparative experimental analysis highlights performance differences among these methods in terms of information retention, computational efficiency, and clinical applicability. Finally, the paper reviews performance evaluation metrics for multimodal fusion and provides recommendations for future research to further promote the widespread adoption of this technology in clinical diagnostics and intelligent healthcare.

Keywords: Multimodal medical image fusion, multimodal database, perioperative period, deep learning, evaluation metrics

Address correspondence to: Yongchu Hu, The Department of Anesthesiology, Second Affiliated Hospital of Navy Medical University, No.415 Fengyang Road, Shanghai 200003, China. E-mail: liuyang1268@smmu.edu.cn.

Introduction

Medical imaging plays a crucial role in diagnosis and clinical treatment. One of the greatest challenges in medicine is achieving accurate disease identification and effective treatment [1]. The exploration of medical imaging began in 1895 with the discovery of X-rays by German physicist Wilhelm Conrad Roentgen. This groundbreaking discovery not only revolutionized the scientific community but also provided a new tool for medical diagnosis. X-ray imaging enables non-invasive observation of the internal structure of the human body, quickly becoming an indispensable part of medical diagnostics.

With the continuous advancement of science and technology, more imaging techniques have emerged, such as MRI, CT, ultrasound (US), and PET. These technologies have greatly enhanced clinical diagnosis, disease monitoring, and surgical planning, improving both the level of medical care and the quality of life for patients. However, despite their effectiveness, single-modality imaging technologies—such as X-rays, MRI, or ultrasound—each have limitations [2]. For example, X-ray imaging is excellent for visualizing bone structures but less effective for soft tissues. MRI excels in soft tissue imaging but has long scan times and is sensitive to metal implants. CT is ideal for imaging bones and high-density tissues, while PET provides valuable functional and metabolic data. Moreover, single-modality imaging often cannot provide both rich anatomical and functional information simultaneously, which hinders early disease diagnosis and treatment.

As a solution to these limitations, multimodal medical image fusion (MMIF) technology has emerged. Image fusion was first proposed in 1985 and has since rapidly advanced, particularly in fields such as infrared and visible light image fusion, material analysis, remote sensing, multi-focus images, and medical image fusion [3].

In recent decades, medical image fusion technology has significantly advanced medical imaging. It can be broadly classified into single-modality fusion and multimodal fusion. Single-modality fusion typically provides less information, which is why most research focuses on multimodal image fusion [4]. MMIF combines images from multiple modalities, integrating their strengths [5]. This technology offers not only more comprehensive and accurate diagnostic information but also enhances treatment decisions and improves outcomes. Furthermore, it holds great potential for early disease detection, treatment evaluation, and prognosis monitoring, making it an indispensable tool in modern medicine. The core principle is to integrate information from various imaging modalities, overcoming the limitations of single-modality imaging by leveraging the strengths of each. Different imaging modalities provide complementary anatomical and functional data [6]. By effectively fusing these different image modalities, doctors can obtain more precise and comprehensive information, enhancing diagnostic accuracy and increasing the likelihood of early detection.

With the advancement of computer vision, artificial intelligence, and deep learning technologies, multimodal fusion methods based on image processing and machine learning (ML) have matured. These methods have become especially valuable in neuroimaging, oncology, and cardiovascular diseases, improving diagnostic efficiency and treatment outcomes [3, 7, 8]. For example, in brain tumor diagnosis, MRI delineates the tumor boundary and brain tissue structure, while PET reveals areas of metabolic activity. The fusion of these images allows for precise determination of the tumor's location, size, and activity, guiding surgical resection and radiotherapy planning [9]. In cancer treatment, PET/CT fusion plays a critical role in accurate positioning, staging, diagnosis, and radiotherapy planning by combining anatomical and functional metabolic information, significantly enhancing diagnostic accuracy and optimizing treatment strategies [10]. Furthermore, this technology provides crucial perioperative support: it enables comprehensive preoperative assessment by displaying lesion and anatomical information; it enables intraoperative navigation through real-time data integration; and it assists postoperative assessment by accurately monitoring residual lesions and tissue recovery. The integration of multimodal information facilitates preoperative planning and prognostic assessment by providing more detailed and accurate pathological data, thereby improving the level of diagnosis and treatment and prognosis.

Table 1. Comparison of several common imaging methods

Imaging Technology	Imaging Principle	Main Advantages	Main Disadvantages	Applications
MRI	Strong magnetic field + RF signals	High soft tissue contras no ionizing radiation, multi-parametric	Long scan time, high cost, metal implants restricted	Neurology, musculoskeletal, soft tissues
CT	X-ray tomography	Fast scanning, high spatial resolution, suitable for emergencies	Ionizing radiation, lower soft tissue contrast	Chest, abdomen, bones, emergencies
PET	Radioactive tracer metabolic imaging	Provides functional & metabolic info, often combined with CT	High radiation dose, low resolution, high cost	Oncology, cardiovascular, neurology
US	High-frequency sound wave reflection	No radiation, real-time imaging, low cost, portable	Low resolution, operator-dependent, poor penetration through bone/gas	Fetal, cardiac, abdominal examinations
SPECT	Radioactive tracer functional imaging	Shows blood flow & metabolism, can combine with CT	Long imaging time, low resolution, requires radioactive material	Cardiology, brain disorders
OCT	Low-coherence optical imaging	Ultra-high resolution, non-invasive	Limited imaging depth, high cost, motion-sensitive	Ophthalmology (retina), cardiovascular

However, MMIF also faces several challenges, including dealing with modality differences, improving computational efficiency of fusion algorithms, and enabling real-time clinical applications. This paper aims to comprehensively review existing MMIF technologies, focusing on traditional methods, model-based methods, and learning-based methods. Through a systematic analysis of the advantages and disadvantages of these methods and a review of commonly used performance evaluation metrics, this paper explores their prospects and challenges in clinical applications. The ultimate goal is to offer valuable references for researchers to further promote the development of multimodal fusion technology, improving diagnostic accuracy and clinical outcomes.

Imaging technology

Each imaging modality in medical diagnosis has its own unique characteristics and provides specific types of information. Different medical imaging modalities utilize various bands of the electromagnetic spectrum to diagnose different medical conditions in the human body [7].

Below are some common medical imaging modalities, briefly summarized in **Table 1** [11-16].

Magnetic resonance imaging (MRI)

MRI utilizes strong magnetic fields and radio-frequency signals to produce high-resolution images, making it ideal for soft tissue imaging, such as the brain, spinal cord, and muscles. It offers excellent soft tissue contrast, no ionizing radiation, and multi-directional imaging capabilities, making it suitable for detailed observation of lesions. However, MRI has several disadvantages, including long scan times, high costs, and limitations for patients with metal implants.

Computed tomography (CT)

CT uses X-rays to scan the body and quickly generate 3D cross-sectional images. It is particularly useful for imaging the chest, abdomen, and bones and plays a crucial role in emergency diagnoses. CT offers fast imaging and high spatial resolution, especially for bone and lung imaging, providing precise views of internal structures and lesions. However, it uses ionizing radiation, which can harm the body with frequent exposure, and it has lower soft tissue contrast.

Positron emission tomography (PET)

PET uses radioactive tracers to observe metabolic activity within the body and is often combined with CT (PET-CT) to provide both anatomical and functional information. PET is valuable for studying tumors, cardiovascular diseases, and neurological conditions, offering detailed insights into metabolism and function. However, it involves radiation exposure, has lower spatial resolution, and is expensive.

Ultrasound imaging

Ultrasound imaging uses high-frequency sound waves to generate real-time images, commonly used for examining fetuses, the heart, and abdominal organs. It is non-invasive, portable, cost-effective, and provides rapid imaging. However, the quality of ultrasound imaging depends on the operator's skill, and its resolution is lower than that of other imaging modalities. Additionally, ultrasound cannot penetrate gas or bone well, limiting its effectiveness in imaging deep tissues.

Single photon emission computed tomography (SPECT)

SPECT uses radioactive tracers to visualize blood flow or metabolic activity and is often employed in diagnosing heart disease and brain disorders. It provides functional and metabolic information and is usually combined with CT (SPECT-CT) for integrated imaging. However, SPECT has longer imaging times, lower resolution, and involves radioactive materials, which pose a risk of radiation exposure.

Optical coherence tomography (OCT)

OCT uses light waves to provide high-resolution imaging, primarily in ophthalmology and increasingly in cardiovascular fields. It offers excellent resolution for non-invasive tissue observation, especially in eye exams. However, its imaging depth is limited to superficial tissues, and it is relatively expensive. Additionally, motion can interfere with imaging quality.

Multimodal imaging in clinical scenarios

Various imaging modalities have their unique advantages and limitations, making them suitable for different medical scenarios. For example, brain tumor diagnosis is a key area for imaging technologies. A meta-analysis on the diagnostic value of PET/CT for brain tumors showed that PET, using high-efficiency tracers, provides valuable diagnostic information. The combination of PET/CT improves diagnostic accuracy and better delineates brain tumor boundaries, while MRI provides clear anatomical structure. Thus, PET/CT and MRI are often combined in brain tumor diagnostics to obtain more precise information [17]. At the same time, OCT plays an important role in early cancer detection [18]. While OCT has limitations in scanning deep tissue sites, its high resolution, superior to other technologies, makes it ideal for cancer screening. It is also used to guide biopsies, provide real-time feedback during surgeries, and monitor tumor responses to treatment.

As mentioned, single-modality imaging technologies have inherent limitations in providing comprehensive spatial, temporal, and functional information, making it difficult to fully capture tissue structure, function, and metabolic activity. Multimodal imaging technology addresses these limitations by fusing data from different modalities. In multimodal image fusion, combining the strengths of these imaging technologies provides more comprehensive and detailed diagnostic information. With continuous technological advancements, multimodal fusion can effectively enhance diagnostic accuracy and improve disease treatment outcomes.

In this section, we discuss some commonly used multimodal medical databases, including MIMIC-IV, Open-i, TCGA, the Cancer Imaging Archive, Open Access Series of Imaging Studies (OASIS), PhysioNet, and recent large-scale databases, such as MedTrinity-25M and CLIMB (Clinical Large-scale Integrative Multimodal Benchmark). These databases cover various data modalities—electronic health records (EHR), medical images, physiological signals (electrocardiogram, electroencephalogram), genomic data, pathological sections, radiology reports, and clinical records—providing researchers with rich multimodal information. They play an important role in clinical research, disease prediction, imaging genomics, and the development of AI-based diagnostic tools.

MIMIC-IV (https://physionet.org/content/mimiciv) primarily includes patient hospitalization data, diagnoses, EHR, vital signs, lab test results, and medical images, making it a crucial resource for clinical prediction and decision support systems [19]. Open-i (https://openi.nlm.nih.gov) is a platform for medical imaging and text integration, offering X-rays, CT, MRI images, and radiology reports, making it valuable for image-text joint learning [20].

TCGA (https://portal.gdc.cancer.gov) contains CT, MRI images, and genomic data for cancer patients, widely used in imaging genomics

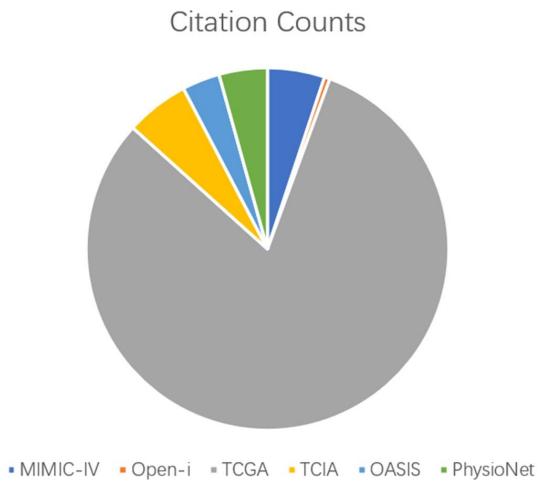

Figure 1. Citations of six databases in PubMed in the past five years.

research [21]. The Cancer Imaging Archive, (https://www.cancerimagingarchive.net) focuses on cancer-related medical imaging, providing high-quality pathology slides, CT, and MRI data to support tumor imaging analysis and radiation oncology research [22]. OASIS (https://www.oasis-brains.org) is dedicated to neuroimaging, containing MRI images and cognitive data from individuals with Alzheimer's disease and normal aging, offering significant value for brain structure research and cognitive disorder prediction [23]. PhysioNet Database (https://physionet.org) includes various physiological signals such as electrocardiogram, electroencephalogram, and cardiac ultrasound, combined with patient medical records, supporting cardiovascular disease research and the development of intelligent diagnostic systems [24].

MedTrinity-25M (https://huggingface.co/datasets/UCSC-VLAA/MedTrinity-25M) provides 25 million images across 10 imaging modalities (CT, MRI, ultrasound, gastroscopy, etc.), with fine-grained annotations for 65 types of lesions, ideal for cross-modal classification, segmentation, and report generation tasks [25].

CLIMB (https://github.com/DDVD233/climb) Integrates 2D images, 3D sequences, monitoring time series, physiological signals, EHR text, and brain network diagrams from 4.51 million patients (19TB of data), covering 96 clinical conditions and 13 fields, with a multi-task evaluation pipeline [26].

The establishment and sharing of these databases, along with advancements in AI and big data technologies, have significantly promoted the cross-modal integration of medical data. This has supported AI innovation in the medical field and fostered research in medical image analysis, intelligent diagnosis, and personalized treatment, etc. **Figure 1** shows the approximate citation counts of the first six databases mentioned above in PubMed, restricted to the past five years. This was achieved by searching for the keyword, such as "MIMIC-IV" in the PubMed database, within a five-year period. **Figure 2** shows several brain images from the OASIS database [27].

MMIF procedure

Multimodal medical image fusion usually involves several key steps. First, medical images from different modality sources undergo preprocessing, including denoising and normalization, to enhance the effect of subsequent processing. Next, image registration is conducted. The source image is aligned with the reference image, and this process is completed based on matched features to provide support for the subsequent fusion step [28]. Then, features are extracted from the image to capture the structural, textural, and functional features in images of different modalities. Finally, fusion rules are employed to highlight key information and features from sub-images, which support later stages of image reconstruction. Image fusion technique is applied by overlapping two input source images to produce a resultant image with excessive and complementary information [29]. Performance metrics are necessary to evaluate and validate the effectiveness of the selected fusion algorithm [30]. The overall MMIF procedure is shown in **Figure 3** [31].

Two prerequisites need attention in the image fusion step. First, all reasonably required medical information present in the input image must appear in the fused image. Second, the fused image should not contain information that is not present in the original input image. Fusion methods are applicable across multi-sensor images from diverse modalities, multi-focus images from the same modality, and are widely employed in multimodal medical images.

MMIF techniques

In MMIF, methods are generally divided into three categories: traditional methods, model-based methods, and learning-based meth-

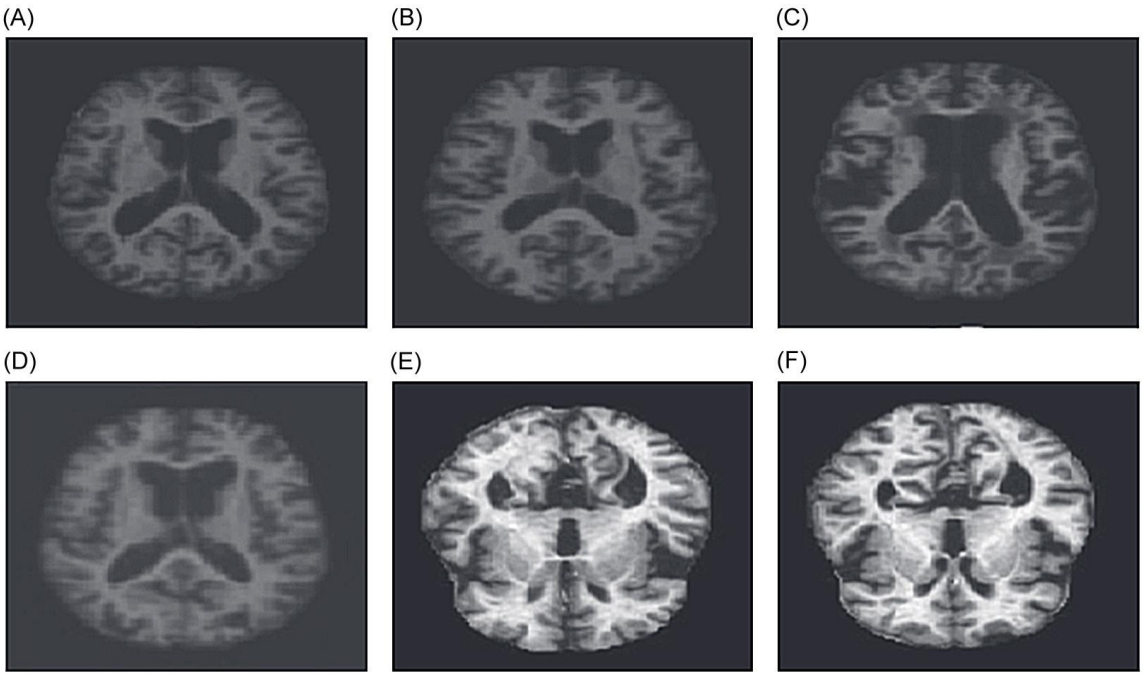

Figure 2. MRI images from OASIS dataset: (A) non-demented aging disease, (B) high-grade mild dementia, (C) mild dementia disease, (D) less extreme dementia disease, (E) Alzheimer's Disease, and (F) healthy control [26].

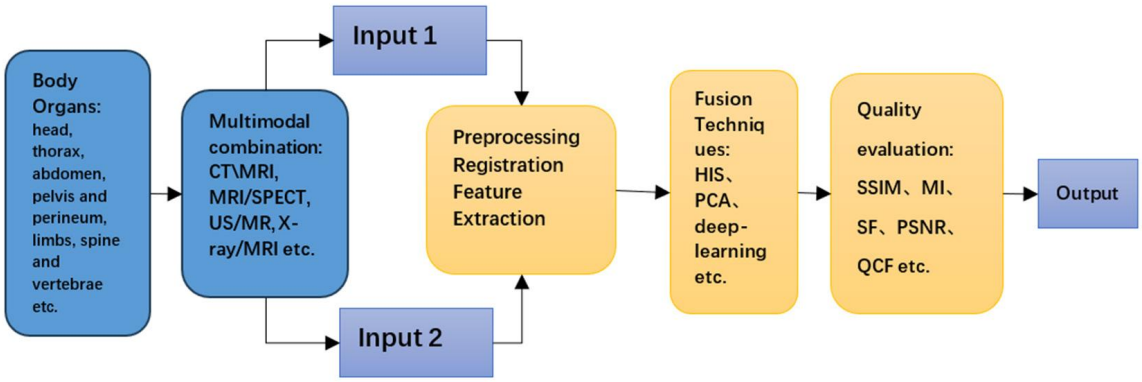

Figure 3. Overall multimodal medical fusion procedure.

ods. Below is a brief introduction to these approaches.

Traditional methods

Traditional methods primarily rely on classic image processing and analysis techniques, often using simple mathematical operations and transformations. Pixel-level fusion is the basic category within these methods, including techniques such as IHS (Intensity-Hue-Saturation) transformation, principal component analysis (PCA), and multi-resolution analysis techniques like Laplace pyramid, wavelet transform, and Contourlet transform [32]. Among these, IHS transformation, wavelet transform, and Laplacian pyramid fusion methods are particularly valuable in practice.

Pixel-level fusion methods combine images at the individual pixel level to make fusion decisions [33, 34]. Since this is applied directly to the initial images, the resulting images exhibit less spatial distortion and a lower signal-to-noise ratio (SNR). In the frequency domain method, images are first converted into the frequency domain using Fourier transform. The fusion process is then performed on the frequency components, followed by an inverse transformation to obtain the final fused image.

(A)

$$\begin{bmatrix} I_0 \\ v_1 \\ v_2 \end{bmatrix} = \begin{bmatrix} 1/3 & 1/3 & 1/3 \\ -\sqrt{2}/6 & -\sqrt{2}/6 & 2\sqrt{2}/6 \\ 1/\sqrt{2} & -1/\sqrt{2} & 0 \end{bmatrix} \begin{bmatrix} R_0 \\ G_0 \\ B_0 \end{bmatrix}$$

(B)

$$\begin{bmatrix} R_{new} \\ G_{new} \\ B_{new} \end{bmatrix} = \begin{bmatrix} 1 & -1/\sqrt{2} & 1/\sqrt{2} \\ 1 & -1/\sqrt{2} & -1/\sqrt{2} \\ 1 & \sqrt{2} & 0 \end{bmatrix} \begin{bmatrix} I_{new} \\ v_1 \\ v_2 \end{bmatrix}$$

Figure 4. Transformation formula: (A) RGB to IHS (B) corresponding inverse transformation.

The IHS method has garnered significant attention among traditional methods of MMIF due to its ability to control image details, simplicity in computation, suitability for real-time applications, and status as a classic technique in image fusion [35]. Below is a brief overview of this method.

IHS transformation is a color space conversion method primarily used to convert the RGB (Red-Green-Blue) color space into the IHS (Intensity-Hue-Saturation) color space. The core idea is to separate the image's color information (hue H, saturation S) from the brightness information (intensity I), allowing for independent processing of each component during image processing, ultimately enhancing the visual effect and information fidelity after fusion.

I represents the brightness or grayscale value of the image (the overall brightness of the color). H represents the type of color, such as red, green, or blue. S represents the purity of the color (the depth of the color). The mathematical equations for IHS transformation are as follows:

$$I = \frac{R + G + B}{3} \tag{1}$$

$$H = \arctan\left(\frac{\sqrt{3}(G - B)}{2R - G - B}\right) \tag{2}$$

$$S = 1 - \frac{\min(R, G, B)}{I} \tag{3}$$

Inverse transformation (from IHS back to RGB):

$$R = I + \mathrm{Scos}(H) \tag{4}$$

$$G = I + \mathrm{Scos}(H - 120^{\circ}) \tag{5}$$

$$B = I + \mathrm{Scos}(H + 120^{\circ}) \tag{6}$$

Figure 4 further shows the RGB-IHS transformation and its inverse transformation process in matrix form.

For instance, Sajid Ullah Khan et al. proposed a novel structural and spectral feature enhancement method in the NSST (Non-Subsampled Shearlet Transform) domain for MMIF [36]. In this domain, the image is decomposed into sub-bands of multiple scales and directions, enabling image processing operations at different scales and directions, such as image fusion, denoising, and feature extraction. First, two pairs of images are generated using the IHS method. The input image is then decomposed using the NSST to obtain low-frequency and high-frequency subbands. The proposed structural information (SI) fusion strategy is applied to the low-frequency subband (LFS), enhancing structural information such as texture and background. Next, PCA is used as the fusion rule for the high-frequency subband (HFS) to extract pixel-level information. Finally, the fused image is obtained through inverse NSST and IHS.

In medical imaging, PET displays metabolic changes in pseudo-color, while MRI provides anatomical structures in grayscale. The fusion of PET and MRI brain images creates a composite image that integrates anatomical structures with metabolic changes, helping doctors effectively diagnose potential diseases. Chen et al. proposed a new fusion method based on IHS and log-Gabor wavelet transform [37]. First, the intensity components of MR and PET images are decomposed using the log-Gabor wavelet transform at an appropriate decomposition scale. Then, a "maximum selection" fusion rule is applied to high-frequency subbands, while a two-stage fusion rule based on a weighted average scheme and visibility measure is used for low-frequency subbands. Finally, an inverse log-Gabor wavelet transform is applied to the fused high- and low-frequency subbands to

obtain new intensity components, along with the original hue and saturation components of the PET image, which are then transformed into a fused color image. This method effectively presents both anatomical structures and color changes, while significantly reducing color distortion.

Additionally, Mozhdeh Haddadpour et al. proposed another PET/MRI fusion technology based on the two-dimensional Hilbert transform (2-D HT) and the IHS method [38]. This approach aims to fuse the anatomical details of MRI images with high spatial resolution and the metabolic characteristics of PET images to facilitate more accurate and convenient clinical diagnosis and treatment. Both methods seek to maximize the preservation and enhancement of the spatial and spectral (functional) information from the input images, ultimately providing reliable support for clinical applications.

The IHS method, however, has several limitations: (i) Spectral Distortion: It may lose spectral information, especially in high-dimensional multispectral images. (ii) Non-linear Instability: It lacks stability for images with strong nonlinear characteristics. (iii) Color Distortion: Large color discrepancies between input images can cause color shifts after IHS fusion. To address these issues, researchers often integrate IHS with wavelet transforms, PCA, deep learning, and other techniques to improve fusion performance.

Model-based methods

Model-based methods use mathematical and statistical models to capture the characteristics of images, leading to more accurate fusion. Sparse representation fusion methods are widely used within this category. These methods assume that images can be represented by a small number of non-zero coefficients under a redundant dictionary. During the fusion process, a common dictionary is first learned, followed by sparse encoding of the source image. The sparse coefficients are then fused, and the fused image is reconstructed using the dictionary.

For example, PET and MRI images fused using the nonparametric Bayesian-based sparse representation (SR-NPB) technique outperformed three other sparse representation techniques—Traditional Sparse Representation (SR), Adaptive Sparse Representation (ASR), and Joint Sparse Representation (JSR)—in both visual and quantitative comparisons [39]. The new approach was also faster in execution, with experiments using 20 sets of PET and MRI scans. Bhardwaj et al. applied a fractional-order BSA (Bird Swarm Algorithm)-based Bayesian fusion strategy using the BRATS brain MRI dataset [40]. This method simplifies the fusion process by using wavelets generated from the original images using the HWT (Haar Wavelet Transform).

In Nayak's study, a bird swarm optimization (BSO) technique was used to develop a novel Bayesian fusion algorithm on the BRATS dataset [41]. The BSO, inspired by the flocking behavior of birds, optimizes the fusion process by simulating the cooperation and information sharing of birds during foraging and migration. This new medical image fusion scheme, BSO, demonstrated superior performance. Discrete wavelet transform was applied to images of different modalities, extracting decomposition coefficients from the four frequency bands: LL (low–low, capturing overall structure), LH (low–high, representing horizontal details), HL (high–low, representing vertical details), and HH (high–high, capturing diagonal details). Bayesian fusion theory, optimized by the BSO algorithm, effectively fused the feature information of different modalities, enhancing image directional sensitivity and reducing redundant coefficients. This method significantly improved the information richness and diagnostic value of the fused image.

In the study of multimodal medical image fusion, various algorithms and methods are constantly being proposed to improve fusion quality. For example, in the study by Das and Bhattacharya, researchers found that multiresolution wavelet decomposition provides more image information than single-resolution methods, particularly in image fusion and denoising [42]. Meanwhile, Li et al. proposed a medical image fusion approach based on joint low-rank and sparse decomposition with dictionary learning for image denoising and enhancement [43]. This method's dictionary learning model includes low-rank and sparse regularization terms, constructing the fused image by combining the low-rank and sparse

Table 2. Comparison of learning methods in multimodal medical image fusion

Method Category	Representative Models	Key Advantages	Typical Applications
Traditional ML Methods	SVM, RF, KNN, PCA	Interpretable, easy to implement, effective for small datasets	Early-stage studies, simple or low-noise image fusion
CNN-based Methods	U-Net, FusionNet	Preserves spatial and texture features, supports hierarchical learning	Fusion of structurally aligned images (e.g., CT+MRI)
GAN-based Methods	FusionGAN, CycleGAN	High-quality outputs, handles nonlinear relationships	High-detail, cross-modality image fusion (e.g., PET+MRI)
Autoencoder-based Methods	Fusion AE, VAE	Good for unsupervised learning, extracts latent representations	Fusion tasks with limited or no annotations
Hybrid Deep Models	Wavelet-CNN, SwinFusion	Multi-scale extraction, blends transform and deep features	Structural reconstruction, diagnosis-oriented fusion
Emerging Methods	Transformer-based	Strong global context modeling, adaptable across modalities	Large-scale fusion, complex multimodal integration

Note: Support vector machines (SVM), random forests (RF), K-nearest neighbors (KNN) and principal component analysis (PCA). Variational Autoencoder (VAE).

components of the source image, thereby improving image quality.

Learning-based methods

Learning-based MMIF methods use machine learning and deep learning techniques to learn features and patterns from large datasets for efficient image fusion. These methods can automatically extract complex features, offer strong generalization performance, and adapt flexibly to the fusion needs of different types of images. Prior to the widespread use of deep learning, traditional machine learning methods such as support vector machines, random forests, K-nearest neighbors and PCA were commonly used. These methods achieved effective information integration through statistical analysis, feature optimization, and pixel-level fusion strategies. However, as the complexity and dimensionality of medical imaging data grew significantly, traditional methods began to show limitations in feature representation and computational efficiency. This has driven the advancement of deep learning technology.

In recent years, deep learning has gained significant traction in fields like text processing, computer vision, and natural language processing, making MMIF more efficient and intelligent [44]. Deep learning techniques, such as convolutional neural networks (CNNs), generative adversarial networks (GANs), and autoencoders, have proven particularly effective. CNNs, such as FusionNet and U-Net, extract local features from medical images via multilayer convolution operations, making them highly suitable for fusion tasks like CT-MRI and PET-MRI [45-49]. GANs, such as FusionGAN and CycleGAN, generate realistic, detailed images through adversarial training, effectively addressing complex, nonlinear fusion challenges. Autoencoder frameworks, like Fusion Autoencoder and Variational Autoencoder, excel at latent feature extraction, compression, and high-quality reconstruction, particularly in unsupervised learning scenarios. Additionally, hybrid models like Wavelet-CNN combine traditional transform-domain techniques with deep learning for improved multi-scale feature extraction and enhanced fusion efficiency. Their characteristics and applicability are summarized in **Table 2**.

Li et al. introduced a novel deep learning architecture designed specifically for infrared and visible image fusion [50]. Unlike traditional convolutional networks, their encoding network consists of convolutional layers, fusion layers, and dense blocks, where the output of each layer connects to all other layers. This architecture aims to extract more useful features from source images during encoding and uses two fusion layers (fusion strategies) to merge these features. Finally, the decoder reconstructs the fused image, optimizing information integration before reconstruction and improving feature extraction during encoding.

To further enhance the detail quality and realism of the fused image, the Generative Adversarial Network (GAN) is used to achieve high-quality medical image fusion through

adversarial training between the generator and discriminator [45-48, 50-53].

Despite the impressive results achieved by current fusion methods, there are still areas for improvement. For example, GAN-based fusion of infrared and visible light images is time-consuming and lacks ground truth, making it difficult to design a comprehensive input for the discriminator to perform high-level tasks. Two existing solutions to this problem involve using visible images as references or learning a generative model through a dual-discriminator approach, where both infrared and visible images serve as input [54, 55]. To address these challenges, Hou et al. proposed a semantic segmentation-based infrared and visible light image fusion GAN (SSGAN) [56]. This method is a deep learning-based, end-to-end fusion network that does not require manual rule design. It uses semantic masks to separate images into foreground (salient semantic features) and background (fine texture details). The foreground represents salient semantic objects, while the background contains finer texture details. Distinct generator pathways extract the semantic features, while the discriminator combines the infrared foreground and visible background to generate images that preserve both semantic clarity and textural detail.

The instability of GANs has prompted the exploration of Transformer architectures. The Transformer's attention mechanism excels at capturing global multimodal relationships and has demonstrated great potential in accurately integrating cross-modal features. With its success in natural language processing and computer vision, researchers have started to explore its application in the field of medical image fusion.

Current fusion rules employed by convolution-based networks for multimodal medical image fusion are often not fine-grained enough. Deep learning-based methods generally concatenate source images or depth features from different modalities and input them into neural networks, which may lead to insufficient utilization of the source image information and limit the comprehensive use of available modalities. To address this, Zhang et al. proposed Transfusion, a transformer-based end-to-end medical image fusion framework [57]. This innovative framework incorporates the Transformer as a fusion strategy, utilizing its self-attention mechanism to integrate the global contextual information of multimodal features and fully fuse them. Additionally, the designed branch networks interact through multi-scale fusion transformers, enabling better utilization of information from different modalities.

Simultaneously, self-supervised learning (SSL) has been developing rapidly [58-62]. SSL does not require a large amount of manually annotated data but instead leverages the structural information within the data to train models and enhance cross-modal alignment and feature representation.

Fang et al. proposed a multimodal brain tumor segmentation framework that utilizes hybrid fusion of modality-specific features via a self-supervised learning strategy, employing fully convolutional networks [63]. Their multi-input architecture, along with the novel hybrid attention fusion scheme, learns independent features from multimodal data, adapts to varying numbers of multimodal inputs, and captures the correlation between them through the attention mechanism.

Inspired by contrastive learning, Zhang et al. developed an SSL framework based on contrastive autoencoding and convolutional information exchange for multimodal medical fusion tasks [64]. Since extracting features from source images in pairs often causes information redundancy, the researchers combined Transformers and CNNs in parallel as autoencoders. This combination preserves both global and local features based on prior knowledge and uses a contribution estimation model to assess the optimal fusion contribution of paired source images. The Transformer-CNN hybrid encoder and contribution estimation model treat paired source images as positive and negative results of reconstructed images, improving fusion quality by mitigating information redundancy through refined feature exchange.

Currently, self-supervised MMIF methods pretrain networks using large natural image datasets via the original image reconstruction task, then achieve image fusion by integrating fusion rules into the trained network. However, they often overlook the domain differences between

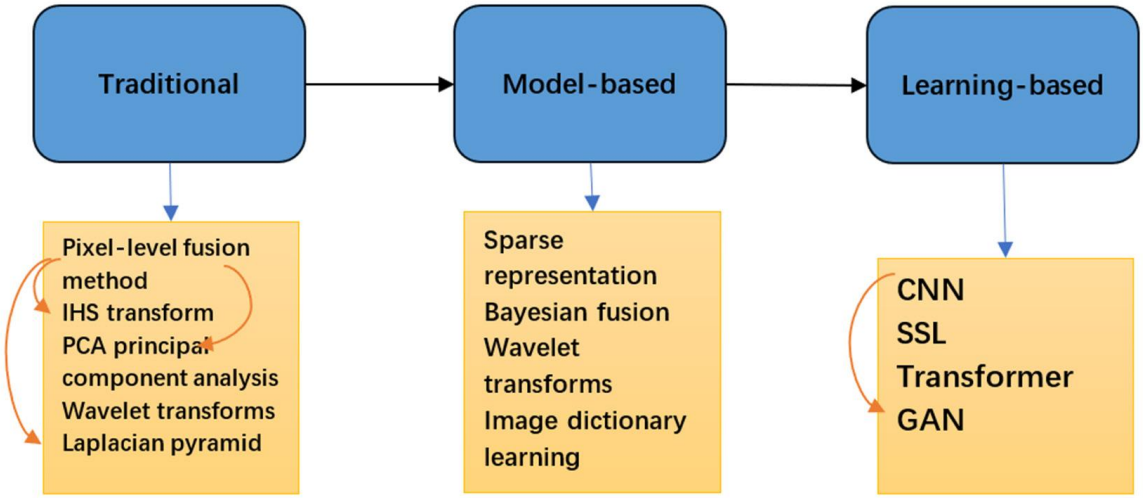

Figure 5. Three fusion approach categories: Traditional methods provide a foundation for model methods, which in turn provide a development foundation for learning methods. "Laplacian Pyramid", "IHS" and "PCA" are pixel-level fusion technologies; GAN is developed based on CNN.

the training and test data. Additionally, most existing MMIF methods are built upon traditional CNN architectures, limiting their ability to model long-range contextual relationships in the source modalities. To overcome this, Zhang et al. proposed a self-supervised transformer for MMIF [65]. Under this framework, random image super-resolution (RSR) is used to train the network. Both RSR and MMIF share similar multi-resolution inputs and objectives: image restoration and enhancement, which helps reduce domain discrepancies between the training and test data. Furthermore, a transformer-based fusion network is introduced to capture both local and global information from the source modalities. By leveraging RSR as a pretext task aligned with fusion objectives, this model reduces domain differences and effectively captures both global and local modality information.

In summary, image fusion methods can be classified into three categories: traditional methods, model-based methods, and learning-based methods. Each method has distinct characteristics and application scenarios, with developmental relationships among them. As shown in **Figure 5**, traditional image fusion methods (e.g., Laplacian pyramid, IHS transform, PCA) are primarily based on pixel-level operations or direct transform-domain processing, laying the theoretical and technical foundation for model-based methods. These model-based methods continue to evolve, ultimately driving the development of learning-based fusion technologies, with deep learning as the core. **Table 3** lists some fusion techniques.

With the continuous growth of medical imaging data and advancements in computing power, learning-based methods are moving toward smarter and more efficient solutions. Future research will likely focus on multimodal feature alignment across different domains, improving the interpretability of fusion methods, and leveraging large-scale pretrained medical imaging models. The development of these technologies will not only enhance diagnostic efficiency but also play a key role in areas such as telemedicine, disease detection, and personalized treatment.

Image fusion quality assessment metrics

The evaluation of MMIF quality is crucial to ensure that the fusion results meet clinical diagnostic needs. Fusion quality assessment methods are typically divided into two categories: subjective and objective evaluation [66]. Subjective evaluation, as the name suggests, relies on human judgment, often performed by clinical experts. It typically involves comparing the fused image with the original images to score the fusion result. The advantage of subjective evaluation is that it directly reflects the practical utility of the fused image and the observer's intuitive assessment. However, it has limitations, including dependence on per-

Table 3. Comparison of several methods

Method Name	Type	Advantages	Disadvantages	Computational Complexity	Image Quality
IHS	Traditional	Intuitive, low computational cost	Spectral loss, unstable for high dimensions	Low	Medium
PCA	Traditional	Dimensionality reduction, feature extraction	Color distortion, sensitive to noise	Medium	Medium
Wavelet Transform	Traditional	Multi-resolution, image detail preservation	High complexity, long processing time	High	High
GAN	Learning-based	High quality image generation, handles complex tasks	Unstable training, requires large data	High	High
CNN	Learning-based	Automatic feature extraction, strong recognition	High computational cost, long training	High	High
Transformer	Learning-based	Integrates multimodal data, self-attention mechanism	Long training, complex model	High	High
Sparse Representation	Model-based	Effective feature representation, robust to noise	Needs high-quality dictionary, complex computation	Medium	Medium

sonal experience and subjective judgment, variability between different observers, and being time-consuming, labor-intensive, and difficult to quantify. As a result, objective evaluation indicators are commonly introduced for automated and repeatable quality assessment. Objective evaluation analyzes the quality of the fused image from multiple perspectives by examining the statistical and structural features of both the fused and source/reference images.

Common objective evaluation indicators focus on different aspects, including the (SSIM), peak signal-to-noise ratio (PSNR), mutual information (MI) and cross entropy (CE).

(1) SSIM assesses the similarity of image structure, brightness, and contrast. Its value range is from 0 to 1, with 1 indicating that the structure of the fused image closely matches that of the original image. The formula is as follows:

$$SSIM(x,y) = \frac{(2\mu_x\mu_y + C_1)(2\sigma_{xy} + C_2)}{(\mu_x^2 + \mu_y^2 + C_1)(\sigma_x^2 + \sigma_y^2 + C_2)} \quad (7)$$

(2) PSNR measures the difference in pixel intensity between the fused image and the reference image. A higher PSNR value indicates better image quality, as it signifies a lower level of distortion between the fused and reference images. The formula is as follows:

$$PSNR = 10\log_{10}\left(\frac{MAX_I^2}{MSE}\right) \quad (8)$$

(3) MI measures the amount of information the fused image retains from the two source images. A larger MI value indicates that the fused image contains more of the original information. The formula is as follows:

$$MI(X,Y) = \sum_{x,y} p(x,y)\log\frac{p(x,y)}{p(x)p(y)} \quad (9)$$

(4) CE evaluates the similarity between the light intensity distribution of the fused image and the source image. A smaller cross-entropy value indicates less information loss [67].

In general, the above objective indicators can quantify fusion quality to some extent, but each focuses on different aspects, making it challenging to fully capture the subjective quality evaluation criteria of the human eye. To improve the consistency between objective evaluation and human perception, recent research has proposed enhanced fusion quality assessment methods. For instance, Wang et al. proposed a super-pixel-level structural similarity evaluation index system [68]. This method first performs superpixel segmentation on the image, dividing it into smaller areas that are perceptually uniform. It then extracts features from the source and fused images within the corresponding superpixel areas to calculate regional structural similarity. This approach helps reduce errors caused by direct pixel comparison of images from different modalities, enabling a more accurate assessment of how well the fused

image retains the source image's structural information. Compared to traditional pixel-by-pixel SSIM, the superpixel-based evaluation is less sensitive to registration errors and offers greater accuracy in fusion quality assessment.

In the future, by integrating human visual perception models with artificial intelligence technologies, fusion quality evaluation methods will more accurately and comprehensively reflect the strengths and weaknesses of fusion results, providing stronger support for the advancement of MMIF technology.

Discussion

MMIF effectively integrates complementary features from different imaging modalities, overcoming the limitations of single-modality imaging and enhancing diagnostic accuracy. Initially, traditional fusion techniques dominated, focusing mainly on spatial and frequency domain methods. However, these methods have limitations in preserving information and accurately representing key diagnostic features. As a result, model-based methods gradually became mainstream, offering greater flexibility and robustness in processing complex image data and integrating probabilistic information, thereby improving diagnostic accuracy.

In recent years, deep learning methods have driven further progress in MMIF. Architectures based on CNNs, GANs, and Transformers have significantly improved MMIF performance with their powerful feature extraction and adaptive learning capabilities. CNNs excel in capturing multi-scale features through their hierarchical learning structure. GANs enhance fusion quality by synthesizing high-fidelity images, bridging modality differences, and improving visual clarity. Transformers, known for their excellent feature extraction and global context modeling, handle long-range dependencies and enhance modality alignment.

Despite the ongoing development of MMIF techniques, challenges remain, including addressing cross-modality differences, optimizing algorithms for efficiency, and achieving clinical applicability. Continued research is crucial for improving these technologies, optimizing fusion performance, and ultimately enabling clinical application.

Looking ahead, MMIF technology holds broad application potential. Possible future development directions include:

• Improving interpretability is key to enhancing user trust and optimizing clinical decision-making. With growing demands for transparency in AI products, enhancing the interpretability of deep learning models is crucial for clinical decision support. Future developments should focus on explaining model decisions. For instance, incorporating attention mechanisms could highlight specific regions of medical images prioritized during fusion, providing visual cues for clinicians. Additionally, feature visualization techniques (e.g., Grad-CAM or saliency maps) could be used to display internal feature representations, clarifying how the model processes multimodal data.

• Future research should aim to improve fusion accuracy by addressing modality differences, enhancing feature alignment, and reducing information redundancy. Researchers could design custom loss functions (e.g., mutual information-based or redundancy-penalizing losses) to minimize overlapping or irrelevant information during fusion.

• The focus is on developing computationally efficient and lightweight models for clinical usability. However, bottlenecks such as high computational complexity, slow inference speed, and resource-intensive models limit real-time clinical applications. Researchers should consider applying model compression techniques, such as pruning (removing redundant neurons) and quantization (reducing weight precision), to create lightweight models without compromising accuracy. Additionally, utilizing advanced hardware or optimizing algorithms with efficient convolution operations and approximate complex functions can help, with custom implementations tailored to clinical hardware limitations.

• To address data scarcity and labeling costs, self-supervised learning and synthetic data augmentation methods are increasingly employed, enabling robust model training without large labeled datasets. For example, self-supervised learning can be used to pre-train a model on an unlabeled multimodal dataset and then fine-tune it on a smaller labeled dataset.

• Research should focus on developing general models that can adapt to various medical imaging modalities and clinical scenarios. This includes applying transfer learning to adapt pre-trained models to new modalities and developing multi-task learning frameworks to enhance the adaptability and versatility of MMIF models.

Overall, continuous innovation and interdisciplinary collaboration are crucial to advancing multimodal medical image fusion technology. Combining medical image fusion technology with genomics, physiological signal monitoring and big data analysis will further promote the implementation of personalized diagnosis and treatment strategies, achieve early diagnosis and precise treatment of diseases, and significantly improve the accuracy of clinical diagnosis and the efficiency of medical decision-making.

Conclusion

The rapid advancement of multimodal image fusion technology has greatly benefited the medical field and human well-being. This paper summarizes the evolution of MMIF technology, beginning with an introduction to mainstream imaging technologies, followed by an analysis of the advantages and limitations of single-modality technologies. It then introduces multimodal image fusion technology, followed by an overview of three MMIF methods: traditional methods, model-based methods, and learning-based methods, with a particular focus on the application of deep learning in recent years. Finally, performance evaluation indicators for multimodal fusion are analyzed, and suggestions for future research directions are provided.

Author contributions: Zhaopeng Zhou: Provide medical theory background support, guide research direction, and participate in discussions on review framework and writing details. Miao Zhou: Provide medical theory background support, participate in the discussion of the review framework and writing details. Wenhui Guo: Guide the overall conception of the review and preside over the revision of the paper. Yongchu Hu: Responsible for the overall conception and review of the paper, and complete the revision and finalization of the paper.

References

[1] George ASH, Shahul A, George AS. Artificial Intelligence in Medicine: A New Way to Diagnose and Treat Disease. Partn Univers Int Res J 2023;2(3):246-259.

[2] Caraiani C, Dong Y, Rudd AG, et al. Reasons for inadequate or incomplete imaging techniques. Med Ultrason 2018;20(4):498-507.

[3] Huang B, Yang F, Yin M, et al. A Review of Multimodal Medical Image Fusion Techniques. Comput Math Methods Med 2020;2020:8279342.

[4] Karim S, Tong G, Li J, et al. Current advances and future perspectives of image fusion: A comprehensive review. Inform Fusion 2023; 90:185-217.

[5] Du J, Li W, Lu K, et al. An overview of multimodal medical image fusion. Neurocomputing 2016;215:3-20.

[6] Sossi V. Multi-modal Imaging and Image Fusion. In: Kiessling F, Pichler BJ, editors. Small Animal Imaging: Basics and Practical Guide. Berlin, Heidelberg. Springer Berlin Heidelberg, 2011. p. 293-314.

[7] Li Y, El Habib Daho M, Conze PH, et al. A review of deep learning-based information fusion techniques for multimodal medical image classification. Comput Biol Med 2024;177:108635.

[8] Haribabu M, Guruviah V, Yogarajah P. Recent Advancements in Multimodal Medical Image Fusion Techniques for Better Diagnosis: An Overview. Curr Med Imaging 2023;19(7):673-694.

[9] Werner P, Barthel H, Drzezga A, et al. Current status and future role of brain PET/MRI in clinical and research settings. Eur J Nucl Med Mol Imaging 2015;42(3):512-526.

[10] Wang SY, Chen XX, Li Y, et al. Application of Multimodality Imaging Fusion Technology in Diagnosis and Treatment of Malignant Tumors under the Precision Medicine Plan. Chin Med J (Engl) 2016;129(24):2991-2997.

[11] Schwenck J, Sonanini D, Cotton JM, et al. Advances in PET imaging of cancer. Nat Rev Cancer 2023;23(7):474-490.

[12] Hussain S, Mubeen I, Ullah N, et al. Modern Diagnostic Imaging Technique Applications and Risk Factors in the Medical Field: A Review. Biomed Res Int 2022;2022:5164970.

[13] Fendler WP, Eiber M, Beheshti M, et al. PSMA PET/CT: joint EANM procedure guideline/SNMMI procedure standard for prostate cancer imaging 2.0. Eur J Nucl Med Mol Imaging 2023;50(5):1466-1486.

[14] Crişan G, Moldovean-Cioroianu NS, Timaru DG, et al. Radiopharmaceuticals for PET and SPECT Imaging: A Literature Review over the Last Decade. Int J Mol Sci 2022;23(9):5023.
[15] Greffier J, Villani N, Defez D, et al. Spectral CT imaging: Technical principles of dual-energy CT and multi-energy photon-counting CT. Diagn Interv Imaging 2023;104(4):167-177.
[16] Piovesan A, Vancauwenberghe V, Van De Looverbosch T, et al. X-ray computed tomography for 3D plant imaging. Trends Plant Sci 2021;26(11):1171-1185.
[17] Treglia G, Muoio B, Trevisi G, et al. Diagnostic Performance and Prognostic Value of PET/CT with Different Tracers for Brain Tumors: A Systematic Review of Published Meta-Analyses. Int J Mol Sci 2019;20(19):4669.
[18] Wang J, Xu Y, Boppart SA. Review of optical coherence tomography in oncology. J Biomed Opt 2017;22(12):1-23.
[19] Johnson AEW, Bulgarelli L, Shen L, et al. MIMIC-IV, a freely accessible electronic health record dataset. Sci Data 2023;10(1):1.
[20] Demner-Fushman D, Antani S, Chachra S, et al. Open-i: Imaging, informatics, natural language processing, and multi-modal information retrieval. 2016.
[21] Liñares-Blanco J, Pazos A, Fernandez-Lozano C. Machine learning analysis of TCGA cancer data. PeerJ Comput Sci 2021;7:e584.
[22] Clark K, Vendt B, Smith K, et al. The Cancer Imaging Archive (TCIA): maintaining and operating a public information repository. J Digit Imaging 2013;26(6):1045-1057.
[23] Marcus DS, Wang TH, Parker J, et al. Open Access Series of Imaging Studies (OASIS): cross-sectional MRI data in young, middle aged, nondemented, and demented older adults. J Cogn Neurosci 2007;19(9):1498-1507.
[24] Jiang S, Ashar P, Shandhi MMH, et al. Demographic reporting in biosignal datasets: a comprehensive analysis of the PhysioNet open access database. Lancet Digit Health 2024; 6(11):e871-e878.
[25] Xie Y, Zhou C, Gao L, et al. MedTrinity-25M: A Large-scale Multimodal Dataset with Multigranular Annotations for Medicine. ArXiv 2025; arXiv:2408.02900.
[26] Dai W, Chen P, Lu M, et al. CLIMB: Data Foundations for Large Scale Multimodal Clinical Foundation Models. ArXiv 2025;arXiv:2503.07667.
[27] Azam MA, Khan KB, Aqeel M, et al. Analysis of the MIDAS and OASIS Biomedical Databases for the Application of Multimodal Image Processing. Intell Technol Appl 2020;581-592.
[28] Mohammed HA. The image registration techniques for medical imaging (MRI-CT). Am J Biomed Eng 2016;6(2):53-58.
[29] El-Gamal FE-ZA, Elmogy M, Atwan A. Current trends in medical image registration and fusion. Egypt Inf J 2016;17(1):99-124.
[30] Princess MR, Kumar VS, Begum M. Comprehensive and Comparative Study of Different Image Fusion Techniques. Int J Adv Res Electr, Electron Instrum Energy 2014;3:11800-11806.
[31] Azam MA, Khan KB, Salahuddin S, et al. A review on multimodal medical image fusion: Compendious analysis of medical modalities, multimodal databases, fusion techniques and quality metrics. Comput Biol Med 2022;144: 105253.
[32] Kaur H, Koundal D, Kadyan V. Image Fusion Techniques: A Survey. Arch Comput Method E 2021;28(7):4425-4447.
[33] Daniel E. Optimum Wavelet-Based Homomorphic Medical Image Fusion Using Hybrid Genetic–Grey Wolf Optimization Algorithm. IEEE Sens J 2018;18(16):6804-6811.
[34] Li S, Kang X, Fang L, et al. Pixel-level image fusion: A survey of the state of the art. Information Fusion 2017;33:100-112.
[35] Basu S, Singhal S, Singh D. A Systematic Literature Review on Multimodal Medical Image Fusion. Multimed Tools Appl 2024;83(6):15845-15913.
[36] Khan SU, Khan F, Ullah S, et al. Multimodal medical image fusion in NSST domain with structural and spectral features enhancement. Heliyon 2023;9(6):e17334.
[37] Chen CI. Fusion of PET and MR Brain Images Based on IHS and Log-Gabor Transforms. IEEE Sens J 2017;17(21):6995-7010.
[38] Haddadpour M, Daneshvar S, Seyedarabi H. PET and MRI image fusion based on combination of 2-D Hilbert transform and IHS method. Biomed J 2017;40(4):219-225.
[39] Shabanzade F, Khateri M, Liu Z. MR and PET Image Fusion Using Nonparametric Bayesian Joint Dictionary Learning. IEEE Sens Lett 2019;3(7):1-4.
[40] Bhardwaj J, Nayak A. Haar wavelet transform-based optimal Bayesian method for medical image fusion. Med Biol Eng Comput 2020; 58(10):2397-2411.
[41] Nayak A, Bhardwaj J. Discrete Wavelet Transform and Bird Swarm Optimized Bayesian Multimodal Medical Image Fusion. Helix 2020; 10(01):7-12.

[42] Arpita D, Bhattacharya M. Evolutionary algorithm based automated medical image fusion technique: Comparative study with fuzzy fusion approach. 2009 World Congress on Nature & Biologically Inspired Computing (NaBIC) 2009; 269-274.
[43] Li H, He X, Tao D, et al. Joint medical image fusion, denoising and enhancement via discriminative low-rank sparse dictionaries learning. Pattern Recognit 2018;79:130-146.
[44] LeCun Y, Bengio Y, Hinton G. Deep learning. Nature 2015;521(7553):436-444.
[45] Bhatnagar G, Wu QMJ, Liu Z. Directive Contrast Based Multimodal Medical Image Fusion in NSCT Domain. IEEE Trans Multimedia 2013; 15(5):1014-1024.
[46] Gupta J, Pathak S, Kumar G. Deep Learning (CNN) and Transfer Learning: A Review. Journal of Physics: Conference Series 2022;2273(1): 012029.
[47] Salehi AW, Khan S, Gupta G, et al. A study of CNN and transfer learning in medical imaging: Advantages, challenges, future scope. Sustainability 2023;15(7):5930.
[48] Bhatt D, Patel C, Talsania H, et al. CNN variants for computer vision: History, architecture, application, challenges and future scope. Electronics 2021;10(20):2470.
[49] Liu JM, Sun HM, Katto J. Learned image compression with mixed transformer-cnn architectures. ArXiv 2023;arXiv:2303.14978.
[50] Li H, Wu XJ. DenseFuse: A Fusion Approach to Infrared and Visible Images. IEEE Trans Image Process 2019;28(5):2614-2623.
[51] Karthika S, Durgadevi M. Generative Adversarial Network (GAN): a general review on different variants of GAN and applications. 2021 6th International Conference on Communication and Electronics Systems (ICCES) 2021;1-8.
[52] Andresini G, Appice A, De Rose L, et al. GAN augmentation to deal with imbalance in imaging-based intrusion detection. Future Gener Comp Syst 2021;123:108-127.
[53] Lim W, Yong KSC, Lau BT, et al. Future of generative adversarial networks (GAN) for anomaly detection in network security: A review. Comput Secur 2024;139:103733.
[54] Ma J, Yu W, Liang P, et al. FusionGAN: A generative adversarial network for infrared and visible image fusion. Inform Fusion 2019;48:11-26.
[55] Ma J, Xu H, Jiang J, et al. DDcGAN: A Dual-Discriminator Conditional Generative Adversarial Network for Multi-Resolution Image Fusion. IEEE Trans Image Process 2020;29:4980-4995.
[56] Hou J, Zhang D, Wu W, et al. A Generative Adversarial Network for Infrared and Visible Image Fusion Based on Semantic Segmentation. Entropy 2021;23:376.
[57] Zhang J, Liu A, Wang D, et al. Transformer-Based End-to-End Anatomical and Functional Image Fusion. IEEE Trans Instrum Meas 2022;71:1-11.
[58] Zhai X, Oliver A, Kolesnikov A, et al. S4L: Self-Supervised Semi-Supervised Learning. 2019 IEEE/CVF International Conference on Computer Vision (ICCV) 2019;1476-1485.
[59] Liu X, Zhang F, Hou Z, et al. Self-Supervised Learning: Generative or Contrastive. IEEE Trans Knowl Data Eng 2023;35(1):857-876.
[60] Jaiswal A, Babu AR, Zadeh MZ, et al. A survey on contrastive self-supervised learning. Technologies 2020;9(1):2.
[61] Hendrycks D, Mazeika M, Kadavath S, et al. Using Self-Supervised Learning Can Improve Model Robustness and Uncertainty. ArXiv 2019;arXiv:1906.12340.
[62] Chen T, Kornblith S, Swersky K, et al. Big self-supervised models are strong semi-supervised learners. Adv Neural Inf Process Syst 2020;33:22243-22255.
[63] Fang F, Yao Y, Zhou T, et al. Self-Supervised Multi-Modal Hybrid Fusion Network for Brain Tumor Segmentation. IEEE J Biomed Health Inf 2022;26(11):5310-5320.
[64] Zhang Y, Nie R, Cao J, et al. Self-Supervised Fusion for Multi-Modal Medical Images via Contrastive Auto-Encoding and Convolutional Information Exchange. IEEE Comput Intell Mag 2023;18(1):68-80.
[65] Zhang J, Liu Y, Liu A, et al. Multimodal Image Fusion via Self-Supervised Transformer. IEEE Sens J 2023;23(9):9796-9807.
[66] Xun S, Li Q, Liu X, et al. Charting the path forward: CT image quality assessment - an in-depth review. J King Saud Univ-Com 2025; 37(5):92.
[67] Mao A, Mohri M, Zhong Y. Cross-Entropy Loss Functions: Theoretical Analysis and Applications. Proceedings of the 40th International Conference on Machine Learning 2023;202: 23803-23828.
[68] Wang E, Yang B. Superpixel-level Structural Similarity Metric for Image Fusion Quality Assessment. 2020 7th International Conference on Information Science and Control Engineering (ICISCE) 2020;1371-1376.

Perioperative Precision Medicine
ISSN: 2957-5443

Zentime

Review Article https://doi.org/10.61189/167468gjipte

Research progress of bone marrow mesenchymal stem cells in the treatment of acute liver failure

Huan Li[1,2], Xiaoyu Tang[1,2], Jiameng Liu[1,2], Wanning Li[1,2], Xin Niu[1,2], Xingchen Yue[1,2], Shangping Fang[1,2]

[1]School of Anesthesiology, Wannan Medical College, Wuhu 241002, Anhui Province, China. [2]Anesthesia Laboratory and Training Center, Wannan Medical College, Wuhu 241002, Anhui Province, China.

Corresponding author: Shangping Fang.

Acknowledgement: This work was supported by Key Project Research Fund of Wannan Medical College (WK2022Z10); Anhui Province College Student Innovation and Entrepreneurship Training Program Project (S202410368031); Anhui Province College Student Innovation Training Program Project (S202510368032).

Declaration of conflict of interest: None.

Received April 15, 2025; Accepted July 25, 2025; Published December 31, 2025

Highlights

- This review focuses on the research of bone marrow mesenchymal stem cells (BM-MSCs) in treating acute liver failure (ALF).
- BM-MSCs are a heterogeneous subset of stromal stem cells that can be isolated from various adult tissues.
- BM-MSCs have the ability to migrate toward damaged tissues and differentiate into hepatocytes. They effectively suppress pro-inflammatory cytokine release and promote hepatocyte proliferation.
- BM-MSCs are a promising target for clinical treatment of acute liver failure.
- BM-MSCs provide a new therapeutic direction for patients with acute liver failure during the perioperative period.

Abstract

Acute liver failure (ALF) is a severe hepatic injury characterized by rapid progression and multifactorial etiology. Clinical manifestations predominantly include severe gastrointestinal symptoms, altered consciousness, coagulopathy, jaundice, and hepatic encephalopathy. Currently, no specific pharmacological agents or established therapeutic regimens exist for ALF. While liver transplantation remains the primary clinical intervention, its application is limited by the shortage of donors. Advances in medical technology and research have led to accumulating experimental evidence suggesting that mesenchymal stem cells (MSCs) can alleviate liver inflammation, improve hepatic histology and function, and enhance survival rates in ALF. MSCs have advanced to clinical trials, with ongoing exploration into the mechanisms underlying their efficacy, highlighting their substantial potential in regenerative medicine. In the future, BM-MSCs may become an important treatment option for patients with acute liver failure during the perioperative period. This review provides a comprehensive overview of the therapeutic mechanisms and key findings associated with stem cells, particularly BM-MSCs, in the treatment of ALF.

Keywords: Acute liver failure, mesenchymal stem cells, therapeutics

Introduction

Acute liver failure (ALF) is a severe hepatic injury caused by factors such as drugs, hepatotoxic substances, viruses, and alcohol, characterized by extensive hepatocyte death and rapid deterioration of liver function. Clinical manifestations include hepatic encephalopathy, intracranial hypertension, infections, coagulation disorders, and hemorrhage. Without timely intensive care or liver transplantation, ALF can lead to multiple organ failure and death [1]. Allogeneic

Address correspondence to: Shangping Fang, Anaesthesiology Experimental Training Center, College of Anesthesiology, Wannan Medical College, No. 22 Wenchang West Road, Yijiang District, Wuhu 241002, Anhui Province, China. Tel: +86-19855362767. E-mail: fangshangping0@163.com.

Table 1. MSCs from different sources

Feature	BMSCs	UCMSCs	ADSCs	hPMSCs
Full Name	Bone Marrow Mesenchymal Stem Cells	Umbilical Cord Mesenchymal Stem Cells	Adipose-Derived Mesenchymal Stem Cells	Human Placental Mesenchymal Stem Cells
Source	Bone Marrow	Umbilical Cord	Adipose Tissue	Placenta
Immunogenicity	Low (potential for mild rejection in allogeneic transplantation)	Very low	No rejection in autologous transplantation	Low
Immunomodulation	Suppresses inflammation via HO-1 and inhibits pyroptosis via IL-10	Significantly mitigates inflammatory responses and modulates macrophage polarization	Suppresses excessive immune responses and ameliorates the inflammatory microenvironment	Not reported
Paracrine Factors	HO-1 activates autophagy	Highly secretes HGF to promote hepatic regeneration	Secretes growth factors promoting angiogenesis	Improves liver function indicators
Differentiation Potential	Multipotent differentiation	Multipotent differentiation (notably strong hepatic differentiation potential)	Multipotent differentiation (moderate hepatic differentiation capacity)	Exhibits prominent anti-fibrotic differentiation potential
Clinical Accessibility	Invasive harvesting, slow expansion kinetics, high cost	Non-invasive source, high yield, rapid expansion	Minimally invasive harvesting, high yield	Non-invasive source

Note: HO-1, heme oxygenase 1; IL-10, Interleukin-10; HGF, hepatocyte growth factor.

liver transplantation remains the only effective treatment for liver failure; however, alternative therapies are urgently needed due to the severe shortage of donors [2]. Numerous studies have shown that transplantation of hepatic stem cells or pluripotent stem cell-derived hepatocyte-like cells in experimental liver disease models can lead to liver repopulation by donor cells and improved survival rates [3].

Mesenchymal stem cells (MSCs) are a heterogeneous subset of stromal stem cells that can be isolated from various adult tissues. MSCs interact with both the innate and adaptive immune systems, modulating effector functions [4]. A growing body of animal studies suggests that MSCs significantly mitigate acute liver injury in ALF through their migratory capacity, hepatogenic differentiation potential, immunomodulatory effects, and paracrine actions [5]. Due to their ability to migrate to injured tissues, differentiate into hepatocytes, suppress inflammatory cytokine release, and promote hepatocyte proliferation, MSCs have emerged as a key focus of research in ALF treatment [6]. The specific characteristics of mesenchymal stem cells from different sources are shown in **Table 1**.

Clinical challenges in allogeneic liver transplantation for ALF

Determining the suitability of allogeneic liver transplantation for ALF presents significant clinical challenges, primarily in the timely identification of transplant indications and contraindications. A critical challenge is precise indication assessment, requiring clinical evaluation to confirm irreversible hepatic injury and distinguish reversible from irreversible etiologies. The latter, characterized by extensive hepatocyte necrosis without regenerative potential, typically necessitates urgent transplantation [7]. While established prognostic scoring systems such as the Model for End-Stage Liver Disease (MELD) help identify patients at highest mortality risk, their predictive accuracy remains limited [2]. Furthermore, the dynamic assessment of contraindications is challenging: absolute contraindications must be rigorously excluded, while managing relative contraindications (e.g., advanced age) requires highly individualized evaluation [3, 8]. The clinical complexity is compounded by the potential for rapid deterioration within hours, necessitating continuous monitoring and dynamic reassessment of transplant eligibility. Additionally,

establishing transplant criteria in special populations is significantly influenced by distinct etiological profiles. Post-transplant outcomes exhibit substantial heterogeneity among these subgroups, even after successful transplantation. A particularly salient challenge is pediatric ALF, especially cases triggered by specific metabolic disorders (e.g., mitochondrial hepatopathies) [6, 9]. Evidence from large registries like the European Liver Transplant Registry (ELTR) indicates significantly reduced long-term survival in these children compared to adult ALF recipients or pediatric patients transplanted for more common metabolic indications [10]. This underscores the unique clinical challenges and heightened post-transplant management requirements associated with metabolic etiologies in pediatric ALF.

Advances in the mechanisms underlying bone marrow-derived mesenchymal stem cell (BMSC) therapy for ALF

BMSCs were first identified in adult mouse bone marrow by Friedenstein AJ et al. during in vitro colony assays in 1976. Recent studies have demonstrated their self-renewal, multipotent differentiation, low immunogenicity, and immunomodulatory functions. BMSCs have recently been applied in clinical trials, while the underlying mechanisms of their efficacy are being extensively investigated [11].

BMSCs ameliorate ALF via modulation of autophagy through the HO-1/PI3K/AKT signaling pathway

Heme oxygenase-1 (HO-1) is an inducible enzyme with anti-apoptotic and immunomodulatory properties [12]. Autophagy, a conserved intracellular catabolic process, may be a critical pathway in MSC-mediated therapy for ALF. Zhang et al. isolated and cultured BMSCs from Sprague-Dawley rats [13]. ALF-induced rats were treated with BMSCs, an HO-1 inducer, or an HO-1 activity inhibitor, followed by assessment of hepatic injury markers and HO-1 activity. The results demonstrated that MSC treatment significantly upregulated HO-1 expression while reducing serum levels of alanine aminotransferase (ALT), aspartate aminotransferase (AST), and total bilirubin (TBIL). In contrast, pharmacological inhibition of HO-1 attenuated the therapeutic efficacy of MSCs and suppressed hepatocellular autophagy. These findings suggest that BMSCs ameliorate ALF through HO-1 upregulation-dependent mechanisms [14]. Wang et al. transplanted BMSCs into D-galactosamine-induced ALF rats. Pharmacological inhibition studies revealed that BMSCs alleviated ALF through HO-1 upregulation, wherein HO-1 activated autophagy via the PI3K/AKT signaling pathway [15]. Amiri F et al. intravenously administered autophagy-impaired BMSCs to mice with ALF [16]. The autophagy-modulated MSC transplantation group exhibited significantly reduced hepatic enzyme activity and lower necrotic scores compared to sham-operated controls (receiving no cell therapy). At 72 hours post-transplantation, mice receiving autophagy-inhibited MSCs demonstrated restoration of hepatic enzyme levels to baseline values. These data indicate that autophagy inhibition in BMSCs enhances their paracrine-mediated hepatic regenerative potential, suggesting a novel strategy to optimize cell-based therapy for ALF [16]. MSCs possess remarkable metabolic and functional supportive capacities in inflammatory diseases [17].

BMSCs mitigate inflammatory responses in ALF through modulation of underlying immune mechanisms

NOD-like receptor protein 3 (NLRP3) plays a pivotal role in inflammatory and immune responses. Wang et al. administered exogenous recombinant rat interleukin (IL)-10, small interfering RNA (siRNA), and the NLRP3 inhibitor MCC950 to mice, demonstrating that either IL-10 injection or BMSC transplantation ameliorated elevated total bilirubin, NH3, inflammatory cytokines, and related enzymes in ALF, suggesting that IL-10 secreted by BMSCs alleviates ALF through inflammasome suppression [18]. Wang JL et al. assessed hepatocyte proliferation using immunohistochemical (IHC) staining, examined key Wnt signaling proteins and cell surface factor expression, and employed IL-4 silencing to explore IL-4's role in BMSC bioactivity [18]. Results indicated that BMSCs ameliorate ALF through IL-4-dependent macrophage polarization toward the M2 anti-inflammatory phenotype [19]. Jiang et al. inhibited the PI3K/AKT/mTOR signaling pathway in vitro with the specific inhibitor LY294002, followed by intravenous BMSC administration into rats

to observe transdifferentiation dynamics [20]. BMSCs migrated to intestinal injury sites and transdifferentiated into intestinal epithelial cells. Compared to the ALF control group, this treatment significantly reduced intrahepatic pro-inflammatory cytokine levels. Additionally, intestinal permeability, mortality rates, and histopathological lesions in the gut were markedly reduced. These findings suggest that BMSC transplantation may serve as a potential therapeutic candidate for endotoxemia in ALF [20]. High mobility group box chromosomal protein 1is a crucial proinflammatory molecule in various inflammatory diseases. Wang et al. demonstrated that soluble receptor for advanced glycation end-products (sRAGE) administration significantly prolonged survival time, improved liver function, reduced inflammatory cytokine levels, and mitigated hepatocyte necrosis in ALF rats [21]. Xiu et al. revealed that CXCR4 overexpression in BMSCs enhanced their migration capacity through PI3K/Akt signaling pathway activation downstream of CXCR4, elucidating the molecular mechanisms and providing novel insights for the clinical application of BMSCs in ALF treatment [22].

Interaction between HO-1 and NLRP3

In ALF, HO-1 (heme oxygenase-1) and the NLRP3 inflammasome are closely interconnected through oxidative stress, endotoxemia, and inflammatory cascades, jointly participating in the pathological process of ALF. HO-1 inhibits NLRP3 activation [23]. The HO-1 metabolic product, carbon monoxide, inhibits NLRP3 inflammasome assembly, while bilirubin inhibits NLRP3 ubiquitination, reducing its binding efficiency with the adaptor protein. In experiments using BMSCs to treat ALF, high HO-1 expression significantly reduced NLRP3 activity [24]. The integrative role of autophagy: HO-1-induced autophagy can selectively degrade NLRP3 inflammasome components, forming a negative feedback loop. When autophagy is inhibited, the protective effect of BMSCs against ALF diminishes, and levels of inflammatory factors in liver tissue increase. HO-1 and NLRP3, acting as central regulators for antioxidant stress and pro-inflammatory responses, form an interactive regulatory network through the “oxidative stress-endotoxin-inflammation” axis in ALF. Therapeutic strategies targeting both may offer new approaches to ALF treatment [25, 26].

Advances in the therapeutic mechanisms of umbilical cord mesenchymal stem cells (UCMSCs) for ALF

Human UCMSCs are derived from the umbilical cord and exhibit broad tissue sources, multilineage differentiation potential, low immunogenicity, and strong self-renewal capacity, showing significant promise in regenerative medicine [27]. In vitro cultured UCMSCs have been shown to attenuate hepatic inflammation in a co-culture model of liver inflammation following preconditioning [28]. Jia et al. conducted a clinical investigation involving patients diagnosed with liver failure and cirrhosis who received stem cell infusions. Peripheral infusion of UCMSCs demonstrated significant therapeutic efficacy in hepatitis B virus-related liver failure, significantly reducing serum levels of ALT, AST, and TBIL. Extended treatment courses were associated with improved therapeutic outcomes [29]. Tao et al. transplanted UCMSCs into ALF mice, observing reduced serum ALT and AST levels along with attenuated inflammatory responses, suggesting UCMSCs alleviate ALF by modulating hepatocyte apoptosis and macrophage polarization, making UCMSC-based therapy a viable alternative for ALF patients [30]. Yu et al. administered HNF4α-overexpressing UCMSCs via tail vein injection into ALF model mice [31]. The HNF4α-UCMSCs group exhibited significantly improved inflammatory responses compared to the CON-UCMSCs group, with reduced inflammatory cell infiltration, diminished apoptosis, and markedly improved survival rates. HNF4α-UCMSCs secreted higher levels of IL-10 than CON-UCMSCs, thereby attenuating macrophage death and promoting M2 macrophage polarization. These findings highlight the superior therapeutic efficacy of HNF4α-UCMSCs over CON-UCMSCs in ALF treatment, providing a novel therapeutic approach for ALF [31]. Yun et al. evaluated UCMSCs in CCl4-induced ALF, assessing toxicity, tumorigenicity, and biodistribution, and found hepatoprotective effects through reduced hepatocyte necrosis and lobular neutrophil infiltration, suggesting that UCMSC therapy could serve as an alternative to liver transplantation [32]. Zhang et al. investigated the therapeutic effects of transplanting passage 5 (P5) and passage 10 (P10) human UCMSCs into rats with ALF [33]. Control group rats died within 48 to 96 hours after saline injection, while the P5-UCMSCs group exhibited a 7-day survival rate of 62.5%, with only 3 mor-

talities. The P10-UCMSCs group showed a 37.5% survival rate, with 3 rats surviving beyond one week. UCMSC transplantation effectively repaired damaged liver tissue, stimulating endogenous liver regeneration and suppressing hepatocyte apoptosis, thereby repopulating the liver and compensating for hepatic function [33]. Guo J et al. administered UMSCs via peripheral infusion to rhesus monkeys (Macaca mulatta) with toxin-induced intraperitoneal injury [34]. Comparative analysis revealed that, relative to the control group, the UMSCs group exhibited significantly decreased levels of proinflammatory cytokines (e.g., TNF-α, IL-1α, IL-1RA, and IL-15) and chemokines (e.g., MCP-1, MIP-1α, and MIP-1β). This suggests that UMSCs effectively suppress the aggregation and maturation of circulating monocytes, concurrently inhibiting their IL-6 secretion. Histological examination demonstrated substantial improvement in liver architecture, restoration of systemic homeostasis, and enhanced survival rates [35].

Advances in adipose-derived mesenchymal stem cell (ADSC) therapy for ALF

ADSCs are typically isolated from a patient's subcutaneous adipose tissue, yielding high cell numbers. ADSCs accumulate at disease sites to suppress excessive immune responses and secrete various growth factors and cytokines. They promote angiogenesis, exert anti-apoptotic effects, and regulate immune cells through cell-cell interactions. ADSCs possess advantages, including high proliferation, clonogenicity, multipotent differentiation, and immunomodulation, making them ideal candidates for ALF therapy [36]. ADSCs have been widely applied in ALF treatment due to their abundant sources, low cost, and simple isolation procedures [37]. Liau et al. established indirect co-culture systems between primary ADSCs and damaged HepG2 cells, observing that ADSCs exhibited early hepatic differentiation markers under the influence of factors released by injured HepG2 cells [37]. Zhang et al. transplanted ADSC-differentiated hepatocytes into mice with liver injury. Histological analysis revealed marked improvement, evidenced by reduced hepatic necrotic areas and significantly decreased serum TBIL levels [37]. Immunofluorescence staining, serological parameters, and biochemical indices showed varying degrees of improvement. These findings indicate that ADSC-derived hepatocytes hold significant promise for therapeutic interventions in liver disease animal models and clinical translation [37]. Chae et al. implanted Foxa2-modified ADSC scaffolds into the dorsal subcutaneous tissue of nude mice. Histopathological damage was significantly alleviated in the treated group. Paracrine cytokines (e.g., IL-10, IL-4, IL-6, and IL-13) were markedly upregulated through paracrine mechanisms, substantially enhancing hepatic regeneration processes. These findings demonstrate the substantial clinical value of ADSCs in treating ALF [38]. Subsequently, Shi et al. isolated porcine ADSCs and transplanted them into rabbits with ACLF, evaluating biochemical parameters, histomorphological scores, ADSC distribution characteristics, and hepatic pathology. Results showed that ADSC transplantation improved survival rates and liver function, demonstrating their therapeutic effects against ALF [39]. Jin et al. engrafted ADSC-differentiated hepatocyte-like cells into ALF model mice. The PBS control group exhibited 100% mortality within 48 hours, whereas the treatment group achieved a 26.7% survival rate, resulting in a significant survival advantage along with effective attenuation of inflammatory responses [40]. Liu et al. transplanted third-passage ADSCs derived from ALF porcine models and healthy donor-derived ADSCs into ALF mice [41]. Both groups exhibited improved hepatic histopathology, liver function, and survival rates, as evidenced by significant reductions in ALT, AST, direct bilirubin, and TBIL, along with attenuated inflammatory cell infiltration and enhanced hepatic lobule regeneration. Notably, the ALF-ADSCs group exhibited elevated expression of porcine hepatocyte-specific genes in recipient livers, suggesting enhanced hepatic differentiation potential in ADSCs isolated from liver-injured porcine donors [41]. Hwang et al. demonstrated that lipid-conjugated heparin-coated ADSCs reduced serum AST and ALT levels more rapidly and alleviated inflammation compared to untreated ADSCs, indicating that this modification significantly enhances therapeutic efficacy against liver injury [42].

Exploratory studies on human placental mesenchymal stem cell (PMSCs) therapy for ALF

In addition to the three common types of MSCs, PMSCs have shown promising potential in treating ALF. Cao et al. established an ALF model in Chinese experimental miniature pigs and trans-

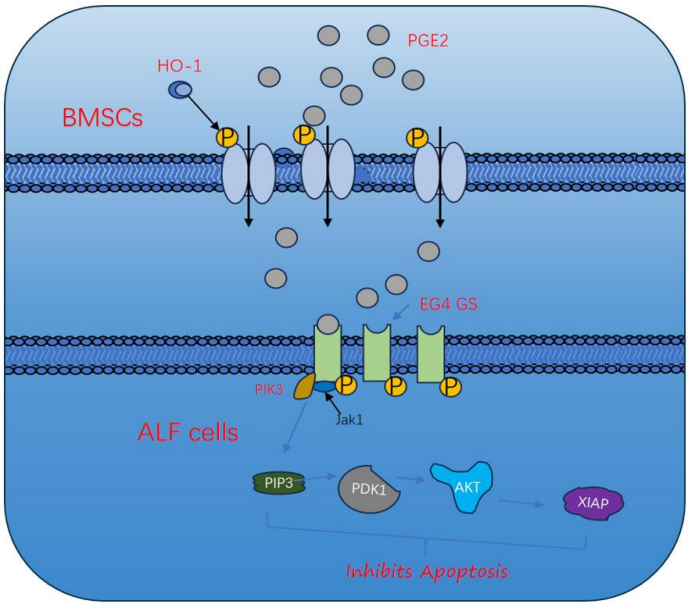

Figure 1. Mechanism of action of BMSCs. HO-1 promotes BMSCs to release PGE2, which binds to EG4 GS on hepatocytes, triggering an enzymatic cascade that activates PIP3, PDK1, and AKT, and subsequently activates XIAP, thereby inhibiting cell apoptosis caused by acute lung injury.

planted PMSCs, observing improved liver function with normalized concentrations of ALT, AST, ALP, CHE, TBIL, and TBA in recipient pigs. Hepatic inflammation and degenerative necrosis were alleviated, while liver regeneration was promoted. The survival time of ALF pigs was significantly prolonged [43]. Yu et al. generated GFP(+) PMSCs through lentiviral GFP (Green Fluorescent Protein) gene transduction, demonstrating that GFP(+) PMSCs expressed multiple liver-promoting factors, and their derived hepatocyte-like cells exhibited typical hepatic phenotypes [44]. Yu et al. administered GFP-labeled PMSCs via tail vein injection to CCl4-induced fibrotic rats, showing improved liver function. This approach also provided insights for the application of adipose-derived stem cell therapy in ALF [45].

Development and prospects

Currently, MSCs exhibit several key capabilities, including homing to injured tissues, targeting damaged sites via inflammatory signals, suppressing cytokine storms, undergoing hepatogenic differentiation, promoting hepatocyte proliferation, and exerting paracrine effects. However, significant challenges remain in the therapeutic application of MSCs for ALF treatment.

Limited research exists on MSC combination therapies, and further investigation is needed to determine whether different delivery vehicles or co-encapsulation strategies could enhance therapeutic efficacy.

Determining the optimal dosage for MSC therapy in ALF remains a critical area for further exploration. The establishment of patient stratification criteria for different transplantation routes (e.g., intravenous vs. intrahepatic injection) in MSC therapy is crucial. Besides, defining the optimal temporal parameters for MSC intervention in ALF is essential for improving clinical outcomes.

Signal path

BMSCs secrete heme oxygenase-1 (HO-1), which exerts anti-inflammatory, antioxidant, and anti-apoptotic effects, thereby ameliorating oxidative stress injury in ALF hepatocytes. Prostaglandin E2 (PGE2) activates G protein-coupled signaling by binding to EP4 receptors on the surface of ALF hepatocytes. This process recruits and phosphorylates Janus kinases (Jaks). Jak1 subsequently phosphorylates phosphatidylinositol 3-kinase (PI3K), which catalyzes the synthesis of phosphatidylinositol (3,4,5)-trisphosphate (PIP3) from phosphatidylinositol (4,5)-bisphosphate (PIP2). PIP3 facilitates phosphoinositide-dependent kinase-1 (PDK1)-mediated phosphorylation of protein kinase B (AKT), generating phosphorylated AKT (p-AKT). Activated AKT suppresses pro-apoptotic factors and upregulates the expression of the X-linked inhibitor of apoptosis protein (XIAP). Collectively, this signaling cascade inhibits apoptotic cell death in ALF hepatocytes. The signaling pathway diagram is shown in **Figure 1**.

Conclusion

This review focuses on elucidating the therapeutic effects of MSCs in ALF. MSCs can be derived from multiple sources, including bone marrow, umbilical cord, adipose tissue, and placenta. They possess the capabilities of self-renewal and multilineage differentiation, coupled with low immunogenicity and immunomodulatory functions. BMSCs can ameliorate ALF by

activating autophagy through the PI3K/AKT signaling pathway via induction of HO-1 expression. In the future, MSCs may potentially become a significant therapeutic alternative to liver transplantation for ALF.

Author contributions: Huan Li performed the conception of the study. Huan Li, Xingchen Yue, Wanning Li, Xin Niu contributed to the literature and collection of materials. Huan Li, Xiaoyu Tang contributed to material analysis and manuscript writing. Huan Li reviewed and refined the manuscript.

References

[1] Tujios S, Stravitz RT, Lee WM. Management of Acute Liver Failure: Update 2022. Semin Liver Dis 2022;42(3):362-378.

[2] Bernal W, Bittermann T, Sheth R, et al. Survival With and Without Liver Transplantation in Critically Ill Patients With Cirrhosis: A 20-Year Experience. Clin Gastroenterol Hepatol 2025; S1542-3565(25)00459-8.

[3] Battistella S, Grasso M, Catanzaro E, et al. Evolution of Liver Transplantation Indications: Expanding Horizons. Medicina (Kaunas) 2024; 60(3):412.

[4] Ding DC, Shyu WC, Lin SZ. Mesenchymal stem cells. Cell Transplant 2011;20(1):5-14.

[5] Shokravi S, Borisov V, Zaman BA, et al. Mesenchymal stromal cells (MSCs) and their exosome in acute liver failure (ALF): a comprehensive review. Stem Cell Res Ther 2022; 13(1):192.

[6] Oh SH, Jeong IS, Kim DY, et al. Recent Improvement in Survival Outcomes and Reappraisal of Prognostic Factors in Pediatric Living Donor Liver Transplantation. Liver Transpl 2022;28(6):1011-1023.

[7] Hu C, Wu Z, Li L. Mesenchymal stromal cells promote liver regeneration through regulation of immune cells. Int J Biol Sci 2020;16(5):893-903.

[8] Schiødt FV, Chung RT, Schilsky ML, et al. Outcome of acute liver failure in the elderly. Liver Transpl 2009;15(11):1481-1487.

[9] Maiwall R, Kulkarni AV, Arab JP, et al. Acute liver failure. Lancet 2024;404(10454):789-802.

[10] Kaliciński P, Grenda R, Szymczak M, et al. Multidisciplinary management of children with acute liver failure - Report on 104 children treated in single center. Pediatr Transplant 2024;28(1):e14654.

[11] Keshavan N, Greenwood M, Prunty H, et al. Gene therapy prevents hepatic mitochondrial dysfunction in murine deoxyguanosine kinase deficiency. Mol Ther Methods Clin Dev 2024; 33(1):101397.

[12] Junge N, Karam V, Hartog H, et al. Update on pediatric liver transplantation in Europe 2022: An ELITA-ESPGHAN report. J Pediatr Gastroenterol Nutr 2025;81(1):82-90.

[13] Owen M, Friedenstein AJ. Stromal stem cells: marrow-derived osteogenic precursors. Ciba Found Symp 1988;136:42-60.

[14] Chen HC, Awale S, Wu CP, et al. Co-cultured bone marrow mesenchymal stem cells repair thioacetamide-induced hepatocyte damage. Cell Biol Int 2020;44(12):2459-2472.

[15] Wang Y, Wang JL, Ma HC, et al. Mesenchymal stem cells increase heme oxygenase 1-activated autophagy in treatment of acute liver failure. Biochem Biophys Res Commun 2019; 508(3):682-689.

[16] Amiri F, Molaei S, Bahadori M, et al. Autophagy-Modulated Human Bone Marrow-Derived Mesenchymal Stem Cells Accelerate Liver Restoration in Mouse Models of Acute Liver Failure. Iran Biomed J 2016;20(3):135-144.

[17] Nie H, An F, Mei J, et al. IL-1β Pretreatment Improves the Efficacy of Mesenchymal Stem Cells on Acute Liver Failure by Enhancing CXCR4 Expression. Stem Cells Int 2020; 2020:1498315.

[18] Wang J, Ren H, Yuan X, et al. Interleukin-10 secreted by mesenchymal stem cells attenuates acute liver failure through inhibiting pyroptosis. Hepatol Res 2018;48(3):E194-E202.

[19] Wang J, Ding H, Zhou J, et al. Transplantation of Mesenchymal Stem Cells Attenuates Acute Liver Failure in Mice via an Interleukin-4-dependent Switch to the M2 Macrophage Anti-inflammatory Phenotype. J Clin Transl Hepatol 2022;10(4):669-679.

[20] Jiang T, Xia G, Yang B, et al. Application of Bone Marrow Mesenchymal Stem Cells Effectively Eliminates Endotoxemia to Protect Rat from Acute Liver Failure Induced by Thioacetamide. Tissue Eng Regen Med 2022;19(2):403-415.

[21] Wang J, Wang H, Shi J, et al. Effects of bone marrow MSCs transfected with sRAGE on the intervention of HMGB1 induced immuno-inflammatory reaction. Int J Clin Exp Pathol 2015;8(10):12028-12040.

[22] Xiu G, Li X, Yin Y, et al. SDF-1/CXCR4 Augments the Therapeutic Effect of Bone Marrow Mesenchymal Stem Cells in the Treatment of Lipopolysaccharide-Induced Liver Injury by Promoting Their Migration Through PI3K/Akt Signaling Pathway. Cell Transplant 2020;29:963689720929992.

[23] Kuo NC, Huang SY, Yang CY, et al. Involvement of HO-1 and Autophagy in the Protective Effect of Magnolol in Hepatic Steatosis-Induced NLRP3 Inflammasome Activation In Vivo and In Vitro. Antioxidants (Basel) 2020;9(10):924.
[24] Lei L, Guo Y, Lin J, et al. Inhibition of endotoxin-induced acute lung injury in rats by bone marrow-derived mesenchymal stem cells: Role of Nrf2/HO-1 signal axis in inhibition of NLRP3 activation. Biochem Biophys Res Commun 2021;551:7-13.
[25] Han J, Jia D, Yao H, et al. GRP78 improves the therapeutic effect of mesenchymal stem cells on hemorrhagic shock-induced liver injury: Involvement of the NF-κB and HO-1/Nrf-2 pathways. FASEB J 2024;38(1):e23334.
[26] Alruhaimi RS, Hassanein EHM, Alnasser SM, et al. Modulation of NF-κB/NLRP3 inflammasome axis, Nrf2/HO-1 signaling and attenuation of oxidative stress mediate the protective effect of ambroxol against cyclophosphamide cardiotoxicity. Biochem Biophys Res Commun 2025; 776:152242.
[27] Qiao Y, Xu Z, Yu Y, et al. Single cell derived spheres of umbilical cord mesenchymal stem cells enhance cell stemness properties, survival ability and therapeutic potential on liver failure. Biomaterials 2020;227:119573.
[28] Hu C, Wu Z, Li L. Pre-treatments enhance the therapeutic effects of mesenchymal stem cells in liver diseases. J Cell Mol Med 2020;24(1):40-49.
[29] Jia Y, Shu X, Yang X, et al. Enhanced therapeutic effects of umbilical cord mesenchymal stem cells after prolonged treatment for HBV-related liver failure and liver cirrhosis. Stem Cell Res Ther 2020;11(1):277.
[30] Tao Y, Wang Y, Wang M, et al. Mesenchymal Stem Cells Alleviate Acute Liver Failure through Regulating Hepatocyte Apoptosis and Macrophage Polarization. J Clin Transl Hepatol 2024;12(6):571-580.
[31] Yu Y, Zhang Q, Wu N, et al. HNF4α overexpression enhances the therapeutic potential of umbilical cord mesenchymal stem/stromal cells in mice with acute liver failure. FEBS Lett 2022;596(24):3176-3190.
[32] Yun JW, Ahn JH, Kwon E, et al. Human umbilical cord-derived mesenchymal stem cells in acute liver injury: Hepatoprotective efficacy, subchronic toxicity, tumorigenicity, and biodistribution. Regul Toxicol Pharmacol 2016;81:437-447.
[33] Zhang Y, Li Y, Li W, et al. Therapeutic Effect of Human Umbilical Cord Mesenchymal Stem Cells at Various Passages on Acute Liver Failure in Rats. Stem Cells Int 2018;2018:7159465.
[34] Guo G, Zhuang X, Xu Q, et al. Peripheral infusion of human umbilical cord mesenchymal stem cells rescues acute liver failure lethality in monkeys. Stem Cell Res Ther 2019;10(1):84.
[35] Nahar S, Nakashima Y, Miyagi-Shiohira C, et al. Cytokines in adipose-derived mesenchymal stem cells promote the healing of liver disease. World J Stem Cells 2018;10(11):146-159.
[36] Zhang S, Zhu Z, Wang Y, et al. Therapeutic potential of Bama miniature pig adipose stem cells induced hepatocytes in a mouse model with acute liver failure. Cytotechnology 2018; 70(4):1131-1141.
[37] Liau LL, Makpol S, Azurah AGN, et al. Human adipose-derived mesenchymal stem cells promote recovery of injured HepG2 cell line and show sign of early hepatogenic differentiation. Cytotechnology 2018;70(4):1221-1233.
[38] Chae YJ, Jun DW, Lee JS, et al. The Use of Foxa2-Overexpressing Adipose Tissue-Derived Stem Cells in a Scaffold System Attenuates Acute Liver Injury. Gut Liver 2019;13(4):450-460.
[39] Shi L, Liu Y, Liu Q, et al. Adipose-derived stem cells can alleviate RHDV2 induced acute liver injury in rabbits. Res Vet Sci 2024;172:105255.
[40] Jin Y, Shi R, Qi T, et al. Adipose-derived stem cells show hepatic differentiation potential and therapeutic effect in rats with acute liver failure. Acta Biochim Biophys Sin (Shanghai) 2023;55(4):601-612.
[41] Liu S, Guo R, Hou X, et al. Adipose-tissue derived porcine mesenchymal stem cells efficiently ameliorate CCl(4)-induced acute liver failure in mice. Cytotechnology 2020;72(3):327-341.
[42] Hwang Y, Kim JC, Tae G. Significantly enhanced recovery of acute liver failure by liver targeted delivery of stem cells via heparin functionalization. Biomaterials 2019;209:67-78.
[43] Cao H, Yang J, Yu J, et al. Therapeutic potential of transplanted placental mesenchymal stem cells in treating Chinese miniature pigs with acute liver failure. BMC Med 2012;10:56.
[44] Yu J, Su X, Zhu C, et al. GFP Labeling and Hepatic Differentiation Potential of Human Placenta-Derived Mesenchymal Stem Cells. Cell Physiol Biochem 2015;35(6):2299-2308.
[45] Yu J, Hao G, Wang D, et al. Therapeutic Effect and Location of GFP-Labeled Placental Mesenchymal Stem Cells on Hepatic Fibrosis in Rats. Stem Cells Int 2017;2017:1798260.

Perioperative Precision Medicine
ISSN: 2957-5443

Zentime

Review Article https://doi.org/10.61189/691939hefazb

The role and research progress of ferroptosis in myocardial injury in sepsis

Jiayin Wang[1,4,5,*], Sixu Chen[2,5,*], Weiqi Lin[3,4,*], Xinyi Xie[1,5], Yutong Sun[3,5], Qin Zhang[3,5], Qixiang Xu[1,4,5], Cuifeng Zhang[2,5]

[1]School of Pharmacology, Wannan Medical College, Wuhu, Anhui, China. [2]School of Anesthesiology, Wannan Medical College, Wuhu, Anhui, China. [3]School of Clinical Medicine, Wannan Medical College, Wuhu, Anhui, China. [4]Anesthesia Laboratory and Training Center, Wannan Medical College, Wuhu, Anhui, China. [5]Wuhu Perioperative Monitoring and Prognostic Technology Research and Development Center, Wannan Medical College, Wuhu, Anhui, China.
[*]The authors contribute equally and co-first authors.

Corresponding authors: Qixiang Xu and Cuifeng Zhang.

Acknowledgement: This work was supported by The Foundation of Wannan Medical College (WK2023ZQNZ08), National university innovation and entrepreneurship training program (202310368014, 202310368049, 202410368014), Anhui Province university innovation and entrepreneurship training program (S202310368095, S202310368087, S202410368004, S202410368009).

Declaration of conflict of interest: None.

Received March 2, 2025; Accepted June 4, 2025; Published December 31, 2025

Highlights

- A comprehensive review of the role of ferroptosis in sepsis-induced myocardial injury is presented.
- The mechanisms of ferroptosis and recent advancements in its involvement in sepsis-induced myocardial injury are discussed.
- Perioperative whole-process risks may induce sepsis, activate ferroptosis and raise myocardial injury risk, while integrating ferroptosis into management can reduce this risk.

Abstract

Sepsis is triggered by the body's dysregulated response to infection, often accompanied by acute organ dysfunction and a high risk of mortality. The incidence of myocardial injury in sepsis patients ranges from 40% to 70%, with complex pathophysiological mechanisms. In recent years, ferroptosis, a novel form of programmed cell death, has attracted widespread attention. Studies suggest that it may play a key role in sepsis-related myocardial injury; however, research in this field is still in the preliminary stage, with some controversial findings and unclear underlying mechanisms. Notably, risks throughout the perioperative period (preoperative stage, intraoperative trauma/infection, and postoperative recovery) can induce sepsis, which further activates the ferroptosis pathway and leads to myocardial injury. Based on this, integrating ferroptosis into the perioperative management system—optimizing risk stratification through marker screening and implementing targeted interventions—holds great significance for reducing the risk of perioperative sepsis-related myocardial injury. This article systematically summarizes the latest research progress on ferroptosis in sepsis-related myocardial injury, explores its potential mechanisms, and screens for potential therapeutic targets by combining the characteristics of perioperative risks, thereby providing references for subsequent clinical research and practice.

Keywords: Sepsis, myocardial injury, ferroptosis, perioperative period, research progress

Address correspondence to: Qixiang Xu, School of Pharmacology, Wannan Medical College, No. 22 Wenchang West Road, Yijiang District, Wuhu 241002, Anhui, China. Tel: +86-18355305112. E-mail: xuqixiang@wnmc.edu.cn. **Cuifeng Zhang**, School of Anesthesiology, Wannan Medical College, No. 22 Wenchang West Road, Yijiang District, Wuhu 241002, Anhui, China. Tel: +86-15551257181. E-mail: zhangcuifeng@wnmc.edu.cn.

Introduction

Sepsis is a severe clinical syndrome, which can also be induced by perioperative infections, trauma, and other factors. Typically caused by infection, it leads to an uncontrolled immune response in the body, thereby triggering a systemic inflammatory response and multi-organ damage [1]. In recent years, ferroptosis, as a form of iron-dependent programmed cell death, has attracted increasing attention. Studies have shown that ferroptosis is closely related to oxidative stress and plays an important role in the pathological process of sepsis [2]. However, the specific role of ferroptosis in sepsis-induced myocardial injury and its molecular mechanism remain to be further explored.

The mechanism of ferroptosis mainly involves the dysregulation of intracellular iron metabolism and the accumulation of lipid peroxides. Studies have found that ferroptosis plays an important role in multiple-organ damage caused by sepsis, including injury to the heart, liver, lung and kidney [3]. Specifically, ferroptosis aggravates myocardial injury in sepsis by promoting the accumulation of intracellular lipid peroxides, leading to cardiomyocyte death [4]. Several studies have shown that inhibiting ferroptosis can improve the survival rates in septic mice and reduce heart damage, providing novel therapeutic avenues for clinical treatment [5].

Multiple signaling pathways regulate ferroptosis in sepsis-induced myocardial injury. For example, p53 is an important regulator of ferroptosis, which helps cells resist external stimuli by modulating the expression of downstream genes [6]. In addition, the Nrf2/GPX4 axis and NCOA4-FTh1-mediated ferritin autophagy are also important mechanisms in the regulation of ferroptosis [7]. These mechanisms not only deepen our understanding of the role of ferroptosis in sepsis-induced myocardial injury, but also provide potential targets for developing targeted therapeutic strategies.

In terms of treatment, the application of iron chelators and ferroptosis inhibitors has shown promising results. For example, Fer-1, a ferroptosis inhibitor, not only significantly improves cardiac function and reduces the cardiac inflammatory response in septic mice, but also can reduce the risk of perioperative septic myocardial injury when used for preoperative pretreatment [8]. Studies have also shown that inhibition of ferroptosis can reduce myocardial injury caused by sepsis and enhance both the structure and function of the heart, providing a new direction for the treatment of sepsis-induced myocardial injury [9].

This article summarizes the research progress of ferroptosis in sepsis-induced myocardial injury, focuses on the regulatory characteristics and mechanisms of ferroptosis during the perioperative period, identifies therapeutic targets, and provides insights for the precise prevention and treatment of perioperative sepsis-induced myocardial injury.

Pathophysiological mechanisms of sepsis

Infection and systemic inflammatory response

Sepsis is a systemic inflammatory response syndrome caused by infection, often accompanied by multiple organ dysfunction. Pathogens (such as bacteria, viruses, or fungi) activate the host immune system by releasing endotoxins or other pathogenic substances, leading to a series of complex physiological reactions. These reactions include the release of cytokines, activation of white blood cells, and increased vascular permeability, all of which trigger a systemic inflammatory response. Although this response serves as the body's defense mechanism against infection, excessive inflammatory response can lead to tissue damage and organ dysfunction, and further aggravate the condition of sepsis [10, 11]. Studies have shown that inflammatory mediators such as tumor necrosis factor (TNF-α) and interleukins (IL-1, IL-6) play a key role in the occurrence and development of sepsis, especially in the process of myocardial injury, which promotes the apoptosis and dysfunction of myocardial cells [12].

Mechanisms of myocardial injury in sepsis

Sepsis-induced myocardial injury is multifactorial. First, the release of inflammatory mediators directly affects cardiomyocyte function, leading to a decreases myocardial contractility. Second, oxidative stress in sepsis aggravates cardiomyocyte damage and increases the generation of reactive oxygen species (ROS), which in turn triggers intracellular lipid peroxidation and leads to the death of cardiomyocytes [14].

In addition, disturbances in iron metabolism play an important role in sepsis-induced myocardial injury. Excessive iron accumulation promotes iron-dependent cell death (ferroptosis), a form of cell death closely related to cardiomyocyte dysfunction [13]. Additionally, specific signaling pathways, such as activation of the NLRP3 inflammasome, are closely related to myocardial injury in sepsis, and inhibiting these pathways may offer protective effects [15, 16].

Effects of iron metabolism disorders on myocardium

Proper functioning of iron metabolism is essential for heart muscle health. Patients with sepsis often experience excessive iron accumulation, which not only triggers oxidative stress but also leads to ferroptosis in cardiomyocytes [17]. Ferroptosis is a novel form of programmed cell death primarily mediated by lipid peroxidation. Studies have shown that during sepsis, the content of iron in myocardial tissue increases significantly, leading to cardiomyocyte dysfunction and death [18]. In addition, iron metabolism disorders may aggravate myocardial injury by disrupting mitochondrial function in myocardial cells [19, 20]. Regulating iron uptake, storage and excretion offers potential new ideas and strategies for the treatment of septic myocardial injury.

The basic mechanism of ferroptosis

Intracellular iron homeostasis

Iron, an essential trace element for cellular proliferation and one of the most abundant metal elements in the human body, is tightly regulated under physiological conditions through uptake, metabolism, and storage processes to maintain homeostasis. Ferritin, the primary iron storage protein, effectively sequesters iron ions, preventing their participation in harmful free radical reactions [21]. Dysregulation of iron homeostasis, particularly iron overload, is a critical trigger for ferroptosis, a regulated form of cell death characterized by lethal lipid peroxidation. Iron overload promotes lipid peroxide accumulation and exacerbates oxidative stress, resulting in cellular injury [4]. During ferroptosis, depletion of intracellular glutathione (GSH) and reduced activity of glutathione peroxidase 4 (GPX4) impair the detoxification of lipid peroxides, allowing ferrous iron (Fe^{2+}) to catalyze Fenton-like reactions that generate excessive ROS, ultimately inducing cell death [22]. Morphologically, ferroptotic cells exhibit distinct mitochondrial abnormalities, including mitochondrial shrinkage, decreased or absent cristae, and increased membrane density [23]. Iron accumulation and lipid peroxidation are key initiating events in membrane oxidative damage during ferroptosis, underscoring the importance of maintaining intracellular iron homeostasis for cell survival.

Ferroptosis and amino acid metabolism

Ferroptosis is an iron-dependent, lipid peroxidation-driven form of programmed cell death, primarily mediated by excessive intracellular iron accumulation, GSH depletion, and impaired GPX4 function [24]. Its sensitivity is closely linked to the dynamic balance of amino acid metabolism [25]. Among these, the cystine/cysteine metabolic axis plays a central role. The system Xc^- antiporter, composed of SLC7A11 and SLC3A2, exports glutamate in exchange for cystine, which is subsequently reduced to cysteine—an essential precursor for intracellular GSH synthesis [26, 27]. GSH serves as a cofactor for GPX4, facilitating the reduction of lipid hydroperoxides. GSH depletion leads to GPX4 inactivation and triggers ferroptosis [28]. Moreover, glutamate accumulation may exacerbate oxidative stress through excitotoxicity, forming a positive feedback loop between metabolism and cell death.

Additional amino acid pathways are also play a role in regulating ferroptosis. Arginine metabolism, through nitric oxide synthase (NOS) or polyamine biosynthesis pathways, modulates the cellular redox state; branched-chain amino acids, such as leucine, can activate the mTOR pathway, thereby suppressing ATF4-mediated antioxidant responses [28-30]. Furthermore, NCOA4-FTH1 phase separation-mediated ferritinophagy regulates iron metabolism and ferroptosis sensitivity, representing a promising therapeutic target [31]. Recent studies have also highlighted the aberrant expression of amino acid transporters, such as LAT1 (SLC7A5), in promoting ferroptosis resistance in tumor cells, suggesting that reprogrammed amino acid metabolism may be a critical mechanism by which cells evade ferroptosis in disease con-

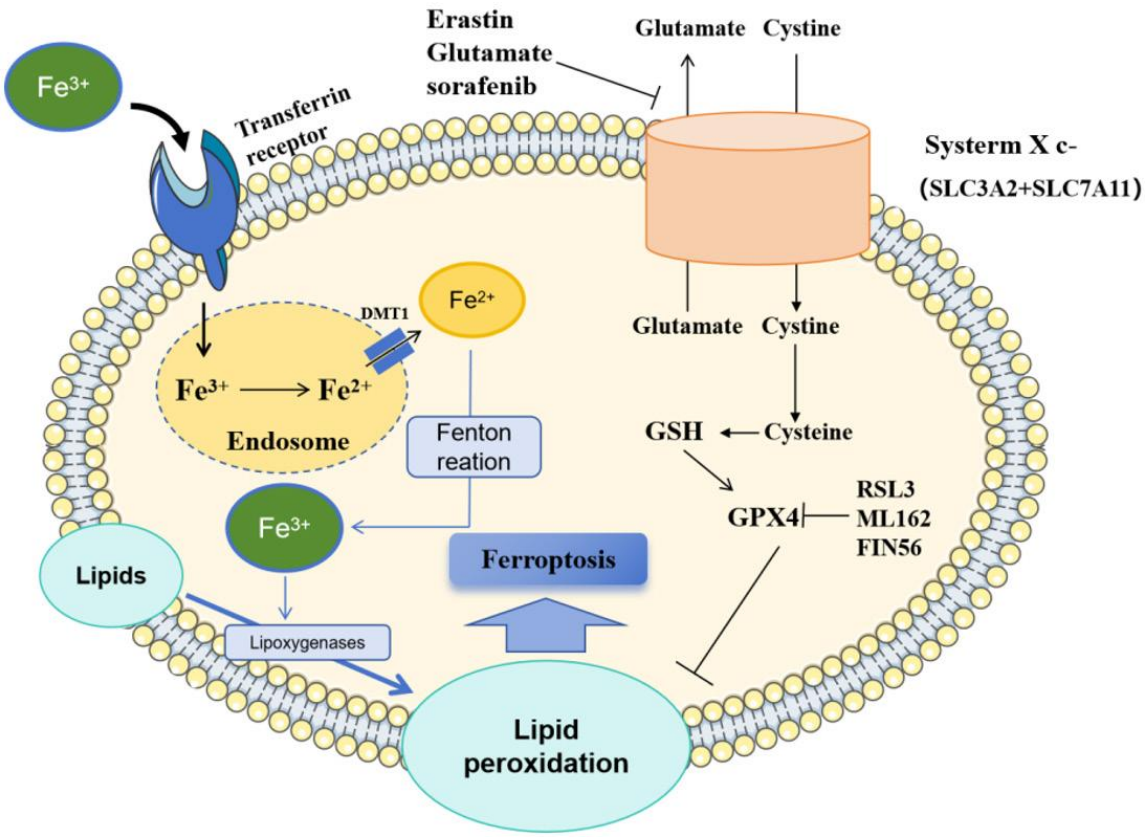

Figure 1. Schematic diagram of the ferroptosis-lipid peroxidation signaling pathway.

texts [32]. A deeper understanding of the crosstalk between ferroptosis and amino acid metabolism may shed light on the metabolic foundations of various diseases and offer novel therapeutic strategies for ferroptosis-associated conditions, including cancer and neurodegenerative disorders.

The link between ferroptosis and lipid peroxidation

Ferroptosis, an important regulatory cell death outcome, is essentially triggered by the dysregulation of lipid peroxidation products. Inflammatory responses induced by bacterial infections lead to the production of large amounts of reactive oxygen species (ROS) [5]. Studies have shown that in the intrinsic association between ferroptosis and lipid peroxidation, ROS act as a core signaling molecule, permeating the entire "oxidative damage-death execution" cascade and forming a triangular regulatory network of iron-ROS-lipid peroxidation [8]. This network can be intuitively understood by combining the **Figure 1**: In the initiation phase, extracellular Fe^{3+} enters the endosome via the transferrin receptor and is reduced to free ferrous ions (Fe^{2+}), which then participate in the Fenton reaction. Fe^{2+} synergizes with ROS to attack the double bonds of polyunsaturated fatty acids (PUFAs) in the cell membrane: ROS (such as •OH) directly participate in hydrogen atom abstraction reactions to generate lipid radicals (L•), while Fe^{2+} accelerates the decomposition of hydrogen peroxide (H_2O_2), amplifying ROS generation efficiency [33]. In the propagation phase, lipid radicals (L•) combine with oxygen to form lipid peroxyl radicals (LOO•), which further drives the vicious cycle of oxidative damage. This process not only consumes PUFAs within the membrane but also continuously generates new ROS (such as singlet oxygen $^1O_2$), forming a "ROS-lipid peroxidation" positive feedback loop that amplifies oxidative damage exponentially.

Under normal physiological conditions, cells eliminate lipid hydroperoxides (LOOH) through the glutathione (GSH)-glutathione peroxidase 4 (GPX4) axis [34]. As shown in **Figure 1**, System Xc^- mediates the entry of cystine into the cell and its conversion to cysteine, which provides

the raw material for GSH synthesis. GSH, as a cofactor of GPX4, helps it scavenge lipid peroxides. Meanwhile, antioxidant enzyme systems such as superoxide dismutase (SOD) and catalase (CAT) can neutralize ROS and maintain redox balance. However, when ferroptosis occurs, it is often accompanied by the depletion of GSH and inhibition of GPX4 activity, which can be caused by inhibitors like Erastin blocking System Xc^- and RSL3 inhibiting GPX4, leading to the dysregulation of lipid peroxidation.

As the "core messenger" in the ferroptosis and lipid peroxidation network, the dynamic regulation of ROS not only determines cell fate but also provides multi-dimensional targets for intervening in oxidative damage-related diseases [35].

Other regulatory mechanisms of ferroptosis

In addition to the aforementioned pathways, ferroptosis is finely regulated by various signaling molecules. For instance, studies have shown that downregulation of nuclear receptor coactivator 4 (NCOA4) inhibits ferritinophagy, thereby reducing intracellular iron accumulation and lipid peroxidation, and ultimately suppressing ferroptosis [36]. Moreover, ferroptosis suppressor protein 1 (FSP1) has been found to reduce Coenzyme Q10 (CoQ10) and inhibit lipid peroxidation, exerting an anti-ferroptotic effect independently of the GPX4 pathway [37]. Jiang et al. demonstrated that nuclear p53 regulates ferroptosis through both transcriptional and post-translational mechanisms, while also exerting antioxidant effects [38]. Conversely, overactivation of heme oxygenase-1 (HO-1) can lead to excessive intracellular ferrous iron accumulation and increased ROS production, thereby promoting ferroptosis [39]. The mevalonate pathway also plays an essential role in ferroptosis regulation: its metabolites, including CoQ10 and isopentenyl pyrophosphate, are involved in modulating ferroptotic sensitivity. Isopentenyl pyrophosphate, derived from decarboxylated mevalonate, affects the maturation of selenocysteine tRNA, thus regulating the synthesis of GPX4 [40]. These signaling molecules act on diverse nodes within the networks of iron metabolism, oxidative stress, and lipid peroxidation, highlighting the multifactorial complexity and versatility of ferroptosis regulation [6].

Mechanisms and research progress of ferroptosis in sepsis-induced myocardial injury

Oxidative stress and inflammatory response

Sepsis is a life-threatening condition resulting from a dysregulated host response to infection [41]. It induces systemic inflammatory responses and oxidative stress, increasing intracellular ROS levels in cardiomyocytes, which disrupt cellular structures and impair cardiac function. Evidence suggests that oxidative stress and inflammation are key inducers of ferroptosis [45]. The mechanism involves three core factors: elevated oxidative stress, iron metabolism dysregulation, and impaired antioxidant defenses [43]. In septic myocardial injury, systemic inflammatory cascades elevate ROS levels, damaging biological membranes and initiating lipid peroxidation, which promotes ferroptosis. Iron overload, frequently observed in sepsis, provides excess free Fe^{2+} that fuels ROS generation via Fenton chemistry, exacerbating myocardial damage [44]. Inflammatory mediators can also modulate iron-related proteins, such as transferrin receptor 1 (TfR1), promoting iron uptake and facilitating ferroptosis [45]. Ferroptosis leads to lipid peroxide accumulation and loss of membrane integrity in cardiomyocytes, further intensifying myocardial injury in sepsis [21, 44]. Dysfunction of the antioxidant system, particularly the system Xc^-–GSH–GPX4 axis, impairs lipid hydroperoxide clearance, accelerating ROS accumulation. Regulatory molecules like acyl-CoA synthetase long-chain family member 4 (ACSL4) and GPX4 exhibit aberrant expression in myocardial injury and are closely associated with cardiac dysfunction severity [46]. Inhibiting ferroptosis has been shown to mitigate septic myocardial injury and improve cardiac function, offering a promising therapeutic strategy [42, 47].

Mitochondrial dysfunction

Sepsis-induced mitochondrial dysfunction significantly contributes to myocardial injury. Most cellular ROS originate from mitochondrial oxidative phosphorylation. Ferroptosis and mitochondrial dysfunction are mutually reinforcing: lipid peroxides generated during ferroptosis attack mitochondrial membranes, causing swelling, cristae disappearance, and outer membrane rupture, impairing mitochondrial function [48]. Ferroptosis disrupts intracellular iron homeostasis, and excess Fe^{2+} catalyzes ROS produc-

tion, damaging mitochondrial respiratory chain complexes, decreasing ATP synthesis, and impairing cardiomyocyte energy metabolism. Moreover, ferroptosis leads to GSH depletion and GPX4 inactivation, preventing the effective clearance of lipid peroxides and ROS, resulting in persistent mitochondrial oxidative stress. Conversely, mitochondrial dysfunction promotes ferroptosis by destabilizing ferritin, facilitating ferritinophagy, and increasing intracellular free iron. As mitochondria are the primary site of ROS generation, their dysfunction amplifies ROS production, creating a vicious cycle of lipid peroxidation and ferroptosis. This bidirectional interaction exacerbates septic myocardial injury and may contribute to organ failure and mortality.

Amino acid metabolism

Ferroptosis alters amino acid metabolism in septic myocardial injury and induces autophagic responses. GPX4 regulates ferroptosis and oxidative stress by converting reduced GSH into oxidized glutathione (GSSG), thereby preventing ferroptosis [49]. In sepsis, oxidative stress decreases GPX4 activity, increasing susceptibility to ferroptosis and worsening myocardial injury [50]. ACSL4, a key enzyme in lipid peroxidation, is upregulated during ferroptosis and correlates with myocardial damage [51]. NCOA4, the selective receptor for ferritin, mediates ferritin degradation and elevates intracellular Fe^{2+} levels during ferroptosis [52]. Inflammatory factors in sepsis upregulate NCOA4 expression, promoting ferritinophagy and iron release, thereby enhancing ferroptosis. Lipocalin-2 (Lcn2) binds iron-loaded siderophores, restricting iron uptake and inhibiting ferroptosis. Lcn2 deficiency increases iron uptake and ferroptosis risk, while Lcn2 upregulation may protect the myocardium by mitigating ferroptosis-induced injury [53]. Elevated myocardial iron levels have been observed in sepsis patients and are positively correlated with myocardial damage severity, highlighting iron dysregulation as a therapeutic target in septic cardiomyopathy [42, 47].

Research progress on ferroptosis in sepsis-induced myocardial injury

Findings from animal model studies

In recent years, animal models have played a pivotal role in elucidating the relationship between ferroptosis and sepsis-induced myocardial injury. Studies have demonstrated that sepsis can induce ferroptosis in cardiomyocytes, a process closely linked to iron metabolism dysregulation and lipid peroxide accumulation [54]. By establishing the cecal ligation and puncture (CLP) model in mice, researchers found that administration of ferroptosis inhibitors significantly reduced myocardial injury and improved cardiac function in septic animals [55]. Additionally, iron chelators such as deferoxamine have been shown to mitigate cardiac damage in septic mice, suggesting that ferroptosis may be a critical mechanism in sepsis-induced cardiomyopathy [5]. These findings deepen our understanding of the pathophysiological mechanisms underlying sepsis-related cardiac injury and provide potential therapeutic targets for intervention.

Preliminary results from clinical studies

In clinical research, the role of ferroptosis in sepsis patients has garnered increasing attention. One study revealed a positive correlation between dysregulated iron metabolism and the severity of myocardial injury in sepsis patients, indicating that ferroptosis may play a key role in this context [9]. Among the regulatory factors, the p53 transcription factor family has been implicated in ferroptosis [56]. Specifically, tetracycline-induced p53 promoter activation and ROS-induced cellular stress responses were shown to promote ferroptosis by suppressing the expression of SLC7A11 [59]. Furthermore, Li et al. reported that ferritinophagy-mediated ferroptosis constitutes a critical mechanism in sepsis-induced cardiac damage. In a lipopolysaccharide (LPS)-induced sepsis model, LPS was shown to upregulate the expression of nuclear receptor coactivator 4 (NCOA4), which promotes ferritin degradation and the release of free iron [60]. This, in turn, activates mitochondrial membrane-associated iron-binding proteins, exacerbating oxidative injury. Clinical data have suggested that ferroptosis inhibitors may be beneficial in improving cardiac function and reducing inflammatory responses in sepsis patients [8]. However, current clinical trials targeting ferroptosis are still limited, and further research is needed to verify the efficacy and safety of such therapies in sepsis-induced myocardial injury.

Therapeutic prospects of targeting ferroptosis

Recent research indicates that ferroptosis plays a significant role in sepsis-related organ dam-

age, including myocardial injury [57]. Targeted therapeutic strategies against ferroptosis mainly include iron chelators, antioxidants, and specific ferroptosis inhibitors [58]. For example, deferoxamine has been shown to effectively prevent iron accumulation, thereby alleviating cardiac injury in sepsis models [5]. Moreover, ferroptosis inhibitors such as ferrostatin-1 and liproxstatin-1 have demonstrated the ability to reduce myocardial damage and improve cardiac function in septic animals [7]. Combining ferroptosis inhibitors with other treatments, such as anti-inflammatory agents or antioxidants, may further enhance therapeutic efficacy [61]. Despite these encouraging findings, several challenges remain, including optimizing dosage, determining appropriate routes of administration, and ensuring long-term safety. Future research should focus on refining ferroptosis-targeted treatment strategies to provide more effective solutions for sepsis-induced myocardial injury. These emerging therapeutic approaches offer new insights and directions for the management of septic cardiomyopathy.

Effects of combination therapy on sepsis-induced myocardial injury

Combination therapy is gaining increasing attention in the treatment of sepsis, particularly in strategies targeting ferroptosis. Studies have shown that the co-administration of certain drugs can significantly enhance therapeutic efficacy. For instance, combining antioxidants with ferroptosis inhibitors has been demonstrated to alleviate oxidative stress and inflammatory responses in sepsis patients, thereby reducing oxidative damage in cardiomyocytes and mitigating myocardial injury [8]. Additionally, certain compounds derived from traditional Chinese medicine, such as ginsenoside Re, have been reported to ameliorate sepsis-induced cardiac injury by modulating ferroptosis pathways and enhancing antioxidant defenses [44]. This combination therapy approach not only improves treatment effectiveness but also provides new possibilities for the clinical management of sepsis-related myocardial injury.

Conclusion

Ferroptosis, as a newly identified form of regulated cell death, is gaining growing attention for its role in sepsis-induced myocardial injury. Studies have shown that ferroptosis is closely associated with cardiomyocyte damage and may play a pivotal role in the pathophysiological processes of sepsis. Although current research has uncovered potential mechanisms and implications of ferroptosis in septic cardiomyopathy, many questions remain unresolved and warrant further investigation.

Discrepancies among studies—stemming from variations in experimental design, model selection, and evaluation criteria—highlight the need for standardized protocols in future research. Establishing uniform methodological frameworks and fostering multicenter collaborations and interdisciplinary communication will be essential for a more comprehensive understanding of ferroptosis in sepsis-induced myocardial injury.

Looking forward, therapeutic interventions targeting ferroptosis hold great promise for improving cardiac function and overall outcomes in sepsis patients. The development of novel drugs or treatment strategies that modulate ferroptosis-related pathways could offer new clinical options. However, the efficacy and safety of these interventions must be rigorously validated through clinical trials to ensure tangible benefits for patients.

In summary, an in-depth exploration of ferroptosis not only broadens our understanding of the mechanisms underlying sepsis-induced myocardial injury but also opens new avenues for clinical intervention. Continued research in this area may ultimately lead to the development of more effective therapeutic strategies, thereby reducing the incidence of cardiac complications in sepsis and improving patient quality of life.

Author contributions: Jiayin Wang, Sixu Chen and Weiqi Lin contributed to the conception of the study and wrote the manuscript draft. Xinyi Xie, Qin Zhang, Haiyi Qian and Yutong Sun contributed to the information collection and analysis. Qixiang Xu and Cuifeng Zhang helped perform the analysis by having constructive discussions and revising the manuscript.

References

[1] Li Y, Ren S, Zhou S. Advances in sepsis research: Insights into signaling pathways, organ failure, and emerging intervention strategies. Exp Mol Pathol 2025;142:104963.

[2] Li JR, Wang HL. The Keap1/Nrf2/ARE signaling pathway can alleviate ferroptosis in sepsis by regulating oxidative stress. Chinese Critical Care Medicine 2021;33(7):881-884.
[3] Zhang P, Liu W, Wang S, et al. Ferroptosisand Its Role in the Treatment of Sepsis-Related Organ Injury: Mechanisms and Potential Therapeutic Approaches. Infect Drug Resist 2024;17:5715-5727.
[4] Wang X, Li J, Zhang Y, et al. HIF1A/BNIP3 pathway affects ferroptosis in sepsis-induced cardiomyopathy through binding to BCL-2. Redox Rep 2025;30(1):2544412.
[5] Huang YH, Zhang GP, Liang H, et al. Inhibition of ferroptosis alleviates myocardial injury in septic mice: The role of lipocalin-2. Journal of Southern Medical University 2022;42(2):256-262.
[6] Gao N, Tang AL, Liu XY, et al. p53-Dependent ferroptosis pathways in sepsis. Int Immunopharmacol. 2023;118:110083.
[7] Wang Y, Zhang Y, Gao M, et al. Lipocalin-2 promotes CKD vascular calcification by aggravating VSMCs ferroptosis through NCOA4/FTH1-mediated ferritinophagy. Cell Death Dis 2024; 15(11):865.
[8] Huang Q, Ding Y, Fang C, et al. The Emerging Role of Ferroptosis in Sepsis, Opportunity or Challenge? Infect Drug Resist 2023;16:5551-5562.
[9] Zeng L, Liu X, Geng C, et al. Ferroptosis in cancer (Review). Oncol Lett 2024;28(1):304.
[10] Wiersinga WJ. Current insights in sepsis: from pathogenesis to new treatment targets. Curr Opin Crit Care 2011;17(5):480-486.
[11] Xiao Y, Yu Y, Hu L, et al. Matrine Alleviates Sepsis-Induced Myocardial Injury by Inhibiting Ferroptosis and Apoptosis. Inflammation 2023;46(5):1684-1696.
[12] Fang X, Fu W, Zou B, et al. Tectorigenin relieved sepsis-induced myocardial ferroptosis by inhibiting the expression of Smad3. Toxicol Res (Camb) 2023;12(3):520-526.
[13] Shen H, Xie K, Tian Y, et al. N6-methyladenosine writer METTL3 accelerates the sepsis-induced myocardial injury by regulating m6A-dependent ferroptosis. Apoptosis 2023;28(3-4):514-524.
[14] Liu C, Zou Q, Tang H, et al. Melanin nanoparticles alleviate sepsis-induced myocardial injury by suppressing ferroptosis and inflammation. Bioact Mater 2022;24:313-321.
[15] Qiu J, Xiao X, Gao X, et al. Ulinastatin protects against sepsis-induced myocardial injury by inhibiting NLRP3 inflammasome activation. Mol Med Rep 2021;24(4):730.
[16] Dan Z, Shi X, Shu C, et al. 4-amino-2-trifluoromethyl-phenyl retinate alleviates lipopolysaccharide-induced acute myocardial injury through activation of the KLF4/p62 axis. Cell Signal 2024;114:111001.
[17] Liu Q, Wu J, Zhang X, et al. Iron homeostasis and disorders revisited in the sepsis. Free Radic Biol Med 2021;165:1-13.
[18] Huang Y, Li L, Li Y, et al. Knockdown of LncRNA Lcn2-204 alleviates sepsis-induced myocardial injury by regulation of iron overload and ferroptosis. J Mol Cell Cardiol 2024;192:79-93.
[19] Zhang J, Song Y, Li Y, et al. Iron homeostasis in the heart: Molecular mechanisms and pharmacological implications. J Mol Cell Cardiol 2023;174:15-24.
[20] Ravingerová T, Kindernay L, Barteková M, et al. The Molecular Mechanisms of Iron Metabolism and Its Role in Cardiac Dysfunction and Cardioprotection. Int J Mol Sci 2020;21(21): 7889.
[21] Han X, Zhang J, Liu J, et al. Targeting ferroptosis: a novel insight against myocardial infarction and ischemia-reperfusion injuries. Apoptosis 2023;28(1-2):108-123.
[22] Zhang L, Jia R, Li H, et al. Insight into the double-edged role of ferroptosis in disease. Biomolecules 2021;11(12):1790.
[23] Dixon SJ, Lemberg KM, Lamprecht MR, et al. Ferroptosis: an iron-dependent form of non-apoptotic cell death. Cell 2012;149(5):1060-1072.
[24] Liu M, Kong XY, Yao Y, et al. The critical role and molecular mechanisms of ferroptosis in antioxidant systems: a narrative review. Ann Transl Med 2022;10(6):368.
[25] Gao M, Monian P, Quadri N, et al. Glutaminolysis and Transferrin Regulate Ferroptosis. Mol Cell 2015;59(2):298-308.
[26] Bannai S, Kitamura E. Transport interaction of L-cystine and L-glutamate in human diploid fibroblasts in culture. J Biol Chem 1980; 255(6):2372-2376.
[27] Sato H, Tamba M, Ishii T, et al. Cloning and expression of a plasma membrane cystine/glutamate exchange transporter composed of two distinct proteins. J Biol Chem 1999;274(17): 11455-11458.
[28] Vučković AM, Bosello Travain V, Bordin L, et al. Inactivation of the glutathione peroxidase GPx4 by the ferroptosis-inducing molecule RSL3 requires the adaptor protein 14-3-3ε. FEBS Lett 2020;594(4):611-624.
[29] Bendavit G, Aboulkassim T, Hilmi K, et al. Nrf2 Transcription Factor Can Directly Regulate

mTOR: LINKING CYTOPROTECTIVE GENE EXPRESSION TO A MAJOR METABOLIC REGULATOR THAT GENERATES REDOX ACTIVITY. J Biol Chem 2016;291(49):25476-25488.
[30] Torrence ME, MacArthur MR, Hosios AM, et al. The mTORC1-mediated activation of ATF4 promotes protein and glutathione synthesis downstream of growth signals. Elife 2021;10:e63326.
[31] Luo C, Liang H, Ji M, et al. Autophagy induced by mechanical stress sensitizes cells to ferroptosis by NCOA4-FTH1 axis. Autophagy 2025; 21(6):1263-1282.
[32] Meira W, Daher B, Parks SK, et al. A Cystine-Cysteine Intercellular Shuttle Prevents Ferroptosis in xCT^{KO} Pancreatic Ductal Adenocarcinoma Cells. Cancers (Basel) 2021; 13(6):1434.
[33] Yan B, Ai Y, Sun Q, et al. Membrane Damage during Ferroptosis Is Caused by Oxidation of Phospholipids Catalyzed by the Oxidoreductases POR and CYB5R1. Molecular Cell 2021;81(2):355-369.e10.
[34] Fan BY, Pang YL, Li WX, et al. Liproxstatin-1 is an effective inhibitor of oligodendrocyte ferroptosis induced by inhibition of glutathione peroxidase 4. Neural Regen Res 2021;16(3):561-566.
[35] Jang S, Chapa-Dubocq XR, Tyurina YY, et al. Elucidating the contribution of mitochondrial glutathione to ferroptosis in cardiomyocytes. Redox Biol 2021;45:102021.
[36] Mou Y, Wu J, Zhang Y, et al. Low expression of ferritinophagy-related NCOA4 gene in relation to unfavorable outcome and defective immune cells infiltration in clear cell renal carcinoma. BMC Cancer 2021;21(1):18.
[37] Huang J, Zhao Y, Luo X, et al. Dexmedetomidine inhibits ferroptosis and attenuates sepsis-induced acute kidney injury via activating the Nrf2/SLC7A11/FSP1/CoQ10 pathway. Redox Rep 2024;29(1):2430929.
[38] Jiang L, Kon N, Li T, et al. Ferroptosis as a p53-mediated activity during tumour suppression. Nature 2015;520(7545):57-62.
[39] Chang LC, Chiang SK, Chen SE, et al. Heme oxygenase-1 mediates BAY 11-7085 induced ferroptosis. Cancer Lett 2018;416:124-137.
[40] Shimada K, Skouta R, Kaplan A, et al. Global survey of cell death mechanisms reveals metabolic regulation of ferroptosis. Nat Chem Biol 2016;12(7):497-503.
[41] Liu Q, Wu J, Zhang X, et al. Iron homeostasis and disorders revisited in the sepsis. Free Radic Biol Med 2021;165:1-13.
[42] Guo J, Wang S, Wan X, et al. Mitochondria-derived methylmalonic acid aggravates ischemia-reperfusion injury by activating reactive oxygen species-dependent ferroptosis. Cell Commun Signal 2024;22(1):53.
[43] Jiang X, Stockwell BR, Conrad M. Ferroptosis: mechanisms, biology and role in disease. Nat Rev Mol Cell Biol 2021;22(4):266-282.
[44] Ye J, Lyu TJ, Li LY, et al. Ginsenoside Re attenuates myocardial ischemia/reperfusion induced ferroptosis via miR-144-3p/SLC7A11. Phytomedicine 2023;113:154681.
[45] Tang LJ, Zhou YJ, Xiong XM, et al. Ubiquitin-specific protease 7 promotes ferroptosis via activation of the p53/TfR1 pathway in the rat hearts after ischemia/reperfusion. Free Radic Biol Med 2021;162:339-352.
[46] Jia B, Li J, Song Y, et al. ACSL4-Mediated Ferroptosis and Its Potential Role in Central Nervous System Diseases and Injuries. Int J Mol Sci 2023;24(12):10021.
[47] Yang F, Wang W, Zhang Y, et al. Effects of ferroptosis in myocardial ischemia/reperfusion model of rat and its association with Sestrin 1. Adv Clin Exp Med 2023;32(2):219-231.
[48] Zhang Y, Zeng Y, Huang M, et al. Andrographolide attenuates sepsis-induced acute kidney injury by inhibiting ferroptosis through the Nrf2/FSP1 pathway. Free Radic Res 2024;58(3):156-169.
[49] Zhang Y, Swanda RV, Nie L, et al. mTORC1 couples cyst(e)ine availability with GPX4 protein synthesis and ferroptosis regulation. Nat Commun 2021;12(1):1589.
[50] Li ZB, Zhou QY, Jiang ZT, et al. Relationship between the expression of ferroptosis-related protein GPX4 in septic myocardial injury and vascular endothelial injury. Journal of Practical Shock (Chinese & English) 2024;8(3):148-151,155.
[51] Tang LJ, Luo XJ, Tu H, et al. Ferroptosis occurs in phase of reperfusion but not ischemia in rat heart following ischemia or ischemia/reperfusion. Naunyn Schmiedebergs Arch Pharmacol 2021;394(2):401-410.
[52] Wu H, Liu Q, Shan X, et al. ATM orchestrates ferritinophagy and ferroptosis by phosphorylating NCOA4. Autophagy 2023;19(7):2062-2077.
[53] Liu J, Song X, Kuang F, et al. NUPR1 is a critical repressor of ferroptosis. Nat Commun 2021; 12(1):647.
[54] Wang D, Qu X, Zhang Z, et al. New developments in the role of ferroptosis in sepsis-induced cardiomyopathy (Review). Mol Med Rep 2025;31(5):118.
[55] Wang XY, Zeng YC, Zhang YX, et al. Hypoxia-inducible factor-1α inhibitor LW6 inhibits myocardial ferroptosis and improves septic myocar-

dial injury in rats. Chinese Journal of Infection Control 2025;(6).

[56] Kang R, Kroemer G, Tang D. The tumor suppressor protein p53 and the ferroptosis network. Free Radic Biol Med 2019;133:162-168.

[57] Wang N, Ma H, Li J, et al. HSF1 functions as a key defender against palmitic acid-induced ferroptosis in cardiomyocytes. J Mol Cell Cardiol 2021;150:65-76.

[58] Du Y, Guo Z. Recent progress in ferroptosis: inducers and inhibitors. Cell Death Discov 2022;8(1):501.

[59] Jiang L, Hickman JH, Wang SJ, et al. Dynamic roles of p53-mediated metabolic activities in ROS-induced stress responses. Cell Cycle 2015;14(18):2881-2885.

[60] Li N, Wang W, Zhou H, et al. Ferritinophagy-mediated ferroptosis is involved in sepsis-induced cardiac injury. Free Radic Biol Med 2020;160:303-318.

[61] Zhang L, Luo YL, Xiang Y, et al. Ferroptosis inhibitors: past, present and future. Front Pharmacol 2024;15:1407335.

Perioperative Precision Medicine
ISSN: 2957-5443

Zentime

Review Article https://doi.org/10.61189/251934gxqfic

Diagnostic performance of deep learning for brachial plexus ultrasound: A systematic review

Jiaen Wu[1], Jiaxun Jiang[1], Zhaopeng Zhou[1], Miao Zhou[2], Liangqing Lin[3], Jinjing Wu[1], Haipo Cui[1]

[1]School of Health Science and Engineering, University of Shanghai for Science and Technology, Shanghai 200093, China. [2]Jiangsu Cancer Hospital, Changzhou 213164, Jiangsu Province, China. [3]Department of Anesthesiology, The First Hospital of Putian, Putian 351100, Fujian, China.

Corresponding author: Haipo Cui.

Declaration of conflict of interest: None.

Received April 9, 2025; Accepted August 13, 2025; Published December 31, 2025

Highlights

- This study compares deep learning methods for brachial plexus ultrasound segmentation, demonstrating improved segmentation efficiency and reduced learning difficulty, which may enhance perioperative regional anesthesia planning and safety.
- U-Net is favored for brachial plexus segmentation due to its enhanced ability to capture contextual features through increased channel utilization.
- Available public brachial plexus datasets are summarized, offering valuable resources for future research and perioperative ultrasound applications.

Abstract

Ultrasound-guided nerve block is a safe and effective regional anesthesia technique; however, accurate identification of the brachial plexus remains challenging due to its small size and low contrast in ultrasound images. Recent advances in deep learning offer promising solutions to enhance brachial plexus segmentation and improve perioperative regional anesthesia precision and safety. This review systematically summarizes current deep learning approaches applied to ultrasound-based brachial plexus segmentation. We highlight key models, including Convolutional Neural Networks, the U-shaped Convolutional Neural Networks and their variants, Mask Region-Based Convolutional Neural Networks, and Generative Adversarial Network-based architectures, and compare their reported performances, with Dice Similarity Coefficients ranging from 0.5865 to 0.882 and Intersection over Union values up to 0.6957. Among them, U-Net remains the most frequently employed due to its balance of accuracy and computational efficiency. Moreover, novel models such as multi-objective brachial plexus segmentation network and BPMSegNet have demonstrated superior segmentation performance by incorporating attention mechanisms and spatial contrast features. Notwithstanding these advancements, challenges persist, particularly limited dataset availability and insufficient model generalization. This review provides a comprehensive overview of recent progress, evaluates comparative performance metrics, and outlines future directions to improve model robustness and clinical applicability and clinical applicability in the perioperative setting.

Keywords: Deep learning, brachial plexus, image segmentation

Introduction

The brachial plexus is a complex network of nerves originating from the anterior rami of cervical and upper thoracic spinal nerves, responsible for the motor and sensory functions of the upper limbs [1]. Injuries to the brachial plexus may result in sensory deficits, neuropathic pain, or even paralysis, significantly diminishing patients' quality of life [2, 3]. Traditional treat-

Address correspondence to: Haipo Cui, School of Health Science and Engineering, University of Shanghai for Science and Technology, No. 516 Jungong Road, Yangpu District, Shanghai 200093, China. E-mail: h_b_cui@163.com.

ment approaches, including pharmacologic analgesia, physiotherapy, and surgical nerve repair, are limited by challenges such as imprecise localization, slow recovery, and significant side effects [3, 4].

Ultrasound-guided brachial plexus block has gained popularity due to its safety, real-time imaging capabilities, and radiation-free operation [5, 6]. Compared with CT or MRI, ultrasound is particularly suitable for bedside procedures and repeated interventions, making it a preferred choice in perioperative regional anesthesia and pain management [7]. However, clinical success relies heavily on operator expertise and precise identification of the low-contrast, small-diameter brachial plexus structures within noisy ultrasound images [8, 9].

In recent years, deep learning, a subfield of artificial intelligence, has revolutionized medical image analysis. Unlike traditional machine learning methods based on hand-crafted features, deep learning leverages multilayer neural networks to automatically learns hierarchical representations from raw data [10]. Notably, Convolutional Neural Networks (CNNs) have demonstrated superior performance in extracting spatial features and patterns in medical images. Architectures such as U-shaped Convolutional Neural Networks (U-Net) and Residual Networks (ResNet) have been widely used for tasks such as organ segmentation, tumor detection, and nerve identification [10, 11]. In ultrasound brachial plexus imaging, improved deep learning models have achieved encouraging outcomes; for instance, U-Net variants have reported Dice coefficients up to 0.658, while modified SegNet models have achieved 96% segmentation accuracy [11, 12].

Despite these advances, challenges persist, including ultrasound image artifacts, anatomical variability, and the scarcity of publicly available datasets. Therefore, a systematic review of current deep learning approaches is essential to guide future developments.

This paper provides a comprehensive review of deep learning applications in brachial plexus segmentation from ultrasound images. We summarize commonly used public datasets, evaluate representative deep learning architectures, and compare model performance using metrics such as Dice coefficient and Intersection over Union (IoU). In addition, current challenges and future directions are discussed. This work aims to provide researchers and clinicians with an informed perspective on the potential and constraints of AI-assisted nerve segmentation. In particular, accurate and automated brachial plexus segmentation can enhance perioperative ultrasound-guided nerve block precision, reduce block failure rates, minimize complications, shorten procedural times, and ultimately improve patient safety and outcomes in upper limb surgeries.

Data and preprocessing

Dataset

High-quality datasets are fundamental for training deep learning models, as they directly determine model accuracy and generalizability. When selecting datasets, not only the size and volume of data but also its diversity and quality should be considered. However, in medical image processing, many datasets remain inaccessible due to patient privacy concerns, which limits the availability of high-quality training data. Fortunately, some researchers and academic competitions have released publicly available datasets. For example, the Ultrasound Nerve Segmentation competition held in mid-2016 focused on identifying brachial plexus nerve structures [13]. **Table 1** summarizes the currently available public ultrasound datasets containing brachial plexus images.

Dataset preprocessing

Although large-scale image datasets can yield satisfactory results in model training, such ideal conditions are rarely achievable in practice. This limitation can be improved through image preprocessing, which effectively enhances the accuracy and performance of deep learning models [16]. Common preprocessing steps include denoising, normalization, and image registration, all of which reduce noise and ensure data consistency [17]. For example, Ly *et al.* applied image rotation to increase sample size and enhance model generalization, while Wang *et al.* employed random cropping and scaling, which were shown to be critical for successful model training [18, 19]. **Table 2** summarizes the preprocessing methods reported in the literature.

Table 1. Medical image dataset

Datasets	Image types	Position	Sample size	Data collection methods	Annotation quality
Ultrasound nerve segmentation	Ultrasonic	Brachial plexus	16780	Details not provided	Expert-trained annotators
Brachial-plexus-segmentation	Ultrasonic	Supraclavicular region	500	Two hospitals not mentioned	Expert-labeled, double-checked
UBPD [14]	Ultrasonic	Brachial plexus	1052	SIEMENS ACUSON NX3 Elite and Philips EPIQ5	Professional anesthesiologists
FLUID-sensitive dataset [15]	MRI	Brachial plexus	274	Standard MRI protocols	Radiologist

Table 2. Preprocessing methods

Reference	Datasets	Preprocessing methods
Wang *et al.* [19]	Kaggle	Random rotation/scaling/shear
Wang *et al.* [20]	Kaggle	Median filtering
Ding *et al.* [14]	UBPD	Bilinear interpolation

Overview of deep learning

The typical workflow for deep learning–based brachial plexus segmentation comprises five stages: (1) dataset preparation, involving the collection and annotation of brachial plexus ultrasound images; (2) image preprocessing, including denoising, normalization, augmentation, and cropping; (3) model selection and training, in which architectures such as CNN and U-Net are applied to extract and learn image features; (4) segmentation inference, in which the trained model is used to segment new images; and (5) performance evaluation, assessing model effectiveness using established metrics. This workflow is illustrated in **Figure 1**, which outlines the end-to-end process from data acquisition to model evaluation. It enables automated and accurate identification of brachial plexus structures, supporting clinical applications such as ultrasound-guided nerve blocks.

CNNs

CNNs are deep learning models particularly effective for image analysis and have been widely applied across various fields. Their core principle lies in hierarchical feature abstraction, progressively extracting feature from low-level texture to high-level semantics representations [21]. The workflow is shown in **Figure 2**.

First, the convolution layer applies filters to the input image to generate feature maps through convolution operations, with different convolution layers capturing different feature levels. The resulting outputs are processed by an activation function, most commonly the Rectified Linear Unit, which introduces nonlinearity and enables the network to learn more complex patterns [22]. Then, the pooling layer down-samples the feature maps to reduce data dimensionality and calculational cost. Finally, the fully connected layer integrates all the features from previous layers and produces the final output through linear transformation and activation.

The advantage of CNN is that it can automatically learn image features, offering greater efficiency than traditional manual feature extraction. Parameter sharing of convolution kernel at different positions reduces the number of model parameters and improves training efficiency. In addition, through convolution and pooling operations, CNN confers certain translation, rotation, and scale invariance, contributing to their robustness. These characteristics have led to remarkable success in tasks such as image classification, target detection, and medical image segmentation.

Classic architectures such as LeNet and GoogLeNet are foundational CNN models, and many modern networks build upon these designs [23, 24]. CNN can also be integrated with other models to enhance accuracy. For instance, Boxtel JV *et al.* employed CNN as a classifier to identify brachial plexus regions in neck ultrasound images, followed by U-Net for segmentation, achieving superior performance compared with the original segmentation model [25].

Mask region-based CNN (R-CNN)

Mask R-CNN is a deep learning model for instance segmentation, achieving pixel-level

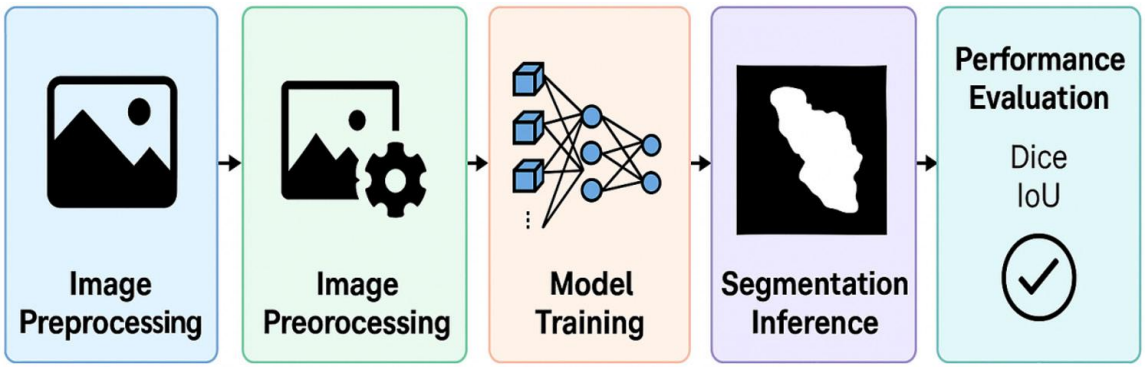

Figure 1. General workflow of deep learning.

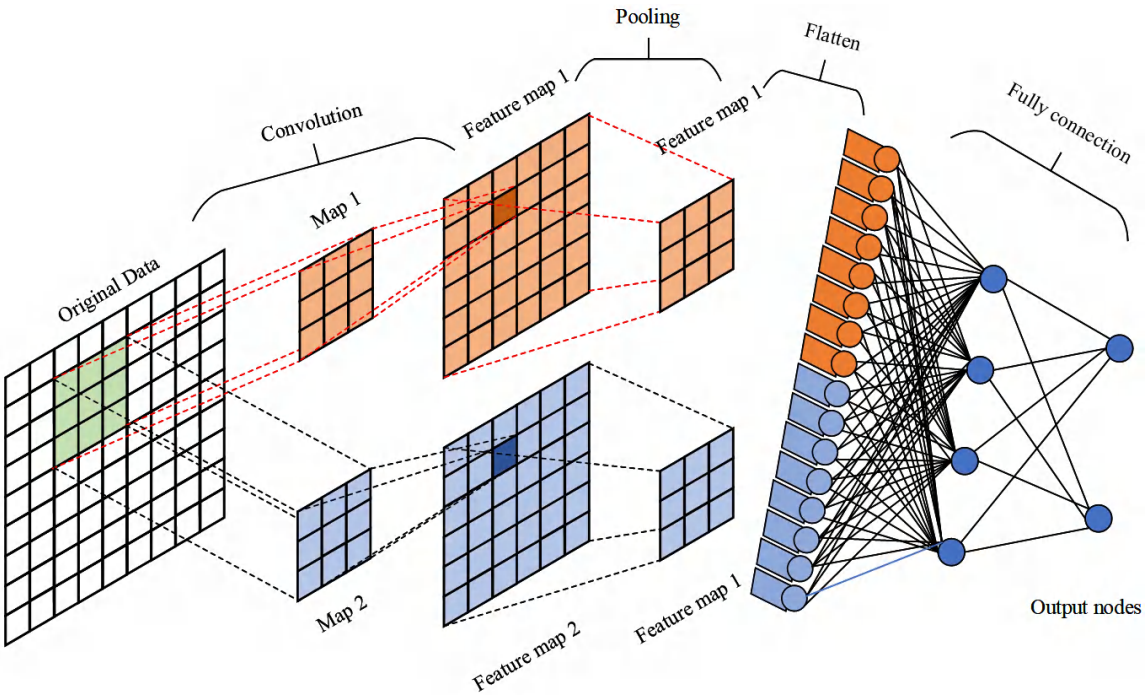

Figure 2. Schematic diagram of convolutional neural network.

accuracy by simultaneously identifying and segmenting individual objects in an image [26]. It extends Faster R-CNN by introducing an additional branch for object mask prediction, thereby enabling instance segmentation alongside target detection. **Figure 3** shows the network structure of Mask R-CNN.

The Mask R-CNN workflow starts with an input image, from which a CNN backbone extracts multi-level feature maps. Then, the Feature Pyramid Network processes these feature maps to construct a multi-scale feature pyramid, allowing the model to detect objects at different scales [27]. Next, a Region Proposal Network generates candidate Regions of Interest that are likely to contain objects [28]. To improve localization accuracy, Mask R-CNN incorporates feature alignment techniques for these Regions of Interest.

For segmentation, Mask R-CNN employs an additional mask branch to predict a binary mask for each Regions of Interest after classification and regression. This mask delineates the exact pixels corresponding to the target object. Model training is guided by a multi-task loss function that integrates classification loss, bounding box regression loss, and mask loss, thereby enabling joint optimization of detection and segmentation. Due to its excellent performance, Mask R-CNN has been widely used in

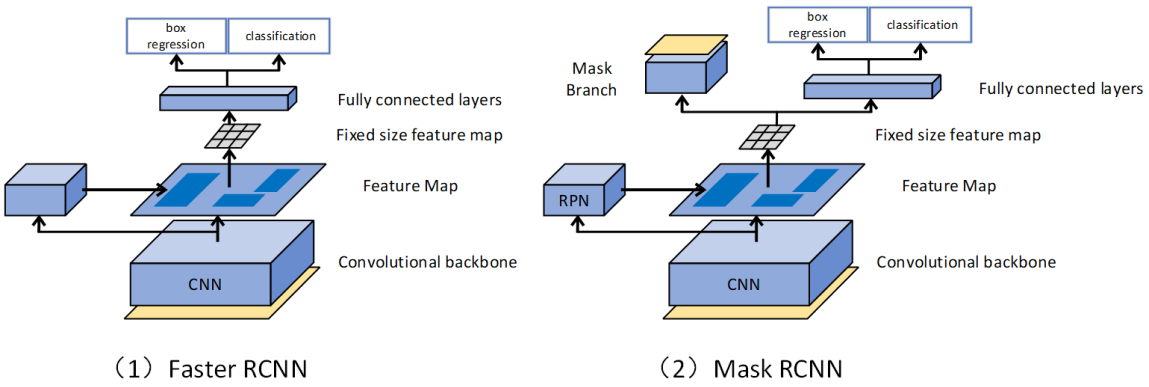

Figure 3. The fundamental architecture of R-CNNs.

autonomous driving, medical image analysis, video surveillance and other fields, providing accurate and efficient solutions for object recognition and segmentation.

Ding et al. developed a multi-objective brachial plexus segmentation network (MallesNet), derived from the Mask R-CNN framework, which achieved higher segmentation accuracy than U-Net and its variants [14]. MallesNet extends Mask R-CNN by enabling simultaneous recognition and segmentation of multiple targets. Notably, it introduces two novel modules: the Spatial Local Contrast Feature extraction module, which calculates multi-scale contrast features to effectively improve small-target recognition, and the Self-Attention Gate, which captures spatial relationships across channels and re-weights feature maps by integrating non-local operations with channel attention. In addition, the up-sampling mechanism of the original Feature Pyramid Network is improved by fine-tuning the feature map using transposed convolution and skip cascade.

U-Net

U-Net, proposed by Ronneberger et al. at the International Biomedical Imaging Challenge in 2015, has become one of the most widely used architectures for medical image segmentation [29]. Its name derives from the characteristic U-shaped structure of the network. Compared with traditional convolutional neural network, U-Net is particularly effective in delineating image boundaries and preserving fine details, thereby improving segmentation accuracy [30]. The two most important components of U-Net include the U-shaped encoder–decoder structure and the skip connection layers.

As shown in **Figure 4**, the encoder uses two consecutive convolutions to extract features and uses a 2×2 max-pooling layer to reduce the image resolution while retaining contextual information. The decoder symmetrically restores the image resolution through transposed convolution (3×3 kernels) and upsampling layers, while integrating encoder features to preserve spatial details.

The skip connection layers directly transfer feature maps from each encoder level to the corresponding decoder level. This design fuses multi-scale encoder features with corresponding decoder features, facilitating the recovery of fine-grained information during reconstruction.

Several improvements to U-Net have been proposed. For instance, Wang et al. enhanced the standard U-Net by incorporating a Recurrent Neural Network (RNN) module into the skip connections to strengthen contextual relevance [19]. Additionally, they introduced an auxiliary loss to improve the accuracy of the model. Their modified model achieved a DICE coefficient improvement of 0.08 compared with the original U-Net model.

ResNet

ResNet is a deep neural network architecture proposed by He et al. in 2015, mainly designed for image recognition and computer vision tasks [31]. In traditional deep neural networks, increasing the number of convolutional and pooling layers was assumed to improve model learning performance. However, this often leads to gradient vanishing or gradient exploding, where gradients become too small or too large, thereby hindering effective training [32]. The

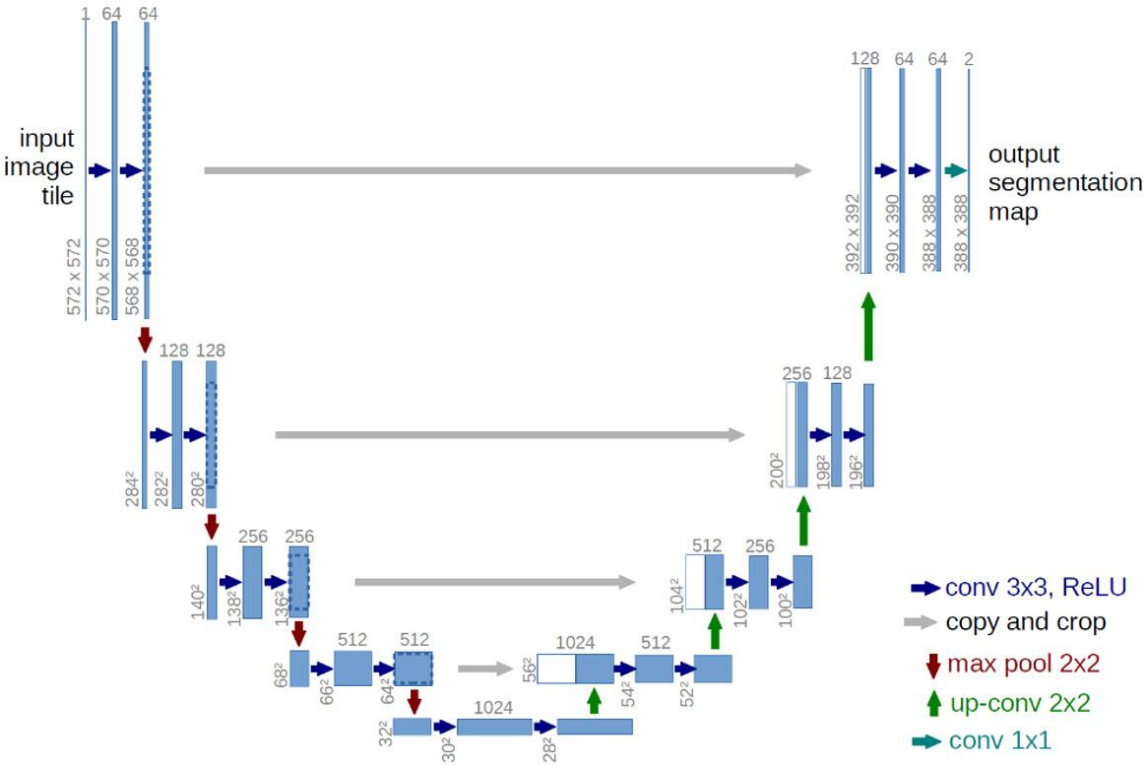

Figure 4. The fundamental architecture of U-Net. This figure was cited from [29].

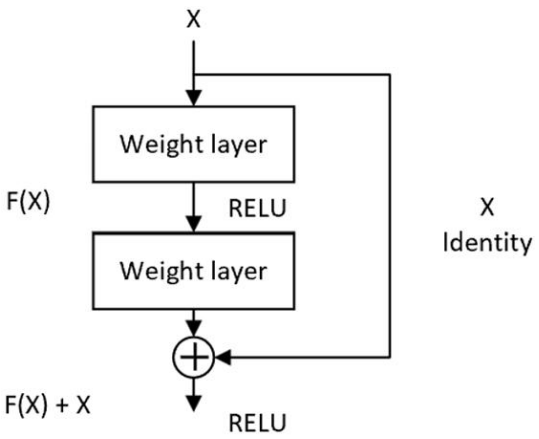

Figure 5. The fundamental architecture of ResNet. ResNet, Residual Neural Network.

core innovation of ResNet is the concept of residual learning, which solves these issues. Instead of directly mapping input to output, each layer learns the residual—the difference between the input and output. As shown in **Figure 5**, this design facilitates more efficient training and enables construction of much deeper networks capable of capturing complex features.

Wang et al. *appl*ied a ResU-Net variant for brachial plexus segmentation [20]. They first used median filtering to reduce speckle noise and then incorporated Dense Convolution and Residual Multi-kernel Pooling modules into the ResU-Net architecture. These modifications reduced spatial information loss and improved the robustness of segmentation at different scales, thereby improving segmentation accuracy. The improved model achieved a Dice coefficient of 0.649, representing an increase of 0.083 compared with the baseline ResU-Net.

Scoring criteria

In image segmentation tasks, model evaluation is essential for assessing how accurately the predicted region matches the ground truth. Since a single metric may not comprehensively capture model performance, multiple evaluation criteria are often applied in combination. Commonly used indicators include IoU or Dice coefficient.

Accuracy

Accuracy is defined as the ratio of true positives (TP) and true negatives (TN) to the total number of samples, as shown in **Table 3** [34].

$$Accuracy = \frac{TP + TN}{TP + FN + FP + TN}$$

Table 3. Confusion matrix [33]

Actual category	Predicted category	
	Positive	Negative
Positive	True Positive (TP)	False Negative (FN)
Negative	False Positive (FP)	True Negative (TN)

This measure is simple and intuitive. However, it can be misleading when the sample categories are unbalanced, as it may overestimate performance when one class dominates the dataset.

IoU

IoU evaluates the overlap between the predicted segmentation and the ground truth by calculating the ratio of their intersection to their union [35].

$$IoU = \frac{TP}{FP + FN + TP}$$

IoU values range from 0 to 1, with values closer to 1 indicating higher similarity between prediction and ground truth. It provides an overall evaluation of segmentation accuracy across category.

Dice coefficient

The Dice coefficient serves as a pivotal metric for evaluating segmentation performance [36]. The goal of image segmentation is to divide an image into regions with similar features, which is usually used to identify and extract specific objects or regions in an image.

$$DICE = \frac{2|A \cap B|}{|A| + |B|}$$

Among them, A is the predicted value, and B is the true value. It compares the degree of overlap between the predicted area and the true labeled area. The Dice coefficient ranges from 0 to 1, with higher values indicating better segmentation accuracy. A Dice score of 1 denotes complete overlap, while 0 indicates no overlap at all.

Chapter summary

In recent years, a variety of deep learning models have been applied to the recognition and segmentation of brachial plexus structures in ultrasound images. Beyond conventional CNNs, models such as U-Net, ResNet, and more advanced architectures have demonstrated the ability to automatically extract image features and achieve accurate nerve segmentation. However, the inherent noise, low contrast, and complex background of ultrasound images, simple models often limit the accuracy of simple models.

To improve the accuracy of recognition and segmentation, researchers have tried to integrate specially designed modules or sub-networks into standard architectures. These modules enhance the capture of global and local context information, enabling the models to better interpret pixel-level relationships and thereby improve segmentation performance in complex imaging scenarios.

In addition, although these modifications increase the computational cost, they enhance the model's ability to manage uncertainty and fuzzy boundaries in ultrasound images. In general, inserting modules or subnetworks represents a key strategy for improving segmentation accuracy in brachial plexus ultrasound and has broad application prospects.

Existing architectures for brachial plexus segmentation

This section classifies and analyzes representative deep learning architectures for brachial plexus segmentation, as summarized in **Table 4**.

Pisda *et al.* evaluated several architectures, including fully convolutional networks, ResNet-34, and LinkNet [37-39]. Among these, LinkNet demonstrated the fastest training speed and most effective transfer learning performance on ultrasound images, with an accuracy of up to 0.8966.

Hafiane et al. briefly compared deep learning and machine learning in medical image recognition in 2017 [40]. They designed a 3-layer CNN (3×3 convolutions, Rectified Linear Unit activation, and max-pooling) that integrated spatial and temporal information. Their results showed that CNNs outperformed support vector machines, with an accuracy of 0.89 [41]. The researchers emphasized that richer data

Table 4. Performance evaluations of models for brachial plexus segmentation

Model	Reference (Year)	Database (Size)	Hardware/Software	Accuracy	Dice	IoU
FCN	Pisda *et al.* (2022)	Kaggle (9970)	NVIDIA GPU + Keras	0.8284	/	0.4800
LinkNet	Kuldeep *et al.* (2022)	Kaggle (9970)	NVIDIA GPU + Keras	0.8966	/	0.5200
CNN + spatial information	Hafiane *et al.* (2017)	Medipole Garonne Hospital (5000)	Not specified	0.8900	/	/
CNN + U-Net	Xi *et al.* (2024)	Beijing Jishuitan Hospital (502)	Not specified	/	0.7480	0.6300
MallesNet	Ding *et al.* (2022)	UBPD (1052)	NVIDIA GTX 1080Ti + TensorFlow	/	0.8460	/
U-Net	Kaggle (2016)	Kaggle (16780)	Not specified	/	0.5865	/
U-Net	Tian *et al.* (2022)	Ningbo Sixth Hospital (340)	NVIDIA GTX 1050ti/NVIDIA RTX 3090 + PyTorch	/	0.6850	/
QU-Net	Long *et al.* (2018)	Collected by themselves (11144)	NVIDIA GTX 1070 + PyTorch	0.6500	/	/
U-Net + EfficientNet	Kong *et al.* (2021)	Kaggle (5635)	NVIDIA GTX 1080 + PyTorch	/	0.7347	0.6957
U-Net + RNN	Wang *et al.* (2021)	Kaggle (5635)	Not specified	/	0.6490	/
M-Net	Abraaham *et al.* (2019)	Kaggle (5635)	NVIDIA GTX 1070 + Keras	/	0.8820	/
ResU-Net	Wang *et al.* (2019)	Kaggle (5633)	NVIDIA GTX 1080 + Keras	/	0.7093	/
YOLOv4	Sugino *et al.* (2024)	Collected by themselves (1612)	NVIDIA A100 + PyTorch	0.8150	/	/
BPMSegNet	Ding *et al.* (2020)	UBPD (1055)	NVIDIA GTX 1080Ti + TensorFlow	/	/	/
CNN+GAN	Liu *et al.* (2018)	Collected by themselves (5800)	Not specified	/	/	0.7320

Note: IoU, Intersection over Union; FCN, Fully Convolutional Network; CNN, Convolutional Neural Network; U-Net, U-shaped Network; RNN, Recurrent Neural Network; ResU-Net, Residual U-Net; GAN, Generative Adversarial Network; BPMSegNet, Brachial Plexus Multi-task Segmentation Network.

further enhance the applicability of CNNs in medical imaging.

Xi et al. trained a U-Net-based segmentation model using patient ultrasound images from Beijing Jishuitan Hospital to identify brachial plexus structures [42]. Manual annotations from experienced anesthesiologists served as the clinical gold standard for comparison. The model achieved a Dice coefficient of 0.748 and an IoU of 0.630, indicating strong overlap with expert-labeled regions. These results demonstrate the clinical potential of deep learning models in accurately and automatically identifying brachial plexus nerves.

Ding et al. enhanced Mask R-CNN by introducing a Spatial Local Contrast Feature module and a Self-Attention Gate to capture multi-channel spatial relationships, and named the improved model MallesNet [14]. This model was applied not only to brachial plexus segmentation but also to the segmentation of surrounding peripheral structures such as veins, arteries, and muscles. Studies have found that leveraging these uncovered structures around the brachial plexus can facilitate the identification of brachial plexus nerves [43]. MallesNet achieved good segmentation performance on the UBPD dataset.

Tian et al. conducted a comparative study on various models for brachial plexus trunk segmentation in ultrasound images [44]. Using a dataset of 340 brachial plexus ultrasound images annotated by three experienced clinicians as the gold standard for model comparison, they evaluated 12 deep learning models and found that U-Net achieved the best segmentation accuracy with an IoU of 0.6850. Although U-Net contained only 7.76 million parameters, its processing speed was limited to 15 images per second. By contrast, LinkNet ranked second with an IoU of 0.6627 but

offered higher processing efficiency, suggesting greater potential for real-time brachial plexus segmentation in the future.

Long et al. believed that the standard U-Net focuses primarily on pixel-level classification, which is insufficient to handle the high noise inherent in brachial plexus ultrasound images [45]. To address this limitation, they proposed QU-Net, incorporating a new loss function that compares pixel-level similarity between predicted and target crops. However, due to the relatively small training dataset, the accuracy rate was only 0.65.

Similarly, Kong et al. addressed the problem of blurred edges in brachial plexus images, which often leads to reduced segmentation accuracy [46]. They modified the U-Net model by incorporating dilated convolutions into the skip connections, thereby reducing noise and mitigating the imbalance between positive and negative samples. This approach achieved a Dice coefficient of 0.7347 and an IoU of 0.6957.

Wang et al. used U-Net as the basic architecture and enhanced it with a RNN module, effectively improving contextual feature extraction [19]. An auxiliary loss function was added to determine the presence or absence of brachial plexus nerves in the image, further improving model accuracy. Their findings indicated that U-Net model is efficient for capturing both global and local information, supporting its clinical applicability.

Abraham et al. tested their approach using Kaggle ultrasound dataset [47]. Differs from U-Net, their M-Net architecture has 5 convolutional layers in the encoder and utilizes average pooling rather than maximum pooling to reduce feature map resolution. Furthermore, they incorporated multi-scale decomposition, which separates signals into different frequency components: noise is primarily concentrated in small-scale (high-frequency) components, while meaningful information is distributed in large-scale (low-frequency) components. By applying thresholding and filtering, M-Net effectively suppressed high-frequency noise while preserving useful signals. Building on this principle, M-Net leverages multi-scale inputs to supervise feature maps, thereby mitigating the impact of image noise on accuracy to some extent. However, the authors noted that M-Net may suffer from overfitting and emphasized the need for larger datasets for validation.

Wang et al. observed that U-Net alone was not accurate enough in low-contrast ultrasound images [20]. To address this limitation, they integrated ResNet with U-Net and introduced Dense Convolution kernels and a Residual Multi-kernel Pooling module, realizing the ResU-Net architecture. This model achieved a Dice coefficient of 0.7093, demonstrating superior performance compared with conventional U-Net.

YOLO (You Only Look Once) is an object detection algorithm designed to achieve fast and efficient object recognition by reframing object detection as a single regression problem [48]. The model divides the image into grids, with each grid simultaneously predicting multiple bounding boxes and categories, which not only accelerates prediction efficiency but also enables detection of multiple objects within a single forward pass. The core advantage of YOLO lies in its excellent balance of speed and accuracy: compared with traditional two-stage detectors such as Faster R-CNN, YOLO greatly improves inference speed by converting the detection problem into a regression problem, while maintaining a high detection accuracy through network optimization and loss function design.

Sugino et al. applied YOLOv4 to brachial plexus ultrasound images, exploring suitable network structures and input image scales for nerve detection [49]. Using two datasets comprising 1,612 labeled brachial plexus ultrasound images, they evaluated the influence of model scaling and input size on performance. Their findings confirmed that YOLOv4's scalable architecture offers an effective trade-off between computational efficiency and segmentation accuracy, while reducing network complexity.

Against gold-standard manual annotations, the optimal model (YOLOv4-P7, 384×384 input) achieved a Dice coefficient of 0.846. Visual comparisons showed close alignment with manual labels, and real-time inference at 192.4 fps ensured practical utility.

SegNet, based on the network architecture of VGG-13, applies an unpooling structure in the decoder to enhance boundary recognition in segmentation task [50]. Ding et al. proposed a

Table 5. Performance comparison to different models on the UBPD dataset

Model	AP@mask/AP@B-box			
	AP@50	AP@60	AP@70	AP@50
Mask R-CNN	43.96/58.00	39.45/48.71	30.41/38.40	27.89/33.11
YOLACT	57.15/62.01	45.95/51.58	42.81/41.28	34.02/30.39
BPMSegNet	58.02/62.97	48.92/56.46	42.06/42.01	37.18/37.62

Note: AP, average precision; AP@50, AP@60, AP@70, precision at intersection-over-union thresholds of 0.50, 0.60, and 0.70, respectively; B-box, bounding box.

novel brachial plexus segmentation network - BPMSegNet, incorporating three key innovations: Spatial Local Contrast Features, self-attention gates, and skip connections with transposed convolutions [51]. BPMSegNet was trained and evaluated on the UBPD dataset, which they also developed, consisting of 1,055 brachial plexus ultrasound images, including nerves and surrounding tissues. For detection, BPMSegNet achieved the best results on multiple metrics, with AP@50, AP@60, AP@70 and AP reaching 62.97, 56.46, 42.01 and 37.62, respectively. In segmentation tasks, it also outperformed competing models, with the highest AP@50, AP@60 and AP scores of 58.02, 48.92 and 37.18, respectively. As shown in **Table 5**, compared with Mask R-CNN and YOLAT, BPMSegNet demonstrated segmentation results more consistent with manual annotations, with smoother edge delineation, while other models exhibited category misjudgment and missed detections [52].

Liu et al. proposed an innovative deep learning model that combines a Generative Adversarial Network (GAN) to achieve accurate segmentation of brachial plexus structure in ultrasound images [53, 54]. A GAN consists of two competing components: a generator and a discriminator. Through adversarial training, the two networks iteratively improve each other's performance, leading to more robust feature learning. The researchers pointed out two major limitations of conventional convolutional CNN-based approaches for nerve segmentation. First, CNNs may overlook subtle anatomical defects, causing suboptimal performance for pixel-level label prediction. In complex ultrasound background, this limitation reduces segmentation accuracy. Second, patient movement or inability to fully cooperate during scanning can cause the nerve region to be mistakenly identified as background, compromising the accuracy of the segmentation.

To solve the first limitation, the researchers designed a deep learning framework integrating a GAN, which consists of two main parts: a segmentation network and a discriminator network. The segmentation network aims to generate segmentation results that closely approximate the true neural structures, while the discriminator acts as a "supervisor", distinguishing between predicted outputs and ground-truth labels. Through adversarial training, the segmentation network progressively improves its performance by attempting to "fool" the discriminator into accepting its predictions as real. To address the second problem, the researchers used dilated convolution to increase the receptive field of the model. This technique allows the model to obtain more contextual information without losing resolution, thereby capturing the characteristics of neural structures over a wider range.

Experimental results demonstrated a significant improvement in segmentation accuracy. Compared with conventional FCN, the GAN-based approach increased the IoU coefficient by 27.8%, providing a more accurate and reliable solution for neural image segmentation in clinical applications. Although adversarial training did not uniformly enhance all performance metrics, it notably improved segmentation accuracy from an anatomical perspective, achieving closer consistency with manual delineation.

Discussion and challenges

Discussion

In this review, we analyzed 15 deep learning models for brachial plexus segmentation, highlighting substantial progress in this field. Early studies primarily applied simple CNNs, and subsequent research introduced more sophisticated architectures. Among them, FCN and U-Net have been intensively used due to their excellent performance. Later, numerous U-Net vari-

ants have since been proposed, often incorporating modules such as residual blocks to enhance feature learning, or adopting multi-task architectures to improve recognition capability. Overall, U-Net–based networks remain the most widely preferred for brachial plexus segmentation. The LinkNet model achieved the highest accuracy (0.8966) on the Kaggle dataset, demonstrating its strong suitability for this benchmark. M-net, proposed by Abraham *et al.* ranked second. Its deeper encoder with additional convolutional layers likely contributed to improved accuracy; however, the added complexity also raises concerns about potential overfitting, underscoring the need for larger datasets for validation.

In addition, several studies emphasized the critical role of data preprocessing [20, 55, 56]. For example, Wang et al. demonstrated that preprocessing the Kaggle dataset increased the Dice coefficient from 0.7063 to 0.7093, highlighting how appropriate preprocessing strategies can yield measurable improvements in segmentation accuracy [20].

Challenges

Despite notable progress, deep learning segmentation of brachial plexus in ultrasound imaging still faces many challenges. First, data scarcity remains the foremost issue. Publicly available datasets are limited due to patient privacy concerns, institutional data protection policies, lack of standardized annotation protocols, and the high cost of expert annotation. Consequently, many studies rely heavily on the Kaggle dataset or on restricted, unpublished data. This limitation constrains model training and hinders generalizability. Although data augmentation and image preprocessing can partially solve this problem, they cannot fundamentally overcome the upper bound imposed by insufficient data.

Furthermore, clinical translation to low-resource clinical settings is another major barrier. Characterized by—introduces additional hurdles. Real-world deployment, particularly in point-of-care scenarios (e.g., portable ultrasound machines), is constrained by limited computational power, memory capacity, and real-time inference requirements. Complex neural architectures that demand substantial GPU acceleration, high-capacity Random Access Memory (RAM), and extensive floating-point operations are often impractical for embedded systems. This challenge is compounded by the need for energy-efficient designs to prevent overheating in portable devices, further restricting model complexity. These challenges not only affect the practicality of the model but also raise important questions about future research directions and technological development.

Looking forward, future research must focus on enhancing model generalization under limited data conditions and identify the best optimization strategy to advance the clinical applicability of deep learning for brachial plexus ultrasound imaging.

Future research directions

As highlighted in the preceding discussion, there is a significant shortage of publicly available brachial plexus datasets, particularly in ultrasound imaging. Therefore, establishing a comprehensive, standardized, and expert-annotated public dataset is of critical importance. As the volume and quality of training data increase, the performance and generalizability of deep learning models are expected to improve substantially, thereby accelerating progress in this research area.

To address this challenge, efforts should be directed at both policy and technical fronts. From a policy perspective, data-sharing agreements and multi-institutional collaborations should be encouraged, supported by ethical frameworks and regulatory guidelines. From a technical perspective, privacy-preserving strategies such as data encryption, federated learning, and differential privacy offer secure solutions for cross-institutional data utilization without compromising patient confidentiality. Collectively, these strategies will enable the development of high-quality datasets and robust models, ultimately enhancing the clinical applicability of deep learning in brachial plexus ultrasound segmentation.

Another important research direction involves improving the practical deployability of deep learning models in real-world clinical environments. While many models demonstrate excellent segmentation accuracy under controlled settings, their high computational requirements often hinder application in low-resource or

point-of-care scenarios. Future studies should focus on optimizing existing algorithms or developing lightweight, efficient architectures capable of supporting real-time segmentation on embedded or portable ultrasound devices. Techniques such as model pruning, quantization, and knowledge distillation can reduce model size and computational cost while preserving accuracy. Moreover, integrating optimized models with ultrasound systems through interoperable software interfaces or plug-in modules will be essential for seamless clinical adoption. Exploring on-device inference, edge computing, and low-latency processing pipelines will further facilitate the development of lightweight, hardware-friendly AI tools that support real-time decision-making, reduce clinician workload, and enhance diagnostic efficiency.

In this context, combining high-quality datasets with optimized algorithms will not only improve segmentation accuracy in brachial plexus ultrasound imaging but also advance the broader field of medical imaging. Such innovations have the potential to streamline clinical workflows and improve patient care outcomes.

Meanwhile, most current studies on brachial plexus segmentation emphasize performance metrics such as Dice and IoU, while few address the interpretability of deep learning models. In clinical scenarios, however, explainability is crucial for building trust among healthcare providers. Future work should consider incorporating interpretability techniques such as Gradient-weighted Class Activation Mapping, which generates visual heatmaps to highlight the most influential regions in the input image, thereby clarifying the model's decision-making process. Similarly, the application of attention mechanisms can provide insight into feature importance during segmentation. These approaches can significantly enhance the clinical acceptance of AI tools in ultrasound-guided procedures.

Conclusion

This review summarizes recent progress in applying deep learning to brachial plexus ultrasound image segmentation, including the availability of public datasets, commonly used segmentation models, and their evaluation metrics. The main contribution of this review is to analyze existing models, highlight emerging trends, and outline future research directions in this field. These insights may assist researchers in developing accurate, robust, and clinically applicable models for ultrasound-guided brachial plexus segmentation.

Author contributions: Jiaen Wu: Responsible for the primary research work of the paper, including literature review, data analysis, and writing the article. Miao Zhou: Responsible for part of the literature review and writing of specific chapters, particularly those related to relevant work and background. Zhaopeng Zhou, Jiaxun Jiang: Participated in data collection and organization, contributing to the discussion of technical details and methods. Jinjing Wu: Participated in the revision and organization of the paper, mainly helping with formatting and language. Haipo Cui: Corresponding Author: Responsible for the overall conception and review of the paper, guiding the research direction, and finalizing and revising the paper.

References

[1] Grzeczka A, Skowroński A, Zdun M. Anatomy of the brachial plexus (Plexus brachialis) and innervation of the thoracic limb of the Caracal (Caracal caracal). Medical Journal of Cell Biology 2024;12(3):107-116.

[2] Hems T. Chapter 44 - Brachial Plexus Injuries. In: Tubbs RS, Rizk E, Shoja MM, et al., editors. Nerves and Nerve Injuries. San Diego. Academic Press, 2015. p. 681-706.

[3] Lovaglio AC, Socolovsky M, Di Masi G, et al. Treatment of neuropathic pain after peripheral nerve and brachial plexus traumatic injury. Neurol India 2019;67(Supplement):S32-S37.

[4] Goldsmith AJ, Brown J, Duggan NM, et al. Ultrasound-guided nerve blocks in emergency medicine practice: 2022 updates. Am J Emerg Med 2024;78:112-119.

[5] Niyonkuru E, Iqbal MA, Zeng R, et al. Nerve Blocks for Post-Surgical Pain Management: A Narrative Review of Current Research. J Pain Res 2024;17:3217-3239.

[6] Zhang L, Pang R, Zhang L. Comparison of ultrasound-guided costoclavicular and supraclavicular brachial plexus block for upper extremity surgery: a propensity score matched retrospective cohort study. Ann Palliat Med 2021;10(1):454-461.

[7] Prajapati N, Chauhan MAZ, Chaudhary D, et al. Efficacy of ultrasound guided peripheral nerve blocks versus conventional methods in regional Anesthesia. Int J Life Sci, Biotechnol Pharm Res 2025;14(1):342-345.

[8] Warman P, Nicholls B. Ultrasound-guided nerve blocks: efficacy and safety. Best Pract Res Clin Anaesthesiol 2009;23(3):313-326.
[9] Liu S, Wang Y, Yang X, et al. Deep Learning in Medical Ultrasound Analysis: A Review. Engineering 2019;5(2):261-275.
[10] Zhang A, Lipton ZC, Li M, et al. Dive into Deep Learning. arXiv 2021;arXiv:2106.11342.
[11] Zhao H, Sun N. Improved U-Net Model for Nerve Segmentation. Image and Graphics. ICIG 2017. Lecture Notes in Computer Science 2017;496-504.
[12] Yan S, Chen X, Tang X, et al. Segmentation of Brachial Plexus Ultrasound Images Based on Modified SegNet Model. Intelligent Data Engineering and Automated Learning – IDEAL 2023 2023;332-344.
[13] Ultrasound Nerve Segmentation. Available at: https://www.kaggle.com/competitions/ultrasound-nerve-segmentation
[14] Ding Y, Yang Q, Wang Y, et al. MallesNet: A multi-object assistance based network for brachial plexus segmentation in ultrasound images. Med Image Anal 2022;80:102511.
[15] Cao W, Howe BM, Wright DE, et al. Abnormal Brachial Plexus Differentiation from Routine Magnetic Resonance Imaging: An AI-based Approach. Neuroscience 2024;546:178-187.
[16] Burger W, Burge M. Digital Image Processing: An Algorithmic Introduction. Springer Cham, 2022.
[17] Bieniecki W, Grabowski S, Rozenberg W. Image Preprocessing for Improving OCR Accuracy. 2007 International Conference on Perspective Technologies and Methods in MEMS Design 2007;75-80.
[18] Lv YC, Jiang Q, Xu YH, et al. Improved brachial plexus nerve segmentation method based on multi-scale feature fusion. J Comput Appl 2023;43(01):273-279.
[19] Wang Y, Geng J, Zhou C, et al. Segmentation of Ultrasound Brachial Plexus Based on U-Net. 2021 International Conference on Communications, Information System and Computer Engineering (CISCE) 2021;482-485.
[20] Wang R, Shen H, Zhou M. Ultrasound Nerve Segmentation of Brachial Plexus Based on Optimized ResU-Net. 2019 IEEE International Conference on Imaging Systems and Techniques (IST) 2019;1-6.
[21] Alzubaidi L, Zhang J, Humaidi AJ, et al. Review of deep learning: concepts, CNN architectures, challenges, applications, future directions. J Big Data 2021;8(1):53.
[22] Agarap AF. Deep Learning using Rectified Linear Units (ReLU). arXiv 2018;arXiv:1803.08375.
[23] Verdhan V. Image classification using LeNet. Computer vision Using Deep learning: Neural Network Architectures with Python and Keras. New York (USA). Apress Berkeley, CA, 2021. p. 67-101.
[24] Szegedy C, Wei L, Yangqing J, et al. Going deeper with convolutions. 2015 IEEE Conference on Computer Vision and Pattern Recognition (CVPR) 2015;1-9.
[25] Boxtel JV, Vousten V, Pluim J, et al. Hybrid Deep Neural Network for Brachial Plexus Nerve Segmentation in Ultrasound Images. 2021 29th European Signal Processing Conference (EUSIPCO) 2021;1246-1250.
[26] He K, Gkioxari G, Dollár P, et al. Mask R-CNN. 2017 IEEE International Conference on Computer Vision (ICCV) 2017;2980-2988.
[27] Lin TY, Dollár P, Girshick R, et al. Feature Pyramid Networks for Object Detection. 2017 IEEE Conference on Computer Vision and Pattern Recognition (CVPR) 2017;936-944.
[28] Ren S, He K, Girshick R, et al. Faster R-CNN: Towards Real-Time Object Detection with Region Proposal Networks. IEEE Trans Pattern Anal Mach Intell 2017;39(6):1137-1149.
[29] Ronneberger O, Fischer P, Brox T. U-Net: Convolutional Networks for Biomedical Image Segmentation. Medical Image Computing and Computer-Assisted Intervention – MICCAI 2015 2015;234-241.
[30] Siddique N, Paheding S, Elkin CP, et al. U-Net and Its Variants for Medical Image Segmentation: A Review of Theory and Applications. IEEE Access 2021;9:82031-82057.
[31] He K, Zhang X, Ren S, et al. Deep Residual Learning for Image Recognition. 2016 IEEE Conference on Computer Vision and Pattern Recognition (CVPR) 2016;770-778.
[32] Hanin B. Which neural net architectures give rise to exploding and vanishing gradients? arXiv 2018;arXiv:1801.03744.
[33] Caelen O. A Bayesian interpretation of the confusion matrix. Ann Math Artif Intel 2017;81(3): 429-450.
[34] Tharwat A. Classification assessment methods. Appl Comput Inform 2020;17(1):168-192.
[35] Cho YJ. Weighted Intersection over Union (wIoU) for evaluating image segmentation. Pattern Recognit Lett 2024;185:101-107.
[36] Eelbode T, Bertels J, Berman M, et al. Optimization for Medical Image Segmentation: Theory and Practice When Evaluating With Dice Score or Jaccard Index. IEEE Trans Med Imaging 2020;39(11):3679-3690.

[37] Pisda K, Jain P, Sisodia DS. Deep Networks for Brachial Plexus Nerves Segmentation and Detection Using Ultrasound Images. Information Systems and Management Science 2021;132-146.

[38] Koonce B. ResNet50. Convolutional neural networks with swift for tensorflow: image recognition and dataset categorization. Apress Berkeley, CA, 2021. p. 63-72.

[39] Chaurasia A, Culurciello E. LinkNet: Exploiting encoder representations for efficient semantic segmentation. 2017 IEEE Visual Communications and Image Processing (VCIP) 2017;1-4.

[40] Hafiane A, Vieyres P, Delbos A. Deep learning with spatiotemporal consistency for nerve segmentation in ultrasound images. arXiv 2017;arXiv:1706.05870.

[41] Pisner DA, Schnyer DM. Chapter 6 - Support vector machine. In: Mechelli A, Vieira S, editors. Machine Learning. Academic Press, 2020. p. 101-121.

[42] Xi Y, Chong H, Zhou Y, et al. Convolutional neural network for brachial plexus segmentation at the interscalene level. BMC Anesthesiol 2024;24(1):17.

[43] Ustuner E, Yılmaz A, Özgencil E, et al. Ultrasound anatomy of the brachial plexus nerves in the neurovascular bundle at the axilla in patients undergoing upper-extremity block anesthesia. Skeletal Radiol 2013;42(5):707-713.

[44] Tian D, Zhu B, Wang J, et al. Brachial Plexus Nerve Trunk Recognition From Ultrasound Images: A Comparative Study of Deep Learning Models. IEEE Access 2022;10:82003-82014.

[45] Long FN, Zhu XS, Gan JZ. Ultrasound Image Segmentation of Brachial Plexus via Convolutional Neural Networks. J Hefei Univ Technol 2018;41(09):1191-1195+1296.

[46] Kong LJ, Wang QW, Bao YC, et al. A Brachial Plexus Ultrasound Image Segmentation Network Based on Deep Learning. Radio Eng 2021;51(09):841-847.

[47] Abraham N, Illanko K, Khan N, et al. Deep Learning for Semantic Segmentation of Brachial Plexus Nervesin Ultrasound Images Using U-Net and M-Net. 2019 3rd International Conference on Imaging, Signal Processing and Communication (ICISPC) 2019;85-89.

[48] Jiang P, Ergu D, Liu F, et al. A Review of Yolo Algorithm Developments. Procedia Comput Sci 2022;199:1066-1073.

[49] Sugino T, Onogi S, Oishi R, et al. Investigation of Appropriate Scaling of Networks and Images for Convolutional Neural Network-Based Nerve Detection in Ultrasound-Guided Nerve Blocks. Sensors (Basel) 2024;24(11):3696.

[50] Badrinarayanan V, Kendall A, Cipolla R. SegNet: A Deep Convolutional Encoder-Decoder Architecture for Image Segmentation. IEEE Trans Pattern Anal Mach Intell 2017;39(12):2481-2495.

[51] Ding Y, Yang Q, Wu G, et al. Multiple Instance Segmentation in Brachial Plexus Ultrasound Image Using BPMSegNet. arXiv 2020;arXiv:2012.12012.

[52] Jiang X, Liu L, Shan C, et al. Recognizing vector graphics without rasterization. arXiv 2021;arXiv:2111.03281.

[53] Liu C, Liu F, Wang L, et al. SEGMENTATION OF NERVE ON ULTRASOUND IMAGES USING DEEP ADVERSARIAL NETWORK. International Journal of Innovative Computing, Information and Control 2018;14(1):53-64.

[54] Goodfellow I, Pouget-Abadie J, Mirza M, et al. Generative adversarial networks. arXiv 2020; arXiv:1406.2661.

[55] Vashishtha V, Aju D. Nerve segmentation in ultrasound images. 2017 Innovations in Power and Advanced Computing Technologies (i-PACT) 2017;1-5.

[56] Wang Y, Zhu B, Kong L, et al. Brachial Plexus Nerve Trunk Segmentation Using Deep Learning: A Comparative Study with Doctors' Manual Segmentation. arXiv 2022;arXiv: 2205.08143.

Perioperative Precision Medicine
ISSN: 2957-5443

Zentime

Research Article https://doi.org/10.61189/924159jtzdps

Application of 0.15% ropivacaine in labor analgesia for primiparous women with severe pain

Sen Lu, Xiangbing Shui, Jianxin Zhang

Department of Anesthesiology, Suzhou BenQ Medical Center, The Affiliated BenQ Hospital of Nanjing Medical University, Suzhou 215010, Jiangsu Province, China.

Corresponding author: Sen Lu.

Acknowledgement: This work was supported by the Suzhou BenQ Medical Center, The Affiliated BenQ Hospital of Nanjing Medical University (SZMJ2209). The authors would like to thank all the guest editors and anonymous reviewers for their constructive comments.

Declaration of conflict of interest: None.

Received July 7, 2025; Accepted December 4, 2025; Published December 31, 2025

Highlights

- Explored the delivery analgesia mode for the special population of first-time mothers with severe pain.
- Explored the effectiveness and safety of high-concentration ropivacaine in epidural labor analgesia.
- Focused on providing humanistic care for the emotional well-being of postpartum women, extending beyond mere pain relief.

Abstract

Objective: To compare the efficacy and adverse reactions between 0.15% ropivacaine combined with sufentanil and 0.1% ropivacaine combined with sufentanil for labor analgesia in primiparous women with severe pain. **Method:** 195 full-term singleton primiparous women with severe pain (visual pain assessment [VAS] ≥6) were randomly allocated to two epidural analgesia groups using different drug formulations. One group received 0.1% ropivacaine + 0.3 μg/mL sufentanil (control group, n=98). The other group was treated with 0.15% ropivacaine and 0.3 μg/mL sufentanil (experiment group, n=97). The following parameters were recorded: analgesia onset time; maximum VAS scores before analgesia, at 20 min after epidural administration, and during labor; number of analgesic pump presses; number of rescue analgesia events; total analgesic drug consumption; modified Bromage score; maternal satisfaction; duration of labor stages; mode of delivery; neonatal Apgar scores at 1 min and 5 min; and incidence of adverse reactions during labor analgesia, such as skin itching, nausea and vomiting, urinary retention, and fever. **Result**: The onset time of analgesia in the experimental group was significantly shorter than that in the control group ($P<0.05$). While the maximum VAS scores in both groups were significantly lower at 20 minutes post-epidural administration and during labor than before delivery analgesia ($P<0.05$), no statistically significant inter-group differences were observed in VAS scores or in the number of pump compressions, rescue analgesia events, dosage of anesthetic drugs, modified Bromage score, or satisfaction ratings. Similarly, no significant differences were found between the two groups in the duration of labor, mode of delivery, and Apgar scores of newborns at 1 and 5 minutes, or the incidence of pruritus, nausea/vomiting, urinary retention, or intrapartum fever. **Conclusion:** For primiparous women with severe labor pain, initial use of 0.15% ropivacaine combined with sufentanil significantly shortens the onset time, provides more comprehensive analgesic effects, achieves higher satisfaction, and does not increase short-term adverse reactions (including motor block) compared to the conventional 0.1% concentration regimen.

Keywords: Labor analgesia, ropivacaine, severe labor pain, primipara

Address correspondence to: Sen Lu, Department of Anesthesiology, Suzhou BenQ Medical Center, The Affiliated BenQ Hospital of Nanjing Medical University, No. 181 Zhuyuan Road, Suzhou 215010, Jiangsu Province, China. E-mail: Sen.Lu@benqmedicalcenter.com.

Introduction

During the long process of childbirth, the mothers will inevitably experience severe pain, triggering extensive physiological stress reactions that affect respiration, circulation, metabolism, uterine contractions, and placental perfusion, potentially endangering the condition of the fetus [1, 2]. Timely and effective labor analgesia is crucial for ensuring the safety of both mother and baby. At present, epidural analgesia is the "gold standard" for labor analgesia, and ropivacaine has become the preferred drug due to its lower cardiac and central neurotoxicity [3, 4]. However, the recommended concentration range of ropivacaine in international guidelines (0.0625%-0.15%) is relatively broad, and evidence regarding its dose-response relationship—particularly among individuals with severe labor pain—remains insufficient [5]. Therefore, optimizing the concentration of ropivacaine is of great clinical necessity, especially for mothers with severe pain and higher analgesic needs. The author found in previous research that appropriately increasing the concentration of ropivacaine can shorten the onset time of analgesia without increasing drug consumption or adverse reactions, while also receiving positive feedback from mothers. Through literature review, the author found that similar clinical studies are not abundant, and the optimal concentration of ropivacaine has not been confirmed. This study aims to evaluate the clinical value of ropivacaine at a concentration of 0.15% in this population by comparing two different concentration regimens.

Materials and methods

Subjects and ethics

After the institutional review board approval, primiparous women carrying a single, live, term fetus and requesting epidural labor analgesia were asked to participate in the study immediately after entering the delivery room. All of the eligible parturients signed an individual informed consent. Prior to analgesia, each parturient was given a detailed explanation of the epidural puncture and catheterization, analgesics used for epidural analgesia, possible accidents such as failed epidural catheterization and inadvertent epidural puncture, and alternative rescues available.

Research object

This study enrolled postpartum women who gave birth in Suzhou BenQ Medical Center from January 2024 to December 2024. Inclusion criteria: full-term (gestational age ≥37 weeks) singleton primiparous women, aged 20-35 years, with a body mass index of 21-29 kg/m^2, American Society of Anesthesiologists physical status I or II, and assessed by an anesthesiologist using a visual pain assessment (VAS) as having severe pain (score ≥6) before labor analgesia. Exclusion criteria: pre-eclampsia, contraindications to neuraxial anesthesia, allergy to opioids or ropivacaine. failure to achieve a sensory block level of T10 within 30 min after epidural administration, accidental dural puncture during the procedure, local anesthetic systemic toxicity, pump malfunction during labor analgesia, and epidural catheter blockage or dislodgement [6].

Randomization assignment

After initial screening, eligible subjects were assigned to either the sole local anesthetic group or the combination group through a randomization sequence generated via the online software QuickCalcs# (Graphad, San Diego, CA). The allocation list was sealed and kept by an independent staff member not involved in the study. Immediately after epidural labor analgesia requested by the parturient, the corresponding allocation number was disclosed to determine the analgesic medication to be give [7]. Except for the parturients and caregivers, the data-collecting and data-analyzing members were blinded to the group assignment.

Grouping and handling

The parturients were divided into Group C (control group) and Group E (experimental group) using a random number table. Study solutions were specially prepared by a researcher who did not participate in subsequent anesthesia procedures or follow-up. The analgesic drugs for Group C and Group E were 0.1% ropivacaine plus 0.3 μg/mL sufentanil and 0.15% ropivacaine plus 0.3 μg/mL sufentanil, respectively [7, 8]. All operations and follow-up were performed by anesthesiologists who were unaware of the grouping situation.

Anesthesia plan

Upon entering the delivery room, all parturients received intravenous access and continuous monitoring of heart rate, blood pressure, peripheral capillary oxygen saturation, fetal heart rate and uterine contraction intensity. When uterine contractions remained inadequate, it was up to the midwife to determine whether to use oxytocin for infusion [8, 9]. With the parturient in the left lateral position, epidural puncture was performed at the L2-3 interspace. After confirming absence of cerebrospinal fluid or blood return, a catheter was inserted and secured. A 5 mL test dose of 1% lidocaine was administered; following a 5-minute observation period with no signs of local anesthetic systemic toxicity or lower-limb motor block, the catheter was fixed. The parturient was then turned to a left-tilt position and given a 10 mL initial bolus of the study analgesic solution. Sensory block level was assessed 15 minutes later. If the block reached T10 or above, a patient-controlled epidural analgesia pump was connected, set to a background infusion of 8 mL/h, a bolus dose of 8 mL, and a lockout interval of 15 minutes. If there was sudden pain during labor (VAS>4), the anesthesiologist would check the position of the epidural catheter and administer 10 mL of 0.2% ropivacaine as remedial analgesia. If the pain did not improve satisfactorily after 15 minutes, it was considered a failure of analgesia. In such cases, the anesthesiologist examined the anesthesia plane and repunctured the catheter, and the case was withdrawn from this study [10, 11].

Observation indicators

① The onset time of analgesia was recorded as the interval from the first epidural injection to the occurrence of effective analgesia (VAS score <4 points during uterine contractions).

② The maximum VAS score was recorded before delivery analgesia, at 20 minutes after epidural administration, and during labor. Pain scores were assessed immediately after each uterine contraction, and the expectant mother recalled the contraction to report the most severe pain experienced during that period.

③ Analgesic efficacy during childbirth was assessed by recording: the number of analgesic pump demands, the dosage of analgesic drugs used, frequency of rescue analgesia, modified Bromage score after analgesia onset (0 points, no motion block, full flexion of hip, knee, and ankle possible; 1 point, unable to flex hip or raise straight leg, but full knee and ankle flexion possible; 2 points, unable to flex knee joint, only ankle flexion possible; 3 points, unable to flex ankle joint or move lower limbs), and the satisfaction rate of analgesia [8, 13]. The modified Bromage score was tested every hour from analgesia initiation until the end of delivery, and the maximum value would be recorded.

④ The duration of labor and the delivery method were documented.

⑤ The Apgar scores of newborns at 1, 5, and 10 minutes after birth were recorded, along with the number of cases in which the Apgar score was ≤7.

⑥ Adverse reactions in parturients were recorded, such as skin itching, nausea and vomiting, urinary retention, lethargy, and intrapartum fever (body temperature ≥37.5 °C during labor).

⑦ The number of cases using oxytocin was recorded.

Sample size calculation

In this study, the sample size was determined based on the onset time of analgesia during labor. According to preliminary research, the time to achieve a pain score below <3 was 12±1.8 minutes with 0.1% ropivacaine and 10±1.1 minutes with 0.15% ropivacaine. Assuming $\alpha=0.05$ and $\beta=0.1$, a total of 164 parturients were needed. To account for potential dropouts and data loss, an increase of about 20% in the number of cases was required, resulting in a total of 200 cases being collected.

Statistical analysis

SPSS 19.0 statistical software was used for analysis. Normal distribution measurement data are expressed as mean±standard deviation ($\bar{X}\pm s$), and one-way analysis of variance was used for inter-group comparison; Non-normal distribution metric data are represented by median and interquartile range, and between-group comparisons were conducted using the Mann Whitney U test. Count data

Table 1. Comparison of baseline characteristics

Group	Cases	Age (year)	Height (cm)	Weight (kg)	Pregnancy (w)	Cervical opening size (cm)
CG	98	27.9±3.8	158.3±4.2	68.5±7.8	39.8±1.1	1.5±0.6
EG	97	27.5±4.2	159.1±3.9	67.2±6.9	39.6±1.0	1.6±0.6

Note: CG, control group; EG, experiment group.

Table 2. Comparison of analgesia onset time

Group	Onset (min)
CG (n=98)	17.8±2.0
EG (n=97)	10.9±1.2
P	<0.001

Note: P<0.05, the onset time of analgesia in the EG group was significantly shorter than that in the CG group.

Table 3. Comparison of VAS scores at different time points

Group	Before analgesia	20 minutes after administration	During labor process	P
CG (n=98)	8 (7-8)	1 (1-2)[a]	2 (2-3)[a]	<0.001
EG (n=97)	8 (6-9)	1 (1-2)[a]	2 (1-2)[a]	<0.001
P	0.74	0.97	0.82	

Note: [a]P<0.05, compared with before analgesia, the VAS scores of 20 minutes after administration and during labor process has significantly decreased.

are presented as an number (percentage), and comparisons between groups were performed using the chi-square test or Fisher's exact test. P<0.05 indicates a statistically significant difference.

Result

During the study period, 200 pregnant women met the inclusion criteria. One patient in group E withdrew from the study due to analgesic pump malfunction, and two patients in each group were excluded following accidental rupture of the dura mater. In the end, a total of 195 patients completed the study. There were no statistically significant differences between the two groups in age, height, weight, gestational age, or size of the cervix during analgesia (**Table 1**).

The onset time of analgesia in group E was significantly shorter than that in group C, and the difference was statistically significant (P<0.001; **Table 2**).

Before analgesia, there was no statistically significant difference in VAS scores between the two groups. After 20 minutes of epidural administration, the VAS scores of both groups were significantly lower than the pre-analgesia values (P<0.001). Similarly, the maximum VAS scores during labor were significantly reduced compared with pre-analgesia levels (P<0.001), but the difference between the two groups was not statistically significant (**Table 3**).

There were no statistically significant differences in the number of analgesic pump demands, modified Bromage score, or the need for rescue analgesia between the two groups of parturients. No analgesia failure occurred in either group during the study. Satisfaction with pain relief was significantly higher in Group E than in Group C (P<0.001; **Table 4**), and the dosage of ropivacaine used in Group C was significantly higher than that in Group E (P<0.001; **Table 4**).

There was no statistically significant difference in the delivery methods between the two groups (**Table 5**). Neonatal Apgar scores of both groups were above 9 points, and the difference was not statistically significant.

One case (1%) of skin itching occurred in Group C, and the parturient complained of mild itching that could be tolerated and was not treated. However, Group E did not experience any skin itching, and the difference between the two groups was not statistically significant. The incidence of nausea/vomiting, urinary retention, and intrapartum fever did not differ significantly between the two groups (**Table 6**). Both groups did not experience drowsiness.

Discussion

Some parturients experience severe pain in the early stages of labor, for which conventional concentrations of ropivacaine often provide inadequate analgesia. Increasing the concentration of local anesthetics is an effective and

Table 4. Comparison of analgesic efficacy during childbirth

		CG (n=98)	EG (n=97)	P	X^2
PCA time (n)		3 (2-3)	3 (2-4)	0.75	
Dosage of analgesic drugs (ml)		76.43 (58.62-96.87)	72.35 (52.43-92.58)	0.64	
Dosage of Ropivacaine (mg)		76.43 (58.62-96.87)	108.53 (78.65-138.87)[a]	<0.001	
Dosage of Sufentanil (μg)		22.93 (17.59-29.06)	21.71 (15.73-27.77)	0.82	
Bromage score [n (%)]	0	97 (99)	95 (98)	0.92	
	1	1 (1)	2 (2)	0.86	
Remedy [n (%)]	0 time	24 (24.5)	32 (33.0)	0.09	2.16
	1 time	42 (42.9)	38 (39.2)	0.62	0.86
	2 time	18 (18.4)	16 (16.5)	0.32	0.25
	3 time	14 (14.2)	11 (11.3)	0.58	0.98
Satisfaction with pain relief [n (%)]		74 (76)	92 (95)[a]	<0.001	

Note: [a]P<0.05, the dosage of ropivacaine used in the EG group was significantly lower than that in the CG group, and the satisfaction with pain relief of the EG group was significantly higher than that of the CG group.

Table 5. Comparison of delivery outcomes

		CG (n=98)	EG (n=97)	P	F
Delivery method [n (%)]	Natural birth	91 (93)	90 (93)	0.92	
	Caesarean section	7 (7)	7 (7)	0.98	
Total volume of blood (ml)		268.4±32.5	263.5±42.3	0.86	
Apgar scores	1 min	9.7±0.4	9.8±0.3	0.65	1.01
	5 min	9.5±0.4	9.3±0.5	0.68	1.25
	10 min	9.8±0.3	9.9±0.2	0.71	1.03
Usage of oxytocin (n)		75	68	0.78	

Table 6. Comparison of adverse reactions [n (%)]

	CG (n=98)	EG (n=97)	P
Pruritus	1 (1)	0 (0)	0.43
Nausea and vomiting	4 (4)	4 (4)	0.93
Urinary retention	5 (5)	4 (4)	0.86
Fever during childbirth	14 (14)	12 (12)	0.45

easy-to-use strategy in such cases [9, 12]. Since the diffusion rate of local anesthetics is logarithmically related to concentration, doubling the concentration of ropivacaine, for example, can shorten the onset time by about one-third [5, 13, 14]. Therefore, initiating analgesia with a higher concentration (0.15%) can significantly shorten the onset of action and improve maternal satisfaction. This clinical practice has confirmed that the use of 0.15% ropivacaine solution throughout the entire process not only has a good analgesic effect, but also does not increase related adverse reactions.

Epidural analgesia is the gold standard for labor pain relief, and ropivacaine has become the preferred choice due to its low cardiac and central nervous system toxicity [15, 16]. The recommended conventional dose is 0.08%-0.15%, so the control group (Group C) used the hospital's standard formula (0.1% ropivacaine + 0.3 μg/mL sufentanil) [17]. The experimental group (Group E) was administered 0.15% ropivacaine combined with a small dose of sufentanil. This concentration was selected based on the finding by Xing et al. that the lowest effective concentration of ropivacaine for labor analgesia is 0.154% [18]. Therefore, selecting a concentration close to the minimum effective concentration is aimed at providing more sufficient baseline analgesia for severely painful mothers, which is theoretically reasonable and clinically targeted.

Both groups in this study showed good analgesic effects during the late stage of labor, with little need for remedial measures. For those in need of remedial analgesia, a single dose of 0.2% ropivacaine was administered. Sng et al. have demonstrated that this concentration acts rapidly and effectively without increasing adverse reactions [19]. In this study, rescue

analgesia was significant (the vast majority only required one attempt without failed withdrawal). Most importantly, even when the concentration was increased to 0.2%, no significant motor block or other related adverse reactions were observed, fully verifying the safety of this remedial plan.

Both groups of mothers achieved good analgesic effects, but the control group gained higher satisfaction scores, which seems to be related to its shorter onset time of analgesia. When pregnant women experience frequent uterine contractions for the first time, they often feel anxious and tense, which may lead to irritability toward surrounding people and situations [20]. When the pain is suppressed, the anxious emotions are often relieved, making the mother more optimistic about the entire delivery process, which can be easily seen from the comparison of the mothers' expressions. Deng et al. evaluated the relationship between intraspinal delivery analgesia and postpartum depression, and the results showed that the incidence of postpartum depression in women who received intraspinal delivery analgesia was significantly lower than that in women who did not [21]. This also indicates that sufficient analgesia can reduce the incidence of depression in women.

Although increasing the concentration of ropivacaine can shorten the onset time of analgesia and improve satisfaction with postpartum analgesia, higher drug concentrations will also be accompanied with more adverse reactions, such as uterine atony, weakened lower limb strength, and severe liver and kidney load [22, 23]. Therefore, the use of higher-concentration ropivacaine has certain limitations. It is primarily suitable for postpartum women who experience severe pain immediately at the beginning of delivery, those who have already experienced severe pain and cannot undergo single-shot spinal anesthesia, or those who have more stringent requirements regarding the onset time of analgesia. The safety and effectiveness of high-concentration ropivacaine in labor analgesia need further verification.

This study is a single-center study that only includes term singleton primiparous women, and the extrapolation of results is limited, especially with respect to other common populations experiencing severe labor pain (such as multiparous women). In the future, multi-center, large-sample studies are needed to verify the effectiveness and safety of the 0.15% concentration in this population. In addition, the observation period is relatively short, recording only short-term adverse reactions (such as motor block and hypotension), without systematic evaluation of potential long-term outcomes (such as postpartum depression and chronic low back pain). Further follow-up is needed, and a more comprehensive study should be designed to clarify the long-term safety of different concentrations of ropivacaine.

Conclusion

In summary, for primiparous women with severe labor pain, the initial use of 0.15% ropivacaine combined with sufentanil for epidural analgesia significantly shortens the onset time, provides more effective analgesia, and does not increase short-term adverse reactions (including motor block), compared to the conventional 0.1% concentration regimen. This clinical protocol effectively meets the pain relief needs of mothers with severe pain, improves satisfaction with the delivery experience, and has favorable clinical applicability.

Author contributions: Xiangbing Shui and Sen Lu contributed to the conception of the study. Jianxin Zhang contributed significantly to analysis and manuscript preparation. Sen Lu performed the data-analyses and wrote the manuscript. Xiangbing Shui and Jianxin Zhang helped perform the analysis with constructive discussions.

References

[1] Shen XF, Yao SL. Expert consensus on childbirth analgesia 2016. The Journal of Clinical Anesthesiology 2016;32(8):816-818.
[2] Li MJ, Xu Q, Li MY. Mechanism of labor pain and commonly used labor analgesia methods. International Journal of Obstetrics and Gynecology 2018;45(2):125-129.
[3] Anim-Somuah M, Smyth RM, Cyna AM, et al. Epidural versus non-epidural or no analgesia for pain management in labour. Cochrane Database Syst Rev 2018;5(5):CD000331.
[4] Consensus of Chinese experts on pain relief during intraspinal delivery 2021.
[5] Deng XM, Yao SL, Yu BW, et al. Modern Anesthesiology (4th edition). People's Medical Publishing House.

[6] National Collaborating Centre for Women's and Children's Health. Intrapartum care: care of healthy women and their babies during childbirth. Journal of Optoelectronics & Advanced Materials 2007;14(1-2):77-83.
[7] Reina MA, Lirk P, Puigdellívol-Sánchez A, et al. Human lumbar ligamentum flavum anatomy for epidural anesthesia: reviewing a 3D MR-based interactive model and postmortem samples. Anesth Analg 2016;122(3):903-907.
[8] Wang X, Xu S, Qin X, et al. Comparison between the use of ropivacaine alone and ropivacaine with sufentanil in epidural labor analgesia. Medicine (Baltimore) 2015;94(43):1882.
[9] Ji TZ, Li R, Zhu HJ, et al. The Effect of Chloroprocaine in Relieving Sudden Pain during Labor Analgesia. The Journal of Clinical Anesthesiology 2021;37(7):698-701.
[10] Zhou HG, Xue L, Xu HM. Clinical efficacy of different concentrations of ropivacaine in elderly patients with upper limb fractures during brachial plexus block guided by B-ultrasound. Chinese Journal of Gerontology 2021;41(21): 4715-4717.
[11] Wang DH, Chen LP, Xue JJ. Comparison of analgesic effects of different concentrations and volumes of ropivacaine for hip joint capsule peripheral nerve block in elderly patients with hip fractures. The Journal of Clinical Anesthesiology 2022;38(5):497-502.
[12] Luo BR, He SJ, Wu Y, et al. The effect of ropivacaine combined with sufentanil epidural analgesia during the latent period of labor on mother and infant. The Journal of Clinical Anesthesiology 2009;25(7):617-618.
[13] Gan JW, Yu YH. The effect of different concentrations of ropivacaine combined with fentanyl on controlled epidural intermittent pulse injection for labor analgesia. The Journal of Clinical Anesthesiology 2019;35(11):1060-1064.
[14] Luo QY, Jiao J, Huang SQ, et al. Comparison of 0.15% ropivacaine and 0.1% ropivacaine combined with sufentanil for epidural labor analgesia. The Journal of Clinical Anesthesiology 2020;36(8):784-788.
[15] Yu YH, Qu Y, Liu ZQ, et al. Consensus of Chinese experts on pain relief during intraspinal delivery 2021.
[16] Wang FB, Wei XG. Research progress on the application of labor analgesia. Modern Medicine Journal of China 2020;22(02):106-108.
[17] Ma H, Wang GL, Wang JK, et al. Expert consensus on prevention and treatment of complications of spinal canal block (2017). 2017.
[18] Xing YH, Zhang LP, He SJ. The lowest effective concentration of ropivacaine for analgesia in the first stage of labor in countrymen. Chinese Journal of Anesthesiology 2004;24(4):316-317.
[19] Sng BL, Woo D, Leong WL, et al. Comparison of computer-integrated patient-controlled epidural analgesia with no initial basal infusion versus moderate basal infusion for labor and delivery: A randomized controlled trial. J Anaesthesiol Clin Pharmacol 2014;30(4):496-501.
[20] Yao SL, Shen XF. Technical and Management Standards for Labor Analgesia. Science and Technology Literature Press, 2020.
[21] Deng CM, Ding T, Li S, et al. Neuraxial labor analgesia is associated with a reduced risk of postpartum depression: a multicenter prospective cohort study with propensity score matching. J Affect Disord 2021;281:342-350.
[22] Song J, Wang DX, Wang BB, et al. The impact of different timing of delivery analgesia on the labor process, delivery mode, and neonatal outcomes of primiparous women. Chinese Journal of Obstetrics and Gynecology 2020;55(7):476-479.
[23] Zhou X, Li J, Deng S, et al. Ropivacaine at different concentrations on intrapartum fever, IL-6 and TNF-α in parturient with epidural labor analgesia. Exp Ther Med 2019;17(3):1631-1636.

Perioperative Precision Medicine
ISSN: 2957-5443

Zentime

Review Article https://doi.org/10.61189/313450skrqzv

Research progress on pharmacological effects and mechanisms of cycloastragenol

Weiqi Lin[1,2,3*], Qin Zhang[1,3*], Sixu Chen[2,4*], Xinyi Xie[3,5], Jiayin Wang[3,5], Yutong Sun[1,3], Qixiang Xu[3,5], Cuifeng Zhang[2,3,4]

[1]School of Clinical Medicine, Wannan Medical College, Wuhu 241002, Anhui, China. [2]Anesthesia Laboratory and Training Center, Wannan Medical College, Wuhu 241002, Anhui, China. [3]Wuhu Perioperative Monitoring and Prognostic Technology Research and Development Center, Wannan Medical College, Wuhu 241002, Anhui, China. [4]School of Anesthesiology, Wannan Medical College, Wuhu 241002, Anhui, China. [5]School of Pharmacology, Wannan Medical College, Wuhu 241002, Anhui, China.
[*]The authors contribute equally.

Corresponding authors: Qixiang Xu and Cuifeng Zhang.

Acknowledgement: This work was supported by the Natural Science Foundation Of The Higher Education Institutions Of Anhui Province (2024AH051958), the Foundation Of Wannan Medical College (WK2023ZQNZ08), the National University Innovation And Entrepreneurship Training Program (202310368014, 202310368049, 202410368014), the Anhui Province University Innovation And Entrepreneurship Training Program (S202310368087, S202410368004, S202410368009), the Wannan Medical College Undergraduate Research Fund Project (WK2024XS01).

Declaration of conflict of interest: None.

Received January 21, 2025; Accepted April 24, 2025; Published December 31, 2025

Highlights

- Cycloastragenol exhibits anti-aging, anti-cancer, and anti-fibrosis effects.
- Although cycloastragenol shows innovative therapeutic potential, further clinical trials are essential to confirm its clinical applicability.
- Cycloastragenol offers innovative therapeutic avenues for enhancing surgical recovery.

Abstract

Cycloastragenol, a key bioactive compound extracted from Astragalus membranaceus, has attracted increasing attention for its therapeutic potential in anti-aging, cancer treatment, and fibrosis prevention. This review summarizes the pharmacological activities of Cycloastragenol at molecular, cellular, and systemic levels, and discusses its efficacy across various disease models and potential perioperative applications. Current evidence demonstrates that Cycloastragenol exerts dose-dependent therapeutic efficacy through specific molecular targets. However, its clinical translation remains limited, particularly in surgical recovery contexts, underscoring the need for further validation through well-designed clinical trials focused on perioperative outcomes.

Keywords: Cycloastragenol, pharmacological effect, mechanisms of action, research progress

Introduction

Cycloastragenol (CAG), a bioactive triterpenoid derived from Astragalus membranaceus, is primarily obtained through enzymatic hydrolysis of its glycosylated precursor astragaloside IV [1, 2]. This structural modification enhances CAG's pharmacokinetic properties by increasing its lipophilicity, thereby facilitating transmembrane permeability and systemic absorption [3].

CAG's robust organoprotection, anti-inflammatory efficacy, and promotion of cellular stress resistance position it as a candidate for improving perioperative outcomes. Emerging evidence have demonstrated CAG's broad pharmacological activities, including telomerase activation, anti-senescence effects, cardioprotection,

Address correspondence to: Qixiang Xu, School of Pharmacology, Wannan Medical College, No.22 Wenchang West Road, Yijiang District, Wuhu 241002, Anhui Province, China. Tel: +86-18355305112. E-mail: xuqixiang@wnmc.edu.cn. **Cuifeng Zhang**, School of Anesthesiology, Wannan Medical College, No.22 Wenchang West Road, Yijiang District, Wuhu 241002, Anhui Province, China. Tel: +86-15551257181. E-mail: zhangcuifeng@wnmc.edu.cn.

neuropsychiatric modulation, and immune regulation [4-8]. These findings have positioned CAG as a promising candidate for therapeutic applications in various disease contexts.

This review systematically examines the molecular mechanisms and therapeutic potential of CAG, with a particular emphasis on its multi-target regulatory effects on key signaling pathways. By integrating recent pharmacodynamic insights and preclinical studies, we aim to elucidate CAG's translational relevance in precision medicine, particularly in the context of managing age-related and chronic diseases, as well as its emerging potential for improving perioperative outcomes. We further propose novel strategies leveraging CAG's multi-target actions for managing age-related decline and chronic conditions, with implications for optimizing perioperative care and enhancing recovery.

Pharmacological effects of cycloastragenol

Anti-aging effects and cognitive protection

Aging is an inevitable biological process, and telomere shortening is a recognized contributor to cell senescence. CAG is currently the only known telomerase activator with potent anti-aging effects [5, 9, 10]. It delays cellular senescence by upregulating telomerase reverse transcriptase (TERT) mRNA expression and elongating telomeres [11]. In 2012, Cao et al. investigated the anti-aging mechanism of CAG using a D-galactose-induced aging mouse model, and demonstrated that CAG administration significantly enhanced total superoxide dismutase (SOD) activity and total antioxidant capacity, reduced malondialdehyde (MDA) levels, and increased hydroxyproline content [10]. Neuroprotective studies revealed that CAG activated the phosphatidylinositol 3-kinase/protein kinase B/mechanistic target of rapamycin (PI3K/Akt/mTOR) and cAMP response element binding pathways, promoted the expression of synaptic plasticity-related proteins, and alleviated cognitive impairment in Alzheimer's disease models [5, 12]. Hong et al. reported that both CAG and astragalusoside IV reduced the expression levels of p16, cleaved-caspase 3, and Bcl-2 Associated X Protein (BAX), while increasing the expression level of Bcl-2 and TERT, thereby protecting nucleus pulposus cells from high-glucose-induced senescence and apoptosis [13]. Similarly, Ikram et al. showed that CAG downregulated the expression of phosphorylated c-jun n-terminal kinase, phosphorylated p38 mitogen-activated protein kinase, and phosphorylated extracellular signal-regulated kinase (p-JNK, p-P38, and p-Erk), while upregulating the expression of nuclear factor erythroid 2-related factor 2, heme oxygenase-1, phosphorylated tropomyosin receptor kinase B, brain-derived neurotrophic factor, and neuronal nuclear protein (Nrf2, HO-1, p-TrKB, BDNF and NeuN). These changes significantly reduced microglial activation and inflammatory cytokine production, improving oxidative stress, metabolic disturbances, neuroinflammation, apoptosis, and memory impairment in AD mouse models [7]. In D-galactose-induced aging mice, CAG treatment (10 mg/kg for 8 weeks) reduced β-amyloid deposition in the hippocampus by 50%, and Morris water maze testing demonstrated a 35% improvement in spatial memory [4]. Additionally, CAG has been shown to significantly improve behavioral performance and hippocampal structure in AD rat models, thereby enhancing cognitive function, memory, and learning ability [14]. A clinical study also demonstrated that oral administration of a CAG-containing formulation in 20 healthy individuals over 6 months led to a 12% increase in telomere length and marked improvement in skin elasticity [15].

Anti-cancer effect

With rapid economic development and improved living standards, the prevalence of cancer in China has increased markedly. In 2022, approximately 4.82 million new cancer cases and 2.57 million cancer-related deaths were reported [16, 17]. Recent studies suggest that CAG demonstrates notable anti-cancer effects [18]. Mechanistically, CAG binds to target tissue protease B and inhibits lysosomal degradation of major histocompatibility complex class I (MHC-I), thereby promoting MHC-I accumulation on the cell membrane (**Figure 1**). This enhances tumor antigen presentation and augments the cytotoxic activity of $CD8^+$ T cells [19]. Deng et al. reported that combining CAG with a programmed death-1 antibody significantly improved survival in tumor-bearing mice [19]. In colorectal cancer organoid models, CAG in combination with anti-programmed death-1 upregulated MHC-I expression and enhanced the cytotoxicity of $CD8^+$ T cells against tumor cells. Furthermore, CAG also has been shown to inhibit matrix metalloproteinase (MMP)-2 activity and its associated calcification effects, contributing to the amelioration of abdominal aortic aneurysm [20].

Anti-fibrotic effect

Fibrosis is a progressive pathological condition characterized by excessive deposition of extracellular matrix, resulting in tissue distortion and

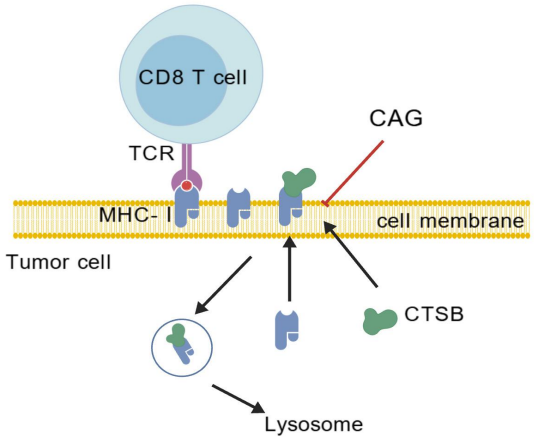

Figure 1. The main anti-cancer pathways of CAG. CD8 T cell, cytotoxic tlymphocyte; TCR, T cell receptor; MHC-I, major histocompatibility complex I; CAG, cycloastragenol; CTSB, Cathepsin B.

gradual loss of organ function [21]. Fibrosis can affect any solid organ, particularly the lungs, liver, heart, and kidneys, and is closely associated with chronic diseases such as diabetes and hypertension. Statistics suggest that about 45% of deaths in Western countries are related to fibrosis-associated diseases [22]. CAG has demonstrated significant anti-fibrotic activity across various organs. In a liver fibrosis mouse model, CAG reduced serum levels of alanine aminotransferase and aspartate aminotransferase, decreased the expression of collagen I and α-smooth muscle actin (α-SMA) in hepatic tissues, and lowered the level of key enzymes and metabolites [1]. In CCl_4-induced hepatic fibrosis in mice, CAG upregulated MMP8, MMP9, MMP12, and interleukin- 6 (IL-6) expression, contributing to fibrosis resolution [23]. In cardiac fibrosis, Dong et al. showed that CAG alleviated isoproterenol-induced myocardial fibrosis and cardiac dysfunction by inhibiting the expression of oxidative stress-related factor NADPH oxidase 4, suppressing phosphorylation of key proteins in the nuclear factor κappa B (NF-κB) signaling pathway (p-IκBα, NF-κB, p-p65), and transforming growth factor-β (TGF-β) expression and inducible nitric oxide synthase transcription [24]. In addition, preliminary studies combining network pharmacology, molecular docking, and animal experiments suggest that CAG may attenuate renal fibrosis in mice by targeting MMP3 and MMP2, reducing collagen fiber deposition, and lowering the expression of TGF-β1, α-SMA, MMP3, and MMP2 in renal tissues [25]. Although clinical data in humans are lacking, preclinical studies in murine models support the therapeutic potential of CAG in hepatic fibrosis [23].

Anti-inflammatory and anti-oxidative stress effects

Oxidative stress arises from an imbalance between oxidative and antioxidant processes, often accompanied by excessive accumulation of reactive oxygen species (ROS). This imbalance can induce tissue inflammation, which in turn exacerbates oxidative stress, forming a vicious cycle that ultimately leads to tissue damage [26].

At the molecular level, CAG exerts bidirectional regulatory effects on key signaling pathways (**Figure 2**). It suppresses nuclear translocation of NF-κB p65 and reduces p-NF-κB p65 expression, leading to significant downregulation of pro-inflammatory cytokines (e.g., TNF-α, IL-1β, and IL-6), while upregulating anti-inflammatory cytokines (e.g., IL-4 and IL-10) [27-33]. Simultaneously, CAG facilitates dissociation of Nrf2 from Kelch-like ECH-associated protein 1 (Keap 1), promotes its nuclear translocation, and enhances the transcription of antioxidant genes such as HO-1 and Aquaporin 9 (AQP9). It also decreases ROS and MDA levels, elevates SOD activity, and modulates apoptosis by reducing the Bax/Bcl-2 ratio, inhibiting caspase-3 activity, and suppressing cytochrome C release [28, 30-36].

At the cellular level, CAG inhibits CD69/CD25 activation marker expression on $CD3^+$ T cells, blocks lymphocyte progression from G0/G1 to S/G2/M phase, and promotes microglial polarization from the M1 to M2 phenotype, demonstrating anti-inflammatory effects [31, 37]. It also mitigates cisplatin-induced inflammation in HK-2 cells by reducing IL-6 and IL-18 levels, suppresses ROS production and mitochondrial cytochrome C release in HT22 cells, and upregulates cleaved caspase-3 and Bcl-2 expression to attenuate oxidative stress damage [29, 35]. Additionally, Liu et al. found that CAG reduced ROS and MDA levels, enhanced SOD activity, and improved viability in C2C12 cells [34]. Network pharmacology studies further revealed its ability to ameliorate primary hepatocyte injury in mice, decrease alanine aminotransferase and aspartate aminotransferase levels in culture supernatants, inhibits p-NF-κB p65 expression, and upregulates adenosine 5'-monophosphate-activated protein kinase, Nrf2, and HO-1 at both gene and protein levels to alleviate alcoholic liver injury [33].

At the tissue and organ level, CAG provides protection against acute myocardial infarction by inhibiting inflammation and cardiomyocyte apoptosis [27]. It also alleviates intestinal inflammation in ulcerative colitis models, im-

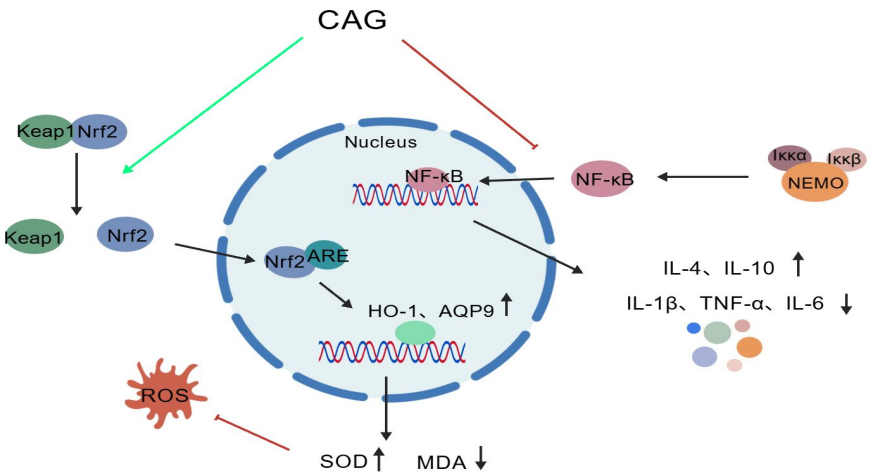

Figure 2. Bidirectional regulatory mechanisms of CAG in anti-inflammatory and antioxidant responses. CAG, cycloastragenol; Nrf2, nuclear factor erythroid 2-related factor 2; Keap1, Kelch-like ECH-associated protein 1; ARE, Antioxidant Response Element; HO-1, heme oxygenase 1; AQP9, Aquaporin 9; SOD, superoxide dismutase; MDA, malondialdehyde; ROS, reactive oxygen species; NF-κB, nuclear factor κappa B; IKKβ, inhibitor of kappa B kinase; IKKα, IκB kinase α; NEMO, nuclear factor-κappa B essential modulator; IL-4, Interleukin 4; IL-10, Interleukin 10; IL-6, Interleukin 6; IL-1β, Interleukin-1 beta; TNF-α, tumor necrosis factor-α.

proves hepatic function in alcoholic liver injury, mitigates cisplatin- and gentamicin-induced renal injury, and prevents airway hyperresponsiveness and mucus hypersecretion in asthmatic mice [28, 29, 32, 33, 38]. Li et al. have demonstrated that CAG reduces neuronal damage in ischemic stroke models by regulating p53 acetylation and the Bax/Bcl-2 ratio [30]. Furthermore, a study confirmed that CAG promoted hepatic regeneration via upregulating AQP9 expression in hepatocytes, which enhances gluconeogenesis and reduces oxidative stress [36].

Notably, clinical studies have shown that CAG modulates the Th1/Th17/Th2 cytokine balance in peripheral blood mononuclear cells (PBMCs) of acute myocardial infarction patients, highlighting its clinical translational potential [27].

Other Effects

Maintenance of skin health

CAG demonstrates multifaceted therapeutic potential in skin diseases through molecular pathway modulation and cellular homeostasis regulation. As the body's primary defense system, skin integrity is crucial. In diabetes-induced ulcerative models, CAG promoted wound healing by increasing SOD activity by 40% and upregulating endothelial eNOS expression by 2.1-fold [39]. In melanocytes, CAG regulates pigmentation via coordinated upregulation of MITF/TYRP1/2 by 1.8-2.3 fold, alongside modulation of p38 MAPK phosphorylation. These effects reduce pro-apoptotic Bax expression by 65%, lower MDA levels by 48%, and elevate catalase (CAT) activity by 35%, thereby attenuating oxidative stress and delaying vitiligo progression [40].

CAG also preserves dermal architecture through extracellular matrix remodeling via fibroblast activation. It upregulates MMP1/9/13 by 2.1-2.7 fold and enhances collagen and hyaluronic acid synthesis by 58% [41]. In keratinocytes, CAG exerts dual regulatory effects by inhibiting proliferation by 45% while inducing autophagy (LC3-II increased by 2.3 fold) and upregulating laminin and palmitoyltransferase (1.6 fold), thereby contributing to the maintenance of the physicochemical skin barrier [42]. These findings collectively position CAG as a promising candidate for managing diverse dermatological disorders through multi-targeted mechanisms.

Regulation of bone metabolism

Bone homeostasis is essential for maintaining skeletal integrity. It not only supports locomotion, but also regulates systemic calcium and mineral metabolism. Disruption of this balance can lead to osteoporosis, fractures, and other bone-related disorders [43]. Current research focuses on two major pathological mechanisms: excessive bone resorption caused by overactive osteoclasts and impaired bone formation due to reduced osteoblast activity [44]. Studies have shown that CAG not only alleviates the inhibition of osteogenic differentiation induced by glucocorticoids by activating telomerase but also inhibits the formation and function of osteoclasts by targeting the intracel-

lular signaling pathway induced by RANKL [45, 46]. In glucocorticoid-induced avascular necrosis of the femoral head, CAG inhibits osteoclast activity and prevents bone loss [47]. In addition, CAG serves as an exogenous enhancer of chondrogenesis from human adipose-derived mesenchymal stem cells, facilitating the formation of cartilage and maintaining the phenotypic stability of active chondrocytes [48]. These findings indicate that CAG holds therapeutic potential in improving bone loss and enhancing cartilage regeneration, contributing to overall skeletal health.

Others

Beyond these established effects, CAG also demonstrates anti-obesity potential. It reduces lipid accumulation by downregulating key adipogenic transcription factors such as PPARγ and C/EBPα, while upregulating Gli1, a pivotal Hedgehog signaling mediator [49]. CAG also protects against doxorubicin-induced podocyte injury through modulation of metabolic pathways including glycerophospholipid, amino acid, glutathione, and purine metabolism. In cerebral ischemia-reperfusion models, CAG significantly improves neurological function scores while reducing cerebral infarct volumes, demonstrating neuroprotective efficacy against focal cerebral ischemia-reperfusion injury [50, 51].

Pharmacokinetics of CAG

CAG, the principal bioactive component of Astragalus membranaceus, predominantly exists in its natural form as saponin derivatives such as astragaloside IV. Pharmacokinetic profiling indicates that CAG exhibits limited oral bioavailability due to its dependence on gut microbiota-mediated hydrolysis for activation [52]. Following both intraperitoneal and oral administration, active metabolites are detectable in systemic circulation, with peak plasma concentrations observed within 0.5-0.75 hours [52].

The compound is eliminated via dual routes, including renal (urinary) and hepatobiliary (fecal) routes [53]. Notably, enterohepatic recirculation contributes to characteristic biphasic or multiphasic plasma concentration-time profiles, owing to reabsorption of biliary-excreted metabolites [54]. Pharmacokinetic analyses in rodent models demonstrate moderate metabolic turnover, evidenced by an elimination half-life of 3-5 hours. At an oral dose of 10 mg/kg in rats, CAG exhibits dose-proportional pharmacokinetics, with a peak plasma concentration of 1,152 ng/mL and increasing AUC values [8].

Mechanistically, biotransformation primarily involves CYP450-mediated phase I oxidation and phase II glucuronidation [54]. However, the specific CYP450 isoforms and detailed metabolic pathways remain to be fully elucidated.

Discussion

Innovativeness

CAG emerges as a novel therapeutic agent, offering distinct advantages over conventional pharmacological interventions due to its multi-modal mechanisms of action. Unlike traditional antioxidants like vitamin C and E, which primarily mitigate oxidative stress with limited efficacy, or targeted therapies like rapamycin, which carry immunosuppressive risks, CAG activates telomerase to elongate telomeres, thereby delaying aging-associated pathologies, including osteoporosis, Alzheimer's disease, and cardiovascular dysfunction. This is complemented by its ability to extend cellular replicative lifespan and slow senescence progression [6].

In oncology, CAG circumvents severe myelosuppression, hepatorenal toxicity, and immunosuppression commonly associated with conventional DNA synthesis inhibitors (e.g., cyclophosphamide). Instead, it exerts synergistic antioxidant, anti-inflammatory, and tissue-regenerative effects, achieving tumor suppression with minimal off-target cytotoxicity.

For fibrotic disorders, where glucocorticoid therapies pose metabolic risks and integrative approaches often lack mechanistic clarity, CAG uniquely modulates fibrotic progression via dual suppression of profibrotic factor secretion and telomerase-mediated senescence delay. This mechanism concurrently addresses metabolic dysregulation, demonstrating enhanced safety profiles in hepatic fibrosis and chronic kidney disease compared to established therapies.

CAG also demonstrates therapeutic innovation in the management of chronic renal failure, offering cost-effective functional preservation and metabolic regulation superior to resource-intensive hemodialysis or transplantation. In respiratory diseases, CAG overcomes the limitations of glucocorticoid resistance and systemic side effects through dual anti-inflammatory and tissue-repair mechanisms, effectively mitigating disease progression in both stable and acute phases of chronic obstructive pulmonary disease and bronchitis.

Distinct from single-target drugs, CAG's poly-

Table 1. Pharmacological effects of cycloastragenol and its direct targets

Pharmacological effect	Direct target
Counteract aging and ameliorate cognitive dysfunction	TERT
Anti-cancer effect	CTSB-MHC-I
Anti-fibrotic effect	MMPs, TGF-β
Anti-inflammatory and anti-oxidative stress effect	Nrf2/ARE, NF-κB

Note: TERT, telomerase reverse tranase; CTSB, Cathepsin B; MHC-I, major histocompatibility complex I; MMPs, Matrix metalloproteinases; TGF-β, Transforming growth factor beta; Nrf2, Nuclear Factor erythroid 2-Related Factor 2; ARE, Antioxidant Response Element; NF-Kb, recombinant nuclear factor kappa B.

pharmacological nature enables synergistic therapeutic outcomes for complex comorbidities, positioning it as a cornerstone for developing low-toxicity combination therapies. Its natural origin and cost-effectiveness further enhance its clinical translation potential across diverse medical disciplines.

Safety profile

CAG demonstrates a favorable safety profile at low therapeutic doses (25-100 μM), with no significant cytotoxicity observed in cellular or animal models. However, cytostatic effects emerge at higher concentrations, necessitating dose optimization for clinical applications [6]. Preclinical studies in abdominal aortic aneurysm models reveal that daily administration of 125 mg/kg effectively attenuates disease progression while maintaining an acceptable safety margin, with no severe adverse events documented during treatment [55]. These findings collectively confirm its controllable toxicity window when administered within established dosage parameters.

Comparative analysis

CAG exerts its anti-fibrotic effects through strategic inhibition of TGF-β/Smad signaling, thereby suppressing fibroblast activation, collagen biosynthesis, and pathological extracellular matrix remodeling. Concurrently, it enhances hepatic sinusoidal endothelial cell functionality to ameliorate microcirculatory dysfunction. In contrast, its anticancer activity is driven by cathepsin B (CTSB)-mediated lysosomal regulation, where CAG preserves MHC-I integrity and amplifies tumor antigen presentation. This mechanism potentiates $CD8^+$ T cell immunity and synergistically enhances the efficacy of programmed death-1 antibodies through coordinated upregulation of antigen-processing machinery and immune transcription factors.

While both therapeutic actions involve modulation of the PI3K/Akt pathway, their downstream cascades exhibit mechanistic divergence: anticancer effects activate immune surveillance and tumor cell cycle arrest, whereas antifibrotic responses counteract NF-κB-driven inflammation and epithelial-mesenchymal transition to facilitate tissue regeneration.

Conclusion

CAG demonstrates polypharmacological efficacy through coordinated modulation of ROS and inflammatory cytokines (e.g., TGF-β1, TNF-α), orchestrating multi-pathway regulation across the Keap1/Nrf2/HO-1, NF-κB, Wnt, MAPK, and apoptotic cascades (**Table 1**). Its therapeutic actions extend to telomerase activation and dynamic control of inflammatory-oxidative-apoptotic axes, collectively enabling multi-organ protective effects in pulmonary, cardiovascular, hepatic, and renal systems through spatially resolved mechanism networks.

While CAG appears to exhibit an enhanced safety profile compared to conventional therapeutics, clinical translation requires rigorous validation via large-scale trials. Current investigations have primarily focused on telomerase activation and antioxidant capacity, leaving other molecular targets insufficiently characterized. Despite evidence suggesting pleiotropic signaling modulation, comprehensive system-level analyses of its cross-pathway regulatory networks are still lacking. Furthermore, fundamental questions remain regarding its gut microbiota crosstalk and tissue-specific mechanism prioritization, necessitating integrated multi-omics approaches to fully elucidate its therapeutic architecture.

Author Contributions: Weiqi Lin, Jiayin Wang, and Sixu Chen contributed to the conception of the study and wrote the manuscript draft; Xinyi Xie, Qin Zhang, and Yutong Sun contributed to the information collection and analysis; Qixiang Xu and Cuifeng Zhang helped perform the analysis by having constructive discussions and revising the manuscript.

References

[1] Wu HY, Gu YQ, Zhou HC, et al. Effects of cyclo-

astragenol on carbon tetrachloride-induced hepatic fibrosis and glycolysis in mice. China Pharm 2022;33(14):1677-1681+1687.
[2] Shen CY, Jiang JG, Yang L, et al. Anti-ageing active ingredients from herbs and nutraceuticals used in traditional Chinese medicine: pharmacological mechanisms and implications for drug discovery. Br J Pharmacol 2017;174(11):1395-1425.
[3] Liao R, Xie W. Optimization of the Preparation Process of Cycloastragaloside IV through Orthogonal Experiment Design. Mod Chin Med 2015;35(05):188-190.
[4] Yung LY, Lam WS, Ho MK, et al. Astragaloside IV and cycloastragenol stimulate the phosphorylation of extracellular signal-regulated protein kinase in multiple cell types. Planta Med 2012;78(2):115-121.
[5] Ip FC, Ng YP, An HJ, et al. Cycloastragenol is a potent telomerase activator in neuronal cells: implications for depression management. Neurosignals 2014;22(1):52-63.
[6] Wan Y, Xu L, Wang Y, et al. Preventive effects of astragaloside IV and its active sapogenin cycloastragenol on cardiac fibrosis of mice by inhibiting the NLRP3 inflammasome. Eur J Pharmacol 2018;833:545-554.
[7] Ikram M, Jo MH, Choe K, et al. Cycloastragenol, a Triterpenoid Saponin, Regulates Oxidative Stress, Neurotrophic Dysfunctions, Neuroinflammation and Apoptotic Cell Death in Neurodegenerative Conditions. Cells 2021;10(10):2719.
[8] Zheng WY, Ran FP, Jia T, et al. Effects of cycloastragalus combined with IL-7 and IL-15 on the proliferation of human umbilical cord blood T cells in vitro. Immunol J 2019;35(11):965-971.
[9] Lv JQ, Zhao RH, Shan SF, et al. Effects of yogurt derived peptides on telomere length in human hepatocyte cell aging model and its related mechanism. Mod Prev Med 2021;48(24):4497-4503+4517.
[10] Cao YL, Li WL, LY W, et al. Anti-aging Function of Cycloastragenol in Aging Mice Induced by D-galactose. Chin J Experimental Tradit Med Formulae 2012;18(19):208-211.
[11] Ullah M, Sun Z. Klotho Deficiency Accelerates Stem Cells Aging by Impairing Telomerase Activity. J Gerontol A Biol Sci Med Sci 2019;74(9):1396-1407.
[12] Zhang Y, Gao D, Yuan Y, et al. Cycloastragenol: A Novel Senolytic Agent That Induces Senescent Cell Apoptosis and Restores Physical Function in TBI-Aged Mice. Int J Mol Sci 2023;24(7):6554.
[13] Hong H, Xiao J, Guo Q, et al. Cycloastragenol and Astragaloside IV activate telomerase and protect nucleus pulposus cells against high glucose-induced senescence and apoptosis. Exp Ther Med 2021;22(5):1326.
[14] Alharbi KM, Alshehri SA, Almarwani WA, et al. Effects of Cycloastragenol on Alzheimer's Disease in Rats by Reducing Oxidative Stress, Inflammation, and Apoptosis. Curr Alzheimer Res 2024;21(2):141-154.
[15] Weiss RA, Weiss MA. Evaluation of a novel anti-aging topical formulation containing cycloastragenol, growth factors, peptides, and antioxidants. J Drugs Dermatol 2014;13(9):1135-1139.
[16] Zhao WJ, Yin ZY, Wang YX, et al. 2024 Interpretation on Cancer Statistics, 2024 and Comparison of Cancer Prevalence Between China and America. Cancer Res Prev Treat 2024;51(08):630-641.
[17] Han B, Zheng R, Zeng H, et al. Cancer incidence and mortality in China, 2022. J Natl Cancer Cent 2024;4(1):47-53.
[18] Park D, Jung JH, Ko HM, et al. Antitumor Effect of Cycloastragenol in Colon Cancer Cells via p53 Activation. Int J Mol Sci 2022;23(23):15213.
[19] Deng G, Zhou L, Wang B, et al. Targeting cathepsin B by cycloastragenol enhances antitumor immunity of CD8 T cells via inhibiting MHC-I degradation. J Immunother Cancer 2022;10(10): e004874.
[20] Melin LG, Dall JH, Lindholt JS, et al. Cycloastragenol Inhibits Experimental Abdominal Aortic Aneurysm Progression. Biomedicines 2022;10(2):359.
[21] Chen X, Yang Y, Sun S, et al. CX3C chemokine: Hallmarks of fibrosis and ageing. Pharmacol Res 2024;208:107348.
[22] Li Y, Gao R, Shan Y, et al. Research progress on mechanism of ginsenosides against organ fibrosis Chin Tradit Herb Drugs 2022;53(07):2237-2246.
[23] Luangmonkong T, Puphancharoensuk P, Tongsongsang V, et al. Hepatoprotective Efficacy of Cycloastragenol Alleviated the Progression of Liver Fibrosis in Carbon-Tetrachloride-Treated Mice. Biomedicines 2023;11(1):231.
[24] Dong X, Fan HW, Hu BX, et al. Effects of cycloastragenol on cardiac fibrosis induced by isoproterenol in mice. Chin J Pathophysiol 2020;36(03):385-393.
[25] Wu M, Ren MX, YS T. Study on the Mechanism of Cycloastragenol in Treating Renal Fibrosis Based on Network Pharmacology. Res Pract Chin Med 2024;38(03):40-46.
[26] Dikic D, Bogdanovic A, Markovic D, et al. Inflammation Promotes Oxidative and Nitrosative Stress in Chronic Myelogenous Leukemia. Biomolecules 2022;12(2):247.
[27] Ren YS, Li HH, Yao JC, et al. Application quantitative proteomics approach to identify differentially expressed proteins associated with cardiac protection mediated by cycloas-

tragenol in acute myocardial infarction rats. J Proteomics 2020;222:103691.
[28] Bagalagel A, Diri R, Noor A, et al. The therapeutic effects of cycloastragenol in ulcerative colitis by modulating SphK/MIP-1alpha/miR-143 signalling. Basic Clin Pharmacol Toxicol 2022;131(5):406-419.
[29] Tang L, Li X, Qin Y, et al. The construction of oligonucleotide-cycloastragenol and the renoprotective effect study. Front Bioeng Biotechnol 2022;10:1027517.
[30] Li M, Li SC, Dou BK, et al. Cycloastragenol upregulates SIRT1 expression, attenuates apoptosis and suppresses neuroinflammation after brain ischemia. Acta Pharmacol Sin 2020;41(8):1025-1032.
[31] Chen T, Li Z, Li S, et al. Cycloastragenol suppresses M1 and promotes M2 polarization in LPS-stimulated BV-2 cells and ischemic stroke mice. Int Immunopharmacol 2022;113(Pt A):109290.
[32] Wang W, Ma XX, WD C. Protective effect of cycloastragenol on acute kidney injury induced by gentamicin in mice. J Xinxiang Med Univ 2019;36(08):715-719.
[33] Xu QX, Ren MX, Liu YL, et al. Exploring the model of action of Cycloastragenol in treating alcoholic liver injury based on network pharmacology. J Qiqihar Med Univ 2022;43(23):2201-2208.
[34] Liu L, Ma BB, Li MJ, et al. Cycloastragenol Prevents the Oxidative Damage Induced by t-BHP in C2C12 Cells through Nrf2/HO-1 Pathway. Chin J Cell Biol 2021;43(11):2134-2141.
[35] Hao RJ, Lu YW, Yu GR. Anti-Oxidative Stress Injury Effect of Cycloastragenol on HT22 Cells Induced by H2O2 Based on Nrf2 Pathway. Inf Tradit Chin Med 2021;38(12):7-12.
[36] Li Y, Yang X, Bao T, et al. Radix Astragali decoction improves liver regeneration by upregulating hepatic expression of aquaporin-9. Phytomedicine 2024;122:155166.
[37] Sun C, Jiang M, Zhang L, et al. Cycloastragenol mediates activation and proliferation suppression in concanavalin A-induced mouse lymphocyte pan-activation model. Immunopharmacol Immunotoxicol 2017;39(3):131-139.
[38] Zhu X, Liu B, Ruan Z, et al. TMT-Based Quantitative Proteomic Analysis Reveals Downregulation of ITGAL and Syk by the Effects of Cycloastragenol in OVA-Induced Asthmatic Mice. Oxid Med Cell Longev 2022;2022:6842530.
[39] Xu HL, Zhang L, Chen H, et al. Effect of Cycloastragenol on Wound Healing of Diabetic Skin Ulcers in Rats Based on Wnt/β-catenin Pathway. Pharmacol Clin Chin Mater Med 2024;40(06):59-66.
[40] Wu HL, Wang W, Zhang SJ, et al. The Effect and Mechanism of Cycloastragenol in the Treatment of Vitiligo. Prog Mod Biomed 2023;23(01):35-40+46.
[41] Yang MH, Hwang ST, Um JY, et al. Cycloastragenol exerts protective effects against UVB irradiation in human dermal fibroblasts and HaCaT keratinocytes. J Dermatol Sci 2023;111(2):60-67.
[42] Xia J, Zhang Y, Wang Q, et al. Cycloastragenol restrains keratinocyte hyperproliferation by promoting autophagy via the miR-145/STC1/Notch1 axis in psoriasis. Immunopharmacol Immunotoxicol 2024;46(2):229-239.
[43] Liu X, Chen M, Liu Q, et al. LncRNA PTCSC3 is upregulated in osteoporosis and negatively regulates osteoblast apoptosis. BMC Med Genomics 2022;15(1):57.
[44] Zhang K, Shi Z, Ren Y, et al. [Kcnq1ot1 promotes osteogenic differentiation and suppresses osteoclast differentiation]. Nan Fang Yi Ke Da Xue Xue Bao 2021;41(1):31-38.
[45] Wu J, Zeng Z, Li Y, et al. Cycloastragenol protects against glucocorticoid-induced osteogenic differentiation inhibition by activating telomerase. Phytother Res 2021;35(4):2034-2044.
[46] Wang G, Ma C, Chen K, et al. Cycloastragenol Attenuates Osteoclastogenesis and Bone Loss by Targeting RANKL-Induced Nrf2/Keap1/ARE, NF-kappaB, Calcium, and NFATc1 Pathways. Front Pharmacol 2021;12:810322.
[47] Wang G, Ma C, Mo L, et al. Cycloastragenol prevents bone loss via inhibiting osteoclast activity in glucocorticoid-induced osteonecrosis of the femoral head: An in vivo study. J Orthop Translat 2024;45:178-187.
[48] Szychlinska MA, Calabrese G, Ravalli S, et al. Cycloastragenol as an Exogenous Enhancer of Chondrogenic Differentiation of Human Adipose-Derived Mesenchymal Stem Cells. A Morphological Study. Cells 2020;9(2):347.
[49] Kim JT, Chen J, Zhou Y, et al. Cycloastragenol inhibits adipogenesis and fat accumulation in vitro and in vivo through activating Hedgehog signaling. Food Sci Biotechnol 2024;33(3):711-720.
[50] Guo M, Cui T, Zhang LC, et al. Protective Effect of Cycloastragenol on Doxorubicin-Induced Podocytes Injury Based on Metabolomics by LC-MS Technology. Chin Pharm J 2022;57(11):910-917.
[51] Yi ZL, WJ G. Protective Effects of Cycloastragenol on Focal Cerebral Ischemia Reperfusion Injury in Rats. J Chengde Med Univ 2015;32(03):186-188.
[52] Wang XZ, Yao JC, Wang EL, et al. Pharmacokinetic Study of SD Rats and Beagle Dogs after Oral Administration or Injection of Cycloastragenol. Chinese J Pharm 2023;54(05):779-784+804.
[53] Ma PK, Wei BH, Cao YL, et al. Pharmacokinet-

ics, metabolism, and excretion of cycloastragenol, a potent telomerase activator in rats. Xenobiotica 2017;47(6):526-537.

[54] Wei BH. Metabolic Transformation of Cycloastragenol in Rats and Its Effects on Hepatic CYP450 Enzymes. Beijing University of Chinese Medicine 2014.

[55] Wang Y, Chen C, Wang Q, et al. Inhibitory effects of cycloastragenol on abdominal aortic aneurysm and its related mechanisms. Br J Pharmacol 2019;176(2):282-296.

Perioperative Precision Medicine
ISSN: 2957-5443

Zentime

Review Article https://doi.org/10.61189/577707zkzsmw

Tailoring perioperative analgesia: Selecting ketamine or dexmedetomidine based on patient-specific factors

Edward Sun[1], Meikun Wang[2], Zongda He[3], Mingyue Li[4], Jingping Wang[5]

[1]University of British Columbia, Vancouver, Canada BC V6T 1Z4. [2]Department of Anesthesia, First Hospital, Jilin University, Changchun 130021, Jilin Province, China. [3]King's College, London, UK WC2R 2LS. [4]Department of Anesthesia, Second Hospital, Jilin University, Changchun 130021, Jilin Province, China. [5]Department of Anesthesia, Critical Care and Pain Medicine, Massachusetts General Hospital, Harvard Medical School, Boston 02114, MA, USA.

Corresponding author: Jingping Wang.

Declaration of conflict of interest: None.

Received July 5, 2025; Accepted September 5, 2025; Published December 31, 2025

Highlights

- Ketamine and dexmedetomidine offer effective non-opioid perioperative analgesia, each with distinct cardiovascular, hepatic, and neurological profiles.
- Dexmedetomidine provides stable sedation and potential neuroprotection, making it particularly suitable for patients with hepatic dysfunction and those undergoing neurosurgery.
- Ketamine helps maintain hemodynamic stability and possesses anti-inflammatory and anti-depressant properties, making it beneficial for high-risk or unstable patients.
- Agent selection should be tailored to individual comorbidities, with combination therapy offering potential synergistic advantages.

Abstract

Ketamine and dexmedetomidine are widely used non-opioid agents for perioperative analgesia and sedation, each with distinct mechanisms and side effect profiles. Dexmedetomidine, an α2-adrenergic agonist, is preferred in patients with hepatic dysfunction due to its stable sedation and lower risk of delirium, though it may cause side effects such as bradycardia and hypotension. Ketamine, a non-competitive N-methyl-D-aspartate receptor antagonist, increases heart rate and blood pressure via catecholamine release and provides additional benefits such as anti-inflammatory, neuroprotective, and antidepressant properties. Although both agents have overlapping clinical roles, selection should be guided by patient comorbidities, including cardiac, hepatic, and neurological conditions. This review summarizes current evidence to support individualized decision-making in postoperative pain management.

Keywords: Ketamine, dexmedetomidine, pain management

Introduction

Dexmedetomidine is a selective, non-opioid α2-adrenergic receptor agonist widely used for short-term sedation and pain management [1]. In the central nervous system, it binds to α2-adrenergic receptors in the locus coeruleus, inhibiting pain transmission. Peripherally, it hyperpolarizes presynaptic membranes in the posterior horn and postsynaptic membranes of interneurons, thereby impeding nociceptive signaling to the brain [2]. Although primarily recognized as a sedative–anxiolytic due to its high α2-adrenergic receptor affinity, dexmedetomidine is also employed for analgesia and has been used in the treatment of hypertension [3]. It is typically administered via intravenous titration due to its short half-life, requiring careful monitoring for dose-dependent adverse effects, despite its favorable sympatholytic and sedative profile [3].

Address correspondence to: Jingping Wang, Department of Anesthesia, Critical Care and Pain Medicine, Massachusetts General Hospital, 55 Fruit Street, Boston 02114, MA, USA. Tel: +86-617-643-2729. E-mail: jwang23@MGH.Harvard.edu.

Ketamine, introduced as an anesthetic in 1964, is another non-opioid analgesic that primarily acts by antagonizing the N-methyl-D-aspartate (NMDA) receptor [4, 5]. In addition to NMDA antagonism, ketamine may exert partial agonist effects at μ and κ opioid receptors, although this remains under debate [6]. It also interacts with other targets, such as muscarinic acetylcholine receptors, and may inhibit gamma-aminobutyric acid activity, contributing to its distinct psychoactive side effect profile [7]. Ketamine exists as two enantiomers, (S)-ketamine and (R)-ketamine, with the S-enantiomer demonstrating greater potency at the NMDA receptor [5]. Beyond its anesthetic use, ketamine has been applied in treating depression and in experimental models of psychosis [5].

Despite differing mechanisms and chemical structures, dexmedetomidine and ketamine share overlapping roles in clinical practice. Both agents are widely used by anesthesiologists and critical care providers. However, a comprehensive comparison of their use in patients with comorbidities such as hepatic, cardiac, or neurological diseases is still lacking. This review aims to address this gap by highlighting how organ-specific conditions influence pharmacodynamics and clinical outcomes. Additionally, we propose a practical decision-making framework and explore the potential of combination therapy to maximize benefits while minimizing side effects.

Mechanistic insights supporting clinical applications

Analgesia and sedation of dexmedetomidine

Dexmedetomidine offers several advantages that make it an ideal anesthetic and analgesic agent in both the operating room and intensive care unit. As a non-opioid medication, it avoids many of the common side effects associated with opioid use, such as nausea, constipation, dependency, and respiratory depression [8, 9].

Dexmedetomidine exerts its sedative and analgesic effects through selective activation of α2-adrenergic receptors, particularly the α2A subtype, G protein–coupled receptors, located in the locus coeruleus of the brainstem [10-12]. Activation of G proteins inhibits adenylyl cyclase, leading to reduced cyclic adenosine monophosphate production [13]. Lower cyclic adenosine monophosphate enhances potassium channel conductance, causing potassium efflux and hyperpolarization of noradrenergic neurons. Simultaneously, calcium channel suppression reduces calcium influx, further inhibiting neurotransmitter release [13, 14]. The synergistic effect of hyperpolarization and calcium-channel inhibition results in decreased neuronal firing and reduced norepinephrine release, thereby jointly suppressing nociceptive signal propagation in the ascending pain pathway (**Figure 1a**).

Anti-inflammatory effect of dexmedetomidine

Both clinical and preclinical studies have demonstrated the anti-inflammatory properties of dexmedetomidine [15]. This effect is believed to be mediated, at least in part, through modulation of intracellular signaling pathways such as Jun N-terminal kinases and p38 mitogen-activated protein kinases [16]. In rat primary astrocyte cultures, high concentrations of dexmedetomidine (0.1, 1, and 10 μM) modulated JNK and mitogen-activated protein kinase activity and significantly attenuated inflammation [17]. However, at lower concentrations (0.01 μM), no significant changes were observed in tumor necrosis factor-alpha (TNF-α) and interleukin-6 (IL-6) expression [17]. Given the evolutionary conservation of the mitogen-activated protein kinase family, it is reasonable to hypothesize that similar effects may occur in mammalian, including human, astrocytes at higher concentrations (**Figure 1b**).

Further supporting its anti-inflammatory potential Xiang et al. demonstrated that dexmedetomidine modulates the cholinergic anti-inflammatory pathway to downregulate systemic cytokine levels [18]. In a lipopolysaccharide (LPS)-induced inflammation model, dexmedetomidine significantly reduced TNF-α, interleukin-1β, and IL-6 levels compared to saline controls [18] These preclinical findings were mirrored in a clinical trial involving 86 patients undergoing intestinal surgery, in which dexmedetomidine not only suppressed inflammatory cytokines but also improved anesthesia recovery time and Mini-Mental State Examination scores [19].

Neuroprotection and immunomodulatory effects of dexmedetomidine

In a study, Oriby et al. reported that dexmedetomidine attenuated neurocognitive impairments [20]. This neuroprotective effect is believed to stem from the drug's ability to counteract necrosis, apoptosis, oxidative stress, and immune responses. One proposed mechanism involves the reduction of catecholamine release during neurosurgical procedures, limiting oxidative stress and enhancing neuronal protection in vulnerable brain regions [19]. Supporting this,

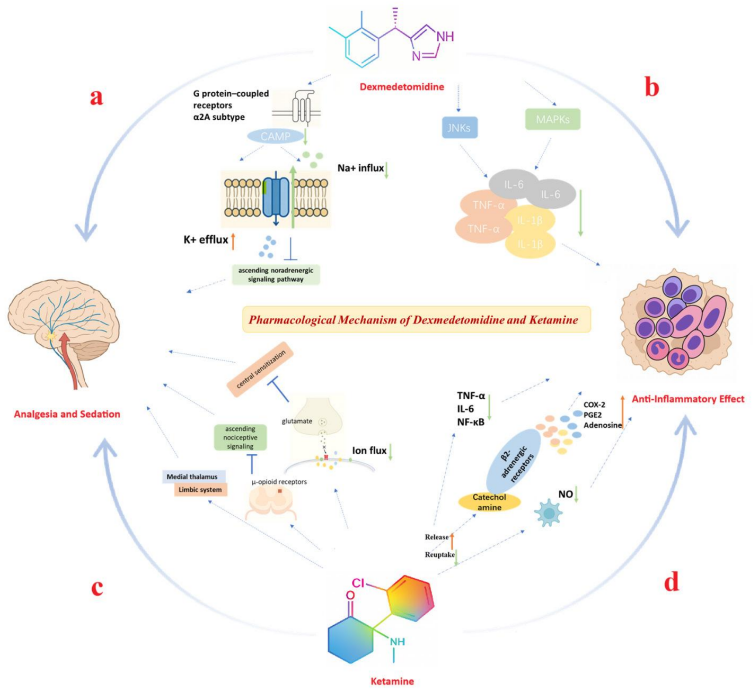

Figure 1. Pharmacological Mechanism of Dexmedetomidine and Ketamine. (a) Analgesia and Sedation of Dexmedetomidine; (b) Anti-Inflammatory Effect of Dexmedetomidine; (c) Analgesia and Sedation of Ketamine; (d) Anti-Inflammatory Effect of Ketamine. CAMP, cyclic adenosine monophosphate; Na+, sodium ion; K+, potassium ion; JNKs, c-Jun N-terminal kinases; MAPKs, mitogen-activated protein kinases; TNF-α, tumor necrosis factor-alpha; IL-6, interleukin-6; IL-1β, interleukin-1 beta; NMDA, N-methyl-D-aspartate; NO, nitric oxide; NF-κB, nuclear factor kappa-B; COX-2, cyclooxygenase-2; PGE_2, prostaglandin E_2.

Schoeler et al. demonstrated in organotypic hippocampal slice cultures that dexmedetomidine promoted neuroprotection in traumatic brain injury models through activation of extracellular signal-regulated kinases [21]. Oxidative stress, a key contributor to postoperative cognitive dysfunction, is also directly mitigated by dexmedetomidine. The drug has been shown to lower malondialdehyde levels and promote the nuclear translocation of peroxisome proliferator-activated receptor gamma coactivator 1-alpha, enhancing mitochondrial function and cellular resilience against oxidative damage [22].

Beyond its neuroprotective actions, dexmedetomidine also modulates immune responses implicated in postoperative cognitive dysfunction. Excessive cytokine release and lymphocyte activation are known contributors to neuroinflammation in the perioperative period. Research shows that dexmedetomidine downregulates both innate and adaptive immune activity by modulating cytokine levels and immunological signaling pathways, further supporting its potential to reduce neuroinflammation and cognitive impairment after surgery [23, 24].

Clinical data, though limited, suggest potential neuroprotective effects of dexmedetomidine in humans. For example, retrospective studies in aneurysmal subarachnoid hemorrhage patients showed better neurological outcomes in those receiving dexmedetomidine, potentially due to reduced oxidative stress and inflammation. While no randomized clinical trials have directly measured proliferator-activated receptor gamma coactivator 1-α expression, these findings are consistent with preclinical data indicating mitochondrial preservation via the AMPK/proliferator-activated receptor gamma coactivator 1-α pathway [25].

Analgesia and sedation of ketamine

Ketamine is a non-competitive NMDA receptor antagonist used for analgesia and anesthesia in perioperative settings [26]. It blocks the NMDA receptor channel in a non-competitive manner. When glutamate dissociates and the ion channel closes, ketamine remains trapped inside, preventing normal ion flux, impairing receptor function, and attenuating central sensitization [27]. Ketamine also interacts with μ-opioid receptors and neurons in the presynaptic spinal dorsal horn. It reduces the release of excitatory neurotransmitters from presynaptic neurons in the spinal dorsal horn and inhibits ascending nociceptive signaling (**Figure 1c**) [28]. For its sedative effects, ketamine acts on multiple brain regions, including the thalamocortical and limbic systems. It suppresses excitatory activity in the medial thalamus while enhancing activity in the limbic system, such as the hippocampus and amygdala, leading to a dissociative state characterized by profound sedation with preserved airway reflexes and spontaneous breathing [29].

Due to its engagement with multiple receptors in both the central and peripheral nervous systems, and its slow dissociation (slow “off-rate”) from these targets, ketamine is an effective option for both acute and chronic pain management [27, 28]. Ketamine is often combined safely with sedatives like midazolam and propofol for enhanced analgesic and sedative

effects [30]. Additionally, ketamine is favored in emergency and intensive care unit settings for acute non-cancer pain because it does not cause respiratory depression and has minimal hemodynamic disruption [31, 32].

It is worth noting that the analgesic and anesthetic effects of ketamine are dose-dependent. At concentrations around 200 ng/mL, ketamine can produce anesthesia by blocking voltage-gated sodium (Na^+) channels in neurons and lipid bilayers [33]. Additionally, ketamine interacts with muscarinic receptors and voltage-sensitive calcium channels, which may further enhance its analgesic and anesthetic properties [33]. At higher plasma concentrations (-2000 ng/mL), ketamine induces hypnosis, likely through combined blockade of NMDA receptors and hyperpolarization-activated cyclic nucleotide-gated potassium channel 1 [27]. Its dose-dependent pharmacological profile allows clinicians to tailor administration for different outcomes, making it a versatile agent [34].

Anti-inflammatory effect of ketamine

Ketamine also exhibits anti-inflammatory properties [35]. In a study by Lankveld et al. using an equine macrophage cell line, ketamine inhibited LPS-induced production of IL-6 and TNF-α in a dose-dependent manner [36]. Similarly, Yang et al., using a rat model, found that high doses (50 mg/kg) of ketamine reduced LPS-induced lung injury [37]. TNF-α, IL-6, nuclear factor kappa-light-chain-enhancer of activated B cells, and neutrophil infiltration were all significantly decreased in the ketamine group, indicating reductions in oxidative stress and inflammatory damage [37].

Ketamine also modulates the catecholaminergic system by stimulating catecholamine release and inhibiting its reuptake [35]. This accumulation overstimulates β2-adrenergic receptors, resulting in adenosine release [38]. Adenosine then triggers a cascade that includes cyclooxygenase-2 and prostaglandin E2 synthesis, ultimately enhancing anti-inflammatory cytokine production by mononuclear cells [35]. Ketamine further reduces nitric oxide production in immune-stimulated macrophages, contributing to its dose-dependent immunomodulatory effects [39]. Importantly, ketamine is capable of reducing exaggerated inflammation without inhibiting essential immune responses, which is better characterized as an anti-proinflammatory rather than a traditional anti-inflammatory agent (**Figure 1d**) [35].

Although most evidence for ketamine's neuroprotective effects comes from preclinical models of ischemic stroke and traumatic brain injury, emerging clinical data support these mechanisms in humans. An electrocorticography study in acute stroke patients demonstrated that ketamine suppressed cortical spreading depolarizations, a phenomenon strongly associated with secondary neuronal damage and infarct expansion. This suggests that ketamine's NMDA receptor antagonism may attenuate excitotoxic cascades in acute neurological injury [40].

Anti-cancer and antidepressant of ketamine

Studies have also explored ketamine's anti-cancer effects. Saito et al. compared ketamine and MK-801 in neuroglioma and lung cancer cells, finding that ketamine significantly inhibited cell proliferation, migration, and induced apoptosis in a dose-dependent manner [41]. However, this was associated with increased reactive oxygen species, leading to cellular apoptosis [41]. Malsy et al. tested ketamine, S-ketamine, and MK-801 on pancreatic cancer cells and found reduced proliferation and migration, though apoptosis did not significantly differ from controls [42]. In contrast, ketamine induced apoptosis in gastric cancer models [43]. These findings suggest that ketamine's anti-cancer effects may vary by cancer type and dose.

Beyond its anesthetic applications, ketamine has gained attention as a rapid-acting antidepressant. Several proposed hypotheses involve mechanisms independent of NMDA receptor antagonism, including modulation of glutamatergic transmission, enhancement of synaptic plasticity, and regulation of intracellular signaling pathways [44].

Adverse effects and clinical evidence

Dexmedetomidine

While dexmedetomidine can enhance hemodynamic stability, it often induces hypotension and bradycardia due to its potent α2-adrenergic receptor selectivity [45]. These cardiovascular effects are dose-dependent: a loading dose of 1 μg/kg given over less than 10 minutes, or a continuous infusion rate exceeding 0.7–1.0 μg/kg/h, is associated with a higher incidence of hypotension and bradycardia. In contrast, a maintenance dose of 0.2–0.4 μg/kg/h provides effective sedation and analgesia while minimizing the risk of severe hemodynamic instability [46]. These cardiovascular effects may be poorly tolerated in patients with structural heart disease or other cardiovascular comorbidities [47].

The drug's suppression of sympathetic nervous system activity can complicate intraoperative blood pressure and heart rate management. Respiratory depression is another potential concern with dexmedetomidine. In a clinical trial of 40 patients, Abdollahpour et al. observed a lower respiratory rate in those receiving dexmedetomidine compared to the placebo group [34]. Additionally, the PaO_2/FiO_2 ratio was significantly higher in the treatment group, possibly indicating improved oxygenation [34]. Other common side effects include nausea, vomiting, and chills, which can prolong recovery and increase hospitalization time [47].

Ketamine

Neurotoxicity, addiction, nausea, delirium, and myocardial depression are common side effects of ketamine, particularly with chronic administration [28, 48]. Its adverse effects may vary based on patient characteristics and are generally categorized as cardiovascular, central nervous system-related, or hepatic [28]. In a study by Coull et al., 13 healthy young volunteers exhibited reduced performance in color discrimination and timing perception tasks after receiving ketamine at 100 ng/mL plasma levels [49]. Another study found that ketamine at doses of 0.4 and 0.8 mg/kg caused dose-dependent impairments in memory, attention, and executive function, indicating cognitive side effects even in healthy individuals [50]. These neurocognitive side effects are closely linked to plasma concentration and dosage: mild perceptual disturbances are typically observed at plasma levels around 200 ng/mL, corresponding to subanesthetic doses of approximately 0.3–0.5 mg/kg IV, whereas higher doses (1–2 mg/kg IV) can elevate plasma levels to 2,000 ng/mL or more, resulting in profound dissociation, hallucinations, and severe short-term cognitive impairment [48]. Additionally, co-administration with alcohol or other central nervous system depressants may result in severe respiratory depression or even death.

Cardiovascular side effects are also a concern. A study by Christ et al. involving 25 ventilated patients with catecholamine-dependent heart failure found that ketamine significantly reduced heart rate, cardiac index, and stroke volume index compared to sufentanil [51]. These effects may stem from negative inotropic or myocardial depressant properties, though the exact mechanism remains unclear. In contrast, a placebo-controlled study by Liebe et al. found ketamine increased heart rate and blood pressure (without inducing hypertension) [52]. This apparent discrepancy can be explained by the patients' catecholamine reserves and sympathetic tone. Ketamine generally exerts indirect sympathomimetic effects by promoting catecholamine release and inhibiting reuptake, resulting in increased blood pressure and heart rate in patients with adequate sympathetic reserve. However, in patients with advanced heart failure or catecholamine depletion, this indirect mechanism is impaired, and ketamine's direct negative inotropic effect on myocardial contractility predominates, resulting in decreased cardiac output and hypotension. Interestingly, women experienced greater and earlier increases in diastolic blood pressure than men. Other studies have shown that S-norketamine, the primary metabolite of S-ketamine, appears to attenuate its stimulatory effects on cardiac function [53].

Hepatotoxicity is another consideration. In a clinical case series by Jakobsen et al., three out of six patients with complex regional pain syndrome developed elevated liver enzymes after three weeks of continuous S-ketamine infusion, with cumulative doses ranging between 500–700 mg [54]. Enzyme levels, including alanine transaminase, alkaline phosphatase, aspartate transaminase, and γ-glutamyl transferase, returned to normal after treatment cessation, indicating that liver injury may be reversible. The underlying mechanism is not fully understood, but possible explanations include reduced hepatic oxygen delivery, increased lipid peroxidation with free radical formation, and immune-mediated hepatitis [28].

Patient-specific considerations

Building upon the previously discussed mechanisms of action, clinical advantages, and potential adverse effects, the following section examines dexmedetomidine and ketamine in the context of common patient situations, aiming to provide practical insights for clinical decision-making.

Cardiovascular considerations

Dexmedetomidine and ketamine have distinct cardiovascular profiles that significantly influence anesthetic decision-making, particularly in patients with underlying cardiac disease. Dexmedetomidine acts via central sympatholysis, suppressing catecholamine release and reducing sympathetic tone. This leads to decreased heart rate, myocardial contractility, and blood pressure, which may manifest clinically as bradycardia, sinus arrest, or hypotension [19, 53]. As such, it may be less suitable for patients with pre-existing bradycardia or hypotension.

In contrast, ketamine stimulates sympathetic activity by enhancing catecholamine release, producing positive inotropic and chronotropic effects that increase heart rate, blood pressure, and cardiac output [53]. These properties make ketamine advantageous in hemodynamically unstable patients. However, in those with depleted catecholamine or norepinephrine stores, such as in prolonged heart failure or septic shock, this effect may paradoxically result in myocardial depression, tachycardia, and hypotension [53].

In patients with coronary artery disease, ketamine's increased myocardial oxygen demand and shortened diastolic perfusion time raise concerns about ischemic complications [54]. A large trial by Turan et al. in 3,357 cardiac surgery patients showed that Dexmedetomidine did not significantly reduce atrial fibrillation or delirium [55]. Conversely, a review by Mazzeffi et al. highlighted ketamine's usefulness in maintaining hemodynamic stability in patients with ventricular dysfunction [56].

Neurological considerations

Dexmedetomidine is widely used in neurosurgical procedures, such as awake craniotomy, due to its sedative, anxiolytic, and mild analgesic effects, all while preserving respiratory function [57, 58]. Kulikov and Lubnin demonstrated its ability to maintain spontaneous ventilation and patient cooperation during intracranial surgery. In contrast, ketamine has shown superior postoperative analgesia in certain settings[58]. For example, in a randomized trial of laparoscopic cholecystectomy, ketamine outperformed dexmedetomidine in pain control, while both agents, when combined with total intravenous anesthesia, effectively reduced opioid use and improved recovery profiles [59].

Beyond surgical sedation, ketamine also exhibits unique psychiatric and neuroprotective properties. It has been effective in managing agitation, cognitive impairment, and treatment-resistant depression, where dexmedetomidine shows limited benefit. Ketamine has also been applied in the treatment of anti-NMDA receptor encephalitis, particularly in patients with movement disorders or status epilepticus [60, 61]. While paradoxical, these benefits are likely attributable to ketamine's complex receptor interactions, meriting further investigation.

In patients with stroke or subarachnoid hemorrhage, both agents have been explored for their neuroprotective potential. Von der Brelie et al. reported a lower incidence of delayed cerebral ischemia in ketamine-treated patients with SAH [62]. Studies suggest that dexmedetomidine can reduce brain edema, vasospasm, and neurological deficits, although clinical data remain inconclusive [63].

Hepatic considerations

Both dexmedetomidine and ketamine undergo hepatic metabolism, and their pharmacokinetics are notably affected by liver function [64, 65]. Dexmedetomidine is generally well tolerated in patients with hepatic dysfunction, even when administered continuously for over 48 hours. It may provide hepatoprotective benefits during procedures involving hepatic vascular occlusion and has been used safely in liver transplantation to maintain hemodynamic stability and reduce ischemic injury [66, 67].
However, Dexmedetomidine's clearance is dependent on hepatic perfusion. In patients with obstructive jaundice or severe liver impairment, metabolism is delayed, and dose reduction is advised to prevent prolonged sedation and delayed estuation [68, 69].

Ketamine is generally considered safe for short-term use in hepatic impairment, but chronic or repeated exposure, particularly in recreational settings, has been linked to hepatobiliary complications, including cholestasis and sclerosing cholangitis [70]. Therefore, careful consideration of dosing and duration is essential in patients with compromised liver function.

Combination therapy: Dexmedetomidine and ketamine

The combination of dexmedetomidine and ketamine has emerged as a promising strategy to optimize analgesia and sedation while minimizing adverse effects. Their complementary pharmacodynamics can potentially balance hemodynamic responses. A meta-analysis by Li et al. concluded that their co-administration in pediatric patients led to more stable heart rate and oxygen saturation than either agent alone and was associated with improved safety [71].

In clinical practice, this combination has been successfully applied in pediatric sedation, TIVA protocols, and enhanced recovery pathways. A study has shown that the dexmedetomidine–ketamine combination improves intraoperative behavior in uncooperative pediatric dental patients compared to dexmedetomidine alone, despite lower drug acceptance [72]. The addition of ketamine to dexmedetomidine provids

more stable hemodynamics and deeper sedation during awake fiberoptic intubation [73]. This pharmacological synergy may allows for reduced dosages, better control of postoperative pain, and lower opioid requirements, without significantly increasing the risk of cardiovascular or respiratory complications. Nonetheless, further high-quality studies are needed to establish standardized dosing regimens and define patient populations most likely to benefit.

Medication considerations in special populations

Elderly individuals often exhibit increased pharmacodynamic sensitivity and reduced hepatic and renal clearance, which necessitates cautious dosing of both dexmedetomidine and ketamine [74]. Dexmedetomidine's sympatholytic effects may exacerbate age-related autonomic dysfunction, leading to clinically significant bradycardia or hypotension, particularly at loading doses ≥1 μg/kg or maintenance infusions above 0.7 μg/kg/h. Additionally, ketamine's dissociative and cognitive side effects may heighten the risk of postoperative delirium in older adults, especially at doses >1 mg/kg [46]. Therefore, lower initial doses and slower titration are recommended in geriatric patients, alongside vigilant hemodynamic and cognitive monitoring.

Beyond its co-administration with ketamine, dexmedetomidine alone is increasingly used in pediatric sedation for diagnostic imaging, procedural anesthesia, and ICU management [75]. It provides effective anxiolysis without significant respiratory depression [76]; however, its prolonged half-life may delay recovery in short-duration procedures. Ketamine remains a widely accepted pediatric sedative due to its cardiovascular stability, but it can induce hypersalivation, emergence agitation, or hallucinations [77]. Co-administration with anticholinergic agents (e.g., glycopyrrolate) or benzodiazepines is often employed to mitigate these effects. Both agents require individualized dosing based on age, weight, and comorbidities, with attention to developmental pharmacokinetics.

Limited data are available regarding the safety of dexmedetomidine or ketamine in pregnancy. Dexmedetomidine readily crosses the placenta and has been associated with reduced fetal heart rate variability, likely due to central sympatholysis [78]. Its use is generally avoided unless maternal benefit clearly outweighs fetal risk.

Economic considerations

From a cost-effectiveness perspective, dexmedetomidine is generally more expensive than ketamine due to its higher acquisition cost and the need for continuous infusion. However, studies have shown that its opioid-sparing effects, reduced incidence of delirium, and shortened intensive care unit stay may partially offset these costs by reducing the total cost of perioperative care [79]. Although ketamine is inexpensive and easily accessible, it may increase the cost of postoperative monitoring due to its psychoactive effects and potential for cognitive impairment [80]. Therefore, individualized drug selection based on patient comorbidities and expected postoperative course may achieve the best balance between clinical efficacy and medical expenditures.

Conclusion

The perioperative and critical care use of dexmedetomidine and ketamine should be tailored to individual patient characteristics, particularly in the context of cardiac, neurological, and hepatic comorbidities. While both agents offer minimal respiratory depression and valuable non-opioid analgesic effects, their contrasting pharmacodynamic profiles necessitate context-specific selection. Co-administration may provide synergistic benefits in select populations, but further research is warranted to establish optimal dosing strategies and define patient subgroups most likely to benefit.

Author contributions: Edward Sun and Zongda He wrote the draft of the manuscript. Meikun Wang and Mingyue Li contributed to the editing and refinement of the manuscript. Jingping Wang designed the study, reviewed and critically revised the article. All authors made a significant contribution to the work reported and have given final approval for the current version to be published.

References

[1] Kaur M, Singh PM. Current role of dexmedetomidine in clinical anesthesia and intensive care. Anesth Essays Res 2011;5(2):128-133.
[2] Bao N, Tang B. Organ-Protective Effects and the Underlying Mechanism of Dexmedetomidine. Mediators Inflamm 2020;2020:6136105.
[3] Carollo DS, Nossaman BD, Ramadhyani U. Dexmedetomidine: a review of clinical applications. Curr Opin Anaesthesiol 2008;21(4):457-461.
[4] Foster AC, Fagg GE. Neurobiology. Tak-

ing apart NMDA receptors. Nature 1987;329(6138):395-396.
[5] Morgan CJ, Curran HV. Ketamine use: a review. Addiction 2012;107(1):27-38.
[6] Persson J. Ketamine in pain management. CNS Neurosci Ther 2013;19(6):396-402.
[7] Oye I, Paulsen O, Maurset A. Effects of ketamine on sensory perception: evidence for a role of N-methyl-D-aspartate receptors. J Pharmacol Exp Ther 1992;260(3):1209-1213.
[8] Zhang X, Leng Y, Yuan X, et al. Efficacy of perioperative dexmedetomidine in postoperative pain and neurocognitive functions in orthopedic surgery: a systematic review and meta-analysis with trial sequential analysis of randomized controlled trials. Int J Surg 2025;111(5):3525-3542.
[9] Benyamin R, Trescot AM, Datta S, et al. Opioid complications and side effects. Pain Physician 2008;11(2 Suppl):S105-S120.
[10] Afonso J, Reis F. Dexmedetomidine: current role in anesthesia and intensive care. Rev Bras Anestesiol 2012;62(1):118-133.
[11] Andersen JH, Grevstad U, Siegel H, et al. Does Dexmedetomidine Have a Perineural Mechanism of Action When Used as an Adjuvant to Ropivacaine?: A Paired, Blinded, Randomized Trial in Healthy Volunteers. Anesthesiology 2017;126(1):66-73.
[12] Coursin DB, Coursin DB, Maccioli GA. Dexmedetomidine. Curr Opin Crit Care 2001;7(4):221-226.
[13] Giovannitti JA, Thoms SM, Crawford JJ. Alpha-2 adrenergic receptor agonists: a review of current clinical applications. Anesth Prog 2015;62(1):31-39.
[14] Bhana N, Goa KL, McClellan KJ. Dexmedetomidine. Drugs 2000;59(2):263-268; discussion 269-270.
[15] Liaquat Z, Xu X, Zilundu PLM, et al. The Current Role of Dexmedetomidine as Neuroprotective Agent: An Updated Review. Brain Sci 2021;11(7):846.
[16] Luna C, Mendoza N, Casao A, et al. c-Jun N-terminal kinase and p38 mitogen-activated protein kinase pathways link capacitation with apoptosis and seminal plasma proteins protect sperm by interfering with both routes^{+}. Biol Reprod 2017;96(4):800-815.
[17] Zhang X, Wang J, Qian W, et al. Dexmedetomidine inhibits tumor necrosis factor-alpha and interleukin 6 in lipopolysaccharide-stimulated astrocytes by suppression of c-Jun N-terminal kinases. Inflammation 2014;37(3):942-949.
[18] Xiang H, Hu B, Li Z, et al. Dexmedetomidine controls systemic cytokine levels through the cholinergic anti-inflammatory pathway. Inflammation 2014;37(5):1763-1770.
[19] Chen R, Kang Z, Wang Y, et al. The Anti-inflammatory Effect of Dexmedetomidine Administration on Patients Undergoing Intestinal Surgery: A Randomized Study. Drugs R D 2021;21(4):445-453.
[20] Oriby ME, Elrashidy AA, Elsharkawy A, et al. Effects of ketamine or dexmedetomidine on postoperative cognitive dysfunction after cataract surgery: A randomized controlled trial. Indian J Anaesth 2023;67(2):186-193.
[21] Schoeler M, Loetscher PD, Rossaint R, et al. Dexmedetomidine is neuroprotective in an in vitro model for traumatic brain injury. BMC Neurol 2012;12:20.
[22] Li F, Wang X, Deng Z, et al. Dexmedetomidine reduces oxidative stress and provides neuroprotection in a model of traumatic brain injury via the PGC-1α signaling pathway. Neuropeptides 2018;72:58-64.
[23] Ko H, Kayumov M, Lee KS, et al. Immunological Analysis of Postoperative Delirium after Thoracic Aortic Surgery. J Chest Surg 2024;57(3):263-271.
[24] Erdogan Kayhan G, Gul M, Kayhan B, et al. Dexmedetomidine ameliorates TNBS-induced colitis by inducing immunomodulator effect. J Surg Res 2013;183(2):733-741.
[25] Zhang Z, Mu X, Zhou X. Dexmedetomidine alleviates inflammatory response and oxidative stress injury of vascular smooth muscle cell via α2AR/GSK-3β/MKP-1/NRF2 axis in intracranial aneurysm. BMC Pharmacol Toxicol 2022;23(1):81.
[26] Vadivelu N, Schermer E, Kodumudi V, et al. Role of ketamine for analgesia in adults and children. J Anaesthesiol Clin Pharmacol 2016;32(3):298-306.
[27] Sleigh J, Harvey M, Voss L, et al. Ketamine – More mechanisms of action than just NMDA blockade. Trends in Anaesthesia and Critical Care 2014;4(2):76-81.
[28] Niesters M, Martini C, Dahan A. Ketamine for chronic pain: risks and benefits. Br J Clin Pharmacol 2014;77(2):357-367.
[29] Krystal JH, Karper LP, Seibyl JP, et al. Subanesthetic effects of the noncompetitive NMDA antagonist, ketamine, in humans. Psychotomimetic, perceptual, cognitive, and neuroendocrine responses. Arch Gen Psychiatry 1994;51(3):199-214.
[30] Sinner B, Graf BM. Ketamine. Handb Exp Pharmacol 2008;(182):313-333.
[31] Bruder ED, Kamer KJ, Guenther MA, et al. Adrenocorticotropic hormone and corticosterone responses to acute hypoxia in the neonatal rat: effects of body temperature maintenance. Am J Physiol Regul Integr Comp Physiol 2011;300(3):R708-R715.
[32] Bell RF, Kalso EA. Ketamine for pain management. Pain Rep 2018;3(5):e674.
[33] Hirota K, Lambert DG. Ketamine: its mechanism(s) of action and unusual clinical uses. Br

J Anaesth 1996;77(4):441-444.
[34] Abdollahpour A, Saffarieh E, Zoroufchi BH. A review on the recent application of ketamine in management of anesthesia, pain, and health care. J Family Med Prim Care 2020;9(3):1317-1324.
[35] Loix S, De Kock M, Henin P. The anti-inflammatory effects of ketamine: state of the art. Acta Anaesthesiol Belg 2011;62(1):47-58.
[36] Lankveld DP, Bull S, Van Dijk P, et al. Ketamine inhibits LPS-induced tumour necrosis factor-alpha and interleukin-6 in an equine macrophage cell line. Vet Res 2005;36(2):257-262.
[37] Yang J, Li W, Duan M, et al. Large dose ketamine inhibits lipopolysaccharide-induced acute lung injury in rats. Inflamm Res 2005;54(3):133-137.
[38] McCallion K, Harkin DW, Gardiner KR. Role of adenosine in immunomodulation: review of the literature. Crit Care Med 2004;32(1):273-277.
[39] Li CY, Chou TC, Wong CS, et al. Ketamine inhibits nitric oxide synthase in lipopolysaccharide-treated rat alveolar macrophages. Can J Anaesth 1997;44(9):989-995.
[40] Sakowitz OW, Kiening KL, Krajewski KL, et al. Preliminary evidence that ketamine inhibits spreading depolarizations in acute human brain injury. Stroke 2009;40(8):e519-522.
[41] Saito J, Zao H, Wu L, et al. "Anti-cancer" effect of ketamine in comparison with MK801 on neuroglioma and lung cancer cells. Eur J Pharmacol 2023;945:175580.
[42] Malsy M, Gebhardt K, Gruber M, et al. Effects of ketamine, s-ketamine, and MK 801 on proliferation, apoptosis, and necrosis in pancreatic cancer cells. BMC Anesthesiol 2015;15:111.
[43] Zhao S, Shao L, Wang Y, et al. Ketamine exhibits anti-gastric cancer activity via induction of apoptosis and attenuation of PI3K/Akt/mTOR. Arch Med Sci 2020;16(5):1140-1149.
[44] Zanos P, Gould TD. Mechanisms of ketamine action as an antidepressant. Mol Psychiatry 2018;23(4):801-811.
[45] Talke P, Li J, Jain U, et al. Effects of perioperative dexmedetomidine infusion in patients undergoing vascular surgery. The Study of Perioperative Ischemia Research Group. Anesthesiology 1995;82(3):620-633.
[46] Weerink MAS, Struys M, Hannivoort LN, et al. Clinical Pharmacokinetics and Pharmacodynamics of Dexmedetomidine. Clin Pharmacokinet 2017;56(8):893-913.
[47] Piao G, Wu J. Systematic assessment of dexmedetomidine as an anesthetic agent: a meta-analysis of randomized controlled trials. Arch Med Sci 2014;10(1):19-24.
[48] Peltoniemi MA, Hagelberg NM, Olkkola KT, et al. Ketamine: A Review of Clinical Pharmacokinetics and Pharmacodynamics in Anesthesia and Pain Therapy. Clin Pharmacokinet 2016;55(9):1059-1077.
[49] Coull JT, Morgan H, Cambridge VC, et al. Ketamine perturbs perception of the flow of time in healthy volunteers. Psychopharmacology (Berl) 2011;218(3):543-556.
[50] Morgan CJ, Mofeez A, Brandner B, et al. Acute effects of ketamine on memory systems and psychotic symptoms in healthy volunteers. Neuropsychopharmacology 2004;29(1):208-218.
[51] Christ G, Mundigler G, Merhaut C, et al. Adverse cardiovascular effects of ketamine infusion in patients with catecholamine-dependent heart failure. Anaesth Intensive Care 1997;25(3):255-259.
[52] Liebe T, Li S, Lord A, et al. Factors Influencing the Cardiovascular Response to Subanesthetic Ketamine: A Randomized, Placebo-Controlled Trial. Int J Neuropsychopharmacol 2017;20(11):909-918.
[53] Kamp J, van Velzen M, Aarts L, et al. Stereoselective ketamine effect on cardiac output: a population pharmacokinetic/pharmacodynamic modelling study in healthy volunteers. Br J Anaesth 2021;127(1):23-31.
[54] Jakobsen CJ, Torp P, Vester AE, et al. Ketamine reduce left ventricular systolic and diastolic function in patients with ischaemic heart disease. Acta Anaesthesiol Scand 2010;54(9):1137-1144.
[55] Turan A, Duncan A, Leung S, et al. Dexmedetomidine for reduction of atrial fibrillation and delirium after cardiac surgery (DECADE): a randomised placebo-controlled trial. Lancet 2020;396(10245):177-185.
[56] Mazzeffi M, Johnson K, Paciullo C. Ketamine in adult cardiac surgery and the cardiac surgery Intensive Care Unit: an evidence-based clinical review. Ann Card Anaesth 2015;18(2):202-209.
[57] Tasbihgou SR, Barends CRM, Absalom AR. The role of dexmedetomidine in neurosurgery. Best Pract Res Clin Anaesthesiol 2021;35(2):221-229.
[58] Kulikov AS, Lubnin AY. Dexmedetomidine: new opportunities in anesthesiology. Anesteziol Reanimatol 2013;(1):37-41.
[59] Efe Mercanoglu E, Girgin Kelebek N, Turker G, et al. Comparison of the Effect of Ketamine and Dexmedetomidine Combined with Total Intravenous Anesthesia in Laparoscopic Cholecystectomy Procedures: A Prospective Randomized Controlled Study. Int J Clin Pract 2022;2022:1878705.
[60] Rueda Carrillo L, Garcia KA, Yalcin N, et al. Ketamine and Its Emergence in the Field of Neurology. Cureus 2022;14(7):e27389.

[61] MacMahon M, Naysmith MR, McCallion S, et al. Ketamine Infusion Associated with Improved Neurology in a Patient with NMDA Receptor Encephalitis. Case Rep Crit Care 2013;2013:383125.

[62] Von der Brelie C, Seifert M, Rot S, et al. Sedation of Patients with Acute Aneurysmal Subarachnoid Hemorrhage with Ketamine Is Safe and Might Influence the Occurrence of Cerebral Infarctions Associated with Delayed Cerebral Ischemia. World Neurosurg 2017;97:374-382.

[63] Lin N, Vutskits L, Bebawy JF, et al. Perspectives on Dexmedetomidine Use for Neurosurgical Patients. J Neurosurg Anesthesiol 2019;31(4):366-377.

[64] Zanos P, Moaddel R, Morris PJ, et al. Ketamine and Ketamine Metabolite Pharmacology: Insights into Therapeutic Mechanisms. Pharmacol Rev 2018;70(3):621-660.

[65] Rolle A, Paredes S, Cortínez LI, et al. Dexmedetomidine metabolic clearance is not affected by fat mass in obese patients. Br J Anaesth 2018;120(5):969-977.

[66] Al Nasrallah N, Thomas M, Kuehl S, et al. The Use of Dexmedetomidine for Longer Than 48 Hours With Evaluation of Its Secondary Outcome in Patients With Liver Disease. Chest 2016;150(4):228A.

[67] Nia K, Sanaie S, Ghojazadeh M, et al. Use of Dexmedetomidine in Liver Disease: A Systematic Review and Meta-Analysis. Hepatitis Monthly 2019;19:1-7

[68] Song JC, Gao H, Qiu HB, et al. The pharmacokinetics of dexmedetomidine in patients with obstructive jaundice: A clinical trial. PLoS One 2018;13(11):e0207427.

[69] Gaertner J, Fusi-Schmidhauser T. Dexmedetomidine: a magic bullet on its way into palliative care-a narrative review and practice recommendations. Ann Palliat Med 2022;11(4):1491-1504.

[70] LiverTox: Clinical and Research Information on Drug-Induced Liver Injury. National Institute of Diabetes and Digestive and Kidney Diseases, Bethesda (MD), 2012.

[71] Li HP, Liu KP, Yao L. Dexmedetomidine in combination with ketamine for pediatric procedural sedation or premedication: A meta-analysis. Am J Emerg Med 2021;50:442-448.

[72] El-Rouby SH, Y OC, A ME, et al. The effect of dexmedetomidine-ketamine combination versus dexmedetomidine on behavior of uncooperative pediatric dental patients: a randomized controlled clinical trial. J Appl Oral Sci 2024;32:e20240057.

[73] Jamgade D, Fultambkar G, Dara S, et al. A prospective randomized controlled study comparing intravenous dexmedetomidine plus ketamine combination with intravenous dexmedetomidine alone for awake fibreoptic nasotracheal intubation. Ain-Shams Journal of Anesthesiology 2021;13(1):16.

[74] Luca E, Schipa C, Cambise C, et al. Implication of age-related changes on anesthesia management. Saudi J Anaesth 2023;17(4):474-481.

[75] Smith HAB, Besunder JB, Betters KA, et al. 2022 Society of Critical Care Medicine Clinical Practice Guidelines on Prevention and Management of Pain, Agitation, Neuromuscular Blockade, and Delirium in Critically Ill Pediatric Patients With Consideration of the ICU Environment and Early Mobility. Pediatr Crit Care Med 2022;23(2):e74-e110.

[76] Mahmoud M, Mason KP. Dexmedetomidine: review, update, and future considerations of paediatric perioperative and periprocedural applications and limitations. Br J Anaesth 2015;115(2):171-182.

[77] Jang YE, Kim JT. Effective and safe pediatric sedation. Anesth Pain Med (Seoul) 2024;19(Suppl 1):S36-S48.

[78] Yu M, Han C, Jiang X, et al. Effect and Placental Transfer of Dexmedetomidine During Caesarean Section Under General Anaesthesia. Basic Clin Pharmacol Toxicol 2015;117(3):204-208.

[79] Aggarwal J, Lustrino J, Stephens J, et al. Cost-Minimization Analysis of Dexmedetomidine Compared to Other Sedatives for Short-Term Sedation During Mechanical Ventilation in the United States. Clinicoecon Outcomes Res 2020;12:389-397.

[80] Abdildin Y, Tapinova K, Nemerenova A, et al. The impact of ketamine on outcomes in critically ill patients: a systematic review with meta-analysis and trial sequential analysis of randomized controlled trials. Acute Crit Care 2024;39(1):34-46.